

Identification and characterization of host targets of *Ralstonia solanacearum* TAL effector Brg11

Dissertation

der Mathematisch-Naturwissenschaftlichen Fakultät
der Eberhard Karls Universität Tübingen
zur Erlangung des Grades eines
Doktors der Naturwissenschaften
(Dr. rer. nat.)

vorgelegt von
Dousheng Wu
aus Hunan/China

Tübingen
2019

Gedruckt mit Genehmigung der Mathematisch-Naturwissenschaftlichen Fakultät der
Eberhard Karls Universität Tübingen.

Tag der mündlichen Qualifikation:

20.09.2019

Dekan:

Prof. Dr. Wolfgang Rosenstiel

1. Berichterstatter:

Prof. Dr. Thomas Lahaye

2. Berichterstatter:

Prof. Dr. Ulrike Zentgraf

Table of Contents

Abbreviations	1
Zusammenfassung.....	2
Summary	5
Publications.....	7
1 Introduction	9
1.1 The role of type III effectors in plant-pathogen interactions.....	9
1.2 Transcription activator-like effectors and their host targets	10
1.3 <i>R. solanacearum</i> and bacterial wilt disease	12
1.3.1 An introduction to <i>R. solanacearum</i> and its virulence factors	12
1.3.2 Gene knockout and complementation as tools to study the function of <i>R. solanacearum</i> virulence genes	13
1.3.3 The <i>R. solanacearum</i> type III effectors	14
1.4 Previous work on RipTAL Brg11	14
1.5 Polyamines and their regulation in plants	16
1.6 5'UTR-mediated translational regulation in plants.....	17
2 Aims of this work.....	19
3 A modular toolbox for Golden-Gate-based plasmid assembly streamlines the generation of <i>Ralstonia solanacearum</i> species complex knockout strains and multi-cassette complementation constructs	20
4 Metabolomics of tomato xylem sap during bacterial wilt reveals <i>Ralstonia solanacearum</i> produces abundant putrescine, a metabolite that accelerates wilt disease.....	33
5 A pathogen effector subverts translational regulation to boost host polyamine levels	54
6 Discussion.....	106
6.1 Golden-Gate based cloning simplifies gene functional studies in <i>R. solanacearum</i>	106
6.2 Identification of ADCs as Brg11 host targets ---- What makes Brg11 different with TALEs from <i>Xanthomonas</i> ?	108
6.3 ADCs are new members of <i>R. solanacearum</i> type III effector target genes .	109

6.4 Induction of new transcription start sites by Brg11 and its biological impact.	110
6.5 Translational regulation of <i>ADC</i> and other polyamine pathway genes.....	111
6.6 Polyamines represent a centre hub in host-microbe interactions.....	114
6.7 Bacteria type III effectors mediate inhibition of competitive microbes.....	117
6.8 Outlook	118
References	120
Acknowledgments	129
Curriculum vitae	131

Abbreviations

AD	activation domain
ADC	arginine decarboxylase
bp	base pair
CRISPR	clustered regulary interspaced short palindromic repeats
DNA	desoxyribonucleic acid
EBE	effector binding element
EPS	extracellular polysaccharide
ETI	effector triggered immunity
GG	Golden Gate
mRNA	messenger RNA
NLS	nuclear localization signal
PAM	protospacer adjacent motif
PAMP	pathogen associated molecular pattern
PCR	polymerase chain reaction
PRR	pattern recognition receptor
PTI	PAMP triggered immunity
Rip	Ralstonia injected protein
RipTAL	Ralstonia injected protein transcription activator like
RVD	repeat variable diresidue
RNA	ribonucleic acid
RACE	rapid amplification of cDNA ends
ROS	reactive oxygen species
sgRNA	single guided ribonucleic acid
T3SS	type III secretion system
T3E	type III effector
TALE	transcription activator like effector
TSS	transcription start site
UTR	untranslated region
uORF	upstream open reading frame

Zusammenfassung

Das Bakterium *Ralstonia solanacearum* ist ein verheerendes Pathogen für Pflanzen und Verursacher der bakteriellen Welke bei einer großen Anzahl von Spezies, darunter einige wichtige Kulturpflanzen. Während der Infektion injiziert *R. solanacearum* verschiedene Effektorproteine in pflanzliche Wirtszellen, welche auf unterschiedlichen Wegen in zelluläre Prozesse eingreifen um den Verlauf der Krankheit zu fördern. Brg11 ist ein Effektor aus dem *R. solanacearum* Laborstamm GMI1000, welcher Homologie zu *transcription activator like effectors* (TALEs) aus *Xanthomonas* aufweist. TALEs binden an *effector binding elements* (EBEs) in den Promotoren der Wirtszelle und aktivieren so auf transkriptioneller Ebene Wirtszielgene um entweder den Verlauf der Krankheit zu fördern oder aber die Resistenz der Pflanze hervorzurufen. Vorangegangene *in planta* Studien konnten zeigen, dass Brg11 Reportergene mit einer kompatiblen *EBE* im Promotor auf transkriptioneller Ebene aktivieren kann. Das pflanzliche Zielgen von Brg11 sowie die Bedeutung dieses Effektors für die bakterielle Virulenz sind bisher jedoch unklar.

Ich begann meine Arbeit mit der Etablierung eines modularen *Golden-Gate* (GG)-basierten Toolkits, welches die Assemblierung von *R. solanacearum* Gen-*knockout* sowie Komplementationskonstrukten vereinfacht. Dieses Toolkit enthält eine Reihe von Klonierungsvektoren sowie verschiedene funktionale Module, die alle kompatibel zu einem bereits etablierten GG-Toolkit für *in planta* Genexpression sind. Dieses Toolkit wird genetische Forschung an *R. solanacearum* erleichtern.

Im zweiten Teil der Arbeit habe ich die Zielgene von Brg11 mithilfe von Transkriptomanalysen und *target site* Vorhersage identifiziert. Dies konnte zeigen, dass Brg11 auf transkriptioneller Ebene ausschließlich die Expression der aus Tomate (*Solanum lycopersicum*) stammenden *Arginin Decarboxylasen 1* und *2* (*SIADC1/2*) aktiviert. Eine Mutationsanalyse zeigte, dass die Brg11-abhängige Aktivierung von *SIADC1/2* auf der Integrität der Brg11-Zielsequenzen (*Brg11-EBEs*) beruht, welche *upstream* der kodierenden Sequenzen von *SIADC1/2* lokalisiert sind. Untersuchungen der Wirts-Genome von *R. solanacearum* zeigte in jedem Fall mindestens ein *ADC*-Gen mit einer Brg11-kompatiblen *EBE* *upstream* der kodierenden Sequenz von *ADC*. Die Quantifizierung von *ADC*-Transkriptmengen zeigte eine Brg11-abhängige Aktivierung der Transkription in Aubergine, *Nicotiana*

benthamiana und *Nicotiana tabacum*. Zusammengefasst deuten diese Ergebnisse darauf hin, dass *ADC*-Gene konservierte Ziele von Brg11 unter phylogenetisch getrennten Wirtspflanzen von *R. solanacearum* sind.

Im dritten Teil meiner Arbeit befasste ich mich mit den molekularen Eigenschaften von Brg11-induzierten *ADC*-Transkripten. 5' RACE PCR Experimente zeigten, dass Brg11 *ADC*-Transkripte induziert, welche im Vergleich zu den nativen ~300 bp kürzer sind. Ein Vergleich der translationalen Aktivität zwischen nativen und Brg11-induzierten Transkripten zeigte für letztere eine höhere translationale Aktivität. Durch Mutationsanalysen konnte ein konserviertes GC-reiches Motiv von ~50bp Länge in der 5'UTR von nativen *ADC*-Transkripten (*ADC*-Box) identifiziert werden. Dieses Motiv reprimiert möglicherweise die Translation durch die Bildung einer vorhergesagten RNA Sekundärstruktur. Da Brg11-induzierte Transkripte eine kürzere 5'UTR und damit keine *ADC*-Box vorweisen, sind diese Transkripte nicht durch die translationale Regulation der Wirtspflanze betroffen, was zu einer höheren *ADC*-Expression führt.

Im vierten Teil dieser Arbeit wurde untersucht inwieweit die Brg11-vermittelte Aktivierung von *ADC* zur Virulenz von *R. solanacearum* beiträgt. Es ist bekannt, dass *ADC*-Proteine die Umwandlung von Arginin zu Agmatin katalysieren und limitierende Enzyme der Polyaminbiosynthese sind. Metabolomische Analysen zeigten einen Anstieg der Polyamine Agmatin und Putrescin, jedoch nicht von Spermidin und Spermin. Erhöhte Putrescin-Konzentrationen gehen oft mit Abwehrreaktionen der Pflanze gegen Krankheitserreger einher. Analysen des *in planta* Wachstums zeigten, dass Brg11-induzierter, erhöhter Putrescin-Gehalt mit dem reduzierten Wachstum von *Pseudomonas syringae* pv. *tomato* DC3000 korreliert, jedoch keinen Einfluss auf das Wachstum von *R. solanacearum* hat. Diese Beobachtungen lassen vermuten, dass der Brg11-bedingte Anstieg an Putrescin in der Wirtspflanze das Wachstum von *R. solanacearum*-Konkurrenten wie *P. syringae* inhibiert.

Die Ergebnisse dieser Arbeit legen ein neues Konzept nahe nach dem Typ-III-Effektoren ternäre Mikroben-Host-Mikroben Interaktionen vermitteln um bakterielle Virulenz zu steigern. Ebenfalls wird in dieser Arbeit der erste Hinweis geliefert, dass es sich bei der Polyaminbiosynthese um einen bisher unbeachteten regulatorischen Knotenpunkt als Ziel für mikrobielle Effektoren handelt. Des Weiteren führte diese

Arbeit zur Identifikation der *ADC*-Box, einem *cis*-Element in den 5'UTRs der *ADC*-Transkripte von Landpflanzen, welches die Expression von *ADC*-Genen kontrolliert und so als Regulator der Polyaminbiosynthese wirkt. Diese Ergebnisse bieten neue Möglichkeiten für die molekulare Züchtung von schädlingsresistenten Pflanzen.

Summary

Ralstonia solanacearum is a devastating bacterial plant pathogen that causes bacterial wilt disease across a wide range of plant species including numerous important crops. During infection, *R. solanacearum* injects effector proteins into host cells that interfere in various ways with cellular processes to promote disease. Brg11 is an effector present in the *R. solanacearum* strain GM11000 that shares homology to transcription activator-like effectors (TALEs) from *Xanthomonas*. TALEs bind to effector binding elements (EBEs) in host promoters and transcriptionally activate downstream host genes to either promote disease or trigger resistance. Previous *in planta* studies revealed that the TALE-like Brg11 protein transcriptionally activates reporter genes that contain a compatible EBE in their promoters. However, the plant target(s) of Brg11 and their contribution to bacterial virulence is still unclear.

I started my work by establishing a modular, Golden-Gate (GG)-based toolkit that simplifies assembly of *R. solanacearum* gene knockout and complementation constructs. This toolkit contains a series of vector backbones and functional modules that are all compatible with a previously established GG-toolkit for *in planta* gene expression. This toolkit will foster genetic studies in *R. solanacearum*.

In the second part of my work I identified Brg11 host target genes by the combined use of transcriptome profiling and target site prediction. This work uncovered, that *R. solanacearum* Brg11 transcriptionally activates exclusively tomato (*Solanum lycopersicum*) arginine decarboxylase 1 and 2 genes (*SIADC1/2*). Mutational studies demonstrate that Brg11-dependent activation of *SIADC1/2* relies on integrity of Brg11 target sites (*Brg11-EBEs*) that are located upstream of the *SIADC1/2* coding sequences. Inspection of *R. solanacearum* plant host genomes shows in each case at least one *ADC* gene with a Brg11 compatible EBE upstream of the *ADC* coding sequence. Quantification of *ADC* transcript levels demonstrated Brg11-dependent activation in eggplant, *Nicotiana benthamiana* and *N. tabacum*. In summary these observations suggest that *ADC* genes are conserved targets of Brg11 across phylogenetically distinct plant hosts of *R. solanacearum*.

The third part of my work focused on the molecular characterization of Brg11-induced *ADC* transcripts. 5'RACE PCR revealed that Brg11 induces *ADC* transcripts with 5'UTRs that are ~300 bp shorter than native *ADC* transcripts. Comparison of

translational activity of native vs. Brg11-induced, short *ADC* transcripts revealed that the latter have higher translational activity. Mutational studies revealed that a conserved ~50 bp GC-rich motif in the 5'UTR of native *ADC* transcripts, termed *ADC-box*, attenuates translation possibly by forming a RNA secondary structure. Since Brg11-induced *ADC* transcripts have a short 5'UTR lacking the *ADC-box* these transcripts bypass translational regulation installed by the host, resulting in high *ADC* expression.

How Brg11-mediated *ADC* activation contributes to *R. solanacearum* virulence was studied in part four of this work. *ADC* proteins are known to catalyze conversion of arginine to agmatine and are rate-limiting enzymes of polyamine biosynthesis. Metabolic studies revealed a Brg11-dependent increase of agmatine and diamine putrescine but not of the polyamines spermidine and spermine. Elevated putrescine is often associated with plant defense reactions. Quantification of *in planta* growth indeed revealed that the Brg11-induced increase in putrescine levels correlates with reduced *in planta* growth of *Pseudomonas syringae* pv. *tomato* DC3000 but notably had no impact on growth of *R. solanacearum*. These observations suggest a model where Brg11-mediated increase of host putrescine results in reduced growth of microbial niche competitors of *R. solanacearum*.

Observations of this work suggest a novel concept in which type III effectors mediate ternary microbe-host-microbe interactions to promote bacterial virulence. This work also suggests polyamine biosynthesis as a yet unrecognized regulatory hub that is manipulated by microbial type III effectors. Furthermore this work resulted in the identification of the *ADC-box*, a *cis* element present in 5'UTRs of land plant *ADC* transcripts that controls *ADC* expression levels and thus serves as a regulator of polyamine biosynthesis. These findings provide opportunities for molecular breeding of pest-resistant plants.

Publications

1. **Wu, Dousheng**, Schandry, Niklas & Lahaye, Thomas. A modular toolbox for Golden-Gate-based plasmid assembly streamlines the generation of *Ralstonia solanacearum* species complex knockout strains and multi-cassette complementation constructs. *Molecular Plant Pathology* (2018) **9** (2018): 1511–1522.

The author's contribution:

- Participation in the design of the experiments
 - Cloning of plasmids listed in Table S2 and S3
 - Carrying out experiments shown in Fig. 2 (B-E) and Fig. 6 (B-D)
 - Preparation of the manuscript together with Thomas Lahaye and Niklas Schandry
2. M. Lowe-Power, Tiffany, G. Hendrich, Connor, von Roepenack-Lahaye, Edda, Li, Bin, **Wu, Dousheng**, Mitra, Raka, L. Dalsing, Beth, Ricca, Patrizia, Naidoo, Jacinth, Cook, David, Jancewicz, Amy, Masson, Patrick, Thomma, Bart, Lahaye, Thomas, J. Michael, Anthony & Allen, Caitilyn. Metabolomics of tomato xylem sap during bacterial wilt reveals *Ralstonia solanacearum* produces abundant putrescine, a metabolite that accelerates wilt disease. *Environmental Microbiology* (2018) 20(4): 1330–1349

The author's contribution:

- Participation in the discussion of the manuscript
3. **Wu, Dousheng**, Von Roepenack-Lahaye, Edda, Buntru, Matthias, de Lange, Orlando, Schandry, Niklas, L Pérez-Quintero, Alvaro, Weinberg, Zasha, M. Lowe-Power, Tiffany, Szurek, Boris, J. Michael, Anthony, Allen, Caitilyn, Schillberg, Stefan & Lahaye, Thomas. A pathogen effector subverts translational regulation to boost host polyamine levels. *Cell Host & Microbe* (in revision)
(<https://dx.doi.org/10.2139/ssrn.3376660>)

The author's contribution:

- Participation in the design of the experiments
- Cloning of the plasmids used in this study
- Carrying out experiments shown in Fig.1, Fig. 2, Fig. 3, Fig. 4 (B and D), Fig. 6, Fig. S1, Fig. S2, Fig. S3, Fig. S4, Fig. S5 (B),

- Carrying out experiments shown in Fig. 5 (A-G) and Fig. S8 together with Edda Von Roepenack-Lahaye,
- Preparation of the manuscript together with Thomas Lahaye

1 Introduction

1.1 The role of type III effectors in plant-pathogen interactions

Plants possess a highly effective immune system to detect and defend against potential microbes (Chisholm et al., 2006; Jones and Dangl, 2006). The first level of this system is based on perception of pathogen-associated molecular patterns (PAMPs) by plant transmembrane pattern recognition receptors (PRRs). The response to PAMPs have been termed PAMP-triggered immunity (PTI). PTI responses are usually accompanied with MAP kinase signaling, boost of reactive oxygen species, transcriptional activation of defense related genes and accumulation of callose (Nürnberg et al., 2004). PTI can halt further colonization to most non-adapted pathogens due to the conserved character of PAMPs (e.g. bacterial flagellin and elongation factor) across species (Zipfel, 2014).

To successfully infect plants and cause disease, pathogens evolved a needle-like type III secretion system (T3SS) that directly injects proteins into plant cell (Buttner and He, 2009; Chisholm et al., 2006). These proteins are referred to as type III effectors and promote bacterial virulence by interfering with host cell functions including immunity. Phytopathogenic bacteria usually deliver 15 to 30 effectors per strain into host cells (Jones and Dangl, 2006). The N-terminal region of effector proteins contains a noncleavable type III secretion signal that mediate direct translocation of effectors from the bacterial into the host cell (Buttner and He, 2009). Inside plant cells, bacterial effectors can localize to different subcellular compartments where they manipulate diverse host cell functions to benefit the bacteria growth.

The major function that has been assigned to effectors is the suppression of PTI response. Effectors inhibit PTI through multiple mechanisms (e.g. interfere with PRR biogenesis, PRR co-receptors and PRR-associated cytoplasmic kinases) (Macho and Zipfel, 2015). For example, the effector AvrPto from *Pseudomonas syringae* targets host PRRs such as FLS2 and EFR to suppress their kinase activity and block PTI signaling (Xiang et al., 2008, 2010). Except for directly targeting PTI pathways, more and more studies show that effectors can also disturb other plant cellular functions such as phytohormone signaling pathways, metabolism, proteasome-

dependent protein degradation, vesicle trafficking, gene expression and cytoskeleton formation (Büttner, 2016; Macho, 2016). For example, transcription activator-like effectors (TALEs) from *Xanthomonas* promote disease through activation of host target gene expression (Boch et al., 2014).

In addition to suppress PTI and other cellular functions, some effectors function as avirulence proteins and are recognized by specific plant resistance (*R*) genes. The recognition of a given effector by a corresponding *R* protein induces another layer of plant immunity, called effector-triggered immunity (ETI) (Chisholm et al., 2006; Jones and Dangl, 2006). ETI is a more robust form of resistance that is typically associated with a localized cell death reaction and stops pathogen growth (Cui et al., 2014). Thus bacterial effectors can function as both virulence and avirulence factors, they play important roles in plant-pathogen interactions.

1.2 Transcription activator-like effectors and their host targets

TALEs are effector proteins predominantly found in plant pathogenic bacteria *Xanthomonas* (Boch and Bonas, 2010). Recently, TALE-like proteins are also found in other organisms such as *R. solanacearum* (de Lange et al., 2013). They form a unique class of effectors due to their special structure and function (Figure 1). TALEs have a signal peptide required for T3SS-mediated delivery into host cells in their N-terminus, a nuclear localization signal and an activation domain required for *in planta* localization and gene activation in their C-terminus. The centre region of TALEs typically consists of 33-34 amino acids repeats (Bogdanove et al., 2010). The amino acids are identical among different repeats except for position 12 and 13, which are termed repeat-variable diresidue (RVD). TALEs bind to effector binding elements (*EBEs*) in host promoters and transcriptionally activate downstream genes to promote disease or trigger resistance (Boch et al., 2014; Bogdanove et al., 2010). The *EBEs* that TALEs bind to are determined by their RVDs, with each RVD recognizes one DNA base (Boch et al., 2009; Moscou and Bogdanove, 2009). The correlation between certain TALE RVDs and corresponding DNA bases is also known as the TALE code. Based on the TALE code, several algorithms have been developed for TALE target *EBE* prediction (Doyle et al., 2012; Pérez-Quintero et al., 2013). Code-assisted TALE *EBE* prediction in combination with transcriptome profiling provides a robust tool for the isolation of direct TALE host target genes.

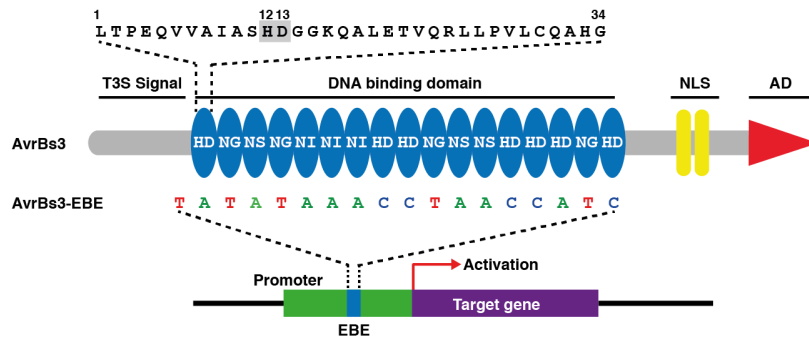


Figure 1 TALE structure and its working model.

The most popular TALE AvrBs3 is shown here as an example. AvrBs3 contains a N-terminal type III secretion signal (T3S Signal), a centre DNA binding domain, a nuclear localization signal (NLS) and a C-terminal activation domain (AD). The centre DNA binding domain consists of 17 repeats. Each repeat contains 34 amino acids and the first repeat is shown on the top of the figure. The 34 amino acids are identical among all the repeats except for the position 12 and 13 which are called repeat-variable diresidue (RVD). The RVDs of AvrBs3 are shown in oval with white text. Each RVD recognizes and binds to one nucleotide with a thymine (T) preceding in a given promoter. These nucleotides are called effector binding element (EBE). AvrBs3 binds to the EBE and transcriptionally activates the downstream target genes (Boch et al., 2009).

The majority of TALE-induced host genes are involved in disease development. The first susceptible (S) gene activated by TALEs was identified in rice. *X. oryzae* pv. *oryzae*, which causes bacterial blight of rice, injects PthXo1 into rice that transcriptionally activates *Os8N3* gene to promote bacterial growth (Yang et al., 2006). *SWEET* gene family that encode sugar transporters are the most popular TALE target genes, since either the same *SWEET* gene or different members of the *SWEET* family can be activated by different TALEs (Antony et al., 2010; Streubel et al., 2013; Yu et al., 2011). This notion has been further expanded with the findings that *SWEET* genes from multiple plant species such as cassava and cotton were also activated by TALEs from corresponding *Xanthomonas* strains (Cohn et al., 2014; Cox et al., 2017). TALE-mediated induction of host *SWEET* genes is considered to increase sugar transportation from phloem cells to the apoplast and thus provide the bacteria with more nutrition (Chen, 2014). Except for *SWEET* genes, several other TALE-induced S genes have been identified recently. *X. citri* subspecies *citri*, the casual agent of citrus canker disease, secretes PthA4 that induces the transcription factor *CsLOB1* to promote pustule formation and bacterial growth (Hu et al., 2014). Tal2g from *X. oryzae* pv. *oryzicola* that causes bacterial leaf streak of rice activates a sulfate transporter gene to increase lesion expansion and bacterial exudation (Cernadas et al., 2014).

TALEs also mediate activation of host *R* genes. These include *Xa10*, *Xa23* and *Xa27* from rice, *Bs3* and *Bs4C* from pepper (Gu et al., 2005; Römer et al., 2007; Strauss et al., 2012; Tian et al., 2014; Wang et al., 2014). Activation of such *R* genes triggers a hypersensitive response and prevents pathogen growth. TALE-targeted host *S* and *R* genes show a high degree of sequence and functional diversity, indicating that TALEs disturb a variety of cellular processes to promote disease or trigger resistance (Boch et al., 2014).

1.3 *R. solanacearum* and bacterial wilt disease

1.3.1 An introduction to *R. solanacearum* and its virulence factors

R. solanacearum, the causal agent of bacterial wilt, is considered as the second most important plant pathogenic bacterium based on its scientific and economic impact (Mansfield et al., 2012). It has an extremely broad host range, infecting more than 200 plant species. The common hosts include tomato, eggplant, pepper, potato, tobacco, ginger, peanut and banana. Due to its high genetic diversity and wide geographical distribution, *R. solanacearum* is divided into four phylotypes (phylotype I, II, III and IV) and recognized as a 'species complex' (Genin and Denny, 2012; Peeters et al., 2013a). As a soil-borne pathogen, *R. solanacearum* survives in soil, infects plants through root and multiplies in xylem vessels. At later stages of infection, *R. solanacearum* secretes large amount of extracellular polysaccharide

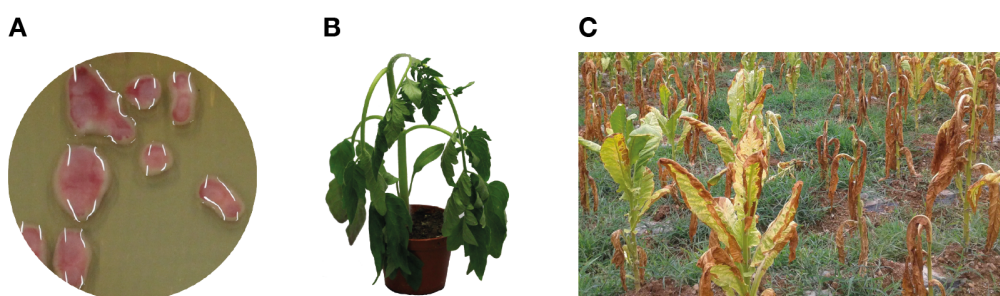


Figure 2 Bacterial wilt disease caused by *R. solanacearum*.

A, Colony morphology of *R. solanacearum* on agar plate supplemented with Triphenyl Tetrazolium Chloride. Typical *R. solanacearum* colonies are irregularly shaped and highly fluidal. The white liquid-like things surrounding the colony are EPS. **B**, The typical symptoms of bacterial wilt. Shown here is an infected tomato plant. The whole plant is wilted due to no water transportation from the root to the upper parts of the plants. **C**, Bacterial wilt disease in field condition. Shown here is a tobacco field in which all the tobacco plants are totally wilted and dried due to bacterial wilt disease.

(EPS) into the xylem blocking water transport from the root to the top (Figure 2A). The typical symptom of this disease is wilting (Figure 2B). In some severe cases, the whole plant is wilted, leading to devastating losses of plant yield (Figure 2C).

The *R. solanacearum* infection relies on several virulence factors such as motility, cell wall degrading enzymes, the T3SS and EPS (Coll and Valls, 2013; Tans-Kersten et al., 2007; Kang et al., 2002). Among these virulence factors, the T3SS is considered as the main pathogenicity determinant in *R. solanacearum*. Mutations in genes encoding regulatory or structural proteins of the T3SS can make the *R. solanacearum* nonpathogenic. The *R. solanacearum* T3SS is encoded by about 20 *hrp* genes and the expression of this system is tightly regulated (Coll and Valls, 2013). Upon contact with the plant, the *R. solanacearum* outer membrane receptor PrhA senses the plant signal and activates the expression of the T3SS through a cascade of transcriptional regulators (Brito et al., 2002). Activation of *hrpB*, a key regulator that located at the bottom of this cascade, directly controls expression of many type III effector genes (Occhialini et al., 2005).

1.3.2 Gene knockout and complementation as tools to study the function of *R. solanacearum* virulence genes

The genome of the model *R. solanacearum* strain GMI1000 encodes a total of 5, 129 predicted proteins (Salanoubat et al., 2002). Generating gene knockout mutants and complementation strains and determining their disease phenotypes are fundamental means to explore gene functions. In *R. solanacearum*, gene knockout constructs can be assembled using overlap extension PCR in combination with classical cloning, by which the flanking regions of the gene of interest are added up- and downstream of an antibiotic resistance gene and ligated into a cloning vector. The construct is then transformed into *R. solanacearum* and integrated into the bacteria genome via homologous recombination, leading to the replacement of the gene of interest with the antibiotic selection marker and thus a gene knockout (Jacobs et al., 2013). For endogenous gene or reporter gene complementation, a classical and Gateway cloning compatible plasmid system, called the '*Ralstonia* chromosome' plasmid series (pRC), has been established (Monteiro et al., 2012). The pRC vectors are based on a safe genomic insertion site to stably integrate gene constructs into the *R. solanacearum* genome. Though the pRC vectors enable cloning of any

promoter:gene combination, this system has limited flexibility in terms of exchange of promoters or genes of interest or tags. Therefore, establishing a more flexible genetic modification toolkit will facilitate gene functional studies in *R. solanacearum*.

1.3.3 The *R. solanacearum* type III effectors

Type III effectors secreted by *R. solanacearum* are uniformly designated as Rip (*Ralstonia* injected proteins) (Peeters et al., 2013b). Till so far 94 type III effector orthologous groups have been predicted in the *R. solanacearum* species complex and 71 of them are experimentally validated for the T3SS dependent translocation (Cunnac et al., 2004; Peeters et al., 2013b). Each individual strain typically encodes 60 to 71 effectors. About half of the effectors are conserved among different *R. solanacearum* strains and called core effectors, while the others are strain specific (Deslandes and Genin, 2014).

Though so many effectors have been identified in *R. solanacearum*, relatively few of them are functionally studied. The major challenge is that single effector mutation has no significant impact on the bacterial virulence, at least in the lab conditions (Cunnac et al., 2004). RipP2 is the most well studied effector in *R. solanacearum*. RipP2 interacts with RRS1, a Toll/Interleukin1 receptor-NB-LRR protein, in *Arabidopsis* and this interaction triggers a resistance reaction against the bacteria (Deslandes et al., 2003). The host targets of many other *R. solanacearum* effectors remain unknown. However, some effectors are assigned to a putative function and a few of them have been functionally validated via reporter assays. For example, RipTAL shares homology with TALEs from *Xanthomonas* and has been shown to localize to plant nucleus and work as a transcriptional activator *in planta* (de Lange et al., 2013).

1.4 Previous work on RipTAL Brg11

RipTAL was named due to its protein structure homology to TAL effectors from *Xanthomonas*. An initial screening found that many *R. solanacearum* strains have this effector (Heuer et al., 2007). Benefit from the discovery of the DNA code of TALEs (Boch et al., 2009; Moscou and Bogdanove, 2009), the DNA binding specificities of a few representative RipTALs were decoded in 2013 (de Lange et al., 2013; Li et al., 2013). Brg11 is a RipTAL from the *R. solanacearum* model strain

GMI1000 and has been shown to contribute to bacterial fitness in eggplant leaves (Macho et al., 2010). Similar to TALEs, Brg11 contains a N-terminal type III secretion signal, a central repeat domain, a C-terminal nuclear localization signal and activation domain (Figure 3A and B). Single Brg11 repeat contains 35 amino acids. The amino acids at position 12 and 13 are polymorphic between different repeats and defined as RVDs responsible for DNA recognition and binding (Figure 3A). Each RVD binds to one base pair at the DNA level with its own binding preferences (Figure 3C). What makes Brg11 different with TALEs is that the DNA base at the 0 position for Brg11 is a guanine (G₀), while for TALEs is a thymine (T₀) (Figure 1, Figure 3B). When these inferred DNA sequences, also termed as *EBE*, were integrated into a minimal *Bs3* promoter fused to a *uidA* reporter, co-delivery of the promoter-reporter with Brg11 into *N. benthamiana* lead to reporter gene activation, demonstrating that Brg11 works as a transcription activator *in planta* (de Lange et al., 2013).

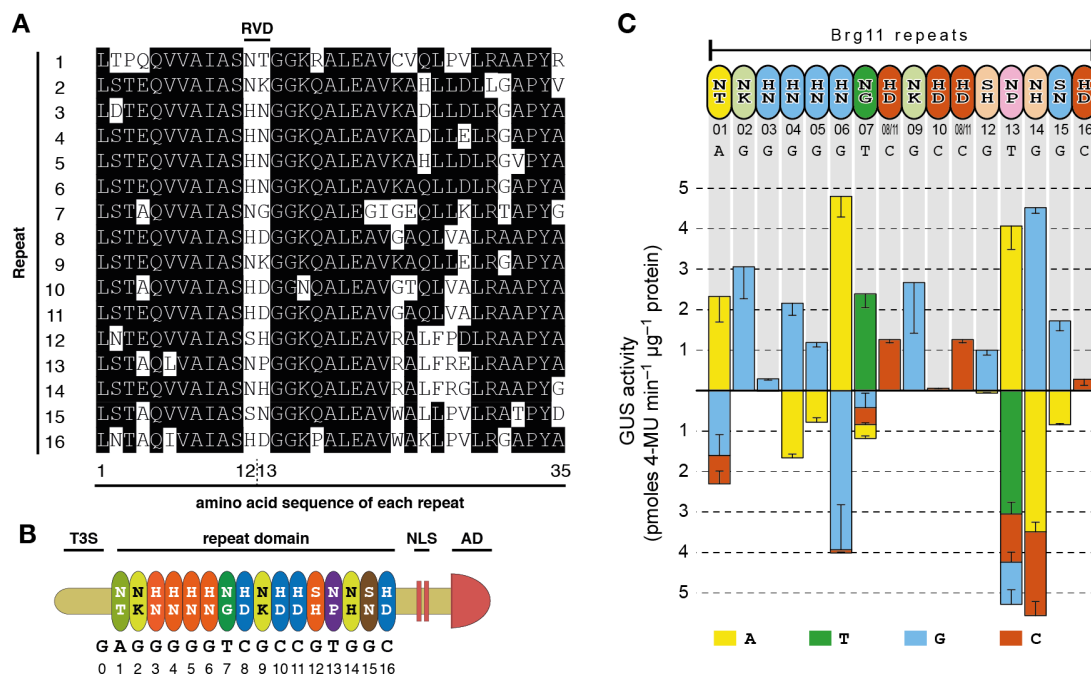


Figure 3 Prior work on RipTAL Brg11.

This figure is taken from de Lange *et al.*, New Phytologist 2013. **A**, Amino acid sequence of Brg11 repeats. Brg11 contains 16 repeats with each repeat 35 amino acids. The amino acids at position 12 and 13 are defined as RVD. **B**, A simplified illustration of Brg11. The RVD sequences of Brg11 are shown. Each RVD binds to one nucleotide. T3S, type III secretion signal; NLS, nuclear localization signal; AD, activation domain. **C**, The binding preference of each repeat to DNA bases. GUS activity indicates the binding affinity.

R. solanacearum is divided into four phylotypes based on its geographical distribution. Brg11 homologies were found in *R. solanacearum* of all phylotypes,

though RipTALs predominantly exist in phylotype I and IV strains (Schandry et al., 2016). RipTALs from different phylotypes not only show differences in the N- and C-terminal regions but also show polymorphisms in the central repeat domain. However, some RipTALs can bind to the *EBEs* of the others, especially RipTALs from *R. solanacearum* strains with a wide host range (Schandry et al., 2016), suggesting that different RipTALs might target the same genes in host plants. Although the binding specificities of RipTALs have been determined, the host target genes remain unknown.

1.5 Polyamines and their regulation in plants

Polyamines are aliphatic polycationic compounds that present in almost all living organisms including plants (Gill and Tuteja, 2010). The most common polyamines are the diamine putrescine, the triamine spermidine and the tetraamine spermine. The synthesis of putrescine in plants may be achieved by two pathways. One of these pathways starts with the decarboxylation of arginine by the enzyme arginine decarboxylase (ADC), leading to the production of agmatine. Agmatine is then synthesized to N-carbamoylputrescine by agmatine iminohydrolase. Consequently, N-carbamoylputrescine is converted into putrescine by N-carbamoylputrescine amidohydrolase. The second pathway is the direct conversion of ornithine into putrescine by ornithine decarboxylase. The synthesis of higher polyamines relies on decarboxylated S-adenosylmethionine as aminopropyl donor, which is generated by S-adenosylmethionine decarboxylase (AdoMetDC). Decarboxylated S-adenosylmethionine is then used by spermidine synthase to add an aminopropyl group to putrescine forming spermidine. In a consecutive aminopropyl reaction, spermine is synthesized by spermine synthase through adding an aminopropyl group to spermidine (Jimenez-Bremont et al., 2014).

Polyamines are essential for normal cell growth, proliferation and differentiation (Michael, 2016). The concentration of polyamines is tightly regulated in eukaryotic cells, as higher levels of polyamines are toxic. The fine regulation is achieved by various ways from biosynthesis, transport to degradation. Polyamines can modulate the translation of most of the enzymes involved in their synthesis and catabolism through feedback mechanisms (Perez-Leal and Merali, 2012). For example, plant *AdoMetDC* genes contains two small upstream open reading frames (uORF) in their

5'UTRs. One of the uORF-encoded peptide can repress the translation of the main *AdoMetDC* ORF under high polyamine conditions and this translational regulation is important for plant polyamine homeostasis (Hanfrey et al., 2005).

The relative abundance of polyamines in plants varies with species and the developmental stages, and undergoes notable changes during abiotic and biotic stress responses (Jimenez-Bremont et al., 2014). Research indicates that the activity of polyamine biosynthetic enzymes and polyamine levels in infected tissues increase during microbial colonization (Walters, 2003). For example, rust fungus *Puccinia hordei* infection increases spermidine level in barley (Greenland and Lewis, 1984), while both spermidine and putrescine were increased in barley after infection with the powdery mildew fungus *Blumeria graminis* (Walters et al., 1985). It has also been shown that polyamines are involved in bacteria-host interactions. *Pseudomonas syringae* infection up-regulates *ADC* gene expression in Arabidopsis and the pathogen grows better when the *ADC2* gene was knocked out (Kim et al., 2013b).

1.6 5'UTR-mediated translational regulation in plants

Regulation of gene expression in eukaryotes is a complex and tightly controlled process. The untranslated regions (UTRs), including the 5' UTR and 3' UTR, and introns are the key regions involved in gene expression regulation (Barrett et al., 2012). In plants, UTRs control gene expression through multiple mechanisms, such as alternative polyadenylation, riboswitching, adenosine methylation, nonsense-mediated decay, alternative splicing and short-peptide translation (Srivastava et al., 2018).

The 5' UTR of many eukaryotic mRNAs contains a short uORF. In plants, including Arabidopsis, maize and rice, about 30% to 40% of transcripts have at least one uORF (Von Arnim et al., 2014). Most uORFs have the canonical start codon ATG, however, some predicted uORFs are potentially translated from non-AUG start codons such as CTG or GTG (McGillivray et al., 2018). Several plant uORFs have been demonstrated to regulate the main ORF (mORF) translation in response to the levels of some key metabolites such as polyamines, sucrose and ascorbate (Guerrero-González et al., 2014; Hanfrey et al., 2005; Laing et al., 2015; Rahmani et al., 2009). uORFs suppress translation of the downstream mORF by slowing or

stalling ribosome movement. If the stop codon of the uORF is located upstream of the exon junction complex, it can be recognized as a premature termination codon to activate nonsense-mediated mRNA decay (Hellens et al., 2016).

The nucleotide content and structure of the 5'UTR also plays an important role in regulating gene expression. Normally 5'UTRs that allow efficient translation are short, less GC rich and relatively unstructured (Kochetov et al., 1998), while 5'UTRs of genes with low protein expression are longer, more GC rich and have a higher degree of predicted secondary structure (Pickering and Willis, 2005). For example, guanine-rich nucleic acid sequences in 5'UTRs can fold into a very stable non-canonical tetrahelical structure called G-quadruplex and strongly repress translation. Bioinformatic analysis have shown that these G-quadruplex structures are often highly conserved (Beaudoin and Perreault, 2010).

2 Aims of this work

Previous studies have demonstrated that the *R. solanacearum* type III effector Brg11 localizes to the nucleus and works as a transcription activator *in planta*. Each repeat of Brg11 recognizes and binds to one base pair and the binding specificity of all Brg11 repeats have been determined. However, these assays were done with *Agrobacterium tumefaciens* mediated transient gene expression in *N. benthamiana*. It remains unknown which host genes are targeted by Brg11 during infection and how activation of these genes contribute to *R. solanacearum* virulence. The aims of this work are:

- 1) Establish a cloning toolkit for gene knockout and complementation in *R. solanacearum*.
- 2) Isolate the direct target genes of Brg11 in tomato.
- 3) Since the Brg11 containing *R. solanacearum* strain has a broad host range, the second aim would be to check if Brg11 activates the same target genes in other host species.
- 4) Investigate if Brg11 induces distinct transcripts compare to the native target transcripts, and if so, how would this make a difference.
- 5) Characterize how Brg11 mediated host target gene activation contributes to disease.

The overall goal of this project is to understand how Brg11 promotes bacterial wilt diseases at the molecular level, which should further provide insight on the control of this devastating plant disease.

3 A modular toolbox for Golden-Gate-based plasmid assembly streamlines the generation of *Ralstonia solanacearum* species complex knockout strains and multi-cassette complementation constructs

This chapter is identical to the publication:

Wu, Dousheng, Schandry, Niklas & Lahaye, Thomas

A modular toolbox for Golden-Gate-based plasmid assembly streamlines the generation of *Ralstonia solanacearum* species complex knockout strains and multi-cassette complementation constructs

Molecular Plant Pathology (2018) **9** (2018): 1511–1522

Technical Advance

A modular toolbox for Golden-Gate-based plasmid assembly streamlines the generation of *Ralstonia solanacearum* species complex knockout strains and multi-cassette complementation constructs

DOUSHENG WU[†], NIKLAS SCHANDRY[‡] AND THOMAS LAHAYE^{*}

Center for Plant Molecular Biology, Eberhard-Karls-University Tübingen, Tübingen 72076, Germany

SUMMARY

Members of the *Ralstonia solanacearum* species complex (*Rssc*) cause bacterial wilt, a devastating plant disease that affects numerous economically important crops. Like other bacterial pests, *Rssc* injects a cocktail of effector proteins via the bacterial type III secretion system into host cells that collectively promote disease. Given their functional relevance in disease, the identification of *Rssc* effectors and the investigation of their *in planta* function are likely to provide clues on how to generate pest-resistant crop plants. Accordingly, molecular analysis of effector function is a focus of *Rssc* research. The elucidation of effector function requires corresponding gene knockout strains or strains that express the desired effector variants. The cloning of DNA constructs that facilitate the generation of such strains has hindered the investigation of *Rssc* effectors. To overcome these limitations, we have designed, generated and functionally validated a toolkit consisting of DNA modules that can be assembled via Golden-Gate (GG) cloning into either desired gene knockout constructs or multi-cassette expression constructs. The *Ralstonia*-GG-kit is compatible with a previously established toolkit that facilitates the generation of DNA constructs for *in planta* expression. Accordingly, cloned modules, encoding effectors of interest, can be transferred to vectors for expression in *Rssc* strains and plant cells. As many effector genes have been cloned in the past as GATEWAY entry vectors, we have also established a conversion vector that allows the implementation of GATEWAY entry vectors into the *Ralstonia*-GG-kit. In summary, the *Ralstonia*-GG-kit provides a valuable tool for the genetic investigation of genes encoding effectors and other *Rssc* genes.

Keywords: effector, Golden-Gate cloning, modular cloning, *Ralstonia solanacearum* species complex (*Rssc*), type III secretion system (T3SS).

INTRODUCTION

The *Ralstonia solanacearum* species complex (*Rssc*) unites a large number of phytopathogenic bacterial species that are globally distributed (Prior *et al.*, 2016; Safni *et al.*, 2014). The *Rssc* complex has been classified into four phylotypes based on genetic similarity which coincide with distinct geographical distributions (Prior and Fegan, 2005). Members of the *Rssc* cause disease on over 200 plant species, including numerous economically important crops. *Rssc* members infect predominantly solanaceous plants, such as potato, tomato, pepper and aubergine, but also Cucurbitaceae, such as watermelon. In addition to these dicotyledonous hosts, *Rssc* members also infect economically important monocot crops, including banana (Ailloud *et al.*, 2015; Genin and Denny, 2012; Prior *et al.*, 2016). Essential for pathogenicity are bacterial effector proteins that are injected by *Rssc* members into host cells via a molecular syringe termed the type III secretion system (T3SS) (Deslandes and Genin, 2014; Peeters *et al.*, 2013). The elucidation of the mechanistic principles of effector-mediated plant susceptibility will probably provide opportunities for the rationalized design of *Rssc*-resistant crops. Accordingly, the identification of *Rssc* effectors and the investigation of their *in planta* function have been a major focus of *Rssc* research. The generation of *Rssc* mutant strains that lack a given effector gene and the subsequent stable integration of genes encoding epitope-tagged effectors are commonly used approaches to unravel effector function. In addition, effector genes are often introduced as transgenes into host cells to study their *in planta* function. A major bottleneck in genetic studies of *Rssc* effectors is the assembly of DNA constructs for the genetic modification of *Rssc* strains.

A widely used approach for chromosomal insertions has been established by Monteiro *et al.* (2012) using the '*Ralstonia* chromosome' plasmid series (pRC). The pRC vector series relies on a safe harbour chromosomal insertion site to stably integrate gene constructs into the chromosome of *Rssc* strains (Cruz *et al.*, 2014; Monteiro *et al.*, 2012). Cloning into the pRC vector series is facilitated by either classical restriction–ligation cloning or GATEWAY reactions. Knockout constructs can be generated using overlap

*Correspondence: E-mail: Thomas.lahaye@zmbp.uni-tuebingen.de

†These authors contributed equally to this work.

‡Present address: Gregor-Mendel Institute of Molecular Plant Biology, Dr. Bohr Gasse 3, Vienna 1030, Austria

extension polymerase chain reaction (PCR) methods, where a chromosomal region is added up- and downstream of a gene conferring antibiotic resistance. The construct is subsequently transformed into *Rssc* strains containing this chromosomal region and integration into the chromosome takes place via homologous recombination, resulting in the replacement of a gene of interest (GOI) with a resistance marker, leading to a genomic knockout (Dalsing and Allen, 2014; Jacobs *et al.*, 2012, 2013). However, so far, no unified cloning platform has been established that enables the straightforward generation of knockout and complementation constructs. Different constructs and cloning approaches are needed to: (i) integrate expression constructs into *Rssc*; (ii) generate gene knockout strains in *Rssc*; and (iii) generate transgenic plants expressing *Rssc* effector genes.

Previously, we have established a toolkit for application in plants that facilitates the modular assembly of expression constructs by Golden-Gate (GG) cloning (Binder *et al.*, 2014). Here, we present a related GG-based toolkit for the genetic modification of *Rssc* strains. The presented toolkit provides a straightforward approach to assemble complex, multi-gene constructs from standardized, reusable cloning modules and to insert them into any chromosomal site in the genome of given *Rssc* strains. Notably, modules of the newly developed *Ralstonia*-GG-kit are fully compatible with the previously established plant-GG-kit. Thus, the very same modules can be used in both contexts, the *Ralstonia*- and the plant-GG-kit, which streamlines side-by-side investigations of *Rssc* effectors and other virulence factors in the context of isolates belonging to the *Rssc* and its host plants.

RESULTS

Establishment of a GG-based cloning procedure for the streamlined generation of knockout constructs for *Rssc* strains

In the first step of our GG-based cloning procedure for the creation of gene knockout constructs for *Rssc* strains, two primer pairs are used to PCR amplify 5' and 3' regions of the given GOI (Fig. 1A, Table S1, see Supporting Information). If possible, the chosen genomic regions should not contain *Bsal* recognition sites as this interferes with the subsequent cloning procedure. If *Bsal* sites are present in the chosen genomic regions, these must be removed by site-directed mutagenesis. Otherwise, no restrictions apply to the selection of the genomic regions to be amplified. In addition to the gene-specific parts of the primers, these contain, at their 5' termini, *Bsal* recognition sites followed by defined nucleotide sequences which, after cleavage of derived PCR products, translate into defined four-base-pair overhangs facilitating subsequent directional multi-fragment ligation (Fig. 1). Blunt-end cloning of PCR products results in so-called level one (LI) modules which, after validation by sequencing, are assembled into

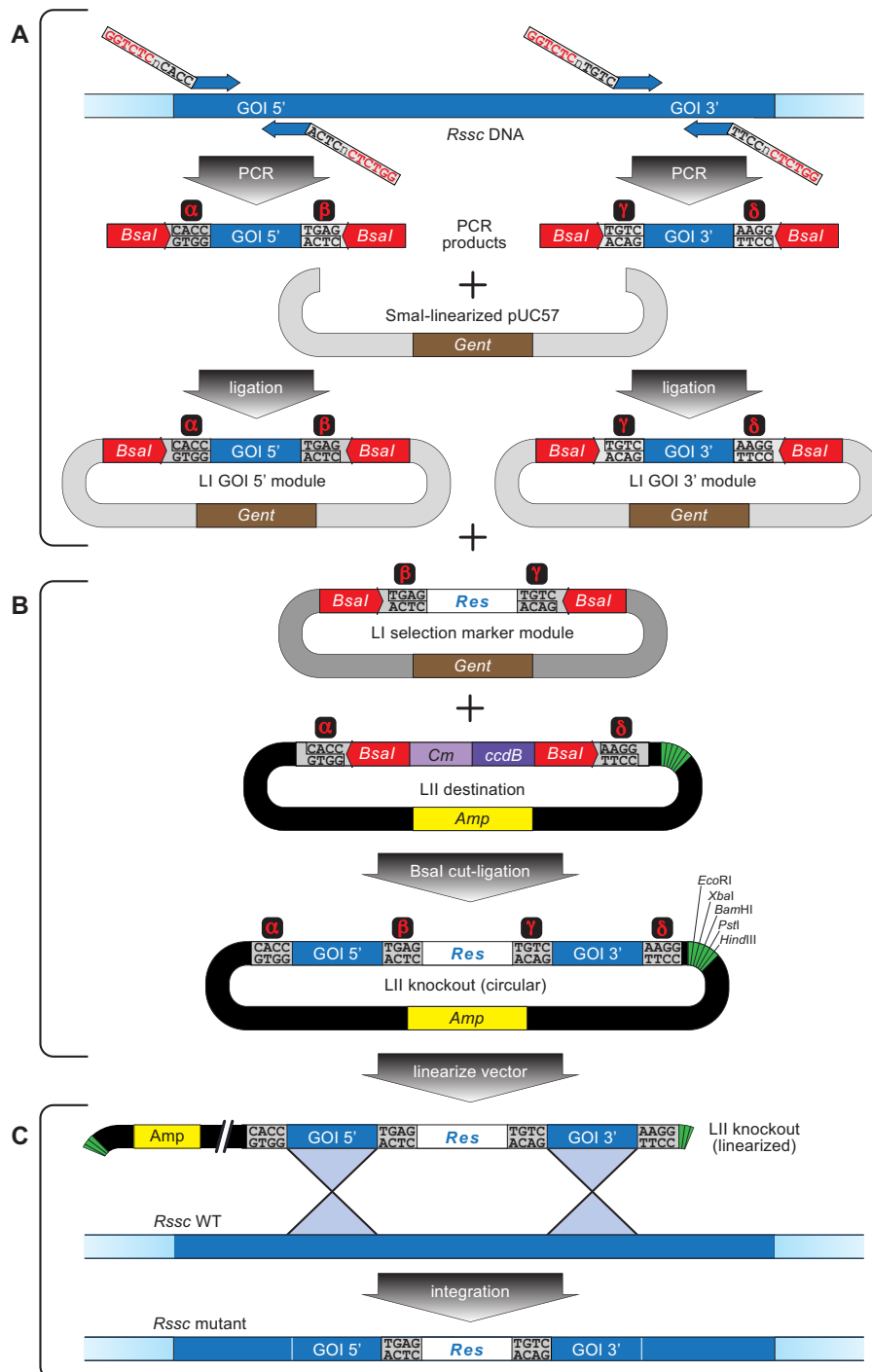
multi-cassette LII modules. LI modules containing genomic fragments (LI GOI 5' module and LI GOI 3' module) are fused to both ends of an LI selection marker module and integrated into an LII destination vector to be used for recombination-based transfer into an *Rssc* strain (Fig. 1B). To maximize flexibility of the *Ralstonia*-GG-kit, several distinct LI selection marker modules have been generated which are available for selection in *Rssc* and which mediate resistance against spectinomycin, gentamycin, kanamycin, tetracycline or chloramphenicol (Table S2, see Supporting Information). Selection markers to be transferred (collectively designated as 'Res' in Fig. 1) are combined with a gentamycin selection marker present in the vector backbone that is intended for selection in *Escherichia coli*. The only exception is the LI vector containing the gentamycin resistance for transfer into an *Rssc* strain, which contains an ampicillin resistance gene in the vector backbone for selection in *E. coli* (Table S2). Directional cloning of the two genomic fragments (LI GOI 5' module and LI GOI 3' module), together with the selection marker module, into a desired target vector (LII destination) is achieved by incubation with *Bsal* endonuclease and DNA ligase. This results in the release of DNA fragments which, as a result of the presence of defined compatible sticky overhangs (Fig. 1; for simplicity, compatible overhangs are designated with identical Greek letters), assemble into the desired ligation product (LII knockout). The desired ligation product is devoid of *Bsal* sites, thus facilitating simultaneous cleavage and ligation (cut-ligation). To simplify the selection of *E. coli* transformants containing the desired LII knockout plasmids, the LII destination vector should preferably have an *E. coli* selection marker that is distinct from the *E. coli* selection marker used in the three LI modules. The LII knockout vector contains a multiple cloning site with several unique endonuclease recognition sites that can be used to linearize the knockout vector (Fig. 1B). Subsequently, the linearized LII knockout vector will be transformed into *Rssc* strains, as described previously (Bertolla *et al.*, 1997), resulting in the desired integration event (Fig. 1C).

Proof-of-principle experiments validate the functionality of GG-generated vectors for the generation of *Rssc* knockout strains

To validate the functionality of our GG-based knockout strategy, we tested our modular toolbox by creating knockout strains in the *Rssc* reference strain GMI1000. We targeted bacterial genes that are known to be crucial for the *in planta* virulence of GMI1000 and which thus should cause changes in the infection phenotypes of corresponding mutant strains. We selected *epsB*, *hrpB* and *hrcV* genes as targets as the corresponding mutant strains are known to be significantly reduced in virulence or non-virulent (Macho *et al.*, 2010; Milling *et al.*, 2011; Vasse *et al.*, 2000). For the generation of *epsB* and *hrpB* knockouts, their coding sequence (CDS) was replaced by a gentamycin resistance gene (Fig. 2A). In the

case of the GMI1000 *hrcV* gene, a gene disruption mutant was created by inserting the gentamycin resistance gene into the *hrcV* CDS (Fig. 2A). We constructed the LII knockout vectors according to our toolbox design (Fig. 1) and transformed the linearized vector into GMI1000. Mutant strains were first selected on agar plates containing gentamycin. Subsequently DNA of resistant strains was

analysed with primer pairs adjacent to the target gene (*epsB* and *hrpB*) or within the target gene (*hrcV*) to confirm the presence of the desired integration event (Fig. 2A). The size of the observed PCR products derived from GMI1000 wild-type and putative knockout strains supported the presence of the envisaged mutational events (Fig. 2B). Typically, 80%–90% of colonies growing



on selective agar contained the desired integration event, demonstrating the high efficiency of GG-generated knockout constructs.

Next, we tested the infection phenotypes of the newly generated GMI1000-derived mutant strains. The *Rssc hrpB* and *hrcV* genes are involved in type III secretion (T3S) of effector proteins from the bacterial pathogen into host plants. Accordingly, their expression is essential for the full virulence of *Rssc* strains on tomato host plants (Macho *et al.*, 2010; Vasse *et al.*, 2000). The *Rssc epsB* gene is involved in the biosynthesis of extracellular polysaccharides (EPSs) and the *epsB* knockout strain has been shown to be significantly reduced in virulence on tomato (Milling *et al.*, 2011). In agreement with the previously published infection phenotypes, our newly generated GMI1000-derived mutant strains ($\Delta hrpB$, $\Delta hrcV$ and $\Delta epsB$) failed to cause wilting symptoms on host plants on inoculation of tomato roots at 7 days post-infection (Fig. 2C). This observation provides supporting evidence that our GG-based knockout strategy indeed resulted in the desired mutational events. GMI1000 wild-type and mutant strains were characterized further by blunt-end syringe infiltration of tobacco leaves. In this assay, the GMI1000 wild-type and mutant strain $\Delta epsB$ triggered a hypersensitive response (HR). By contrast, the $\Delta hrpB$ and $\Delta hrcV$ strains did not trigger HR in tobacco leaves (Fig. 2D). These observations indicate that the HR observed in tobacco is effector-triggered immunity (ETI) and confirm that modified EPS levels in the $\Delta epsB$ mutant strain do not significantly affect effector delivery. To confirm that the newly generated knockout strain $\Delta epsB$ indeed contains modified EPS levels, we also analysed this mutant strain on Kelman's tetrazolium chloride (TZC) agar plates. Wild-type GMI1000 grows on TZC agar plates as large, elevated, fluid colonies, with a white or pale-red centre. By contrast, $\Delta epsB$ grows as smaller deep-red colonies (Kelman, 1954). Consistent with this, $\Delta epsB$ showed a dark-red colony morphology on TZC plates (Fig. 2E). In summary, the PCR analysis, infection phenotypes and colony morphology of the newly generated mutant strains are in agreement with the expectations and confirm that the GG-based knockout strategy produced the desired mutational events.

Establishment of a GG-based vector for the integration of expression cassettes into a permissive site of the GMI1000 genome

Gene knockout strains must be functionally complemented with wild-type genes to confirm that the observed changes in the knockout strains are a result of a mutation in the targeted gene and not the consequence of a mutation at a distinct genomic locus. Given that we had established a GG-based knockout strategy for *Rssc* strains, we wanted to expand our toolkit in a way that facilitated the generation of multi-cassette constructs to be integrated at a permissive chromosomal site. Previous studies in the *Rssc* reference strain GMI1000 have shown that the intergenic region between *Rsc0178* (*glms*) and *Rsc0179* is a permissive site, suitable for the stable integration of expression constructs (Monteiro *et al.*, 2012). Accordingly, we first designed and generated a vector containing the described genomic regions flanking the desired genomic integration site 203336/7 in the GMI1000 chromosome (Fig. 3). To do so, we PCR amplified genomic segments up- and downstream of the permissive site (202375-3336 [UP] 203337-4307 [DOWN]; Monteiro *et al.*, 2012). The PCR primers used for the amplification of UP and DOWN fragments contain *Bsal* recognition sites in their 5' termini, in addition to their *Rssc* strain-specific parts, and defined downstream bases in the *Bsal* cleavage site for subsequent cut-ligation-based fragment assembly. The genomic DOWN segment contained two *Bsal* recognition sites that were removed by site-directed mutagenesis (Fig. 3). Next, *Bsal* cut-ligation was carried out to fuse sequence-validated LI UP and DOWN modules to opposite ends of the *LacZ* reporter gene and to integrate these three module blocks into the LII destination vector. In the resulting plasmid of this *Bsal* cut-ligation, designated LIII_1–6_Amp_RC, the *LacZ* gene is flanked by *Bpil* sites, which facilitate the removal of the *LacZ* reporter gene and the integration of the desired expression cassettes via *Bpil* cut-ligation. Thus, the integration of the desired fragments into the target vector can be traced by blue–white selection. Notably, the LIII_1–6_amp_RC vector, as it is, provides a basis for the

Fig. 1 Golden-Gate (GG)-based assembly of *Ralstonia solanacearum* species complex (*Rssc*) gene knockout constructs. (A) Polymerase chain reaction (PCR)-amplified 5' and 3' regions of a given gene of interest (GOI 5', GOI 3'; blue bars) are blunt-end ligated into linearized cloning vector. Primers (angled bars) contain a *Bsal* recognition site (red type) in addition to their gene-specific parts (narrow blue bars) in their 5' termini and defined downstream bases in the *Bsal* cleavage sites (bold black type). *Bsal*-generated overhangs facilitate subsequent directional cloning of sequence-validated clones into the gene knockout LII destination vector. For simplicity, the distinct types of four-base-pair overhangs are designated with red Greek letters in black boxes. (B) Combined use of *Bsal* and DNA ligase (cut-ligation) allows the simultaneous transfer of the *Rssc* selection marker (*Res*), together with the flanking GOI 5' and GOI 3' fragments, into the gene knockout vector (LII destination, black backbone). (C) The gene knockout vector (LII knockout) is linearized with a suitable endonuclease that cleaves in the vector backbone [available enzymes of the multiple cloning site (green bar) are displayed], but not in the transferred DNA segment. The linearized LII knockout vector is transformed into *Rssc* strains and integrated into its genome by homologous recombination. The antibiotic resistance gene (*Res*) present in the transferred gene segment allows the selection of strains containing the insertion. The presence of the insertion at the desired chromosomal location can be confirmed by PCR-based analysis (see Fig. 2). Light and dark blue bars indicate coding and non-coding sequences, respectively. Grey and black bars indicate vector backbone DNA. Red arrows indicate *Bsal* recognition sites with the tip of the arrow pointing towards its cleavage site. Selection markers are indicated by yellow (ampicillin, *Amp*), purple (chloramphenicol, *Cm*; gyrase-specific toxin, *ccdB*) and brown (gentamycin, *Gent*) boxes. Note that boxes with selection markers represent not only the coding sequence, but also promoter and terminator sequences.

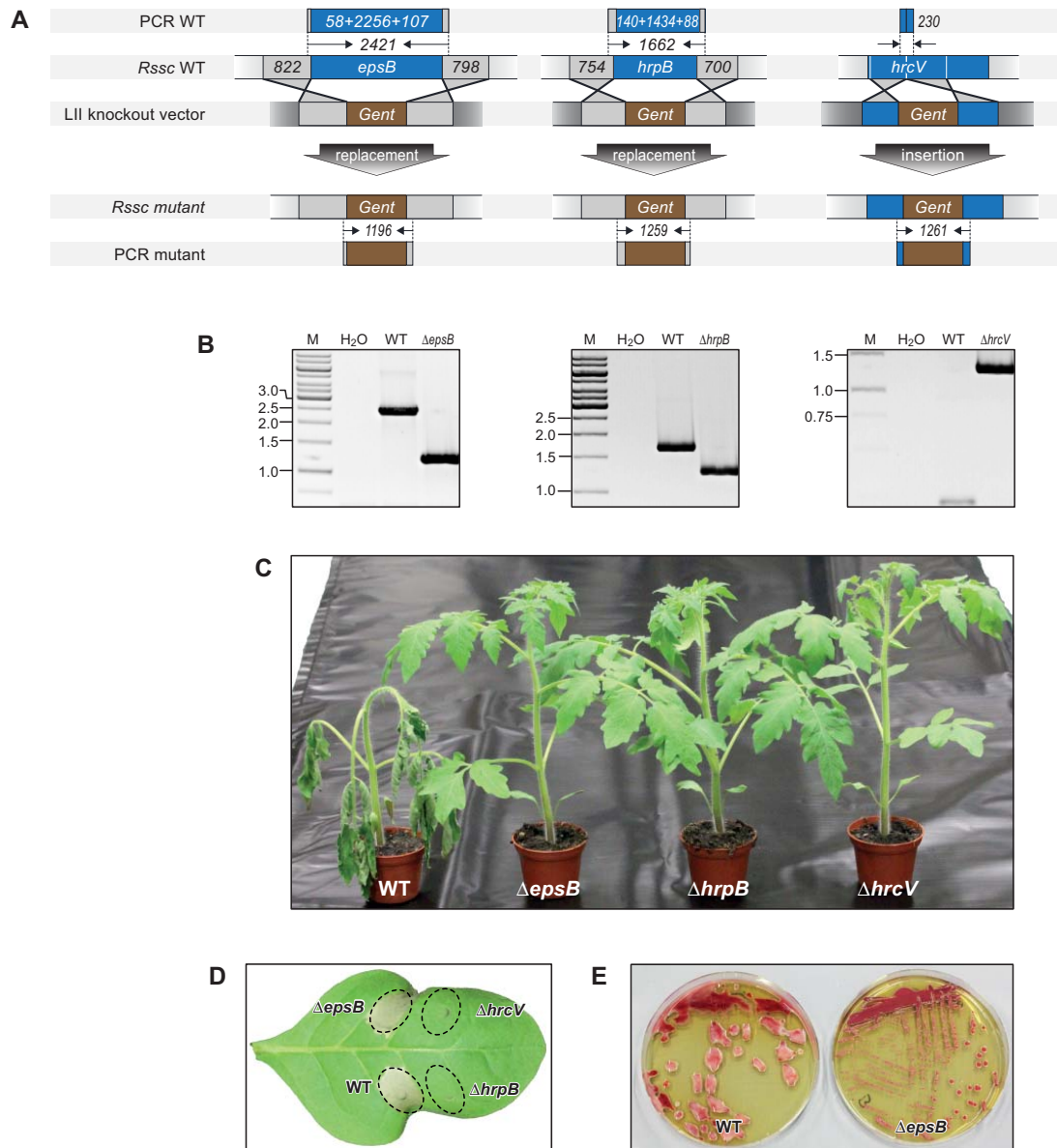


Fig. 2 Validation of chromosomal knockout strains in *Ralstonia solanacearum* species complex (*Rssc*) reference strain GMI1000. (A) Graphical display of *Rssc* *epsB*, *hrpB* and *hrcV* wild-type (WT), gene knockout derivatives and corresponding polymerase chain reaction (PCR) products. (B) Diagnostic PCR on WT, *Rssc* mutants ($\Delta epsB$, $\Delta hrpB$ and $\Delta hrcV$) and a water control (H₂O). Numbers on the right indicate the fragment lengths of a molecular weight DNA marker (M). Fragment sizes are given in kilobases. (C) Infection phenotypes caused by *Rssc* WT and depicted mutant strains on tomato cultivar Moneymaker. Three-week-old tomato plants were root-cut inoculated with WT GMI1000 and the depicted mutant strains. Wilting symptoms were recorded daily after inoculation. The photograph shown here includes one representative plant from each strain-infected plant group at 7 days post-inoculation. (D) Infection phenotypes caused by blunt-end syringe infiltration of *Rssc* WT and displayed mutant strains into *Nicotiana tabaccum* cv. Bottom Special. The bacterial suspension of the depicted strains was adjusted to an optical density at 600 nm (OD_{600}) = 0.1 and infiltrated into *N. tabaccum* leaves. Photographs were taken at 2 days post-inoculation. (E) *Rssc* WT and $\Delta epsB$ mutant strains display distinct colony morphology when grown on agar plates. Symbols as explained in Fig. 1. *Gent*, Gentamycin.

integration of desired expression cassettes into the GMI1000 permissive site 203336/7. In addition, the GG-based cloning scheme can be easily adapted to generate an LIII integration vector for any other desired site in any *Rssc* strain's genome.

Establishment of LI modules for GG-based assembly of expression cassettes to be used in *Rssc* strains

In a previously established GG-based toolkit for the construction of expression vectors (plant-GG-kit), multi-cassette constructs are

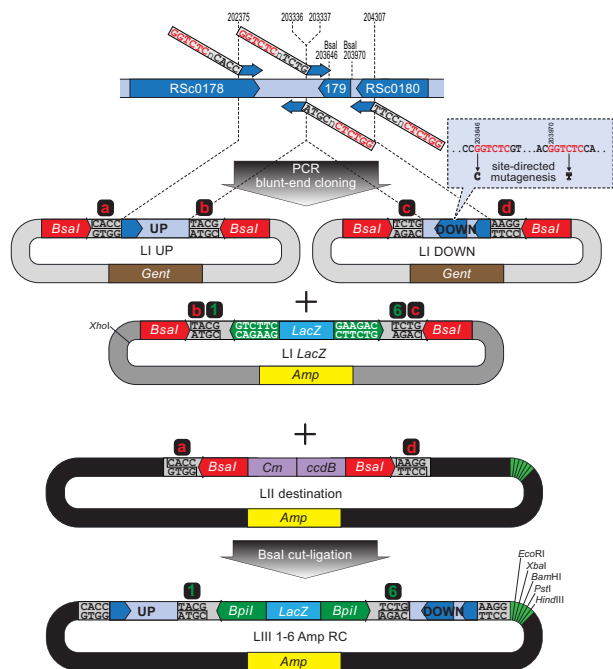


Fig. 3 Golden-Gate (GG)-based assembly of a destination vector for chromosomal insertions into the *Ralstonia solanacearum* species complex (*Rssc*) reference strain GMI1000. Genomic regions up- (UP) and downstream (DOWN) of the intergenic target site in GMI1000 (nucleotide position: 203336/7) are polymerase chain reaction (PCR) amplified. Primers (angled bars) contain *Bsal* recognition sites (red type) in their 5' termini and defined bases in the downstream *Bsal* cleavage sites (bold black type) that facilitate subsequent GG-based transfer. Two *Bsal* recognition sites present in the DOWN segment (203646-51 and 203970-5) are indicated. These *Bsal* recognition sites were removed by PCR mutagenesis on the cloned level I DOWN fragment as indicated (box framed with broken line). A *Bsal* cut-ligation mediates fusion of the up- and downstream regions (UP, DOWN) to a *LacZ* reporter gene and cloning into the transfer vector backbone (LI destination; black backbone). The ligation product (LI 1-6 Amp RC) contains a β -galactosidase (*LacZ*) gene which facilitates the integration of the desired gene constructs via *Bpil* cut-ligation in conjunction with blue-white selection. *Bsal* and *Bpil* recognition sites are indicated with red and green arrows, respectively, with the tip pointing towards their cleavage sites. Four-base-pair overlaps generated by *Bsal* and *Bpil* cleavage are, for simplicity, designated by lowercase red letters and green digits in black boxes, respectively. Note that, because of the arrangement of *Bsal* and *Bpil* recognition sites in LI *LacZ*, both enzymes will produce the same four-base-pair overhang. Accordingly, this overhang is designated with a red letter and a green digit. *Gent*, Gentamycin; *Amp*, Ampicillin; *Cm*, Chloramphenicol; *ccdB*, gyrase-specific toxin.

assembled by fusion of up to six LI modules (Binder *et al.*, 2014). Distinct LI modules are joined by compatible four-base-pair overhangs generated by *Bsal* cleavage. For simplicity, the four-base-pair overhangs present at the termini of these distinct LI modules are designated with upper case letters A–G (Fig. 4). The six-module design is intended to join promoter (LI A-B), N-terminal epitope tag (LI B-C), GOI (LI C-D), C-terminal tag (LI D-E), transcriptional terminator (LI E-F) and a selection marker (LI F-G). The previously established toolbox (Binder *et al.*, 2014) contained

LI modules that were intended for application in a plant context. To establish a similar toolkit for the genetic modification of *Rssc* strains, we constructed a series of new LI modules (Table S2). We first added to our *Ralstonia* GG-toolbox a set of promoters that were cloned as LI A-B modules. The *Rssc eps* promoter shows strong expression and has been widely used for overexpression studies (Monteiro *et al.*, 2012). The *hrpB* and *Gala7* promoters are T3S-associated *Rssc* promoters which have been used to drive the expression of bacterial effector genes (Cunnac *et al.*, 2004; Lohou *et al.*, 2014). We also cloned the *Tfd* terminator from phage fd (Kokotek and Lotz, 1989) as an LI E-F module which has been used previously in the context of the *Rssc* (Monteiro *et al.*, 2012). To provide flexibility with respect to the selection marker, all commonly used antibiotic resistance genes, including gentamycin, kanamycin, spectinomycin, tetracycline and chloramphenicol, were cloned together with the promoter and terminator as selection marker (LI F-G) modules. As our toolbox was designed to be

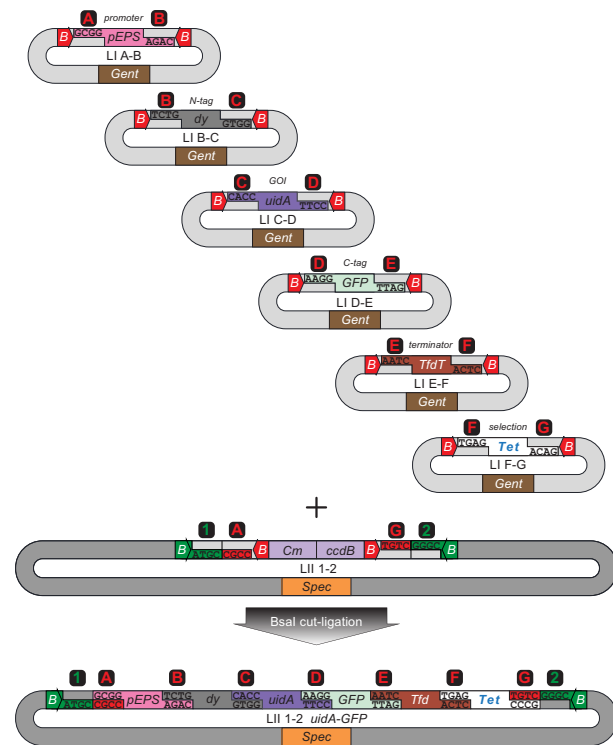


Fig. 4 Golden-Gate (GG)-based assembly of a multi-cassette expression construct for insertion into the GMI1000 genome. LI modules are assembled into an LII module by *Bsal* cut-ligation. For simplicity, compatible four-base-pair overhangs are denoted by identical red upper-case letters. Up to six level I modules can be merged into one LII module. If less than six modules are required, empty dummy (dy) modules provide the overhangs required to seal the gaps. The assembled LII module is transferred by *Bpil* cut-ligation into an LIII module (Fig. 5). Symbols as explained in Fig. 1. *Gent*, Gentamycin resistance; *GFP*, Green fluorescent Protein; *tet*, tetracyclin resistance; *pEPS*, *eps* Promoter; *tfdT*, *tfd* Terminator; *uidA*, β -glucuronidase (GUS) reporter; *spec*, spectinomycin resistance; *ccdB*, gyrase-specific toxin.

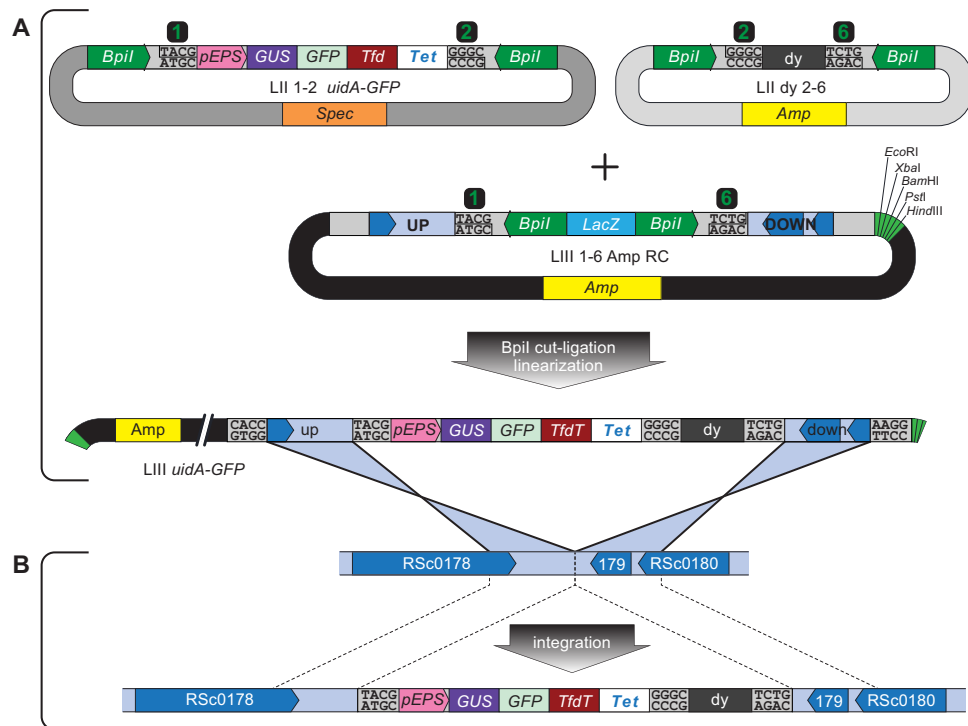


Fig. 5 Homology-based integration of a multi-cassette fragment into the reference strain GMI1000. (A) The desired construct to be integrated (e.g. LII 1–2 *GUS-GFP*, see Fig. 4 for details on assembly) contains a given gene [e.g. *uidA-GFP* (translational fusion)] driven by a constitutive promoter (*pEPS*) and is fused to a transcriptional terminator (*TfdT*). The gene construct also contains a tetracycline selection marker (*Tet*). LII 1–2 *uidA-GFP* is transferred, together with a dummy (*dy*) fragment, which generates the required overhangs for the transfer of LII 1–2 *GUS-GFP* into LIII 1–6 Amp RC. Up to five different LII modules can be integrated via *Bpil* cut-ligation into LIII 1–6 Amp RC (see Binder *et al.*, 2014). (B) The gene insertion vector (LIII *uidA-GFP*) is linearized with a suitable restriction enzyme, transfected into the *Ralstonia solanacearum* species complex (*Rssc*) strain, integrated by homologous recombination and selected for resistance to tetracycline. The gene insertion can be validated by polymerase chain reaction (PCR) (see Fig. 6). Green arrows indicate *Bpil* recognition sites with the tip pointing towards the cleavage site. Otherwise, the symbols are as explained in Fig. 1. Gent, Gentamycin resistance; GFP, Green fluorescent Protein; tet, tetracycline resistance; pEPS, eps Promoter; tfdT, tfd Terminator; *uidA*, β -glucuronidase (*GUS*) reporter; spec, spectinomycin resistance; *GUS*, β -glucuronidase; *ccdB*, gyrase-specific toxin.

compatible with LI modules of the previously established GG-based toolkit for application in plants (Binder *et al.*, 2014), we can make use of the established epitope tags [e.g. green fluorescent protein (GFP), yellow fluorescent protein (YFP), mCherry, haemagglutinin (HA) and myc] that are available as both N-terminal tag (LI B-C) and C-terminal tag (LI D-E) modules (Table S2). In addition to these epitope tags, we cloned the V5 epitope tag as an LI B-C (N-terminal tag) and LI D-E (C-terminal tag) module. Furthermore, the *uidA* gene, encoding a β -glucuronidase (*GUS*) reporter, was cloned as an LI C-D module. Basic information on all newly generated LI modules and previously established LI modules (Binder *et al.*, 2014) that are applicable in the context of *Rssc* is summarized in Tables S2 and S3 (see Supporting Information).

GG-based assembly of a *uidA-GFP* expression cassette for use in *Rssc* strains

To demonstrate the functionality of GG-assembled expression modules, we first focused on the construction of an expression

cassette containing the *uidA* gene. The *uidA* reporter gene was chosen as an *Rssc* strain expressing this reporter is easily traceable in infected tomato plants (Kumar *et al.*, 2016). The expression construct was generated by fusing an *eps* promoter (LI A-B), the *uidA* CDS (LI C-D), the GFP CDS (LI D-E), a *Tfd* terminator (LI E-F) and a tetracycline resistance gene (LI F-G) via *Bsal* cut-ligation into an LII destination vector (Fig. 4). As we omitted an N-terminal tag module (LI B-C), an LI B-C dummy (*dy*) module was added to the *Bsal* cut-ligation to bridge the gap between LI A-B (*epsB* promoter) and LI C-D (*uidA* CDS) modules. In the resulting plasmid (LII 1–2 *uidA-GFP*), the expression cassette is flanked by *Bpil* sites facilitating its transfer via *Bpil* cut-ligation. For simplicity, *Bpil*-generated overhangs present in distinct LII modules are designated with green digits (1–6) in black boxes.

LIII_1–6-Amp_RC, which contains a central cloning site flanked by two genomic segments for recombination-based integration of expression cassettes into *Rssc* strain genomes, has been designed for the integration of up to five distinct LII modules (Fig. 5A). Integration of less than five LII modules

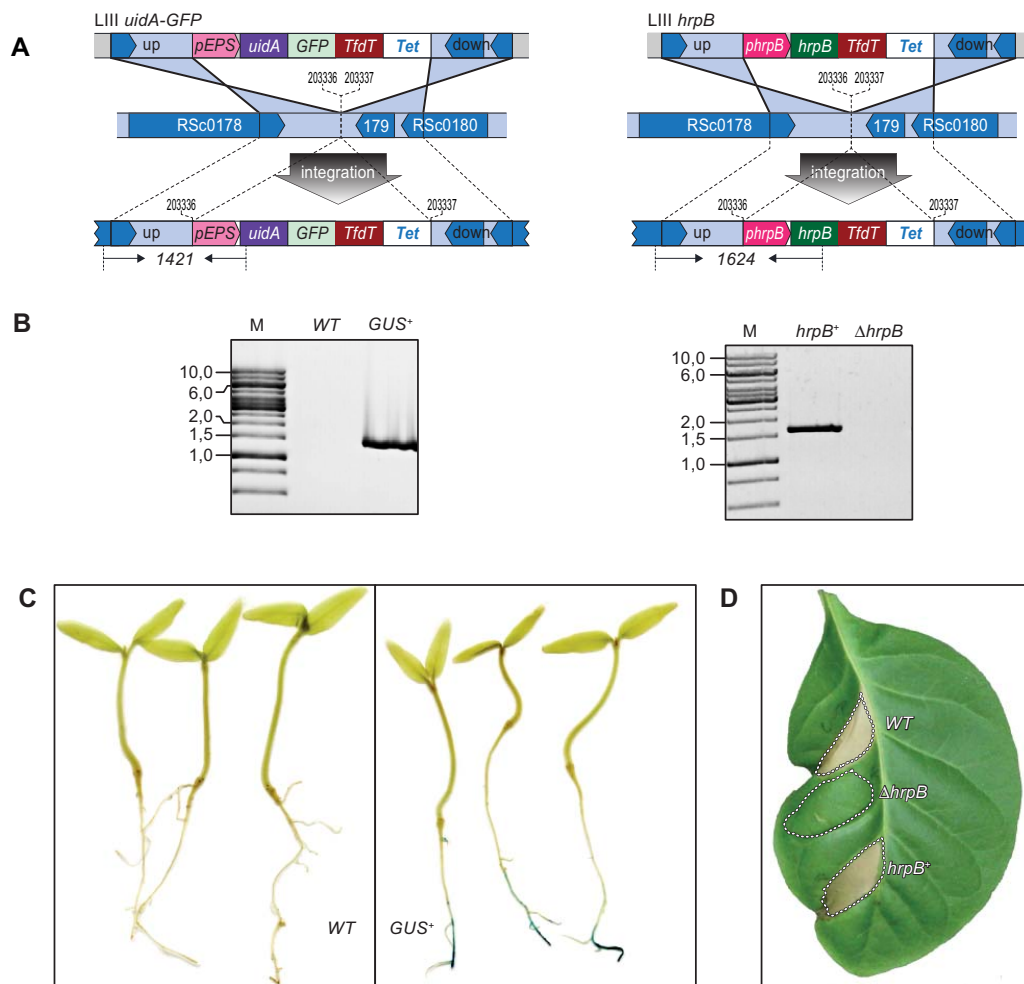


Fig. 6 Chromosomal integration of Golden-Gate (GG)-generated gene constructs into *Ralstonia solanacearum* species complex (*Rsc*) reference strain GMI1000. (A) Graphical display of the integration of a *GUS-GFP* transgene into the wild-type *Rsc* strain (left) and the *hrpB* gene into the $\Delta hrpB$ mutant strain (right). The amplified region and the expected size of diagnostic polymerase chain reaction (PCR) fragments are indicated at the bottom in italic type. (B) Diagnostic PCR on wild-type (WT), a *GUS-GFP*-complemented *Rsc* wild-type strain (*GUS-GFP*⁺) and a complemented mutant strain (*hrpB*⁺). (C) β -Glucuronidase (GUS) staining of tomato seedlings infected with an *Rsc* *GUS-GFP* strain shows blue staining of the vasculature. (D) Integration of the GG-generated *hrpB* transgene into the *hrpB* mutant strain complements its capability to trigger cell death in *Nicotiana tabacum* cv. Bottom Special. Symbols as explained in Fig. 1. Gent, Gentamycin resistance; GFP, Green fluorescent Protein; tet, tetracycline resistance; pEPS, eps Promoter; tfdT, tfd Terminator; uidA: β -glucuronidase (GUS) reporter; spec, spectinomycin resistance; GUS, β -glucuronidase; ccdB, gyrase-specific toxin.

into LIII_1–6-Amp_RC requires the use of dummy modules which have been established previously (Binder *et al.*, 2014). For example, integration of LII 1–2 into LIII_1–6-Amp_RC required the dummy module LII dy 2–6 (Fig. 5A; Table S3). The resulting LIII vector (LIII *uidA-GFP*) contains the expression cassette flanked by the two genomic regions required for integration at a predefined permissive site in the GMI1000 genome. The assembled integration vector LIII *uidA-GFP* was linearized by *Xba*I cleavage, transformed into GMI1000 and transformants were selected on agar plates containing tetracycline (Fig. 5B).

Analysis of the *Rsc* strain containing the *uidA-GFP* expression cassette confirms the functionality of the expression construct

We carried out diagnostic PCR on colonies that grew on tetracycline-containing agar plates and thus probably contain the cassette with the *uidA* gene. The chosen diagnostic PCR primers bind upstream of the predefined integration site and within the *uidA* CDS (Fig. 6A). Thus, PCR with these primers is expected to yield an amplification product only if the expression cassette is integrated into the predefined genomic target. PCR analysis indeed generated a fragment of the expected size only in the

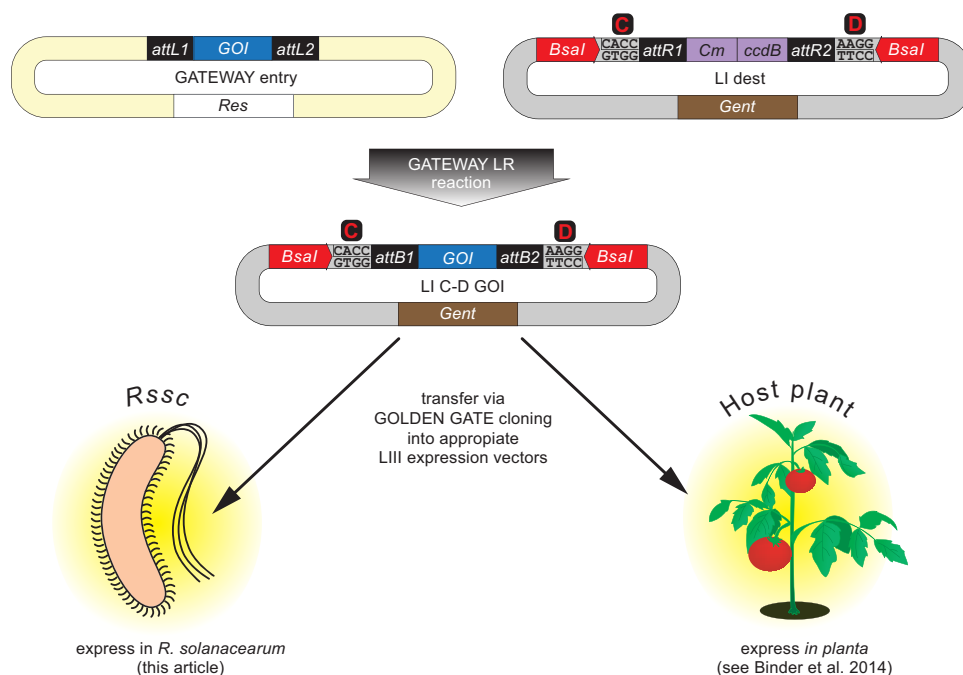


Fig. 7 A conversion vector allows simple implementation of GATEWAY entry vectors into Golden-Gate (GG)-compatible LI modules. *attL1*, *attL2*, *attR1*, *attR2*, *attB1* and *attB2* are interconvertible GATEWAY recombination sites. All other symbols are as explained in Fig. 1. *Rssc*, *Ralstonia solanacearum* species complex. GOI, gene of interest; Cm, chloramphenicol resistance gene; *ccdB*, gyrase-specific toxin; Gent, Gentamycin resistance gene; LI, Level I.

transformed *Rssc* strain, but not in the wild-type strain, suggesting that, in the studied strain, the expression cassette indeed integrated at the desired position (Fig. 6B). To validate the functionality of the *uidA* gene, we infected tomato seedlings with the *uidA*-containing strain and the wild-type *Rssc* strain. Infection with the *uidA*-containing strain caused a strong blue staining of tomato roots (Fig. 6C). By contrast, inoculation with the wild-type strain did not cause blue staining in infected tomato roots. These data demonstrate that the *uidA* gene is expressed and functional in the tested strain. Moreover, these data show that the newly generated LI modules used in the expression construct (e.g. *eps* promoter, *Tfd* terminator and tetracycline resistance) and the proposed GG-based pipeline for the generation of integration vectors are functional.

Complementation of a GMI1000 *hrpB* mutant strain

Once we had demonstrated that the GG-based integration vectors could be used to transfer expression cassettes into the *Rssc* wild-type strain, we wanted to test whether the same strategy could be applied to complement *Rssc* mutant strains. For this purpose, we intended to complement the newly generated mutant strain $\Delta hrpB$ (Fig. 2). To do so, we fused LI modules containing the *hrpB* promoter, the *hrpB* CDS, the *Tfd* terminator and a tetracycline resistance marker via *Bsal* and subsequent *BpiI* cut-ligation into the integration vector LIII 1–6 Amp RC, resulting in LIII *hrpB* (Fig. 6A). The integration vector LIII *hrpB* was linearized with *XbaI*, transformed into the mutant strain $\Delta hrpB$ and putative transformants were selected on agar plates containing gentamycin and tetracycline. A diagnostic PCR with primers upstream of the

integration site and inside the *hrpB* CDS produced a fragment of the expected size only in the complemented mutant strain (*hrpB*⁺), but not in the mutant strain $\Delta hrpB$, suggesting that the *hrpB* expression cassette had been integrated at the predestined site (Fig. 6B). To validate the functionality of the expression cassette, we inoculated tobacco leaves with $\Delta hrpB$, the complemented mutant strain *hrpB*⁺ and the *Rssc* wild-type strain GMI1000. An HR was observed on infection with the wild-type and the complemented mutant strain *hrpB*⁺, but not with the $\Delta hrpB$ mutant (Fig. 6D). These findings demonstrate that GG-based integration vectors can be used to complement *Rssc* mutant strains.

A conversion vector facilitates the rapid implementation of GATEWAY entry vectors into the GG-based toolkit for the *Rssc*

Before the advent of GG-based cloning, recombination-based GATEWAY cloning was a major breakthrough for the streamlining of cloning procedures. In GATEWAY cloning, the given GOI is first cloned into a so-called GATEWAY entry clone in which the GOI is flanked by *attL1* and *attL2* sites. Corresponding expression vectors are generated via GATEWAY L/R recombination of the GOI from the entry vector into a destination vector. The resulting expression clones contain *attB1* and *attB2* sites flanking the GOI. In the past, scientists have devoted substantial efforts towards the generation of GATEWAY entry clones that could be easily transferred into any desired destination vector. A GATEWAY-based toolkit has also been established for *Rssc* (Monteiro *et al.*, 2012). Given that much effort has been devoted to the generation of such

GATEWAY entry clones, we decided to design a GATEWAY to GG conversion vector (designated as GW-to-GG_LI) that allows the implementation of GATEWAY entry clones into our GG-based cloning concept. The newly generated conversion vector contains an *attR* GATEWAY cassette that is flanked by *Bsal* recognition sites. A GATEWAY LR reaction of a given GATEWAY entry clone with GW-to-GG_LI results in a GOI flanked by *attB* and *Bsal* sites (Fig. 7). *Bsal* cleavage of such vectors results in the generation of C- and D-type sticky overhangs and, accordingly, such vectors can be used in *Bsal* cut-ligation (Fig. 5). In summary, the conversion vector GW-to-GG_LI facilitates streamlined implementation of GATEWAY entry vectors into GG-assembled expression cassettes.

DISCUSSION

We have designed, generated and functionally validated a GG-based toolkit for the genetic modification of the *Rssc*. The *Ralstonia*-GG-kit extends the molecular tools available for the genetic modification of the *Rssc* by providing a simple, standardized GG-based cloning strategy for the generation of gene knockout constructs, as well as for the assembly of multi-cassette expression constructs. Conceptually, the *Ralstonia*-GG-kit is based on a previously established GG-based toolkit for the generation of expression constructs to be used *in planta* (plant-GG-kit) (Binder *et al.*, 2014). The modular assembly of expression constructs relies, in both toolkits, on identical four-base-pair overhangs for promoter, epitope tag, GOI and transcriptional-terminator modules. The use of identical overlaps for functionally equivalent modules facilitates the shared use of N- and C-terminal epitope tags for expression in a plant and *Rssc* context. Furthermore, it allows that one GOI can be studied in a plant and *Rssc* context. This is relevant for the genetic analysis of *Rssc* effector genes which are known to be injected into plant host cells. For example, the very same GOI (LI C-D) module encoding an *Rssc* effector protein can be fused to promoters suitable for expression in *Rssc* or to a plant-specific promoter, using modules of the *Ralstonia*- and plant-GG-kit, respectively. The *Ralstonia*-GG-kit also includes a conversion vector (GW-to-GG_LI) that allows the implementation of GATEWAY entry clones (Fig. 7). In summary, the design of the newly established *Ralstonia*-GG-kit allows the implementation of modules from the previously established plant-GG-kit, as well as the implementation of GATEWAY entry modules.

In our GG-based toolkit, we used *Bsal* for the assembly of gene knockout constructs (Figs 1 and 2) and a combination of *Bsal* and *BpI* for the generation of expression cassettes (Figs 3–6). Hence, the sequences to be assembled must be devoid of corresponding recognition sites, which seems, at first glance, to be a substantial constraint of the GG-based approach. Yet, in our experience, appropriate design of the cloning strategy typically overcomes these constraints. For example, in the generation of gene knockout constructs, the choice of suitable 5' and 3' regions

is rather flexible and thus, in most cases, it is possible to select genomic regions that are devoid of *Bsal* recognition sites. If genomic regions containing *Bsal* sites cannot be omitted, site-directed mutagenesis can be used to mutate individual bases within recognition sites. We carried out site-directed mutagenesis of the LI DOWN module as the chosen region of the GMI1000 genome contains two *Bsal* recognition sites that would interfere with subsequent cut-ligations (Fig. 3). Integration of the two point mutations had no obvious detrimental impact on homology-based integration and showed the feasibility of this approach.

If desired fragments are large and contain several *Bsal/BpI* recognition sites, conventional PCR-based mutagenesis can be challenging. In such cases, we advise users of our toolkit to make use of a previously developed GG-based PCR mutagenesis protocol (Engler *et al.*, 2008). In this approach, chosen primers cover *Bsal/BpI* recognition sites, but contain single nucleotide mismatches that eliminate recognition sites in the PCR product. *Bsal* or *BpI* sites at the far end of the PCR products allow subsequent fusion of the mutagenized segments via cut-ligation.

A previously published toolkit for the generation of expression constructs to be integrated into *Rssc* genomes is based on GATEWAY technology (Monteiro *et al.*, 2012), and has significantly simplified the generation and integration of expression constructs. However, this toolkit is tailored towards use in GMI1000 (*Rssc* phylotype I) and phylotype II, but cannot be readily extended to other phylotypes lacking this particular insertion site. The toolkit presented here enables genetic studies beyond phylotypes I and II of the *Rssc* once a permissive site has been identified in the genome. In our view, the truly modular nature of GG-cloning also offers a far greater level of combinatorial flexibility in the generation of expression constructs. Another important aspect is that GATEWAY cloning relies on expensive proprietary enzyme mixes. By contrast, type II enzymes required for GG-cloning can be purchased from various commercial manufacturers and, accordingly, the prices are competitive. Given that the amount of cloning reactions that are typically carried out in a laboratory has drastically increased over time, the costs of single reactions are an important part of laboratory management.

In summary, the *Ralstonia*-GG-kit provides a valuable new resource to the scientific community. It offers the possibility to generate highly complex expression cassettes for integration into the genomes of *Rssc* members.

EXPERIMENTAL PROCEDURES

Bacterial strains and growth conditions

The *Rssc* strains used in this study are listed in Table S4 (see Supporting Information). *Rssc* strains were grown in Peptone, 10 g/L; Tryptone, 1 g/L; Yeast extract, 1 g/L (B broth), Peptone, 10 g/L; Tryptone, 1 g/L; Yeast extract, 1 g/L; Glucose 5 g/L; Agar, 15 g/L; Triphenyl Tetrazolium Chloride,

20 mg/L (BGT agar plate) or minimal medium (MM) at 28 °C. *Escherichia coli* top 10 and DB3.1 were used for cloning and were grown in Luria–Bertani (LB) medium at 37 °C. When needed, antibiotics were added to the medium in the following concentrations: ampicillin, 50 µg/mL; gentamycin, 15 µg/mL; kanamycin, 50 µg/mL; spectinomycin, 100 µg/mL; tetracycline, 10 µg/mL; chloramphenicol, 100 µg/mL.

Molecular biology techniques and reagents

PCR amplifications were performed with Phusion Polymerase [New England Biolabs (NEB), Frankfurt am Main, Germany] in a 20-µL reaction mixture containing 4 µL of GC buffer (NEB), 2 µL of 2 mM deoxynucleoside triphosphates (dNTPs) and 1 pmol of each primer. For PCR mutagenesis, the additive PreCES-I (Ralsler *et al.*, 2006) was used. The primers used for PCR and mutagenesis are listed in Table S1. PCR products were analysed by agarose gel electrophoresis and then purified with the GeneJET PCR Purification Kit or GeneJET Gel Extraction Kit (Thermo Scientific, Darmstadt, Germany). Plasmids were extracted with the GeneJET Plasmid Miniprep Kit according to the manufacturer's instructions (Thermo Scientific). *Bsa*I was purchased from NEB. *Bpi*I, *Sma*I, T4 ligase and other routine enzymes were purchased from Thermo Scientific.

Cut-ligation reaction

*Sma*I cut-ligation was used for blunt-end cloning of PCR products into pUC57 Gent. Reactions were performed in a 20-µL volume containing equal amount of vector and PCR fragment, 1 µL of restriction enzyme *Sma*I, 1 µL of T4 DNA ligase and 2 µL of ligase buffer. The mixture was then incubated in a thermocycler with the following program: 30 °C for 2 min, 20 °C for 5 min, 20 cycles, 30 °C for 5 min, 50 °C for 5 min and 80 °C for 5 min. Five microlitres of the reaction mixture were transformed into *E. coli* top 10 competent cells by heat shock and transferred to LB plates supplemented with gentamycin, 5-bromo-4-chloro-3-indolyl-β-D-galactopyranoside (X-Gal) (40 µg/mL) and Isopropyl β-D-1-thiogalactopyranoside (IPTG) (100 µM). White colonies were used for plasmid extraction and sequencing validation. For *Bpi*I and *Bsa*I cut-ligations, 1 µL of each plasmid, 1 µL of *Bpi*I or *Bsa*I, 1 µL of T4 DNA ligase and 2 µL of ligase buffer were used in a 20-µL reaction volume. The mixture was incubated in a thermocycler with the following program: 37 °C for 2 min, 20 °C for 5 min, 40 cycles, 37 °C for 5 min, 50 °C for 5 min and 80 °C for 5 min. Five microlitres of the reaction mixture were transformed into *E. coli* top 10 competent cells by heat shock and transferred to LB plates supplemented with appropriate antibiotics. Positive cloning events were confirmed by enzyme digestion and sequencing.

Rssc transformation

Gene knockout and complementation constructs were transformed into *Rssc* strains as described previously (Monteiro *et al.*, 2012). Briefly, a single colony was grown in MM supplemented with 2% glycerol to reach an optical density at 600 nm (OD₆₀₀) of 0.2 to 0.3. One hundred microlitres of bacterial suspension were mixed with 2 µg of linearized plasmid DNA. The mixture was applied to a 0.45-µm cellulose nitrate membrane placed on a BGT agar plate and incubated at 28 °C for 1–2 days. Bacteria were collected and plated on BGT medium supplemented with appropriate

antibiotics to select for positive transformants. Genetic modifications were confirmed by PCR.

Plant inoculation assay

Tomato plants (cultivar MoneyMaker) were initially grown at 28 °C in a 16-h/8-h day/night cycle and moved to S2 infection chambers 1 day before inoculation. Three-week-old plants were root cut and inoculated by pouring 6 mL of OD₆₀₀ = 0.05 bacterial suspension into the soil. The disease symptoms of each plant were checked daily until all the infected wild-type plants had wilted. Fifteen plants were used for each strain in one independent experiment and the assay was repeated twice. Pathogenicity was also evaluated by leaf infiltration. Leaves of 24-day-old tobacco (cultivar Bottom Special) plants were syringe infiltrated with OD₆₀₀ = 0.1 bacterial suspension. HR was recorded at 24 and 48 h post-inoculation. To trace the *eps* promoter activity *in planta* with the GUS reporter strain, tomato seeds were sown on phytoagar plates, incubated in the dark for 3 days and then grown under normal light conditions for another 2 days. Small seedlings were root cut and inoculated with a drop (5 µL) of OD₆₀₀ = 0.1 bacterial suspension. Roots of inoculated seedlings were used for blue staining at 3 days post-inoculation.

GUS staining

GUS staining was performed as described previously (Strauß *et al.*, 2012). Briefly, whole seedlings were inoculated with a strain containing the *eps* promoter:GUS reporter or a wild-type strain. Inoculated plants were sampled, vacuum infiltrated with the GUS staining solution and incubated at 37 °C for 24 h. Samples were then incubated in 70% ethanol for 2 days to remove any background and fixed with formaldehyde before imaging.

ACKNOWLEDGEMENTS

We would like to thank P. Ricca and M. Epple for the generation of some LI and LII elements. We are grateful to O. de Lange, C. Krönauer and K. Schenstnyi for helpful comments on an earlier version of the manuscript. We also thank S. Genin and N. Peeters for providing the *Rssc* strain GMI1000 and plasmid pNP351, M. Valls for providing some pRC vectors and C. Allen for providing tobacco seeds. This work was supported by funds from the Deutsche Forschungsgemeinschaft (DFG) to T.L. (LA1338/6-1). N.S. also received funding through the institutional strategy of the University of Tübingen (DFG ZUK63).

REFERENCES

- Ailloud, F., Lowe, T., Cellier, G., Roche, D., Allen, C. and Prior, P. (2015) Comparative genomic analysis of *Ralstonia solanacearum* reveals candidate genes for host specificity. *BMC Genomics*, **16**, 270.
- Binder, A., Lambert, J., Morbitzer, R., Popp, C., Ott, T., Lahaye, T. and Parniske, M. (2014) A modular plasmid assembly kit for multigene expression, gene silencing and silencing rescue in plants. *PLoS One*, **9**, e88218.
- Bertolla, F., Van Gijsegem, F., Nesme, X. and Simonet, P. (1997) Conditions for natural transformation of *Ralstonia solanacearum*. *Appl. Environ. Microbiol.* **63**, 4965–4968.
- Cruz, A.P.Z., Ferreira, V., Pianzola, M.J., Siri, M.I., Coll, N.S. and Valls, M. (2014) A novel, sensitive method to evaluate potato germplasm for bacterial wilt resistance using a luminescent *Ralstonia solanacearum* reporter strain. *Mol. Plant–Microbe Interact.* **27**, 277–285.
- Cunnac, S., Boucher, C. and Genin, S. (2004) Characterization of the cis-acting regulatory element controlling HrpB-mediated activation of the type III secretion system and effector genes in *Ralstonia solanacearum*. *J. Bacteriol.* **186**, 2309–2318.

- Dalsing, B.L. and Allen, C. (2014) Nitrate assimilation contributes to *Ralstonia solanacearum* root attachment, stem colonization, and virulence. *J. Bacteriol.* **196**, 949–960.
- Deslandes, L. and Genin, S. (2014) Opening the *Ralstonia solanacearum* type III effector tool box: insights into host cell subversion mechanisms. *Curr. Opin. Plant Biol.* **20**, 110–117.
- Engler, C., Kandzia, R. and Marillonnet, S. (2008) A one pot, one step, precision cloning method with high throughput capability. *PLoS One*, **3**, e3647.
- Genin, S. and Denny, T.P. (2012) Pathogenomics of the *Ralstonia solanacearum* species complex. *Annu. Rev. Phytopathol.* **50**, 67–89.
- Jacobs, J.M., Babujee, L., Meng, F., Milling, A. and Allen, C. (2012) The *in planta* transcriptome of *Ralstonia solanacearum*: conserved physiological and virulence strategies during bacterial wilt of tomato. *mBio*, **3**, e00114–12.
- Jacobs, J.M., Milling, A., Mitra, R.M., Hogan, C.S., Ailloud, F., Prior, P. and Allen, C. (2013) *Ralstonia solanacearum* requires PopS, an ancient AvrE-family effector, for virulence and to overcome salicylic acid-mediated defenses during tomato pathogenesis. *mBio*, **4**, e00875–13.
- Kelman, A. (1954) The relationship of pathogenicity in *Pseudomonas solanacearum* to colony appearance on a tetrazolium medium. *Phytopathology*, **44**, 693–695.
- Kokotek, W. and Lotz, W. (1989) Construction of a *LacZ*-kanamycin-resistance cassette, useful for site-directed mutagenesis and as a promoter probe. *Gene*, **84**, 467–471.
- Kumar, R., Barman, A., Phukan, T., Kabyashree, K., Singh, N., Jha, G., Sonti, R.V., Genin, S. and Ray, S.K. (2016) *Ralstonia solanacearum* virulence in tomato seedlings inoculated by leaf clipping. *Plant Pathol.* **66**, 835–841.
- Lohou, D., Turner, M., Lonjon, F., Cazalé, A.C., Peeters, N., Genin, S. and Vailleau, F. (2014) HpaP modulates type III effector secretion in *Ralstonia solanacearum* and harbors a substrate specificity switch domain essential for virulence. *Mol. Plant Pathol.* **15**, 601–614.
- Macho, A.P., Guidot, A., Barberis, P., Beuzon, C.R. and Genin, S. (2010) A competitive index assay identifies several *Ralstonia solanacearum* type III effector mutant strains with reduced fitness in host plants. *Mol. Plant–Microbe Interact.* **23**, 1197–1205.
- Milling, A., Babujee, L. and Allen, C. (2011) *Ralstonia solanacearum* extracellular polysaccharide is a specific elicitor of defense responses in wilt-resistant tomato plants. *PLoS One*, **6**, e15853.
- Monteiro, F., Sole, M., van Dijk, I. and Valls, M. (2012) A chromosomal insertion toolbox for promoter probing, mutant complementation, and pathogenicity studies in *Ralstonia solanacearum*. *Mol. Plant–Microbe Interact.* **25**, 557–568.
- Peeters, N., Carrere, S., Anisimova, M., Plener, L., Cazale, A.C. and Genin, S. (2013) Repertoire, unified nomenclature and evolution of the type III effector gene set in the *Ralstonia solanacearum* species complex. *BMC Genomics*, **14**, 859.
- Prior, P. and Fegan, M. (2005) Recent developments in the phylogeny and classification of *Ralstonia solanacearum*. In: *Proceedings of the 1st International Symposium on Tomato Diseases* (Allen, C., Prior, P. and Hayward, C., eds), pp. 127–136. American Phytopathological Society: Minnesota, USA.
- Prior, P., Ailloud, F., Dalsing, B.L., Remenant, B., Sanchez, B. and Allen, C. (2016) Genomic and proteomic evidence supporting the division of the plant pathogen *Ralstonia solanacearum* into three species. *BMC Genomics*, **17**, 90.
- Ralsler, M., Querfurth, R., Warnatz, H.J., Lehrach, H., Yaspo, M.L. and Krobitsch, S. (2006) An efficient and economic enhancer mix for PCR. *Biochem. Biophys. Res. Commun.* **347**, 747–751.
- Safni, I., Cleenwerck, I., De Vos, P., Fegan, M., Sly, L. and Kappler, U. (2014) Polyphasic taxonomic revision of the *Ralstonia solanacearum* species complex: proposal to emend the descriptions of *Ralstonia solanacearum* and *Ralstonia syzygii* and reclassify current *R. syzygii* strains as *Ralstonia syzygii* subsp. *syzygii* subsp. *nov.*, *R. solanacearum* phylotype IV strains as *Ralstonia syzygii* subsp. *indonesiensis* subsp. *nov.*, banana blood disease bacterium strains as *Ralstonia syzygii* subsp. *celebesensis* subsp. *nov.* and *R. solanacearum* phylotype I and III strains as *Ralstonia pseudosolanacearum* sp. *nov.* *Int. J. Syst. Evol. Microbiol.* **64**, 3087–3103.
- Strauß, T., Van Poecke, R., Strauß, A., Romer, P., Minsavage, G.V., Singh, S., Wolf, C., Strauß, A., Kim, S., Lee, H.-A., Yeom, S.-I., Parniske, M., Stall, R.E., Jones, J.B., Choi, D., Prins, M. and Lahaye, T. (2012) RNA-seq pinpoints a *Xanthomonas* TAL-effector activated resistance gene in a large crop genome. *Proc. Natl. Acad. Sci. USA*, **109**, 19 480–19 485.
- Vasse, J., Genin, S., Frey, P., Boucher, C. and Brito, B. (2000) The *hrpB* and *hrpG* regulatory genes of *Ralstonia solanacearum* are required for different stages of the tomato root infection process. *Mol. Plant–Microbe Interact.* **13**, 259–267.

SUPPORTING INFORMATION

Additional Supporting Information may be found in the online version of this article at the publisher's website:

Table S1 Primers used in this study.

Table S2 LI modules.

Table S3 Backbone vectors and dummy elements.

Table S4 *Ralstonia solanacearum* species complex (*Rssc*) strains used in this study.

4 Metabolomics of tomato xylem sap during bacterial wilt reveals *Ralstonia solanacearum* produces abundant putrescine, a metabolite that accelerates wilt disease

This chapter is identical to the publication:

M. Lowe-Power, Tiffany, G. Hendrich, Connor, von Roepenack-Lahaye, Edda, Li, Bin, Wu, Dousheng, Mitra, Raka, L. Dalsing, Beth, Ricca, Patrizia, Naidoo, Jacinth, Cook, David, Jancewicz, Amy, Masson, Patrick, Thomma, Bart, Lahaye, Thomas, J. Michael, Anthony & Allen, Caitilyn

Metabolomics of tomato xylem sap during bacterial wilt reveals *Ralstonia solanacearum* produces abundant putrescine, a metabolite that accelerates wilt disease

Environmental Microbiology (2018) 20(4): 1330–1349

Metabolomics of tomato xylem sap during bacterial wilt reveals *Ralstonia solanacearum* produces abundant putrescine, a metabolite that accelerates wilt disease

Tiffany M. Lowe-Power,¹ Connor G. Hendrich,¹ Edda von Roepenack-Lahaye,² Bin Li,³ Dousheng Wu,² Raka Mitra,⁴ Beth L. Dalsing,¹ Patrizia Ricca,² Jacinth Naidoo,⁵ David Cook,^{6†} Amy Jancewicz,⁷ Patrick Masson,⁷ Bart Thomma,⁶ Thomas Lahaye,² Anthony J. Michael³ and Caitilyn Allen^{1*}

¹Department of Plant Pathology, University of Wisconsin – Madison, Madison, WI 53706, USA.

²Leibniz Institute of Plant Biochemistry, Zentrum für Molekularbiologie der Pflanzen (ZMBP), Universität Tübingen, Tübingen, Germany.

³Department of Pharmacology, University of Texas Southwestern Medical Center, Dallas, TX 75390, USA.

⁴Department of Biology, Carleton College, Northfield, MN 55057, USA.

⁵Department of Biochemistry, University of Texas Southwestern Medical Center, Dallas, TX 75390, USA.

⁶Laboratory of Phytopathology, Wageningen University, Wageningen, The Netherlands.

⁷Department of Genetics, University of Wisconsin, Madison, Madison, WI 53706, USA.

Summary

***Ralstonia solanacearum* thrives in plant xylem vessels and causes bacterial wilt disease despite the low nutrient content of xylem sap. We found that *R. solanacearum* manipulates its host to increase nutrients in tomato xylem sap, enabling it to grow better in sap from infected plants than in sap from healthy plants. Untargeted GC/MS metabolomics identified 22 metabolites enriched in *R. solanacearum*-infected sap. Eight of these could serve as sole carbon or nitrogen sources for *R. solanacearum*. Putrescine, a**

polyamine that is not a sole carbon or nitrogen source for *R. solanacearum*, was enriched 76-fold to 37 μM in *R. solanacearum*-infected sap. *R. solanacearum* synthesized putrescine via a SpeC ornithine decarboxylase. A ΔspeC mutant required $\geq 15 \mu\text{M}$ exogenous putrescine to grow and could not grow alone in xylem even when plants were treated with putrescine. However, co-inoculation with wildtype rescued ΔspeC growth, indicating *R. solanacearum* produced and exported putrescine to xylem sap. Intriguingly, treating plants with putrescine before inoculation accelerated wilt symptom development and *R. solanacearum* growth and systemic spread. Xylem putrescine concentration was unchanged in putrescine-treated plants, so the exogenous putrescine likely accelerated disease indirectly by affecting host physiology. These results indicate that putrescine is a pathogen-produced virulence metabolite.

Introduction

Crop pathogens threaten global food security. Among these is *Ralstonia solanacearum*, which causes bacterial wilt, a high impact plant disease that disrupts the host vascular system. *R. solanacearum* is globally distributed, infects an expanding host range of over 450 plant species, and is not effectively managed in the field (Elphinstone, 2005). Bacterial wilt inflicts large losses on economically important crops such as tomato, potato and banana.

R. solanacearum is a soil-borne pathogen that locates its plant hosts by sensing and chemotaxing toward root exudates (Tans-Kersten *et al.*, 2001; Yao and Allen, 2006). *R. solanacearum* evades root defenses such as nucleic acid extracellular traps (NETs), and enters roots through wounds or natural openings (Vasse *et al.*, 1995; Tran *et al.*, 2016a). The bacterium then systemically colonizes root and stem xylem, a network of metabolically inert tubes that transport water and minerals up from plant roots. In xylem, *R. solanacearum* forms dense biofilms that restrict sap flow and wilt plants (Vasse *et al.*, 1998; Tran *et al.*, 2016b).

Received 2 August, 2017; revised 29 November, 2017; accepted 3 December, 2017. *For correspondence. E-mail callen@wisc.edu; Tel. (608) 262-9578; Fax (608) 263-2626. †Present address: Department of Plant Pathology, Kansas State University, Manhattan, KS 66506, USA

R. solanacearum deploys virulence factors such as plant cell wall degrading enzymes, type 3 secreted effectors and extracellular polysaccharide (Genin and Denny, 2012; Deslandes and Genin, 2014). However, *R. solanacearum* virulence factors have additive effects, and no single factor completely explains bacterial wilt virulence.

The ability of *R. solanacearum* to flourish inside the plant xylem is poorly understood. Xylem sap is nutrient poor (Fatima and Senthil-Kumar, 2015); most plant carbon is sequestered intracellularly and transported in the phloem. Metabolites are 10- to 100-fold less concentrated in xylem sap than in the phloem or leaf apoplast (Fatima and Senthil-Kumar, 2015; O'Leary *et al.*, 2016). Xylem is also hypoxic, posing further metabolic constraints for *R. solanacearum* growth (Dalsing *et al.*, 2015). Nonetheless, the bacterium grows to high cell densities in this niche (Tans-Kersten *et al.*, 2004). One possible explanation for this paradox is that *R. solanacearum* may alter its xylem habitat by increasing the available nutrients, and/or altering physical or chemical conditions that limit bacterial growth and spread. Microbial pathogens are known to produce metabolites that manipulate and damage their hosts. For example, the plant pathogens *Pseudomonas syringae* and *Sclerotinia sclerotiorum*, respectively, produce coronatine and oxalate to subvert host plant immunity (Melotto *et al.*, 2006; Kabbage *et al.*, 2015). Human dental pathogens degrade tooth enamel with lactate waste, and trimethylamine produced by choline-utilizing gut bacteria promotes heart disease (Sansone *et al.*, 1993; Romano *et al.*, 2015). Little is known about *R. solanacearum* metabolites that harm its plant hosts.

To understand how *R. solanacearum* thrives in the xylem, we used untargeted metabolomics to compare global changes in xylem sap chemistry during bacterial wilt disease of tomato. We found sap from infected plants was enriched in several nutrients that improved *R. solanacearum* growth in sap. Unexpectedly, our metabolomics analysis also revealed high levels of the polyamine putrescine in sap of wilting plants. *R. solanacearum* produced the putrescine in xylem sap, but infection also induced expression of several plant putrescine biosynthesis genes in a type 3 secretion system-dependent manner. Furthermore, treating plants with putrescine accelerated bacterial wilt disease progress. Together these results indicate that this polyamine is a virulence metabolite.

Results

Bacterial wilt disease alters tomato xylem sap to favour R. solanacearum growth

We collected xylem sap from healthy tomato plants and *R. solanacearum*-infected plants that had developed wilt symptoms within the previous 16 h (Fig. 1A). Unless otherwise noted, hereafter *R. solanacearum* refers to strain

GMI1000. Even at this early stage of disease, sap exudation rate was 1.4-fold slower than in healthy plants, consistent with the model that bacterial wilt disease occludes xylem flow (Supporting Information Fig. S1). We filter-sterilized this *ex vivo* xylem sap from healthy and infected plants and measured growth of *R. solanacearum* in these media. Although at this disease stage sap nutrients are continuously depleted by the 10⁹ actively growing *R. solanacearum* cells in each gram of tomato stem, the sap from two different *R. solanacearum*-infected tomato cultivars supported more *R. solanacearum* growth than sap from healthy plants (Fig. 1B). This was true under both aerobic and microaerobic conditions, and five of seven phylogenetically diverse *R. solanacearum* strains grew better in sap from plants infected by *R. solanacearum* strain GMI1000 (Supporting Information Fig. S2). We tested the possibility that healthy sap contained concentrated chemicals or defense proteins that inhibited *R. solanacearum* growth, but supplementing minimal media (MM) with sap from healthy plants improved *R. solanacearum* growth (Fig. 1C). This suggested that sap from *R. solanacearum*-infected plants was enriched in nutrients rather than depleted in growth inhibitors. Nonetheless, *R. solanacearum* growth plateaued by 6 h in the *ex vivo* sap (Fig. 1B) while the bacterium grows exponentially *in planta* for over 72 h.

To identify the nutrients that are enriched in xylem sap of *R. solanacearum*-infected tomato plants, we used untargeted metabolomics to compare the chemical composition of sap from healthy and newly symptomatic *R. solanacearum*-infected plants. The results revealed that bacterial wilt disease changes the chemical composition of tomato xylem sap (Fig. 1D and E and Supporting Information Fig. S3A). GC-MS analysis of sap detected 136 metabolites unmatched to reference database compounds and 118 known compounds, including some previously identified in tomato xylem sap (Dixon and Pegg, 1972; Coplin Sequeira *et al.*, 1974; Zuluaga *et al.*, 2013) (Supporting Information Dataset S1). Overall, nutrients in sap from infected plants were more concentrated; the sap was enriched in 22 known and 17 unknown compounds and depleted in only 1 known and 3 unknown compounds (Fig. 1E). To understand how *R. solanacearum* grew better in sap from infected plants, we determined which of the altered metabolites served as nutrients (Fig. 1E and Supporting Information Fig. S4). *R. solanacearum* grew on trehalose, 3-hydroxybutyrate, alanine, gluconate, β -alanine, galactonate and mannitol as sole carbon sources, and on alanine, glycine and β -alanine as sole nitrogen sources. Galactose, the sole compound depleted in infected sap, also supported growth.

To identify xylem sap metabolites preferentially depleted by *R. solanacearum*, we analyzed *ex vivo* sap following 3 h incubation with either *R. solanacearum* or water

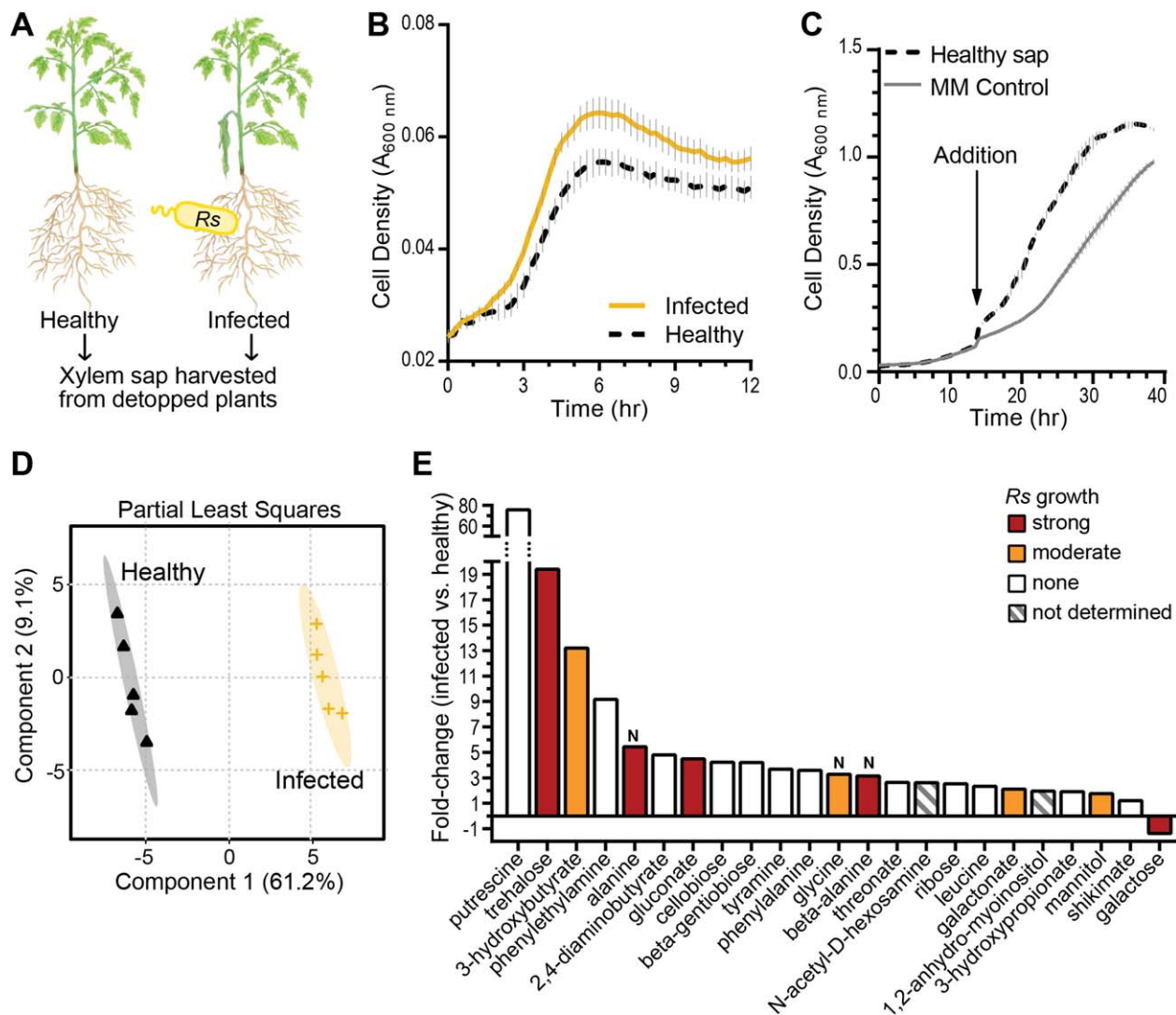


Fig. 1. Bacterial wilt disease changes biological and chemical properties of tomato xylem sap.

A. 'Bonny Best' tomato plants were soil-soak inoculated with *R. solanacearum* GMI1000. At wilt onset, xylem sap was harvested from infected and healthy plants.

B. Growth of *R. solanacearum* in filtered sap from *R. solanacearum*-infected and healthy plants. Data are mean \pm SEM ($n = 3$).

C. Xylem sap from healthy plants improves *R. solanacearum* growth in minimal medium (MM). Vacuum-concentrated sap from healthy plants was added to 1x final concentration to actively growing *R. solanacearum* cultures. Fresh MM was added to the control (AUC = 13.2 ± 0.087). Data are mean \pm SEM ($n = 3$). Area under the curve (AUC) for sap treatment (20.4 ± 0.098) and control treatment (13.2 ± 0.087) were significantly different ($P < 0.001$, t -test). (D, E) Relative chemical composition of xylem sap from healthy and *R. solanacearum*-infected plants was determined by untargeted GC-MS metabolomics ($n = 5$ pools of sap from 4 plants each).

D. Partial least squares analysis of metabolomics data. Shaded areas indicate 95% confidence regions ($n = 5$).

E. Xylem sap metabolites altered by bacterial wilt disease, fold-change relative to sap from healthy plants (t -test FDR < 0.1); bar colors indicate *R. solanacearum* growth on each metabolite as sole carbon or nitrogen ('N') source. Strong and moderate growth are defined in Materials and Methods.

(Fig. 2, Supporting Information Fig. S3B and Dataset S1). *R. solanacearum* growth depleted five compounds: 3-hydroxybutyrate, glucose, pipecolate, gluconate and proline (Fig. 2C). All depleted compounds supported *R. solanacearum* growth except pipecolate (Supporting Information Fig. S5). Together these experiments supported the hypothesis that *R. solanacearum* infection increases available nutrients in plant xylem sap.

R. solanacearum produces putrescine in tomato xylem sap and alters tomato polyamine biosynthesis

Not all enriched compounds were nutrients for the bacterium. *R. solanacearum* could not use the polyamine putrescine as a sole carbon or nitrogen source (Supporting Information Fig. S4), although putrescine was enriched 76-fold in xylem sap from *R. solanacearum*-infected plants (Fig. 1E). Consistent with this result, the *R. solanacearum*

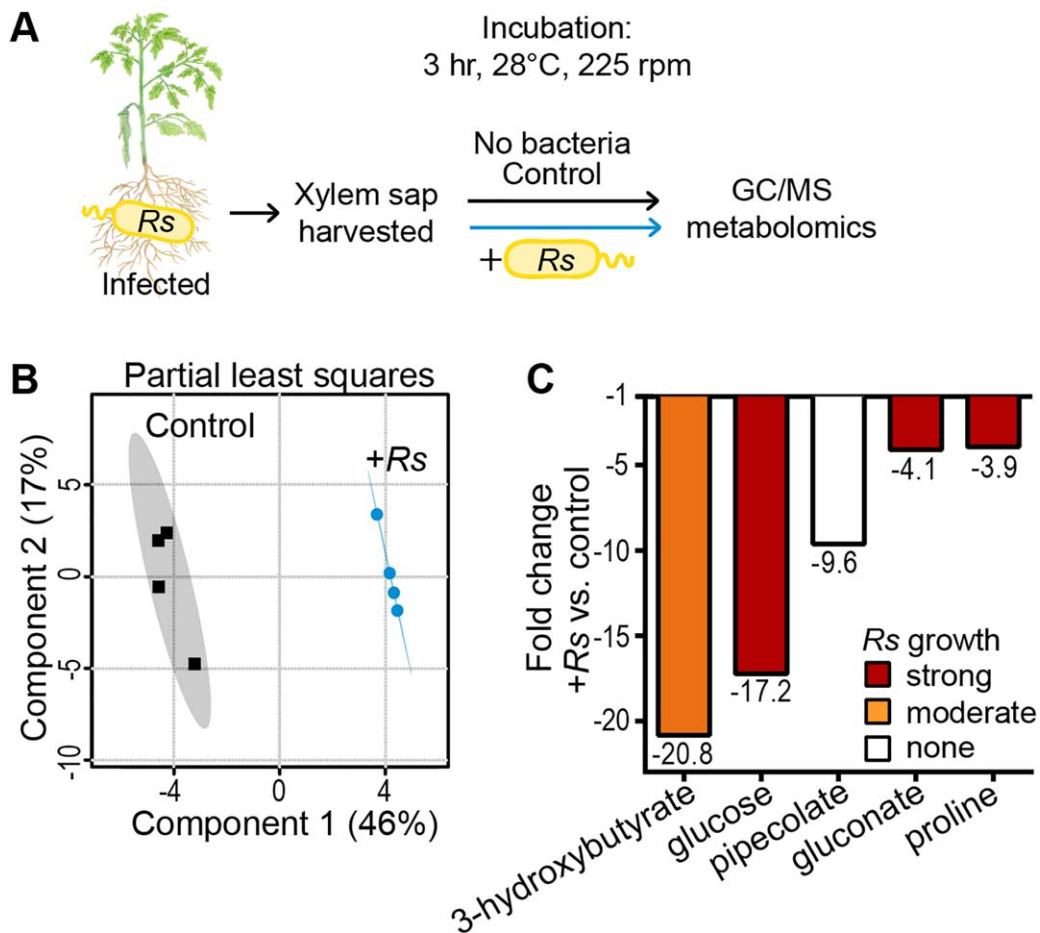


Fig. 2. Xylem sap metabolites consumed during *R. solanacearum* GMI1000 growth.

A. Sap was harvested from infected tomato plants at wilt onset. Pooled sap was incubated with *R. solanacearum* or water for 3 h before GC-MS metabolomic analysis ($n = 4$ pools of 7 plants each).

B. Partial least squares analysis of sap composition metabolomic data. Shaded areas indicate 95% confidence region.

C. Xylem metabolites altered by *R. solanacearum* growth, fold-change relative to sap incubated without *R. solanacearum* (t -test, $FDR < 0.1$) Bar color shows *R. solanacearum* growth on each metabolite as sole carbon or nitrogen ('N') source.

genome lacks homologs of the characterized putrescine catabolism pathways (Samsonova *et al.*, 2003; Kurihara *et al.*, 2005).

Plants accumulate putrescine and other polyamines during drought (Gupta *et al.*, 2016). Because drought stress and bacterial wilt disease both cause wilting, we investigated whether other wilt pathogens also triggered putrescine accumulation. We quantified putrescine in sap from healthy tomato plants and symptomatic plants inoculated with two *R. solanacearum* strains and a tomato wilt fungus, *Verticillium dahliae* (Fig. 3). In sap from healthy plants, putrescine concentration was near the limit of detection ($\sim 1 \mu\text{M}$), but infection with *R. solanacearum* GMI1000 increased sap putrescine levels to $36.9 \mu\text{M}$ after naturalistic soil-soak inoculation (Fig. 3A). Tomato plants inoculated with GMI1000 through a cut leaf petiole, an artificial inoculation method, accumulated less putrescine

(Fig. 4E). Infection with *R. solanacearum* CMR15 and *V. dahliae* modestly increased xylem sap putrescine (Fig. 3A and Supporting Information Fig. S6). Additionally, putrescine accumulated in culture medium of GMI1000 and CMR15 (Fig. 3B).

We first investigated whether *R. solanacearum* GMI1000 produces and exports putrescine in culture and in tomato xylem. Cell pellets of *R. solanacearum* grown in defined medium contained high levels of putrescine and 2-hydroxyputrescine, trace cadaverine levels and no detectable spermidine (Supporting Information Fig. S7). This suggested that *R. solanacearum* produces putrescine, which is consistent with previous findings (Busse and Auling, 1988). All sequenced *R. solanacearum* genomes encode a predicted putrescine synthesis pathway in which a putative arginine (Arg) decarboxylase (ADC, RSc2365) and an agmatinase (RSp1578) convert Arg to putrescine.

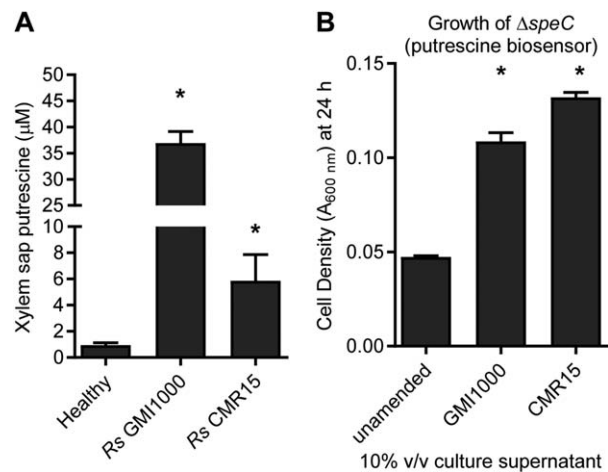


Fig. 3. *R. solanacearum* enriches putrescine in xylem sap and culture medium.

A. Xylem sap was harvested at symptom onset from tomato plants (cv. Money Maker) infected with *R. solanacearum* strains; water-inoculated plants served as controls. Putrescine was measured by LC-MS.

B. Putrescine in spent culture supernatant was detected by growth of the GMI1000 $\Delta speC$ mutant, a sensitive putrescine biosensor as shown in Fig. 4. *R. solanacearum* strains were grown in minimal medium (MM) for 24 h. Culture supernatants were filter-sterilized and added to fresh MM at 10% v/v and inoculated with $\Delta speC$. Growth of $\Delta speC$ mutant was measured at 24 h. Values are mean \pm SEM. (* $P < 0.05$ vs. healthy, t -test with Holm-Bonferroni correction, $n \geq 3$ pools).

However, deletion of RSp1578 did not affect putrescine levels (Supporting Information Fig. S8), showing this gene is not required for putrescine biosynthesis and implying the annotation was incorrect. The RSc2365 decarboxylase that was originally annotated as an ADC belongs to an aspartate aminotransferase-fold family that includes Arg decarboxylases (ADCs), lysine (Lys) decarboxylases, bifunctional Orn/Lys decarboxylases and ornithine (Orn) decarboxylases (ODCs) (Michael, 2016). ODC enzymes convert Orn to putrescine via decarboxylation. Purified RSc2365 protein had ODC activity but no detectable ADC activity. A substrate competition assay revealed that RSc2365 is a bifunctional Orn/Lys decarboxylase with a strong Orn preference (Supporting Information Fig. S7). Accordingly, we renamed RSc2365 'SpeC' like its ortholog, *E. coli* SpeC, an Orn/Lys decarboxylase with strong Orn preference (Michael, 2016). Expression of *speC* is constant in culture and tomato xylem (Jacobs *et al.*, 2012; Khokhani *et al.*, 2017).

To determine how much of the putrescine in xylem sap of infected plants was produced by *R. solanacearum*, we made an *R. solanacearum* $\Delta speC$ mutant. The $\Delta speC$ mutant was an auxotroph that could not grow without at least 15 μ M exogenous putrescine (Fig. 4A and B and Supporting Information Fig. S9), and its growth was poorly complemented by other polyamines (Supporting

Information Fig. S9). This suggests that putrescine is essential for *R. solanacearum* growth even though it cannot be used as a sole carbon or nitrogen source.

The putrescine auxotrophy of the $\Delta speC$ mutant made it a sensitive putrescine biosensor. LC-MS found that xylem sap of *R. solanacearum*-infected tomato plants contained 36.9 μ M putrescine at symptom onset (Fig. 3), so we hypothesized that if tomato plants produced the enriched xylem putrescine, the $\Delta speC$ mutant would be able to grow *in planta*. However, the $\Delta speC$ mutant did not grow after direct inoculation into the xylem (Fig. 4C and Supporting Information Fig. S9) and was avirulent even after 10^8 CFU were directly inoculated into plants (Fig. 4D). At the end of the virulence assay (14 dpi), the *speC* mutant could not be recovered from tomato stem (limit of detection: 500 CFU/g). The inability of the *speC* mutant to grow in tomato stem suggested that *R. solanacearum*, not the tomato plant, produced the putrescine in xylem sap of infected plants. Time-course quantification after cut-petiole inoculation showed that putrescine increased by 72 hpi when GMI1000 populations exceeded 10^9 CFU/g stem (Fig. 4E), whereas sap from healthy and $\Delta speC$ -infected plants contained no detectable putrescine (~ 1 μ M limit of detection). These results indicate that wildtype *R. solanacearum* secretes putrescine in culture and *in planta*.

Finally, we investigated whether *R. solanacearum* infection altered putrescine biosynthesis by the tomato plant host. Tomato produces putrescine via two pathways initiated by either ADCs (SI_ADC1–2) or ODCs (SI_ODC1–3; Supporting Information Fig. S10). ADCs and ODCs are rate-determining steps in plant polyamine biosynthesis, and higher ADC and ODC transcription is correlated with increased plant putrescine production (Jiménez-Bremont *et al.*, 2014). We measured expression of tomato polyamine biosynthesis genes in roots and stems following inoculation of unwounded roots. In tomato seedling roots, *SI_ADC1*, *SI_ODC1* and *SI_SAMDC2* were induced at 24 hpi (Supporting Information Table S1). In stems of symptomatic *R. solanacearum*-infected tomato plants, *SI_ADC1* expression increased by fourfold to fivefold and *SI_ODC3* expression decreased by 1.9-fold relative to healthy controls (Supporting Information Fig. S10B and S10D). To artificially synchronize bacterial wilt disease and track tomato polyamine biosynthesis gene expression over time, we used a cut-petiole inoculation. Under these conditions, *SI_ADC1* expression increased in stem tissue by 48 hpi, when the wildtype *R. solanacearum* population size exceeded 10^8 CFU/g stem (Supporting Information Fig. S10C–D). Although this induction of *SI_ADC1* coincided with the increase in xylem sap putrescine concentration in wildtype-infected plants (Supporting Information Fig. S10D and Fig. 4E), *SI_ADC1* was similarly induced in tomato stem tissue carrying an equal bacterial load of the $\Delta speC$ mutant (Supporting Information Fig. S10C and S10E).

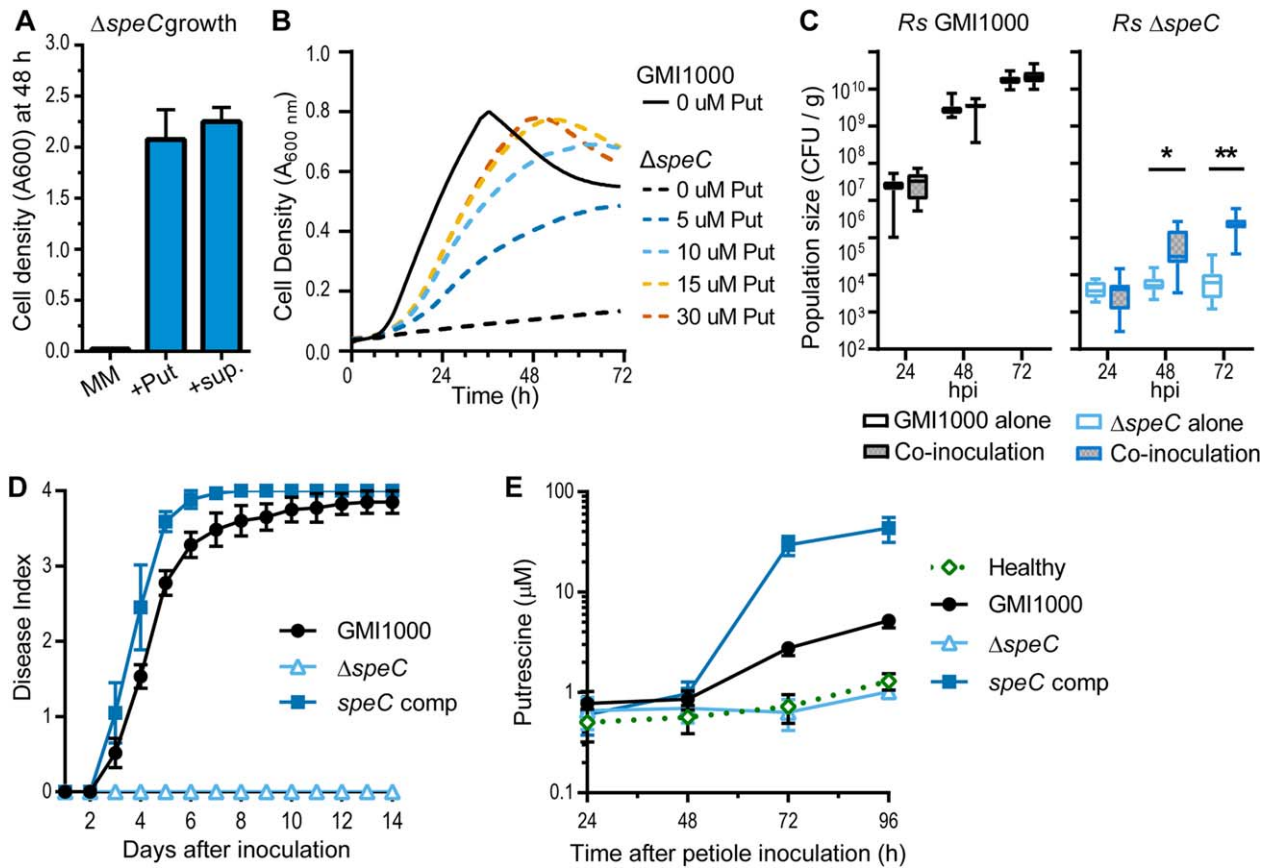


Fig. 4. *R. solanacearum* requires the SpeC ornithine decarboxylase to enrich putrescine in xylem.

A. Growth of the *R. solanacearum* Δ speC mutant in minimal medium (MM), MM plus 100 μ M putrescine (+Put), or MM plus 10% v/v filtered *R. solanacearum* GMI1000 culture supernatant (+sup). Values are mean \pm SEM. ($n=3$).

B. Growth of Δ speC mutant in MM with 0, 5, 10, 15 or 30 μ M putrescine indicates Δ speC mutant requires at least 15 μ M putrescine for maximal growth ($n=3$).

C. Population sizes of GMI1000-kan and the putrescine biosensor Δ speC mutant in tomato cv. Money Maker plants after stem inoculation with 10^3 CFU (alone) or co-inoculation with 10^3 CFU of each strain (* $P < 0.05$ or ** $P < 0.0001$ t -test, $n \geq 10$).

D. Virulence of the Δ speC mutant on tomato cv. Money Maker plants. Wilt index was measured daily following stem inoculation with 10^3 CFU (GMI1000 and complemented *speC* mutant) or 10^8 CFU (Δ speC mutant). Values are means \pm SEM ($n=45$).

E. Putrescine concentration in tomato xylem sap measured by LC-MS after stem inoculation with water (healthy), 10^3 CFU GMI1000, 10^3 CFU complemented Δ speC mutant, or 10^8 CFU Δ speC mutant. Values are mean \pm SEM ($n=3-6$).

Under this condition, putrescine does not accumulate in xylem sap (Fig. 4E). Intriguingly, *SL_ADC1* was not induced in tomato plants infected with a Δ hrcC mutant, which lacks type 3 secretion (Supporting Information Fig. S10E).

Exogenous putrescine accelerates bacterial wilt disease development

Polyamines have pleiotropic effects on plant physiology (Jiménez-Bremont *et al.*, 2014; Gupta *et al.*, 2016). To test the hypothesis that putrescine affects disease development, we treated tomato plant soil and leaves with 0.5 mM putrescine or water 3 h before stem inoculation with *R. solanacearum*. Putrescine treatment accelerated bacterial wilt disease on two susceptible tomato cultivars

(Fig. 5A and Supporting Information Fig. S11) although the concentration of putrescine in xylem sap did not increase (Supporting Information Fig. S11). Putrescine treatment also accelerated symptom development on quantitatively wilt-resistant tomato line H7996 inoculated with resistance-breaking *R. solanacearum* strain UW551 (Fig. 5B). However, putrescine did not break the resistance of H7996 to *R. solanacearum* GMI1000 (Supporting Information Fig. S11). Stomatal conductance and sap exudation rates were both reduced in symptomatic infected plants, but putrescine treatment did not affect these physiological behaviours (Supporting Information Figs S1 and S11).

Putrescine treatment accelerated wilt by increasing bacterial growth and spread in the xylem. At 6 dpi, *R. solanacearum* population sizes in putrescine-treated plants

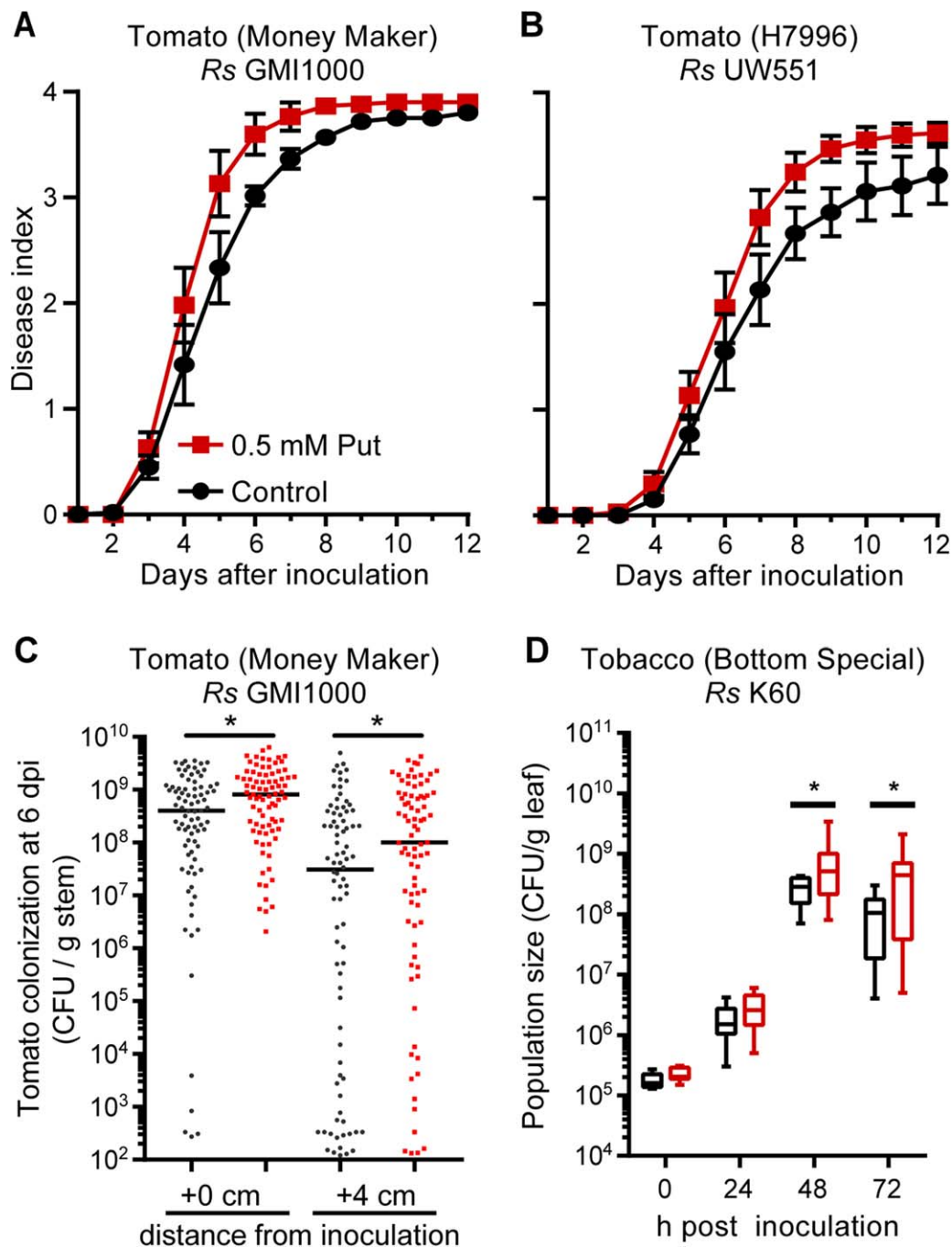


Fig. 5. Exogenous putrescine accelerated bacterial wilt disease.

Putrescine (0.5 mM in water) was applied to roots and leaves of plants 3 h before inoculation with *R. solanacearum* via (A–C) stem inoculation or (D) leaf infiltration. (A and B) Effect of putrescine on wilt symptom development after stem inoculation of (A) susceptible tomato with 50 CFU *R. solanacearum* GMI1000 ($P = 0.0183$, repeated measures ANOVA; values are mean \pm SEM; $n = 60$ plants/treatment) or (B) quantitatively resistant tomato with 5000 CFU *R. solanacearum* resistance-breaking strain UW551 ($P = 0.0403$, repeated measures ANOVA; values are mean \pm SEM; $n = 60$ plants/treatment). Effect of putrescine on *R. solanacearum* (C) growth and spread in tomato stem after stem inoculation of putrescine-treated (red) or control (black) plants, ($*P < 0.05$ Mann–Whitney test, $n > 80$ plants/treatment) and (D) growth in tobacco leaf apoplast after putrescine (red) or water (black) treatment ($*P < 0.05$ *t*-test; $n > 12$ plants/treatment).

were 3.8-fold larger at the site of inoculation and eightfold larger four cm above the inoculation site, as compared to control plants treated with water (Fig. 5C). Consistent with

the accelerated bacterial growth, putrescine treatment increased expression of tomato *PR1b* and *ACO5*, which are markers for the plant salicylic acid and ethylene

defense signaling pathways (Supporting Information Fig. S12). *PR1b* and *ACO5* are also induced by *R. solanacearum* infection (Milling *et al.*, 2011). Moreover, putrescine treatment of tobacco plants increased growth of tobacco pathogenic *R. solanacearum* strain K60 in leaf apoplast (Fig. 5D). Because treating plants with exogenous putrescine did not increase putrescine levels in xylem sap (Supporting Information Fig. S11), putrescine treatment must alter tomato physiology in a way that increases *R. solanacearum* growth in the xylem.

Discussion

Bacterial wilt disease increases xylem sap nutrients

Most previous characterizations of tomato xylem sap used healthy plants (Coplín Sequeira *et al.*, 1974; Chellemi *et al.*, 1998; Zuluaga *et al.*, 2013). It has long been known that xylem sap contains organic acids, amino acids and inorganic ions (nitrate, iron and sulfate), and sucrose was recently detected (Jacobs *et al.*, 2012; Dalsing *et al.*, 2015). The fungal wilt pathogen *V. albo-atrum* enriches amino acids in tomato xylem (Dixon and Pegg, 1972), but data on the effects of *R. solanacearum* infection on xylem sap are limited and inconsistent (Coplín Sequeira *et al.*, 1974; McGarvey *et al.*, 1999). Although differing methods make direct comparisons across studies difficult, these data, together with our observation that *R. solanacearum* grows better in *ex vivo* xylem sap from infected plants, strongly suggest that *R. solanacearum* infection significantly alters this key habitat in ways that favour the pathogen.

We found *R. solanacearum* grows better on xylem sap from infected plants than sap from healthy plants, probably because sap from diseased plants is enriched in at least three nitrogen and seven carbon sources. Although *R. solanacearum* can synthesize many of these nutrients, the rapid growth of the pathogen in xylem suggests they come from the host. Furthermore, the 22 enriched metabolites may not be the complete set of enriched metabolites because this list excludes metabolites *R. solanacearum* consumed at the same rate as they entered the xylem. Consistent with this idea, *R. solanacearum* depleted two nonenriched nutrients (glucose and proline) in *ex vivo* sap within 3 h.

Amino acids and other organic nitrogen compounds are likely important nitrogen sources for *R. solanacearum* in the xylem. Tomato xylem sap contains ~ 1 mM total amino acids and 40 mM nitrate (Dixon and Pegg, 1972; Zuluaga *et al.*, 2013; Dalsing *et al.*, 2015). In the oxygen-limited xylem, *R. solanacearum* uses nitrate primarily as an alternate electron acceptor (Dalsing *et al.*, 2015). Our study suggests the key nitrogen sources fueling bacterial growth in the xylem are alanine, β -alanine, glycine and proline.

We identified galactose, 3-hydroxybutyrate (3HB), gluconate and glucose as important carbon sources for *R. solanacearum* in the xylem. Galactose was the only xylem metabolite depleted by bacterial wilt disease. Interestingly, quorum sensing regulates *R. solanacearum* galactose catabolism such that galactose is only metabolized by *R. solanacearum* at high cell densities, corresponding to successful xylem colonization (Khokhani *et al.*, 2017). 3HB is precursor of the carbon storage molecule polyhydroxybutyrate (PHB), which bacteria often produce when carbon is in excess and redox is constrained (Terpolilli *et al.*, 2016). Microscopy and transcriptomic data suggest PHB metabolism is active when *R. solanacearum* grows in the xylem (Grimault *et al.*, 1994; Brown and Allen, 2004; Jacobs *et al.*, 2012). 3HB was both enriched in infected sap and depleted after *R. solanacearum* grew in *ex vivo* sap. *R. solanacearum* may produce and secrete 3HB to sequester carbon in a form unavailable to the host during early disease. Then, at a late disease stage, when glucose may be limited, *R. solanacearum* may import and polymerize 3HB into PHB to store carbon for survival outside the host. Although plant metabolism could theoretically account for the observed decrease in galactose, tomato plants are an unlikely source for the enriched 3-hydroxybutyrate because the tomato genome does not encode homologs of 3-hydroxybutyrate metabolism and are not known to carry out 3-hydroxybutyrate metabolism (Kanehisa and Goto, 2000).

Although the 1.6-fold glucose enrichment in sap from infected plants was nonsignificant, *R. solanacearum* preferentially consumed glucose in *ex vivo* sap. This suggests glucose is consumed by *R. solanacearum* at the same rate as it enters the xylem. Consistent with this idea, *R. solanacearum* glycolysis genes are highly expressed *in planta* (Brown and Allen, 2004; Jacobs *et al.*, 2012; Khokhani *et al.*, 2017). Our untargeted metabolomic analysis generated relative concentration data. Follow-up studies are needed to determine absolute quantities of nutrients in xylem sap from healthy and diseased plants and to quantify metabolic flux as *R. solanacearum* consumes xylem sap nutrients. These results could refine the existing metabolic model to provide a more biologically complete picture of *R. solanacearum* metabolism in the host (Peyraud *et al.*, 2016).

Xylem vessels are not static. Sap flows through vessels to transport water and minerals to foliar tissue. As in a chemostat, xylem sap continuously supplies nutrients to and removes waste from *R. solanacearum* biofilms. Furthermore, the xylem is a heterogeneous environment, so pooling xylem sap obscures aspects of its chemical ecology. Nutrients are likely more concentrated at the bordered pits that connect the inert xylem vessels to adjacent metabolically active cells, which is consistent with microscopy showing *R. solanacearum* cells clustered at pits (Grimault

et al., 1994; Nakaho et al., 2000). Bacterial consumption and metabolite diffusion within *R. solanacearum* biofilms likely creates a nutrient availability gradient that could support metabolically heterogeneous populations. This spatial heterogeneity could be defined with bacterial biosensors.

What mechanisms cause metabolite enrichment in xylem?

How might plants load nutrients like glucose into xylem during bacterial wilt disease? *R. solanacearum* cell wall-degrading enzymes release cellulose-derived metabolites like cellobiose and gentiobiose (Genin and Denny, 2012). Cellulases and pectinases are known bacterial wilt virulence factors, but their exact mechanisms of action are unknown (Genin and Denny, 2012). Cell wall breakdown could directly release sugars or facilitate leakage of metabolites into the xylem from adjacent tissue.

R. solanacearum may enrich host sap by subverting plant nutrient transport. For example, xylem embolisms formed during bacterial wilt disease could increase nutrients via phloem unloading. The intriguing but unproven phloem unloading hypothesis proposes that plants restore embolisms by moving phloem sugars into the xylem; this solute influx restores sap flow by drawing water into the vessel until the embolizing air is displaced or dissolved (Brodersen et al., 2010; Nardini et al., 2011). If plants use this mechanism to restore xylem function, it would be surprising if xylem pathogens did not manipulate it.

Finally, *R. solanacearum* may use its type 3 secretion system to manipulate the host to load nutrients into the xylem (Deslandes and Genin, 2014). Plant pathogenic *Xanthomonas* spp. use type 3 secreted transcriptional activator-like effectors (TALEs) that induce expression of host SWEET-family sucrose transporter genes (Streubel et al., 2013). These TALEs increase host susceptibility, presumably by raising sucrose levels. *R. solanacearum* GMI1000 has over 70 type 3 effectors, including a TALE that targets an unknown host gene (de Lange et al., 2013; Deslandes and Genin, 2014). It has long been assumed that *R. solanacearum* injects effectors into the living xylem parenchyma cells that are connected to vessels by bordered pits. Recent work confirmed this by visualizing delivery of an *R. solanacearum* effector (PopP2) into living *Arabidopsis* cells surrounding the xylem in petioles (Henry et al., 2017).

What is the source of the enriched putrescine during bacterial wilt disease?

The polyamine putrescine was strikingly enriched in xylem sap from tomato plants infected with *R. solanacearum*. Several lines of evidence indicate *R. solanacearum*

produced this putrescine: (1) Mutant and biochemical analyses showed *R. solanacearum* synthesizes putrescine via the SpeC ornithine decarboxylase; (2) LC-MS showed *R. solanacearum* exports putrescine; (3) Co-inoculation with wildtype *R. solanacearum* partially rescued *in planta* growth of a Δ speC mutant; (4) Plant putrescine synthesis could not rescue the Δ speC mutant's auxotrophy, even though *SI_ADC1* was induced by Δ speC infection.

R. solanacearum secretes putrescine, but the mechanism of putrescine export is unexplored. Because polyamines are positively charged at physiological pH, they require active transport across membranes. *R. solanacearum* has homologs of the PotABCD polyamine importer (Igarashi and Kashiwagi, 2010), which likely allowed exogenous putrescine to rescue Δ speC growth. The *R. solanacearum* genome does not encode homologs of known polyamine exporters (Igarashi and Kashiwagi, 2010; Sugiyama et al., 2016), suggesting *R. solanacearum* uses a novel transport system.

The Δ speC strain proved to be a sensitive putrescine biosensor. *In planta* growth of Δ speC increased by 48 hpi when co-inoculated with wildtype *R. solanacearum*, but LC-MS did not detect increased putrescine until 72 hpi. Δ speC cells nestled in biofilm with putrescine-exporting wildtype cells likely benefited from locally high putrescine levels that were diluted in exuded sap.

Our results raise compelling questions: (1) Do living plant cells import the *R. solanacearum*-produced putrescine? Putrescine uptake by plant cells or putrescine dilution by xylem flow could explain why we detected 10-fold less putrescine in sap of wildtype-infected plants than in culture supernatant containing similar bacterial populations. (2) Does *R. solanacearum* directly increase tomato putrescine synthesis? We observed that induction of *SI_ADC1* by *R. solanacearum* infection required a functional T3SS, which suggests that one or more *R. solanacearum* T3 effectors target host polyamine synthesis. This hypothesis is consistent with bioinformatic predictions that RipTAL-1 targets host genes involved in biosynthesis of polyamines (T. Lahaye, unpublished). Targeting host polyamine metabolism is a virulence strategy for *X. campestris* pv. *vesicatoria* (*Xcv*) and *Heterodera* cyst nematodes (Hewezi et al., 2010; Kim et al., 2013). Both pathogens deploy effectors that interact with plant polyamine biosynthesis enzymes: *Xcv* AvrBsT targets pepper ADC1 and *Heterodera* effector 10A06 increases activity of an *Arabidopsis* spermidine synthase (SPDS2). However the mechanism whereby polyamines promote virulence remains unclear for these pathosystems.

Why does putrescine accelerate bacterial wilt disease?

Polyamines influence virulence traits of many bacteria (reviewed in Di Martino et al., 2013). Polyamines are

essential for biofilm formation in *Yersinia pestis* and induce type 3 secretion gene expression and function in *Salmonella enterica* serovar Typhimurium and *Pseudomonas aeruginosa* (Patel *et al.*, 2006; Zhou *et al.*, 2007; Jelsbak *et al.*, 2012). Polyamines protect bacteria against many membrane stresses, including oxidative damage and cationic peptides like polymyxin B and the histones of neutrophil extracellular traps (NETs) (Goytia and Shafer, 2010; El-Halfawy and Valvano, 2014; Halverson *et al.*, 2015). Putrescine enrichment in xylem sap may affect *R. solanacearum* biofilm, type 3 secretion and resistance to host ROS. However, exogenous application of putrescine to roots and leaves accelerated bacterial wilt disease without detectably increasing putrescine concentration in xylem sap. This suggests that putrescine directly increases host plant susceptibility to *R. solanacearum*.

Putrescine and other polyamines play pivotal and pleiotropic roles in plant biology. Polyamines stabilize membranes, proteins and nucleic acids; regulate plant growth; moderate drought stress; and participate in varied interactions with microbes (Marina *et al.*, 2008; Hewezi *et al.*, 2010; Kim *et al.*, 2013; Jiménez-Bremont *et al.*, 2014; Gupta *et al.*, 2016). Polyamines sometimes benefit pathogens and sometimes boost plant immunity (Jiménez-Bremont *et al.*, 2014). It has been observed that 'In plant-pathogen interactions, the organism that takes control of polyamine metabolism has the advantage' (Jiménez-Bremont *et al.*, 2014). Although the specific roles of polyamines in plant-microbe interactions are uncertain, there are hints. When polyamines contribute to plant defense, it is often because their catabolism releases the plant defense signal H₂O₂ (Marina *et al.*, 2008; Jiménez-Bremont *et al.*, 2014; Gupta *et al.*, 2016). Although *R. solanacearum* induces putrescine catabolism in a resistant host (Aribaud *et al.*, 2010), we found that the activity of the putrescine catabolism enzyme diamine oxidase was 2.3-fold repressed in *R. solanacearum*-infected versus healthy tomato plants. Conversely, polyamines can also reduce H₂O₂ levels directly as antioxidants and indirectly by increasing host catalase activity (Gupta *et al.*, 2016). It would be interesting to determine if putrescine dampens the oxidative defense response of susceptible tomato plants (Milling *et al.*, 2011).

Why does *R. solanacearum* increase putrescine levels in host xylem?

Most free-living organisms make polyamines, usually putrescine and spermidine. Like other β -proteobacteria *R. solanacearum* produces putrescine and 2-hydroxyputrescine (Li *et al.*, 2016). *R. solanacearum* cell lysates lack spermidine, although the *R. solanacearum* GMI1000 genome encodes three spermidine synthase-like proteins that are not typical homologues of known

spermidine synthases (Michael, 2016). *R. solanacearum* is the first example of a bacterium that does not produce spermidine but absolutely requires putrescine (Hanfrey *et al.*, 2011; Kim *et al.*, 2016; Michael, 2016). *R. solanacearum* requires putrescine for growth, but our results suggest that *R. solanacearum*-produced putrescine also affects the plant host. There are precedents: for example, putrescine secreted by the eukaryotic pathogen *Trichomonas vaginalis* triggers host cell death (Garcia *et al.*, 2005).

Is putrescine a virulence metabolite?

Independent lines of evidence suggest the abundant *R. solanacearum*-produced putrescine increases bacterial wilt virulence. *R. solanacearum* manipulated expression of host putrescine biosynthetic genes via its type 3 secretion system, suggesting polyamine levels are important during bacterial wilt disease. Treating plants with exogenous putrescine accelerated bacterial wilt disease on three tomato genotypes, and exogenous putrescine increased bacterial spread and growth in tomato and tobacco plants responding to phylogenetically divergent *R. solanacearum* strains. *R. solanacearum* cannot use putrescine as either a sole carbon or nitrogen source, so putrescine does not improve the bacterium's growth directly by acting as a nutrient. We wondered if exogenous putrescine directly or indirectly upregulates twitching motility or biofilm formation, known *R. solanacearum* virulence factors that are responsive to polyamines in other bacteria (Patel *et al.*, 2006; Skiebe *et al.*, 2012; Di Martino *et al.*, 2013). However, exposing *R. solanacearum* to physiological levels of putrescine did not affect these traits *in vitro* (Supporting Information Fig. S11G). Further, it is unlikely that exogenous putrescine directly affected the xylem-dwelling *R. solanacearum* cells because putrescine treatment did not increase xylem sap putrescine levels, as indicated by both direct LC-MS measurements and by the sensitive Δ *speC* biosensor strain. We therefore favour the hypothesis that pathogen-produced putrescine contributes to virulence by acting on host plant physiology, possibly by reducing reactive oxygen species.

Experimental procedures

Bacterial and fungal strains and routine culturing conditions

Strains used in this study are listed in Supporting Information Table S2. *R. solanacearum* strains were grown at 28°C on CPG medium (1 g l⁻¹ casamino acids, 10 g l⁻¹ peptone, 5 g l⁻¹ glucose and 1 g l⁻¹ yeast extract). Antibiotics were added to media: 20 mg l⁻¹ spectinomycin, 5 mg l⁻¹ tetracycline and 25 mg l⁻¹ kanamycin. *E. coli* were grown on LB medium at 37°C. The Δ *speC* mutant was grown on CPG broth amended with 100 μ M putrescine or on solid CPG amended with 1 mM putrescine. Boucher's minimal medium (MM) pH 7.0

containing 20 mM glucose, 3.4 g l⁻¹ KH₂PO₄, 0.5 g l⁻¹ (NH₄)₂SO₄, 0.125 mg l⁻¹ FeSO₄·7H₂O and 62.3 mg l⁻¹ MgSO₄ was used for experiments requiring defined minimal medium. *Verticillium dahliae* JR2 was grown on potato dextrose agar.

R. solanacearum growth on metabolites present in xylem sap

To assess carbon and nitrogen source utilization, *R. solanacearum* GMI1000 was grown in MM with 10 mM test compounds. MM was prepared as described above without glucose for sole carbon source experiments or without (NH₄)₂SO₄ for sole nitrogen source experiments. Overnight cultures were washed and inoculated into 200 µl MM containing test substrates to a density of OD₆₀₀ = 0.05 in a 96-well flat-bottomed microplate (Corning). Kinetic growth data was collected in a Synergy HTX plate reader with shaking at 28°C and A_{600 nm} measurements recorded every 30 min for 72 h. Relative growth on the metabolites was determined by calculating the mean area under the growth curve (AUC) of three biological replicates. Carbon or nitrogen sources that yielded AUCs of >17, ≥4, or <4 were assigned into strong, moderate or no growth categories respectively. Generally, moderate and strong growth indicates *R. solanacearum* culture grew from A₆₀₀ = 0.03 to a maximum A_{600 nm} of 0.33–0.511 and 0.584–1.145 respectively.

Strain construction

Gene replacement and complementation constructs were created by Gibson assembly (Gibson *et al.*, 2009) (New England Biolabs, Ipswich, MA). The Δ *speC* mutant was created by allelic replacement of the *speC* gene (RSc2365) with the Ω cassette carrying a spectinomycin resistance marker. The 1077 bp region directly upstream of RSc2365, the Ω cassette from pCR8 and the 903 bp region directly downstream of RSc2365 were assembled into the *HindIII* site of pST-Blue. These PCR products were generated with primer sets RSc2365upF/R, omega(c2365)F/R and RSc2365dwnF/R respectively (Supporting Information Table S2). *R. solanacearum* GMI1000 was transformed with *SspI*-linearized pKO-*speC*::Sm by electroporation and transformants were selected with spectinomycin. After initial attempts to select for *speC* deletion were unsuccessful, we added 1 mM putrescine to selection medium, and obtained a Δ *speC* mutant that was confirmed by PCR genotyping. The *speC* complementation vector pRCT-*speC*_com was created by Gibson assembly. The 2.7 kb fragment containing the predicted native promoter and the monocistronic *speC* gene was amplified with the primers *speC*_comF/R (Supporting Information Table S2) and fused into the *XbaI/KpnI* site of pRCT-GWY (Monteiro *et al.*, 2012). *R. solanacearum* GMI1000 was transformed with pRCT-*speC*_com by electroporation, transformants were selected with tetracycline, and strains were confirmed by PCR screening.

The unmarked Δ *hrcC* mutant was produced using pUFR80-*hrcC*, a derivative of a *sacB* positive selection vector (Castaeda *et al.*, 2005). Regions upstream and downstream of the RSp0874 *hrcC* gene were amplified using *hrcC*upF/R and *hrcC*dwnF/R (Supporting Information Table S2). GMI1000 was transformed with pUFR80-*hrcC*, and plasmid integration

was selected with kanamycin medium. Plasmid loss was counter-selected from a Kan^R clone on 5% w/v sucrose, yielding a mixture of wildtype and Δ *hrcC* mutant genotype colonies. PCR screening identified a Δ *hrcC* mutant. The Δ *hrcC* mutant was phenotypically screened for absence of type 3 secretion activity using a tobacco hypersensitive response assay (Poueymiro *et al.*, 2009).

The unmarked Δ RSp1578 mutant was produced using pUFR80-RSp1578. The regions upstream and downstream of RSp1578 were amplified using 1578upF/R and 1578dwnF/R (Supporting Information Table S2). *R. solanacearum* GMI1000 was transformed with pUFR80-RSp1578, and Δ RSp1578 mutants were selected as described for the Δ *hrcC* mutant.

Characterizing growth requirements of Δ *speC* mutant

To determine which polyamines and structurally related molecules compensated for the putrescine auxotrophy of the Δ *speC* mutant, the mutant was grown in MM amended with test substrates. Some growth of the Δ *speC* mutant occurred in unamended MM if 100 µM putrescine was added to the parent overnight Δ *speC* cultures (Supporting Information Fig. S9). To deplete intracellular putrescine stores in Δ *speC* cells before growth experiments, subsequent experiments were conducted with Δ *speC* cells from overnight cultures in unamended CPG, which contains only trace polyamines that supported limited growth of the mutant. Overnight cultures were washed and resuspended to OD₆₀₀ = 0.05 in 200 µl MM amended with 0, 50, 100, 500 µM or 1 mM putrescine, spermidine, cadaverine or agmatine in a 96-well flat-bottomed microplate (Corning). Growth was recorded every 30 min as A₆₀₀ for 48 h in a Synergy HTX plate reader.

To determine whether diverse *R. solanacearum* isolates excreted putrescine to culture supernatant, strains were grown for 24 h in MM to OD₆₀₀ = 1.25. Bacteria were pelleted, and supernatant was sterilized through a 0.22 µm filter. Culture supernatant was added to MM at 10% v/v final concentration, and 5 ml aliquots were inoculated with Δ *speC* cells (OD₆₀₀ = 0.005) that had been putrescine-depleted as described above. Growth was compared to growth in unamended MM (negative control) and MM with 100 µM putrescine (positive control).

Plant growth conditions

Tomato seeds (wilt-susceptible cvs. Bonny Best and Money Maker, and quantitatively wilt-resistant breeding line Hawaii 7996) and tobacco cv. Bottom Special were sown in professional growing mix soil (Sunshine Redimix, Glendale, AZ) in a 28°C climate chamber with a 12 h photoperiod cycle. Tomato seedlings were transplanted 14 days postsowing into individual 4-inch pots containing ~80 g soil. Tobacco plants were transplanted after foliage diameter exceeded 1 cm. Transplants were watered with 50% Hoagland's solution.

Tomato and tobacco inoculation with *R. solanacearum*

Two methods were used to inoculate tomato plants: a naturalistic soil-soaking method and a stem inoculation method that directly introduces *R. solanacearum* into the xylem

(Tans-Kersten *et al.*, 2001). Plants were inoculated 17–21 days after sowing. For the soil soaking method, a suspension of *R. solanacearum* was poured into soil to a final concentration of 5×10^8 CFU g⁻¹ soil (50 ml of OD₆₀₀=0.2). For cut-petiole stem inoculations, 2 µl of a bacterial suspension was placed on the stump of a freshly removed leaf petiole. Inocula ranged from 5×10^1 to 1×10^8 total CFU depending on experiment and bacterial genotype. Tobacco plants were inoculated by leaf infiltration: a 10^5 CFU/ml water suspension of *R. solanacearum* K60 was infiltrated into fully expanded leaves with a needleless syringe. For co-inoculation experiments, kanamycin-marked GMI1000 and the spectinomycin-marked Δ *speC* mutant were introduced at equal concentration. Overnight cultures of each strain were resuspended to OD₆₀₀ of 0.2, mixed 1:1, and diluted to 5×10^5 CFU ml⁻¹ each of GMI1000 and Δ *speC* mutant to deliver 10^3 CFU of each strain (Yao and Allen, 2006). All inoculum concentrations were confirmed with dilution plating.

R. solanacearum disease and colonization assays

For disease assays, symptoms were measured daily using a 0–4 disease index scale (Tans-Kersten *et al.*, 2004): 0: asymptomatic; 1: up to 25% leaflets wilted; 2: up to 50% leaflets wilted; 3: up to 75% leaflets wilted; and 4: up to 100% leaflets wilted. Disease progress experiments were conducted at least three times with 10–15 plants per condition.

Bacterial population sizes *in planta* were determined by homogenizing 100 mg tomato stem or 1 cm² tobacco leaf (~33 mg) in a bead-based Powerlyzer homogenizer (Qiagen, Hilden, Germany). Samples were ground at room temperature in 1 ml sterile water with four 2.38 mm metal beads for two cycles of 2200 r.p.m. for 1.5 min with a 4 min rest between cycles. Homogenate was dilution plated in triplicate on appropriate media, and colonies were counted after 2 days incubation at 28°C. To measure *R. solanacearum* population and spread after putrescine treatment, 50 CFU *R. solanacearum* GMI1000 was cut-petiole inoculated into 26-day-old tomato plants, which have longer stems than 21-day-old plants. After 6 days, bacterial populations were enumerated at the site of inoculation and 4 cm above.

Xylem sap harvest

Xylem sap was harvested from plants 1–3 h after onset of daylight to control for diurnal changes in sap composition (Siebrecht *et al.*, 2003). To ensure adequate water status, plants were watered each evening before morning sampling. Plants inoculated by soil soaking were detopped 2 cm above the cotyledons, and plants inoculated by petiole inoculation were detopped at the site of inoculation. Root pressure forced xylem sap to accumulate on the stump. The sap accumulated after the first 2–3 min was discarded, and the stump was washed with water and gently blotted dry as previous described (Goodger *et al.*, 2005). For the next 20–30 min the sap was frequently transferred into prechilled tubes in a –20°C block or on ice. Samples were flash-frozen and stored at –80°C until analysis. Population sizes in stems were determined as described above.

Bacterial growth in ex vivo xylem sap

Ex vivo xylem sap was harvested as described above. Xylem sap was pooled from at least 3 plants and sterilized through a 0.22 µm filter. Overnight cultures were washed three times, and bacteria were inoculated into 50 µl xylem sap to a final density of OD₆₀₀=0.1 in a half-area 96-well microplate (Corning Inc., Corning, NY), corresponding to A₆₀₀≈0.03 in the microplate wells. Kinetic growth data was collected in a Synergy HTX plate reader with 28°C incubation and variable shaking (BioTek Instruments Inc, Winooski, VT). Microaerobic growth experiments were performed as described (Dalsing *et al.*, 2015). Briefly, the experiments were performed in a plate reader housed in an environment-controlled chamber at 0.1% oxygen and 99.9% N₂ gas.

To determine whether xylem sap from healthy tomato plants inhibited *R. solanacearum* growth, xylem sap from healthy plants was concentrated twofold in a Speed-Vac and added to an equal volume of *R. solanacearum* growing in MM. Overnight cultures were washed and resuspended to OD₆₀₀ = 0.1 in MM before transferring to a 96-half-area-well microplate (50 µl per well). After 14 h growth, 50 µl of twofold concentrated xylem sap was added to the actively growing cultures, yielding a final concentration of 1x xylem sap. Fresh MM (50 µl) was added to control wells. The plate was returned to the plate reader and A_{600 nm} was measured for an additional 24 h.

The lack of growth inhibition of healthy xylem sap was confirmed on solid media using an overlay inhibition assay (Huerta *et al.*, 2015). Briefly, a suspension of *R. solanacearum* cells in semisolid CPG agar was overlaid on solid CPG agar. Wells were excised from the solidified plates with a hole punch. Water, nonconcentrated xylem sap or 10-fold concentrated xylem sap (concentrated in a vacuum concentrator) was added to the wells, and bacterial growth was observed after 48 h incubation at 28°C. The xylem sap did not induce a zone of inhibition, even when added at 10-fold concentration.

GC-MS metabolomics of xylem sap

Sap from soil-soak inoculated plants was used for the untargeted metabolomics experiments. The first experiment compared sap from healthy tomato cv. Bonny Best plants to sap from symptomatic plants infected with *R. solanacearum* GMI1000. To minimize variation, several guidelines were followed when selecting samples for analysis. Although soil-soak inoculations result in asynchronous infections, infected plants showing the first wilt symptoms (<25% leaflets wilted) consistently harbored bacterial populations of $\sim 1 \times 10^9$ CFU g⁻¹ stem. Infected plants displaying the first wilt symptoms (6–10 dpi) and an equal number of healthy plants were selected each day. To ensure that infected plants were at a similar disease state, plants that developed first symptoms during the afternoon were discarded; xylem sap was only sampled from plants that developed wilt symptoms overnight. Additionally, all infected samples came from plants with bacterial density between 1×10^9 and 1×10^{10} CFU per g stem. To avoid distortion of metabolite concentrations due to differential flow rates, only samples with a median sap volume (250–350 µl) were chosen for pooling from the 103 infected and the 69 healthy samples collected. Pools were composed of samples collected across the sampling time. To yield 0.5 to 1 ml, equal

volumes of sap from 4 samples were pooled for each of five biological replicates. For pooling, samples were thawed on ice, and debris was removed from samples by centrifugation at 14 000 r.p.m. for 3 min at 4°C. Mean exudation rate of healthy pools was 0.975 ml min⁻¹, and mean exudation rate of *R. solanacearum*-infected pools was 0.613 ml min⁻¹ (Supporting Information Fig. S1).

The second untargeted metabolomics experiment compared xylem sap from infected plants after incubation with or without *R. solanacearum* GMI1000 for 3 h. Xylem sap was harvested from infected plants as described above. Samples with a median sap volume (150–390 µl) were chosen for pooling from the 134 samples harvested. Each pool was produced from 14 samples. Samples were thawed on ice and sterilized with 0.22 µm filters. Each pool was divided; half was inoculated with a water suspension of *R. solanacearum* strain GMI1000 to OD_{600 nm} = 0.1, and half of the pool received an equal volume of water. Samples were incubated at 28°C with shaking for 3 h. Bacteria were pelleted, and the supernatant was transferred to fresh tubes, flash frozen and stored at -80°C until samples were shipped on dry ice for metabolomics analysis.

GC-MS analysis was performed by West Coast Metabolomics (University of California, Davis). Xylem sap (500 µl) was extracted with 1 ml of ice cold 5:2:2 MeOH:CHCl₃:H₂O. The upper phase was transferred into a new tube and a 500 µl aliquot was dried under vacuum. The residue was derivatized in a final volume of 100 µl. Detailed methods of metabolite derivatization, separation and detection are described (Fiehn *et al.*, 2005). Briefly, samples were injected (0.5 µl, splitless injection) into a Pegasus IV GC (Leco Corp., St Joseph, MI) equipped with a 30 m × 0.25 mm i.d. fused-silica capillary column bound with 0.25 µm Rtx-5Sil MS stationary phase (Restek Corporation, Bellefonte, PA). The injector temperature was 50°C ramped to 250°C by 12°C s⁻¹. A helium mobile phase was applied at a flow rate of 1 ml min⁻¹. Column temperature was 50°C for 1 min, ramped to 330°C by 20°C min⁻¹ and held constant for 5 min. The column effluent was introduced into the ion source of a Pegasus IV TOF MS (Leco Corp., St Joseph, MI) with transfer line temperature set to 230°C and ion source set to 250°C. Ions were generated with a -70 eV and 1800 V ionization energy. Masses (80–500 *m/z*) were acquired at a rate of 17 spectra s⁻¹. ChromaTOF 2.32 software (Leco Corp) was used for automatic peak detection and deconvolution using a 3 s peak width. Peaks with signal/noise below 5:1 were rejected. Metabolites were quantified by peak height for the quantification ion. Metabolites were annotated with the BinBase 2.0 algorithm (Skogerson *et al.*, 2011).

Statistical analyses were conducted in MetaboAnalyst 3.0 (Xia *et al.*, 2015). Although pooled samples were selected from plants with median sap exudation rates, the exudation rate of plants in the healthy pools was 1.2-fold greater than that of plants in the infected pools. Because exudation rate alters sap metabolite concentration (Goodger *et al.*, 2005), we normalized metabolite peak heights by mean exudation rate for each pooled sample. Multivariate and univariate statistics were performed on generalized log transformed peak heights. Metabolites with FDR <0.1 were considered differentially concentrated.

Targeted analysis of putrescine in xylem sap

Putrescine was quantified in tomato cv. Money Maker xylem sap from plants infected with *R. solanacearum* and *V. dahliae* JR2. Plants were inoculated with *R. solanacearum* by soil-soak inoculation and sap was harvested as described above. Three pools of sap from three plants each were lyophilized before analysis. Plants were inoculated with the wilt fungus *V. dahliae* as previously described (Fradin *et al.*, 2009). Briefly, 10-day-old tomato plants were uprooted, rinsed briefly in water and submerged in a *V. dahliae* spore suspension at a concentration of 10⁶ conidia ml⁻¹. The spore suspension was prepared from 1- to 2-week-old *V. dahliae* plates grown on potato dextrose agar and suspended in 20% potato dextrose broth. Following inoculation, plants were potted in metro mix and grown in the greenhouse. At 9 dpi, xylem sap was sampled from healthy and symptomatic *V. dahliae*-infected plants as described above. Three pools of sap from five plants each were lyophilized before analysis.

LC-MS separation and detection of putrescine was performed as reported (Sánchez-López *et al.*, 2009) using an Eksper Micro-LC 200 and a QTRAP4000 (ABSciex, Framingham, MA). Chromatographic separation was achieved on a 150 × 0.5 mm HaloFused C18 column with particle size 2.7 µm (AB Sciex) and column temperature 35°C. A binary gradient at a flow rate of 11 µl min⁻¹ was applied: 0–0.5 min isocratic 90% A; 0.5–4 min, linear from 90% A to 1% A; 4–4.8 min, isocratic 1% A; 4.8–5 min, linear from 1% A to 90% A; 5–5.5 min, linear to 99% A, 5.5–5.8 min, linear to 90% A, 5.8–6 min, isocratic 10% B. Solvent A was water, 0.1% aq. formic acid, 0.05% heptafluorobutyric acid and solvent B was acetonitrile, 0.1% aq. formic acid, 0.05% heptafluorobutyric acid. Injection volume was 2 µl. Analytes were ionized using a TurboV ion source equipped with an Assy 65 µm ESI electrode in positive ion mode. The following instrument settings were applied: nebulizer and heater gas, zero grade air, 25 and 10 psi; curtain gas, nitrogen, 20 psi; collision gas, nitrogen, medium; source temperature, 200°C; ionspray voltage, 5000 V; entrance potential, 10 V; collision cell exit potential, 5 V. The transitions monitored for putrescine were: Q1 mass 89.1 Da, Q3 mass 82.0 Da, declustering potential 22 V, collision energy 14 eV. Acquired MRM data were analyzed using ABSciex MultiQuant software.

Targeted analysis of polyamines in

R. solanacearum cells

To analyze polyamine profiles of *R. solanacearum* cell fractions, *R. solanacearum* GMI1000 and $\Delta speC$ were seeded into 30 ml MM, MM with 500 µM putrescine, or MM with 500 µM spermidine (OD₆₀₀ = 0.015). Cells were grown at 28°C with shaking until to OD₆₀₀ > 0.8. Cell pellets (1.3 × 10¹⁰ CFU) were washed and stored at -80°C until lysis. Pellets were suspended in 750 µl lysis buffer (100 mM MOPS, 50 mM NaCl, 20 mM MgCl₂ pH 8.0) and lysed by ten 30 s rounds of pulsed sonication. During sonication, samples were kept in a salted ice bath. Proteins were precipitated with 225 µl 40% trichloroacetic acid. After 5 min incubation on ice, samples were centrifuged (10 min at > 10 000 × g). The supernatant containing the polyamine lysate was stored at -80°C until benzoyl chloride derivatization.

Polyamines were derivatized by adding 1 ml of 2 N NaOH and 10 μ l benzoyl chloride to 200 μ l cell lysate. Samples were vortexed for 2 min, and incubated at 22°C for 1 h. Saturated NaCl (2 ml) was added, and samples were vortexed for 2 min. After addition of 2 ml diethyl ether, samples were vortexed for 2 min and incubated at 22°C for 30 min. The upper diethyl ether phase containing benzoylated polyamines was removed to a fresh glass tube and evaporated to dryness in a fume hood. For LC-MS analysis, benzoylated samples were dissolved in methanol with 0.1% v/v formic acid and run on an Agilent Infinity LC-MS or Agilent 1100 series LC-MS, with electrospray probes, using a 4.6 \times 150 mm (5 μ m) Agilent Eclipse XDB-C18 column (Agilent Technologies, Santa Clara, CA). Samples were injected using an autosampler. The solvent system was 30% solvent A (HPLC grade water with 0.1% v/v formic acid) and 70% solvent B (HPLC grade acetonitrile with 0.1% v/v formic acid). Column flow at 22°C was 0.5 ml min⁻¹, and the analysis time was 20 min.

To analyze polyamine profile of the *R. solanacearum* Δ RSp1578 mutant, cell lysates grown in MM were prepared as described above. Polyamines were derivatized with dansyl chloride as described (Ducros *et al.*, 2009) with the following modifications. Proteins were precipitated with 1 ml HCl instead of perchloric acid. For HPLC analysis, samples were dissolved in 200 μ l ACN and run on a Zorbax Eclipse Agilent Eclipse XDB-C18 column. A gradient was run using solvent A (water) and solvent B (100% ACN): 2 min 40% B, 15 min gradient 40%–100% B, 2 min 100% B, 7 min 100% B, 4 min gradient 100%–40% B and 2 min 40% B at 37°C, and a flow rate of 0.4 ml min⁻¹ was used.

SpeC overexpression and purification

The *R. solanacearum speC* gene (RSc2365) with codons optimized for expression in *E. coli* was synthesized by GenScript and recombined into BamHI/HindIII sites of pET28b-TEV, yielding pET28b-TEV-speC. Proteins were expressed in *E. coli* BL21(DE3). *E. coli* cells containing the expression construct were grown at 37°C in 40 ml LB with kanamycin. 20 ml of the overnight culture was added to 2 L LB with kanamycin and grown at 37°C. When cells reached mid-log phase (OD₆₀₀ = 0.5), protein expression was induced with 0.2 mM IPTG (isopropyl- β -D-thiogalactopyranoside), and cells were cultured overnight at 16°C. The cells were re-suspended in 100 mM HEPES buffer (pH 8.0), 50 mM NaCl, 5 mM imidazole, 20 μ M PLP, 0.02% Brij-35 detergent and lysed in a cell disruptor at 10 000 psi. The lysate was centrifuged at 18 000 r.p.m. for 60 min to remove unbroken cells, debris and insoluble material. The soluble sample was applied to a 5 ml HiTrap chelating HP column (GE Healthcare, Pittsburg PA) equilibrated with 0.1 M NiSO₄ and buffer A (100 mM HEPES buffer pH 8.0, 50 mM NaCl, 20 μ M PLP, 0.02% Brij-35 and 5 mM imidazole). The 6xHis-tagged SpeC protein was eluted from the column with a gradient of 0%–40% buffer B (100 mM HEPES buffer pH 8.0, 50 mM NaCl, 20 μ M PLP, 0.02% Brij-35 and 500 mM imidazole) over 20 column volumes. Proteins were desalted into 10 mM HEPES (pH 8.0), 150 mM NaCl and 10% glycerol at 4°C using Hi-prep 26/10 desalting column (GE Healthcare). Protein purity was confirmed using SDS-PAGE. Protein concentration was determined in a BioTek Synergy Multi-Mode Microplate reader using the molecular weight

and protein extinction coefficients program, which measures absorbance at 280 nm. Protein yield from the induced cultures harboring the expression constructs was 113.1 mg l⁻¹.

In vitro decarboxylase assay

To identify SpeC substrate(s), decarboxylase activity of purified SpeC was measured with the Infinity Carbon Dioxide Liquid Stable Reagent kit (Thermo Scientific). This kit couples CO₂ production to phosphoenolpyruvate carboxylase and malate dehydrogenase. CO₂ production is indirectly measured as reduced absorbance at 340 nm as malate dehydrogenase oxidizes NADH to NAD⁺. All reactions were performed in 200 μ l volumes and using buffer 100 mM HEPES pH 7.8, 50 μ M PLP, 1 mM DTT, 1 mM of each test substrate (L-ornithine, L-lysine or L-arginine) and 100 μ l 50% CO₂ detection solution from the kit. Purified SpeC protein was added to wells at 0, 25, 50, 100, 200, 400 nM final concentration and mixed well. Samples were incubated at 25°C for 20 min, then reaction kinetics were measured with the BioTek plate reader set to measure A_{340 nm} every 5 s for 20 min at 25°C.

Substrate competition assay for SpeC enzyme

To determine the substrate preference of SpeC decarboxylase, purified enzyme was incubated in equimolar L-ornithine and L-lysine. All reactions were performed in 200 μ l volumes. Reaction buffer was 100 mM HEPES pH 7.8, 50 μ M PLP, 1 mM DTT, 10 mM L-ornithine and 10 mM L-lysine. Reaction was started by adding 2 μ M purified SpeC and mixing well. Reactions were carried out for 1 h at 22°C. The reaction was stopped by adding 1 ml 2 N NaOH, and polyamines were derivatized with benzoyl chloride as described above. Benzoylated reaction products were analyzed by LC-MS. Ornithine decarboxylase activity yielded benzoylated putrescine, and lysine decarboxylase activity yielded benzoylated cadaverine.

qRT-PCR

Expression of tomato polyamine biosynthesis genes in stems of cv. Money Maker was measured in healthy plants and soil-soak inoculated plants showing early symptoms (<25% wilted leaflets). Stem slices (100 mg) were harvested at the site of inoculation, flash frozen, and stored at -80°C until RNA extraction. For time course experiments, the cut-petiole inoculation method was used to ensure synchronous infection. RNA was extracted at 24, 48, 72 and 96 h postinoculation from stem slices at the site of inoculation (including the petiole stump).

RNA was extracted from plant tissue using the RNeasy Plant kit, including DNase treatment (Qiagen). cDNA was synthesized from 200 ng to 1 μ g RNA with SuperScript III (Life Technologies, Carlsbad CA). Absence of DNA contamination was confirmed by running qPCR reactions on RNA. qPCR reactions were run in triplicate with 10 ng cDNA and EvaGreen qPCR mastermix (BullsEye, Madison, WI) in 25 μ l volume in an ABI 7300 Real Time PCR System (Applied Biosystems, Foster City, CA). Relative expression of target genes was calculated by the 2^{- $\Delta\Delta$ CT} method, normalizing to the constantly expressed gene *ACTIN* and to gene expression in

healthy tissue (Milling *et al.*, 2011). All primer sets amplified a 100–200 bp fragment with 95%–105% amplification efficiency. *SI_ODC2* was not investigated because four attempts to design gene-specific primers yielded unacceptable amplification efficiencies. Primers are listed in Supporting Information Table S2.

Tomato root RNA-seq

Bonny Best tomato seed were surface-sterilized by shaking in 10% bleach for 10 min, followed by shaking in 70% ethanol for 5 min. Seeds were washed repeatedly in sterile water and placed in the refrigerator overnight to synchronize germination. The following day, seeds were placed on germination plates (1% water agar) and plates were placed in the dark for three days. Germinated seeds were sown onto the surface of 0.5X Murashige and Skoog Basal Salts Medium plus Gamborg's vitamins (MP Biomedicals, Santa Ana, CA) and 1% Agar and incubated at 28°C with a 12 h light cycle. Root tips were inoculated 2 days later with 1 microliter of water (mock) or a bacterial suspension of *R. solanacearum* strain GMI1000 at $OD_{600}=0.2$, corresponding to approximately 2×10^5 CFU per plant. After 24 h, root segments spanning the inoculation point (1 inch above, down to the root tip) were collected, flash frozen in liquid nitrogen and stored at -80°C prior to RNA isolation. RNA was prepared from 20 to 30 root segments using the Trizol (Life Technologies, Carlsbad, CA) protocol with modifications for tissues with high polysaccharide content. On average, 25 micrograms of total RNA were isolated from each preparation.

For RNA-seq experiments, three independent biological replicates for each condition were sequenced at the University of Wisconsin-Madison Biotechnology Center. Samples were sequenced using paired-end, random primed, multiplexed sequencing on an Illumina HiSeq2000 (Illumina, San Diego, CA). RNA-seq analysis was conducted in the Galaxy environment (<https://galaxyproject.org/>) (Giardine *et al.*, 2005; Blankenberg *et al.*, 2010b; Goecks *et al.*, 2010) at the Minnesota Supercomputing Institute using the Tuxedo Suite software (Trapnell *et al.*, 2012). Sequences were trimmed using Fastq Trimmer to remove low quality bases (Blankenberg *et al.*, 2010a), and sequences shorter than 20 nucleotides were discarded as they can have difficulty with genome alignment. Because this quality control step resulted in some single sequences, both single and paired-end sequences were mapped independently using TopHat (Trapnell *et al.*, 2009), and these files were merged. Transcripts were then assembled using Cufflinks (Trapnell *et al.*, 2010; Trapnell *et al.*, 2012), and a final transcriptome assembly was created using Cuffmerge (Goecks *et al.*, 2010; Trapnell *et al.*, 2010). Differentially expressed genes were identified using Cuffdiff (Trapnell *et al.*, 2012). Expression changes were considered significant for q -values of <0.05 .

Putrescine treatment of plants

Tomato and tobacco leaves and roots were treated with 0.5 mM putrescine in water by spraying leaves until drip-off and pipetting 10 ml into the soil. Water treatment served as a control. After 3 h, tobacco plants were leaf-infiltrated with *R.*

solanacearum K60 as described above, and tomato plants were cut petiole-inoculated with a 2 μl suspension containing 50 CFU *R. solanacearum* GMI1000 on susceptible tomato cvs. Bonny Best and Money Maker. Quantitatively resistant tomato line H7996 was inoculated with 5×10^3 CFU *R. solanacearum* UW551 or 5×10^4 CFU *R. solanacearum* GMI1000. Disease progress assays were conducted as described above. To measure the effect of putrescine on defense gene expression, RNA was extracted from stem at 48 hpi as described above. Xylem sap was harvested at 3 and 24 h post-treatment as described above.

Stomatal conductance

Stomatal conductance was measured with a Licor 6400XT portable photosynthesis system gas analyzer. Settings were used that matched environmental measurements of the growth chamber: 700 ppm reference CO_2 , 400 $\mu\text{mol s}^{-1}$ flow, 27°C leaf temperature, 350 $\mu\text{mol m}^{-2} \text{s}^{-1}$. Equilibrium measurements were recorded on one to three fully expanded leaves per plant two to four h after light onset. Tomato leaves rarely filled the full 2×3 cm gas analyzer chamber, so leaves were subsequently imaged in a custom-rig to normalize stomatal conductance measurements by percent leaf area.

R. solanacearum biofilm and twitching assays

PVC plate biofilm assays were performed as described (Tran *et al.*, 2016b) except that 0 mM, 1 mM or 30 μM putrescine was added to CPG broth. Twitching assays were performed as described (Liu *et al.*, 2001) with freshly poured CPG plates with or without 1 mM putrescine.

Acknowledgements

We thank Alicia Truchon, Kate McCulloh, Duncan Smith and Madeline Hayes for technical assistance, and Devanshi Khokhani, Mehdi Kabbage, Heidi Goodrich-Blair, Jonathan Jacobs, Niklas Schandry and Remi Peyraud for valuable discussions. National Institute of Food and Agriculture, USDA-AFRI-2015-67011-22799, USDA-ARS FNRI MSN168068, USDA-Hatch WIS01776,;National Science Foundation, NSF-IOS 1257479, NSF-IOS 1258082,;National Institutes of Health, T32GM07215, U24DK097154.

References

- Aribaud, M., Jégo, S., Wicker, E., and Fock, I. (2010) *Ralstonia solanacearum* induces soluble amine-oxidase activity in *Solanum torvum* stem calli. *Plant Physiol Biochem* **48**: 787–796.
- Blankenberg, D., Gordon, A., Von Kuster, G., Coraor, N., Taylor, J., Nekrutenko, A., and Team, G. (2010a) Manipulation of FASTQ data with galaxy. *Bioinformatics* **26**: 1783–1785.
- Blankenberg, D., Kuster, G.V., Coraor, N., Ananda, G., Lazarus, R., and Mangan, M. (2010b) Galaxy: a web-based genome analysis tool for experimentalists. *Curr Protoc Mol Biol* **19.10**: 1–21.

- Brodersen, C.R., McElrone, A.J., Choat, B., Matthews, M.A., and Shackel, K.A. (2010) The dynamics of embolism repair in xylem: *in vivo* visualizations using high-resolution computed tomography. *Plant Physiol* **154**: 1088–1095.
- Brown, D.G., and Allen, C. (2004) *Ralstonia solanacearum* genes induced during growth in tomato: an inside view of bacterial wilt. *Mol Microbiol* **53**: 1641–1660.
- Busse, J., and Auling, G. (1988) Polyamine pattern as a chemotaxonomic marker within the proteobacteria. *Syst Appl Microbiol* **11**: 1–8.
- Castañeda, A., Reddy, J.D., El-Yacoubi, B., and Gabriel, D.W. (2005) Mutagenesis of all eight *avr* genes in *Xanthomonas campestris* pv. *campestris* had no detected effect on pathogenicity, but one *avr* gene affected race specificity. *Mol Plant Microbe Interact* **18**: 1306–1317.
- Chellemi, D., Andersen, P., Brodbeck, B., Dankers, W., and Rhoads, F. (1998) Correlation of chemical profiles of xylem fluid of tomato to resistance to bacterial wilt. In *Bacterial Wilt Disease*. Berlin, Germany: Springer, pp. 225–232.
- Coplin, D.L., Sequeira, L., and Hanson, R.S. (1974) *Pseudomonas solanacearum*: virulence of biochemical mutants. *Can J Microbiol* **20**: 519–529.
- Dalsing, B.L., Truchon, A.N., Gonzalez-Orta, E.T., Milling, A.S., and Allen, C. (2015) *Ralstonia solanacearum* uses inorganic nitrogen metabolism for virulence, ATP production, and detoxification in the oxygen-limited host xylem environment. *mBio* **6**: 1–13.
- Deslandes, L., and Genin, S. (2014) Opening the *Ralstonia solanacearum* type III effector tool box: insights into host cell subversion mechanisms. *Curr Opin Plant Biol* **20**: 110–117.
- Di Martino, M.L., Campilongo, R., Casalino, M., Micheli, G., Colonna, B., and Prosseda, G. (2013) Polyamines: emerging players in bacteria-host interactions. *Int J Med Microbiol* **303**: 484–491.
- Dixon, G.R., and Pegg, G.F. (1972) Changes in amino-acid content of tomato xylem sap following infection with strains of *Verticillium albo-atrum*. *Ann Bot* **36**: 147–154.
- Ducros, V., Ruffieux, D., Belva-Besnet, H., Fraipont, F.D., Berger, F., and Favier, A. (2009) Determination of dansylated polyamines in red blood cells by liquid chromatography–tandem mass spectrometry. *Anal Biochem* **390**: 46–51.
- El-Halfawy, O.M., and Valvano, M.A. (2014) Putrescine reduces antibiotic-induced oxidative stress as a mechanism of modulation of antibiotic resistance in *Burkholderia cenocepacia*. *Antimicrob Agents Chemother* **58**: 4162–4171.
- Elphinstone, J.G. (2005) The current bacterial wilt situation: a global overview. In *Bacterial Wilt Disease and the Ralstonia Solanacearum Species Complex*. Caitilyn Allen, P.P., and Hayward, A.L. (ed). St. Paul, MN: APS Press, pp. 9–28.
- Fatima, U., and Senthil-Kumar, M. (2015) Plant and pathogen nutrient acquisition strategies. *Front Plant Sci* **6**: 750.
- Fiehn, O., Wohlgemuth, G., and Scholz, M. (2005) Setup and annotation of metabolomic experiments by integrating biological and mass spectrometric metadata. In *International Workshop on Data Integration in the Life Sciences*. Springer Berlin Heidelberg, pp. 224–239.
- Fradin, E.F., Zhang, Z., Juarez Ayala, J.C., Castroverde, C.D.M., Nazar, R.N., Robb, J., et al. (2009) Genetic dissection of *Verticillium* wilt resistance mediated by tomato *Ve1*. *Plant Physiol* **150**: 320–332.
- Garcia, A.F., Benchimol, M., and Alderete, J. (2005) *Trichomonas vaginalis* polyamine metabolism is linked to host cell adherence and cytotoxicity. *Infect Immun* **73**: 2602–2610.
- Genin, S., and Denny, T.P. (2012) Pathogenomics of the *Ralstonia solanacearum* species complex. *Annu Rev Phytopathol* **50**: 67–89.
- Giardine, B., Riemer, C., Hardison, R.C., Burhans, R., Elnitski, L., Shah, P., et al. (2005) Galaxy: a platform for interactive large-scale genome analysis. *Genome Res* **15**: 1451–1455.
- Gibson, D.G., Young, L., Chuang, R.-Y., Venter, J.C., Hutchison, C.A., and Smith, H.O. (2009) Enzymatic assembly of DNA molecules up to several hundred kilobases. *Nat Methods* **6**: 343–345.
- Goecks, J., Nekrutenko, A., Taylor, J., and Galaxy Team, T. (2010) Galaxy: a comprehensive approach for supporting accessible, reproducible, and transparent computational research in the life sciences. *Genome Biol* **11**: R86.
- Goodger, J.Q.D., Sharp, R.E., Marsh, E.L., and Schachtman, D.P. (2005) Relationships between xylem sap constituents and leaf conductance of well-watered and water-stressed maize across three xylem sap sampling techniques. *J Exp Bot* **56**: 2389–2400.
- Goytia, M., and Shafer, W.M. (2010) Polyamines can increase resistance of *Neisseria gonorrhoeae* to mediators of the innate human host defense. *Infect Immun* **78**: 3187–3195.
- Grimault, V., Gélie, B., Lemattre, M., Prior, P., and Schmit, J. (1994) Comparative histology of resistant and susceptible tomato cultivars infected by *Pseudomonas solanacearum*. *Physiol Mol Plant Pathol* **44**: 105–123.
- Gupta, K., Sengupta, A., Chakraborty, M., and Gupta, B. (2016) Hydrogen peroxide and polyamines act as double edged swords in plant abiotic stress responses. *Front Plant Sci* **7**: 1343.
- Halverson, T.W.R., Wilton, M., Poon, K.K.H., Petri, B., and Lewenza, S. (2015) DNA is an antimicrobial component of neutrophil extracellular traps. *PLoS Pathog* **11**: e100459.
- Hanfrey, C.C., Pearson, B.M., Hazeldine, S., Lee, J., Gaskin, D.J., Woster, P.M., et al. (2011) Alternative spermidine biosynthetic route is critical for growth of *Campylobacter jejuni* and is the dominant polyamine pathway in human gut microbiota. *J Biol Chem* **286**: 43301–43312.
- Henry, E., Toruño, T.Y., Jauneau, A., Deslandes, L., and Coaker, G.L. (2017) Direct and indirect visualization of bacterial effector delivery into diverse plant cell types during infection. *Plant Cell* **29**: 1555–1570.
- Hewezi, T., Howe, P.J., Maier, T.R., Hussey, R.S., Mitchum, M.G., Davis, E.L., and Baum, T.J. (2010) Arabidopsis spermidine synthase is targeted by an effector protein of the cyst nematode *Heterodera schachtii*. *Plant Physiol* **152**: 968–984.
- Huerta, A.I., Milling, A., and Allen, C. (2015) Tropical strains of *Ralstonia solanacearum* outcompete race 3 biovar 2 strains at lowland tropical temperatures. *Appl Environ Microbiol* **81**: 3542–3551.
- Igarashi, K., and Kashiwagi, K. (2010) Characteristics of cellular polyamine transport in prokaryotes and eukaryotes. *Plant Physiol Biochem* **48**: 506–512.
- Jacobs, J.M., Babujee, L., Meng, F., Milling, A., and Allen, C. (2012) The *in planta* transcriptome of *Ralstonia solanacearum*: conserved physiological and virulence strategies during bacterial wilt of tomato. *mBio* **3**: e00114–e00112.

- Jelsbak, L., Thomsen, L.E., Wallrodt, I., Jensen, P.R., Olsen, J.E., and Chakravorty, D. (2012) Polyamines are required for virulence in *Salmonella enterica* serovar Typhimurium. *PLoS One* **7**: e36149.
- Jiménez-Bremont, J.F., Marina, M., Guerrero-González, M.D.L.L., Rossi, F.R., Sánchez-Rangel, D., and Rodríguez-Kessler, M. (2014) Physiological and molecular implications of plant polyamine metabolism during biotic interactions. *Front Plant Sci* **5**: 95.
- Kabbage, M., Yarden, O., and Dickman, M.B. (2015) Pathogenic attributes of *Sclerotinia sclerotiorum*: switching from a biotrophic to necrotrophic lifestyle. *Plant Sci* **233**: 53–60.
- Kanehisa, M., and Goto, S. (2000) KEGG: Kyoto encyclopedia of genes and genomes. *Nucleic Acids Res* **28**: 27–30.
- Khokhani, D., Lowe-Power, T.M., Tran, T.M., and Allen, C. (2017) A single regulator mediates strategic switching between attachment/spread and growth/virulence phenotypes in the plant pathogen *Ralstonia solanacearum*. *mBio* **8**: e00895–e00817.
- Kim, N.H., Kim, B.S., and Hwang, B.K. (2013) Pepper arginine decarboxylase is required for polyamine and γ -aminobutyric acid signaling in cell death and defense response. *Plant Physiol* **162**: 2067–2083.
- Kim, S.H., Wang, Y., Khomutov, M., Khomutov, A., Fuqua, C., and Michael, A.J. (2016) The essential role of spermidine in growth of *Agrobacterium tumefaciens* is determined by the 1,3-diaminopropane moiety. *ACS Chem Biol* **11**: 491–499.
- Kurihara, S., Oda, S., Kato, K., Kim, H.G., Koyanagi, T., Kumagai, H., and Suzuki, H. (2005) A novel putrescine utilization pathway involves γ -glutamylated intermediates of *Escherichia coli* K-12. *J Biol Chem* **280**: 4602–4608.
- de Lange, O., Schreiber, T., Schandry, N., Radeck, J., Braun, K.H., Koszinowski, J., et al. (2013) Breaking the DNA-binding code of *Ralstonia solanacearum* TAL effectors provides new possibilities to generate plant resistance genes against bacterial wilt disease. *New Phytol* **199**: 773–786.
- Li, B., Lowe-Power, T., Kurihara, S., Gonzales, S., Naidoo, J., MacMillan, J.B., et al. (2016) Functional identification of putrescine C- and N-hydroxylases. *ACS Chem Biol* **11**: 2782–2789.
- Liu, H., Kang, Y., Genin, S., Schell, M.A., and Denny, T.P. (2001) Twitching motility of *Ralstonia solanacearum* requires a type IV pilus system. *Microbiology* **147**: 3215–3229.
- Marina, M., Maiale, S.J., Rossi, F.R., Romero, M.F., Rivas, E.I., Garriz, A., et al. (2008) Apoplastic polyamine oxidation plays different roles in local responses of tobacco to infection by the necrotrophic fungus *Sclerotinia sclerotiorum* and the biotrophic bacterium *Pseudomonas viridiflava*. *Plant Physiol* **147**: 2164–2178.
- McGarvey, J., Denny, T.P., and Schell, M. (1999) Spatial-temporal and quantitative analysis of growth and EPS I production by *Ralstonia solanacearum* in resistant and susceptible tomato cultivars. *Phytopathology* **89**: 1233–1239.
- Melotto, M., Underwood, W., Koczan, J., Nomura, K., and He, S.Y. (2006) Plant stomata function in innate immunity against bacterial invasion. *Cell* **126**: 969–980.
- Michael, A.J. (2016) Biosynthesis of polyamines and polyamine-containing molecules. *Biochem J* **473**: 2315–2329.
- Milling, A., Babujee, L., and Allen, C. (2011) *Ralstonia solanacearum* extracellular polysaccharide is a specific elicitor of defense responses in wilt-resistant tomato plants. *PLoS One* **6**: e15853.
- Monteiro, F., Solé, M., van Dijk, I., and Valls, M. (2012) A chromosomal insertion toolbox for promoter probing, mutant complementation, and pathogenicity studies in *Ralstonia solanacearum*. *Mol Plant Microbe Interact* **25**: 557–568.
- Nakaho, K., Hibino, H., and Miyagawa, H. (2000) Possible mechanisms limiting movement of *Ralstonia solanacearum* in resistant tomato tissues. *J Phytopathol* **148**: 181–190.
- Nardini, A., Lo Gullo, M.A., and Salleo, S. (2011) Refilling embolized xylem conduits: is it a matter of phloem unloading? *Plant Sci* **180**: 604–611.
- O'Leary, B.M., Neale, H.C., Geifus, C.M., Jackson, R.W., Arnold, D.L., and Preston, G.M. (2016) Early changes in apoplast composition associated with defence and disease in interactions between *Phaseolus vulgaris* and the halo blight pathogen *Pseudomonas syringae* P_v. *phaseolicola*. *Plant Cell Environ* **39**: 2172–2184.
- Patel, C.N., Wortham, B.W., Lines, J.L., Fetherston, J.D., Perry, R.D., and Oliveira, M.A. (2006) Polyamines are essential for the formation of plague biofilm. *J Bacteriol* **188**: 2355–2363.
- Peyraud, R., Cottret, L., Marmiesse, L., Gouzy, J., Genin, S., and Desveaux, D. (2016) A resource allocation trade-off between virulence and proliferation drives metabolic versatility in the plant pathogen *Ralstonia solanacearum*. *PLoS Pathog* **12**: 1–25.
- Poueymiro, M., Cunnac, S., Barberis, P., Deslandes, L., Peeters, N., Cazale-Noel, A.-C., et al. (2009) Two type III secretion system effectors from *Ralstonia solanacearum* GMI1000 determine host-range specificity on tobacco. *Mol Plant Microbe Interact* **22**: 538–550.
- Romano, K.A., Vivas, E.I., Amador-Noguez, D., and Rey, F.E. (2015) Intestinal microbiota composition modulates choline bioavailability. *mBio* **6**: 1–8.
- Samsonova, N.N., Smirnov, S.V., Altman, I.B., and Ptitsyn, L.R. (2003) Molecular cloning and characterization of *Escherichia coli* K12 *yjgG* gene. *BMC Microbiol* **3**: 2.
- Sánchez-López, J., Camañes, G., Flors, V., Vicent, C., Pastor, V., Vicedo, B., et al. (2009) Underivatized polyamine analysis in plant samples by ion pair LC coupled with electrospray tandem mass spectrometry. *Plant Physiol Biochem* **47**: 592–598.
- Sansone, C., van Houte, J., Joshipura, K., Kent, R., and Margolis, H.C. (1993) The association of mutans streptococci and non-mutans streptococci capable of acidogenesis at a low pH with dental caries on enamel and root surfaces. *J Dent Res* **72**: 508–516.
- Siebrecht, S., Herdel, K., Schurr, U., and Tischner, R. (2003) Nutrient translocation in the xylem of poplar-diurnal variations and spatial distribution along the shoot axis. *Planta* **217**: 783–793.
- Skiebe, E., de Berardinis, V., Morczinek, P., Kerrinnes, T., Faber, F., Lepka, D., et al. (2012) Surface-associated motility, a common trait of clinical isolates of *Acinetobacter baumannii*, depends on 1,3-diaminopropane. *Int J Med Microbiol* **302**: 117–128.
- Skogerson, K., Wohlgemuth, G., Barupal, D.K., and Fiehn, O. (2011) The volatile compound BinBase mass spectral database. *BMC Bioinformatics* **12**: 321.

- Streubel, J., Pesce, C., Hutin, M., Koebnik, R., Boch, J., and Szurek, B. (2013) Five phylogenetically close rice SWEET genes confer TAL effector-mediated susceptibility to *Xanthomonas oryzae* pv. *oryzae*. *New Phytol* **200**: 808–819.
- Sugiyama, Y., Nakamura, A., Matsumoto, M., Kanbe, A., Sakanaka, M., Higashi, K., et al. (2016) A novel putrescine exporter SapBCDF of *Escherichia coli*. *J Biol Chem* **291**: 26343–26351.
- Tans-Kersten, J., Huang, H., and Allen, C. (2001) *Ralstonia solanacearum* needs motility for invasive virulence on tomato. *J Bacteriol* **183**: 3597–3605.
- Tans-Kersten, J., Brown, D., and Allen, C. (2004) Swimming motility, a virulence trait of *Ralstonia solanacearum*, is regulated by FlhDC and the plant host environment. *Mol Plant Microbe Interact* **17**: 686–695.
- Terpolilli, J.J., Masakapalli, S.K., Karunakaran, R., Webb, I.U.C., Green, R., Watmough, N.J., et al. (2016) Lipogenesis and redox balance in nitrogen-fixing pea bacteroids. *J Bacteriol* **198**: 2864–2875.
- Tran, T.M., MacIntyre, A., Hawes, M., and Allen, C. (2016a) Escaping underground Nets: extracellular DNases degrade plant extracellular traps and contribute to virulence of the plant pathogenic bacterium *Ralstonia solanacearum*. *PLoS Pathog* **12**: e1005686.
- Tran, T.M., MacIntyre, A., Khokhani, D., Hawes, M., and Allen, C. (2016b) Extracellular DNases of *Ralstonia solanacearum* modulate biofilms and facilitate bacterial wilt virulence. *Environ Microbiol* **18**: 4103–4117.
- Trapnell, C., Pachter, L., and Salzberg, S.L. (2009) TopHat: discovering splice junctions with RNA-Seq. *Bioinformatics* **25**: 1105–1111.
- Trapnell, C., Williams, B.A., Pertea, G., Mortazavi, A., Kwan, G., van Baren, M.J., et al. (2010) Transcript assembly and quantification by RNA-Seq reveals unannotated transcripts and isoform switching during cell differentiation. *Nat Biotechnol* **28**: 511–515.
- Trapnell, C., Roberts, A., Goff, L., Pertea, G., Kim, D., Kelley, D.R., et al. (2012) Differential gene and transcript expression analysis of RNA-seq experiments with TopHat and Cufflinks. *Nat Protoc* **7**: 562–578.
- Vasse, J., Frey, P., and Trigalet, A. (1995) Microscopic studies of intercellular infection and protoxylem invasion of tomato roots by *Pseudomonas solanacearum*. *Mol Plant Microbe Interact* **8**: 241–251.
- Vasse, J., Montrozier, H., Etchebar, C., Trigalet, A., Araud-Razou, I., Vasse, J., et al. (1998) Detection and visualization of the major acidic exopolysaccharide of *Ralstonia solanacearum* and its role in tomato root infection and vascular colonization. *Eur J Plant Pathol* **104**: 795–809.
- Xia, J., Sinelnikov, I.V., Han, B., and Wishart, D.S. (2015) MetaboAnalyst 3.0—making metabolomics more meaningful. *Nucleic Acids Res* **43**: 251–257.
- Yao, J., and Allen, C. (2006) Chemotaxis is required for virulence and competitive fitness of the bacterial wilt pathogen *Ralstonia solanacearum*. *J Bacteriol* **188**: 3697–3708.
- Zhou, L., Wang, J., Zhang, L.-H., and Ratner, A. (2007) Modulation of bacterial type III secretion system by a spermidine transporter dependent signaling pathway. *PLoS One* **2**: e1291.
- Zuluaga, A.P., Puigvert, M., and Valls, M. (2013) Novel plant inputs influencing *Ralstonia solanacearum* during infection. *Front Microbiol* **4**: 00349.

Supporting information

Additional Supporting Information may be found in the online version of this article at the publisher's web-site:

Fig. S1. Effect of bacterial wilt disease on tomato xylem sap pH and xylem physiology.

(A) Xylem sap pH ($n=5$) and (B) rate of xylem sap exudation from de-topped tomato stems ($*P < 0.0001$ t -test; $n \geq 69$ plants). Samples are from cv. Bonny Best tomato plants soil-soak inoculated with *R. solanacearum* GMI1000 (Infected) or water (Healthy). Sap was harvested when plants displayed first wilting symptoms. (C) Stomatal conductance of Bonny Best tomato leaves was measured with a Licor Photosynthesis instrument. Turgid leaves from healthy plants and apparently turgid and wilted plants from symptomatic plants soil-soak inoculated with *R. solanacearum* GMI1000 were analyzed; $n \geq 18$, letters indicate $P < 0.05$ by ANOVA with Tukey's multiple comparison test.

Fig. S2. Growth of diverse *R. solanacearum* strains in *ex vivo* xylem sap from healthy tomato plants or from plants infected with *R. solanacearum* GMI1000.

(A) Growth of *R. solanacearum* GMI1000 in sap from tomato cv. Money Maker plants resembles growth in sap from GMI1000-infected tomato cv. Bonny Best plants shown in Fig. 1. (B) Aerobic and microaerobic (0.1% O_2) growth of *R. solanacearum* GMI1000 in xylem sap from tomato cv. Bonny Best tomato plants. (C) Growth of diverse *R. solanacearum* strains (phylogroup IIB UW551, phylogroup IIB IBSBF1503, phylogroup IIB UW163, phylogroup IV Blood disease bacterium (BDB) R229, phylogroup IV PSI07, phylogroup IV *R. syzygii* R24) in xylem sap from tomato cv. Bonny Best plants. $n \geq 3$ pools of xylem sap for all growth experiments. Data are mean \pm SEM.

Fig.S3. Loadings for partial least squares analyses of metabolomics data.

(A) Relative amounts of metabolites from healthy tomato sap versus *R. solanacearum*-infected sap as detected by untargeted GC-MS analysis. (B) Comparison of metabolomic changes in *ex vivo* sap after 3 h incubation with *R. solanacearum*.

Fig. S4. Growth of *R. solanacearum* GMI1000 on metabolites enriched or depleted in xylem sap from *R. solanacearum* GMI1000-infected tomato plants versus healthy plants. Metabolites (identified as shown in Fig. 1) were tested as sole carbon sources (black) and sole nitrogen sources (blue) at 10 mM unless otherwise indicated. Dashed lines show negative controls lacking either carbon or nitrogen sources and solid lines show growth on test metabolites. Area under curve (AUC \pm standard error) is indicated for metabolites that supported growth. $N=3$.

Fig. S5. Growth of *R. solanacearum* GMI1000 on metabolites that were depleted in *ex vivo* sap incubated for 3 h with *R. solanacearum*.

Metabolites (identified as shown in Fig. 2 and S3B) were tested as sole carbon sources (black) and nitrogen sources (blue) at 10 mM in minimal medium unless otherwise

indicated. Area under growth curve (AUC \pm standard error) is indicated for metabolites that supported growth. N=3.

Fig. S6. Xylem sap from tomato plants infected with *V. dahliae* has enriched putrescine.

Xylem sap was harvested at symptom onset from tomato plants (cv. Money Maker) infected with the vascular wilt fungus *Verticillium dahliae*; water-inoculated plants served as controls. Putrescine was measured by LC-MS. Values are mean \pm SEM. (* $P < 0.05$ vs. healthy, t -test, $n \geq 3$ pools).

Fig. S7. Polyamine profile of *R. solanacearum* cells and substrate specificity of RSc2365 SpeC.

(A) Polyamine profile of *R. solanacearum* cell pellets grown in defined medium as determined by LC-MS analysis of the cellular benzoylated polyamines. *R. solanacearum* GMI1000 and Δ speC mutant strains were grown in minimal medium with or without 500 μ M putrescine (Put) or spermidine (Spd). Extracted ion chromatograms are shown for dibenzoylated putrescine (296.7; 297.7); tribenzoylated 2-hydroxyputrescine (416.7; 417.7); tribenzoylated spermidine (457.7; 458.7). The mass spectrum for the 2-hydroxyputrescine peak at 4.017 min is indicated by an asterisk in the GMI1000 sample; a peak of 417.2 (m/z) for 2-hydroxyputrescine is found, along with the sodium adduct at +22 (m/z 439.1). Boxes indicate the peaks corresponding to putrescine, 2-hydroxyputrescine and spermidine. Representative results from lysates analyzed in triplicate are shown. (B) Substrate specificity of RSc2365 decarboxylase was determined by an ornithine/lysine substrate competition *in vitro* assay using recombinant SpeC. Purified SpeC protein (2 μ M) was assayed for 1 h at 22°C in the presence of equal amounts (10 mM) of both L-lysine and L-ornithine. After benzoylation of the products, the resulting diamines (putrescine and cadaverine) were detected by LC-MS. Extracted Ion Chromatograms (EIC) for the mass of dibenzoylated putrescine (296.7; 297.7) and dibenzoylated cadaverine (310.7; 311.7) are shown. Identity of the peak for dibenzoylated putrescine (3.440 min) was confirmed by the presence of the corresponding mass (m/z 297.1 and sodium adducted form at m/z 319.1) in the mass spectrum (inset).

Fig. S8. The RSp1578 locus (encoding a putative agmatinase) does not contribute to *R. solanacearum* putrescine production or *R. solanacearum* virulence.

(A) Genomic context of RSp1578 in the *R. solanacearum* strain GMI1000 genome. Dashed line indicates region deleted Δ RSp1578 mutant. (B) Polyamine profile of GMI1000 and Δ RSp1578 mutant. Cell lysate polyamines were derivatized with dansyl chloride. HPLC trace (fluorescence excitation: 333 nm; emission: 518 nm) of representative samples. Peaks corresponding to putrescine, cadaverine and internal standard 1,8-diaminooctane (DAO). Representative results are shown for lysates analyzed in triplicate. (C) Virulence of the Δ RSp1578 mutant on wilt-susceptible tomato cv. Bonny Best after soil soak inoculation (5×10^8 CFU g⁻¹ soil) or stem inoculation (10^3 CFU). Values are mean \pm SEM ($n=45$ plants/treatment).

Fig. S9. *In vitro* and *in planta* growth of Δ speC mutant and its genetic complement.

(A) Genomic context of *speC* gene (RSc2365). Dashed line indicates the region replaced by the spectinomycin cassette in the Δ speC mutant. Solid line indicates the region used to

complement the Δ speC mutant using the predicted native promoter. (B) Effect of overnight culture conditions on growth of Δ speC mutant in minimal medium (MM). Strains were incubated overnight in CPG or CPG with 100 μ M putrescine, washed and resuspended in media as indicated in figure ($n=3$). (C) Growth of GMI1000 (WT), Δ speC mutant, and the complemented Δ speC mutant (*speC* Comp) in MM with (grey bars) or without 30 μ M putrescine (black bars). (D) Structures of putrescine, spermidine, cadaverine and agmatine, and (E) ability of 30 μ M or 100 μ M of these compounds to restore growth of Δ speC mutant when added to MM ($n=3$). (F) Stem population sizes of Δ speC mutant in tomato cv. Money Maker plants was measured 3 days after stem inoculation with 10^3 to 10^8 CFU ($n=5$ plants per condition). (G) Stem population sizes of WT GMI1000, Δ speC mutant and complemented mutant either alone or co-inoculated as indicated in tomato cv. Money Maker plants, measured at indicated times after stem inoculation with 10^3 to 10^8 CFU ($n=5$ plants per condition).

Fig. S10. Expression of tomato putrescine biosynthesis genes during bacterial wilt disease.

(A) Tomato putrescine biosynthesis pathway. (B) Gene expression of tomato cv. Money Maker after naturalistic soil-soak inoculation with *R. solanacearum* (5×10^8 CFU g⁻¹ soil) or water. Stem RNA was extracted from healthy or symptomatic infected plants and analyzed by RT-qPCR with normalization to *ACTIN*. Values are mean \pm SEM ($n=5$) * indicates expression levels differ from healthy plants at $P < 0.005$, one-sample t -test. (C-E) Tomato polyamine biosynthesis gene expression after stem inoculation. Polyamine biosynthesis genes are identified by color as indicated. Tomato plants (cv. Money Maker) were cut-petiole inoculated with 10^3 CFU *R. solanacearum* GMI1000, 10^8 CFU Δ speC (Put⁺), or 10^8 CFU Δ hrcC (T3SS). (C) Population sizes of the three bacterial strains over time in stems directly below the inoculation site. Dashed lines indicate inoculum density at $t=0$. Values are geometric mean \pm SEM ($n=3$). (D) Time-course expression of polyamine biosynthesis genes in tomato stems infected with *R. solanacearum* GMI1000. (E) Expression of *SL_ADC1* at 48 hpi in tomato stem tissue with equal bacterial burden of *R. solanacearum* GMI1000, Δ speC (Put⁺), Δ hrcC (T3SS), relative to gene expression in healthy plants. Values are mean \pm SEM ($n=3$).

Fig. S11. Effects of putrescine treatment on healthy and *R. solanacearum*-infected tomato plants and on *R. solanacearum* behaviour *in vitro*.

Putrescine (0.5 mM) or water (control) was applied to tomato plants by foliar spray and soil soak. (A-B) At 3 h post-putrescine treatment, tomato (A) susceptible Bonny Best ($P=0.0151$ repeated measures ANOVA; $n=180$ plants/treatment) or (B) resistant Hawaii7996 (H7996) ($P=0.8121$; $n=30$ plants/treatment) were stem inoculated with (A) 50 or (B) 50 000 CFU *R. solanacearum* GMI1000. Symptom development was measured using a disease index corresponding to percent of wilted leaflets. Values are means \pm SEM. (C-D) Effect of putrescine treatment on putrescine levels in xylem sap as measured by (C) LC-MS quantification and (D) growth of *R. solanacearum* Δ speC putrescine biosensor strain in xylem vessels. (C) Xylem sap

of noninfected plants was harvested at 3 and 24 h after putrescine treatment, and putrescine was measured with LC-MS. Values are means \pm SEM ($n=3$). (D) Leaves and soil of tomato plants were treated with 0.5 mM putrescine or water every 24 h for three treatments. At 3 h after first treatment, 10^4 CFU $\Delta speC$ were inoculated into the stem. Bacterial population size was determined at 72 h post-inoculation by dilution plating ground stem sections. Horizontal line shows geometric mean ($n=5$). (E) Effect of putrescine on root pressure-driven sap exudation of *R. solanacearum*-infected tomato cv. Money Maker plants. Plants were stem inoculated with 50 CFU *R. solanacearum* GMI1000. Sap exudation rate of detopped plants was measured for 30 min ($n \geq 26$). (F) Leaf stomatal conductance of control or putrescine-treated tomato cv. Money Maker plants was measured by Licor 6400 XT portable photosynthesis system at 24 to 72 h after stem inoculation with 50 CFU *R. solanacearum* GMI1000; ($n \geq 30$ plants/treatment). (G) Effect of putrescine on *R. solanacearum* GMI1000 in crystal violet polyvinylchloride attachment assay. *R. solanacearum* was grown in CPG with 0, 30 μ M, or 1 mM

putrescine. Letters indicate $P < 0.05$ by ANOVA with Tukey's test for multiple comparisons. Values are means \pm SEM ($n=60$).

Fig. S12. Effect of putrescine treatment and *R. solanacearum* infection on expression of tomato defense genes.

Plants were cut petiole- inoculated with 50 CFU and RNA was extracted at 48 hpi. Plant gene expression was normalized to *ACTIN* transcript levels. Values are mean \pm SEM. Letters indicate $P < 0.05$ by ANOVA with Tukey test for multiple comparisons ($n=7$ plants/treatment).

Table S1. Expression of tomato polyamine metabolism genes in healthy and GMI1000-infected tomato (cv. Bonny Best) seedling roots.

Table S2. Strains, plasmids and primers used in this study.

Dataset S1: Relative quantification of metabolites in tomato xylem sap.

(A) Comparison of metabolites in healthy versus *R. solanacearum*-infected sap. (B) Comparison of metabolites in *R. solanacearum*-infected tomato sap with or without 3 h incubation with *R. solanacearum* GMI1000.

5 A pathogen effector subverts translational regulation to boost host polyamine levels

This chapter is identical to the manuscript:

Wu, Dousheng, Von Roepenack-Lahaye, Edda, Buntru, Matthias, de Lange, Orlando, Schandry, Niklas, L Pérez-Quintero, Alvaro, Weinberg, Zasha, M. Lowe-Power, Tiffany, Szurek, Boris, J. Michael, Anthony, Allen, Caitilyn, Schillberg, Stefan & Lahaye, Thomas

A pathogen effector subverts translational regulation to boost host polyamine levels

Cell Host & Microbe (in revision) (<https://dx.doi.org/10.2139/ssrn.3376660>)

A pathogen effector subverts translational regulation to boost host polyamine levels

Dousheng Wu¹, Edda Von Roepenack-Lahaye¹, Matthias Buntru², Orlando de Lange^{1†},
Niklas Schandry^{1‡}, Alvaro L Pérez-Quintero^{3§}, Zasha Weinberg⁴, Tiffany M. Lowe-Power^{5¶},
5 Boris Szurek³, Anthony J. Michael⁶, Caitilyn Allen⁵, Stefan Schillberg², Thomas Lahaye^{1*}

¹Center for Plant Molecular Biology, Eberhard-Karls-University Tübingen, Auf der
Morgenstelle 32, 72076 Tübingen, Germany

²Fraunhofer Institute for Molecular Biology and Applied Ecology IME, Forckenbeckstrasse 6,
52074 Aachen, Germany

10 ³UMR IPME, Institut de Recherche pour le Développement, France

⁴Department of Computer Science and Interdisciplinary Center for Bioinformatics,
Universität Leipzig, D-04107 Leipzig, Germany

⁵Department of Plant Pathology, University of Wisconsin – Madison, Madison, WI 53706,
USA

15 ⁶Department of Biochemistry, University of Texas Southwestern Medical Center, Dallas, TX
75390, USA

[†]Present address: University of Washington, Department of Electrical Engineering, Seattle,
WA, USA

20 [‡]Present address: Gregor Mendel Institute of Molecular Plant Biology (GMI), Austrian
Academy of Sciences, Vienna BioCenter (VBC), Dr. Bohr-Gasse 3, 1030 Vienna, Austria

[§]Present address: Department of Bioagricultural Sciences and Pest Management, Colorado
State University, Fort Collins 80523-1177, USA

[¶]Present address: Plant and Microbial Biology Department, University of California Berkeley,
Berkeley CA 94720-3202; USA

25 *Correspondence to: thomas.lahaye@zmbp.uni-tuebingen.de

Summary

Pathogenic bacteria inject effector proteins into host cells to manipulate cellular processes promoting infection. Transcription-activator-like effectors (TALEs), an effector class found
30 in some plant-pathogenic bacteria, transcriptionally activate host genes to promote disease. We have identified *arginine decarboxylase (ADC)* genes as the sole host targets of Brg11, a TALE-like effector from the bacterial broad-host-range plant pathogen *Ralstonia solanacearum*. Brg11 targets the *ADC-box*, a 50-bp motif upstream of *ADC* genes broadly conserved across land plants. The transcribed *ADC-box* attenuates translation from native
35 *ADC* mRNAs. Yet, Brg11 induces transcription of truncated *ADC* mRNA lacking the 5' *ADC-box*, thus bypassing translational control. ADCs are rate-limiting enzymes of polyamine biosynthesis, and we show that the Brg11-induced elevation of polyamine levels triggers a plant defense reaction that likely inhibits bacterial niche-competitors, but not *R. solanacearum*. Our findings illustrate a novel concept in effector biology whereby bacterial
40 effectors act as mediators of tripartite microbe-host-microbe interactions.

Main Text

Virulence of bacterial pathogens of plants and animals relies on effector proteins that bacteria inject via their type III (T3), type IV (T4), or type VI (T6) secretion systems directly into the cytoplasm of eukaryotic and prokaryotic target cells¹⁻³. Bacterial T4- and T6-effectors are typically injected into antagonistic bacteria where they act as potent toxins^{4,5}. By contrast, bacterial T3 effectors are generally injected into eukaryotic host cells where they manipulate host cells to promote bacterial disease⁶. Analysis of T3 effector knock-out strains in the context of dipartite host-pathogen interactions often failed to uncover a virulence contribution for given T3 effectors. It thus seems plausible that elucidation of T3 effector function requires an appropriate testing environment that considers their functional contributions not only in the context of host-microbe but also in the context of microbe-microbe interactions.

The bacterial protein Brg11, is a T3 effector from the bacterial broad-host-range plant pathogen *Ralstonia solanacearum*^{7,8}. Brg11 is structurally related to transcription activator-like effectors (TALEs) from the bacterial genus *Xanthomonas*, a class of T3 effectors that bind to effector binding elements (EBEs) in plant genomes and activate transcription of downstream host genes to promote disease⁹. Given the homology of *R. solanacearum* Brg11 to *Xanthomonas* TALEs, it is conceivable that Brg11 promotes disease through transcriptional activation of host genes. Previously, we identified a 17 bp sequence that mediates *in planta* Brg11 dependent promoter-reporter activation¹⁰. However, no host promoters containing a Brg11-compatible target site (*Brg11-EBE*) have been identified and thus it is still unclear how Brg11 promotes bacterial disease.

Brg11 targets exclusively host *ADC* genes

To identify Brg11 host target genes we scanned the tomato promoterome for sequences related to the previously identified 17 bp Brg11 target sequence¹⁰. Each of the top 25 predicted *EBEs* was inserted into a minimal promoter and studied for Brg11-dependent activation using promoter-reporter fusions. These assays revealed that only the two sequence-identical *EBEs* upstream of *arginine decarboxylase 1* ([*Solanum lycopersicum*] *SLADC1*) and *arginine decarboxylase 2* (*SLADC2*) genes mediate Brg11-dependent reporter activation (Extended Data Fig. 1). To confirm functionality of these *Brg11-EBEs* in the context of their native promoters, we fused *SLADC1/2* upstream sequences (~350 bp 5' of ATG), to a reporter gene and found that both sequences mediate Brg11-dependent reporter activation (Fig. 1a, b). Notably, mutating the *Brg11-EBEs* in *SLADC1/2* upstream sequences abolished Brg11-dependent reporter activation (Fig. 1a, b), demonstrating that the integrity of the *Brg11-EBEs* is crucial to Brg11-dependent gene activation.

To determine if Brg11 can activate genome-embedded *SLADC1/2* genes, *R. solanacearum* strains with or without Brg11 were delivered into tomato leaves via blunt-end syringe infiltration. The Brg11-containing strain was observed to increase *SLADC1/2* transcript levels approximately two-fold relative to the Brg11-lacking strain (Fig. 1c). Since *R. solanacearum* is a root-adapted pathogen, it seemed plausible that T3SS-mediated delivery of Brg11, and thus activation of *SLADC1/2* genes in leaf tissue, was moderate. We therefore studied *SLADC1/2* activation following T3SS-mediated delivery of Brg11 via the tomato leaf pathogen *X. euvesicatoria*. To do so, we fused the N-terminal translocation domain of an *X. euvesicatoria* effector to either Brg11 or a Brg11-derivative lacking the DNA binding domain (Brg11 Δ DBD) yielding Brg11* and Brg11 Δ DBD*, respectively. We observed that Brg11* induced 15- to 25-fold higher *SLADC1/2* transcript levels relative to Brg11 Δ DBD* (Fig. 1d, Extended Data Fig. 2). To test if Brg11-dependent activation of *SLADC1/2* depends on the

integrity of corresponding upstream *Brg11-EBEs*, we generated heritable mutations in both *Brg11-EBEs* by CRISPR-Cas9 mutagenesis (Fig. 1e). Indeed, Brg11-dependent activation of *SLADC1/2* was abolished in the tomato double mutant lacking functional *Brg11-EBEs* upstream of *SLADC1/2* ($\Delta 1/2$ -*Brg11-EBE*) (Fig. 1c, d). This demonstrates that Brg11 activates the transcription of *SLADC1/2* genes, and that this activation is reliant on the integrity of Brg11 target sites upstream of the *SLADC1/2* coding sequences (CDS).

We then sought to clarify whether Brg11 has other direct target genes besides *SLADC1/2*. Using RNA-seq, tomato transcriptomes were compared 24 hours after inoculation with *X. euvesicatoria* strains containing either Brg11* or Brg11 Δ DBD*. 117 host transcripts, including *SLADC1/2* showed a Brg11-dependent increase (fold-change > 2.0, corrected $p < 0.05$) (Extended Data Fig. 3a, b, Supplementary Table 1). In addition to *SLADC1/2*, *SI12g009000* was the only induced tomato gene with a *Brg11-EBE*-like sequence upstream of its CDS (Extended Data Fig. 3c, d). However, we found that the putative *Brg11-EBE* upstream of *SI12g009000* does not mediate Brg11-dependent reporter activation (Extended Data Fig. 3e). Taken together, these data show that *SLADC1* and *SLADC2* are the only direct target genes of Brg11 in tomato.

The Brg11 containing *R. solanacearum* strain GMI1000 was originally isolated from tomato, but it infects a broad range of important agricultural crops such as eggplant, tobacco, potato, and pepper^{11,12}. We thus hypothesized that Brg11 activates *ADC* genes not only in tomato, but across many or possibly all *R. solanacearum* host species. *In silico* studies uncovered the *Brg11-EBE* sequence upstream of *ADC* genes in all ten investigated host genomes. In four of the host species, however, the *Brg11-EBEs* had polymorphisms with respect to the tomato *Brg11-EBE* (Fig. 2a). Promoter-reporter assays showed however, that these polymorphisms do not disturb Brg11-dependent activation (Fig. 2b). Next, Brg11 was delivered into three representative host species (*Solanum melongena* [eggplant], *Nicotiana*

benthamiana and *Nicotiana tabacum*) to study if Brg11 activates these genome-embedded *ADC* genes. We found Brg11-dependent *ADC* transcript accumulation in all three host species (Fig. 2c-e), suggesting that Brg11 targets *ADC* genes in most, if not all, *R. solanacearum* host plants.

Brg11 induces truncated, highly-active *ADC* mRNAs

*ADC*s are rate-limiting enzymes in polyamine (PA) biosynthesis¹³. Expression of enzymes involved in PA biosynthesis is often translationally controlled by regulatory elements in the 5'UTR of corresponding transcripts¹⁴. TALE-induced and native host transcripts often differ in the length of their 5'UTRs^{15,16}, and thus we wondered if Brg11-induced and native *ADC* transcripts are structurally and functionally distinct. Accordingly, we performed 5' rapid amplification of cDNA ends (RACE) to determine the 5'UTR of *ADC* transcripts in the presence and absence of Brg11. We found that the 5'UTR of Brg11-induced *ADC* transcripts in tomato, eggplant and *N. benthamiana* was consistently >300 bp shorter than the 5'UTR of corresponding native *ADC* transcripts (Fig. 3a-e).

To clarify if the long 5'UTR of native *ADC* transcripts and the short 5'UTR of Brg11-induced *ADC* transcripts differ in translational activity, we cloned long and short 5'UTRs of *SLADC1/2* genes upstream of a *GFP* reporter under transcriptional control of the constitutive 35S promoter (Fig. 3f). The T-DNA contained in addition a constitutively expressed dsRED fluorophore for normalization of GFP reporter read out. Delivery of these reporter constructs into *N. benthamiana* leaves via *Agrobacterium* showed that constructs with the short 5'UTR had 2.5- to 3.5-fold higher GFP intensity relative to constructs containing the long 5'UTR (Fig. 3g, h). No significant differences were observed in reporter mRNA levels (Extended Data Fig. 4a), suggesting that different 5'UTRs do not cause differences in mRNA stability. We complemented these *in planta* assays with *in vitro* translation assays using tobacco cell lysates^{17,18}. In agreement with the *in planta* assays, the *in vitro* studies showed that

constructs containing the short 5'UTR had approximately 4-fold higher GFP intensity relative to constructs containing the long 5'UTR (Extended Data Fig. 5a). Quantification of reporter mRNA levels after *in vitro* translation showed no significant differences in transcript levels (Extended Data Fig. 5b). These results suggest that Brg11-induced host *ADC* transcripts with truncated 5'UTRs have higher translational activity than native *ADC* transcripts.

An ancient *cis*-element limits translation of *ADC* mRNAs

The low translational activity observed for long 5'UTRs of native *SLADCI/2* transcripts suggests the presence of *cis*-elements that inhibit translation. In addition to small upstream ORFs (uORFs), GC-rich regions within the 5'UTR can repress translation since they lead to secondary RNA structures that impede ribosomal scanning for the initiation codon^{19,20}. We identified a ~50 bp GC-rich sequence motif in the 5'UTR of native *ADC* transcripts that is conserved in genomes of seed plant species (embryophyta [gymnosperms and angiosperms]) and we designated it as the *ADC-box* (Extended Data Fig. 6). Notably, the uORF and the transcribed *ADC-box* are both present in the long 5'UTR of native *SLADCI/2* transcripts, but absent from the short 5'UTR of Brg11-induced *SLADCI/2* transcripts (Fig. 4a). To determine the functional relevance of the uORF and the *ADC-box*, we generated corresponding *SLADCI* deletion derivatives and tested their translational activity by the *in vivo* and *in vitro* assays described above. In both assays, deletion of the *ADC-box* significantly increased translational activity, and in contrast, deletion of the uORF only slightly increased translational activity (Fig. 4b, Extended Data Fig. 4b, 5c). These results suggest that the *ADC-box* has a more profound inhibitory effect on translation of *ADC* transcripts than the uORF. It is worth noting that native *ADC* transcripts from several plant species lack an uORF (e.g., *Poaceae* species), but they do contain an *ADC-box* (Extended Data Fig. 7), suggesting that uORFs but not the *ADC-box* are functionally dispensable in these *ADC* transcripts.

Based on the conserved angiosperm sequences, we predicted an RNA secondary structure for the *ADC-box* that utilizes four consecutive GC-rich stretches, termed GC1-4, (Fig. 4c). This predicted structure consists of two RNA duplex regions (RDRs) formed by complementary pairings of GC1 to GC4 (RDR α) and GC2 to GC3 (RDR β). The bases predicted to form RDR β , but not the bases predicted to form RDR α are conserved in seed plants and seedless land plants (mosses and ferns) (Fig. 4e). This suggests that the *ADC-box* is an ancient element of translational regulation that was present in non-vascular plants (Fig. 4f), and that evolved further during speciation of seed plants. To study functional relevance of the GC-rich elements, we mutated GC1 (Δ GC1), GC2 (Δ GC1), or both GC-rich stretches (Δ GC1/2) within the long 5'UTR of native *SLADCI* transcripts and tested their translational activity. Individual mutations of either GC1 or GC2 moderately increased translational activity compared to the long 5'UTR of native *SLADCI* transcripts. The Δ GC1/2 double mutant had translational activity comparable to that of the short 5'UTR of Brg11-induced *SLADCI* transcripts (Fig. 4d). No significant differences were observed for reporter mRNA levels (Extended Data Fig. 4c), suggesting that reporter mRNAs do not differ in stability. Altogether, mutational analysis of the *ADC-box* demonstrates its inhibitory impact on translation and is consistent with the tentative RNA secondary structure.

Brg11 boosts host polyamine levels

ADCs catalyze conversion of arginine to agmatine, and this enzymatic activity provides a simple proxy for ADC expression. To determine ADC activity, we established a mass spectrometry (MS) based assay in which conversion of ^{13}C arginine to ^{13}C agmatine was quantified in homogenized tissue of pathogen-infected tomato leaves (Extended Data Fig. 8a-d). Delivery of Brg11 into tomato leaves via *R. solanacearum* or *X. euvesicatoria* resulted in 8- and 25-fold increase in ^{13}C agmatine levels, respectively (Fig. 5a, b). Importantly, Brg11 did not increase ^{13}C agmatine levels in the tomato double mutant Δ 1/2-*Brg11*-*EBE*,

demonstrating that the integrity of the *Brg11-EBEs* upstream of *SIADC1/2* is crucial to *in planta* function of Brg11. The ADC inhibitor DL- α -difluoromethylarginine (DFMA)²¹ reduced the observed increase in ¹³C agmatine by 4-fold, confirming that increase of ¹³C agmatine is the consequence of increased ADC activity (Extended Data Fig. 8e, f). These results show that pathogen-mediated delivery of Brg11 into plant cells causes increased ADC activity.

In plants, the ADC product of agmatine is converted to putrescine, a PA that serves either as a precursor for the longer PAs spermine and spermidine, or can be catabolized to γ -aminobutyric acid (GABA)^{22,23}. To determine Brg11-induced changes in metabolite composition, we inoculated tomato leaves with *X. euvesicatoria* strains containing either Brg11* or Brg11 Δ DBD* and profiled metabolites 24 hours post inoculation. MS-based analysis did not reveal significant Brg11-dependent changes for spermine, spermidine, or GABA levels. By contrast, Brg11 induced a five- and four-fold increase in agmatine and putrescine levels, respectively (Fig. 5c-g). Since the observed cellular concentration of putrescine is about 100-fold higher than that of agmatine, it can be concluded that Brg11 is causing the most significant metabolic change in putrescine levels.

ADCs attenuate *in planta* growth of *P. syringae*

Plant *ADC* genes are involved in defense reactions against microbial pathogens²⁴, and thus we wondered how *R. solanacearum* would benefit from such changes. *R. solanacearum* strains containing or lacking Brg11 grew similarly in tomato leaves (Fig. 6a) suggesting that elevated ADC activity is neither beneficial nor detrimental to *in planta* growth of *R. solanacearum*. Recent studies on *R. solanacearum*-infected tomato roots uncovered microbes that suppress bacterial wilt disease²⁵, so we speculated that activation of host *ADC* genes inhibits growth of bacterial niche competitors of *R. solanacearum*. To test this hypothesis, we studied *in planta* growth of the tomato leaf pathogens *X. euvesicatoria* and *Pseudomonas*

syringae. While these two pathogens do not colonize roots and thus are unlikely direct niche competitors of *R. solanacearum*, they provide a conceptual test system to clarify if *ADC* gene activation can attenuate *in planta* growth of plant-associated microbes. We first studied *in* 215 *planta* growth of *X. euvesicatoria* strains containing either Brg11* or Brg11ΔDBD*, and found that both strains grew similarly in tomato leaves (Fig. 6b). To see if *ADC* gene activation affects *in planta* growth of *P. syringae*, we co-infiltrated *P. syringae* with *X. euvesicatoria* strains delivering either Brg11* or Brg11ΔDBD*. We found that *X. euvesicatoria* strains containing Brg11* but not strains containing Brg11ΔDBD* attenuated 220 growth of co-cultivated *P. syringae* suggesting that activation of *SLADC1/2* has an inhibitory effect on *P. syringae* (Fig. 6c). To obtain further evidence that *SLADC1/2* genes are involved in resistance against *P. syringae* we used CRISPR-Cas9 mutagenesis to induce heritable mutations in the CDS of *SLADC1/2*. Inoculation of tomato wild-type and the *Sladc1/2* double mutant revealed that the population size of *P. syringae* was almost ten-fold higher in the 225 *Sladc1/2* double mutants, confirming that *SLADC1/2* genes are involved in plant resistance against *P. syringae* (Fig. 6d). By contrast, population sizes of *R. solanacearum* and *X. euvesicatoria* were indistinguishable in *Sladc1/2* double mutants and tomato wild-type plants (Fig. 6e, f). In summation, our findings are consistent with a model where Brg11-mediated activation of *ADC* genes attenuates growth of microbes that are possibly detrimental to *R.* 230 *solanacearum*.

DISCUSSION

T3 effectors generally target key components of the host's immune system to promote bacterial disease ²⁶. We discovered that the *R. solanacearum* type III effector Brg11
235 exclusively targets plant *ADC* genes, implying that *ADC* genes are crucial to plant immune reactions. Since the presence of Brg11 in *R. solanacearum* was neither beneficial nor detrimental in the context of this dipartite plant-pathogen interaction we propose a tripartite interaction model where Brg11 induces changes in host cells that in turn attenuate growth of microbes occupying the same habitat as *R. solanacearum* (Extended Data Fig. 9).

240 Polyamines are ubiquitous in plant and animal cells and their homeostasis is maintained in both kingdoms predominantly by *cis*-elements of transcript UTRs that control translational regulation of PA anabolic/catabolic enzymes ²⁷. Our work resulted in the identification of the *ADC*-box, a novel *cis*-element that is conserved across all land plant species (Fig. 4e). In native *ADC* mRNAs the *ADC*-box is located in the 5'UTR and attenuates
245 translation (Fig. 4b, d). Maintaining PA homeostasis is essential for plant cell survival ²⁸, and thus the *ADC*-box is likely part of a general feedback control mechanism that avoids the synthesis of cell-toxic PA levels. *R. solanacearum* Brg11 bypasses translational control by inducing *ADC* mRNAs with a short 5'UTR lacking the *ADC*-box, thus boosting host PA levels (Extended Data Fig. 10).

250 Our metabolic profiling revealed that the Brg11-mediated increase in host *ADC* activity causes the most pronounced increase in putrescine levels (Fig. 5). If host putrescine levels affect not only *R. solanacearum*, but are also relevant to the pathogenesis of other plant-associated microbes, one would expect that these microbes deliberately interfere with putrescine levels. Indeed, a TALE from the Brassica pathogen *X. campestris* is predicted to
255 activate a host *ADC* gene and thus to increase putrescine levels ²⁹. Reciprocally, several *P. syringae* strains produce the diffusible toxin phaseolotoxin that inhibits plant anabolic

pathways that cause an increase putrescine levels ³⁰. Similarly, the *P. syringae* toxin coronatine, a well-known suppressor of plant defense, induces expression of *Arabidopsis* NATA1, an enzyme that induces acetylation of putrescine, and thus the reduction of
260 putrescine levels ³¹.

To conclude, there is ample evidence to support the notion that *R. solanacearum* and *Xanthomonas* strains deliberately increase putrescine levels, while *P. syringae* pointedly decreases putrescine levels. Therefore, it is plausible that putrescine levels represent a central hub that is targeted by phytopathogenic microbes in an effort to manipulate plant immune
265 reactions for their own selfish interests.

Figure 1

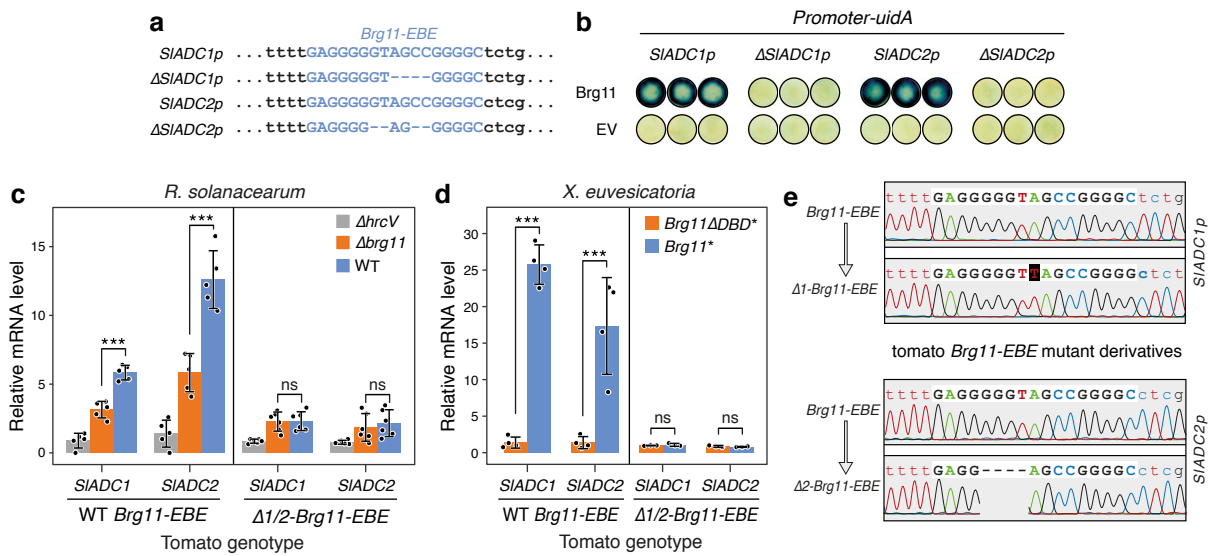


Figure 1 | The *R. solanacearum* effector Brg11 transcriptionally activates tomato *ADC* genes in a *Brg11-EBE* dependent manner.

a, Schematic display of promoter-reporter constructs studied in **(b)**. Upper case blue font indicates the *Brg11-EBE* and mutated derivatives (Δ) within the *SIADC1/2* promoters (*SIADC1/2p*). Hyphens indicate deleted nucleotides. **b**, Gene activation by Brg11 depends on integrity of the *Brg11-EBE*. Depicted promoter-*uidA* fusions were co-delivered with either 35S promoter-driven *brg11* (Brg11) or an empty vector control (EV) into *N. benthamiana* leaves via *A. tumefaciens*. GUS staining was carried out two days post infiltration. **c**, **d**, Delivery of Brg11 into tomato leaves activates *SIADC1/2* genes in a *Brg11-EBE*-dependent manner. The bars represent *SIADC1/2* mRNA levels of depicted tomato genotypes measured by qPCR upon inoculation of depicted *R. solanacearum* (**c**) and *X. euvesicatoria* (**d**) strains. Data are mean \pm SD; *** $P < 0.001$ (Student's t-test); ns, not significant; solid circles show values of individual biological samples. **e**, CRISPR-Cas9 mediated mutations in the *Brg11-EBEs* of *SIADC1p* and *SIADC2p*. Mutations in the *Brg11-EBE* of *SIADC1* and *SIADC2* promoters are indicated by black background and hyphens, respectively.

Figure 2

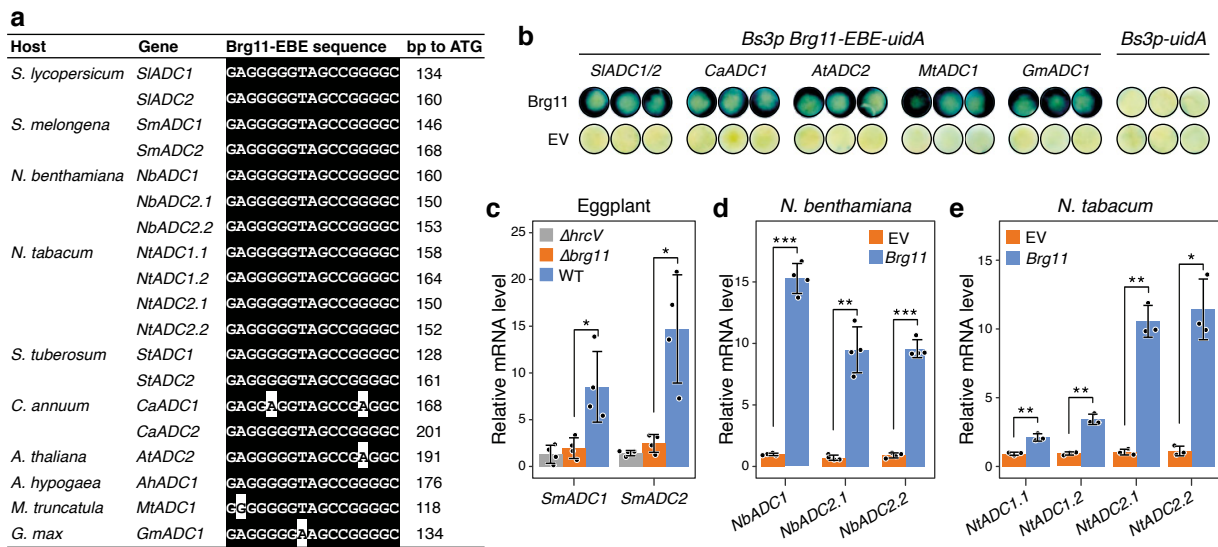


Figure 2 | Brg11 targets ADC genes across different *R. solanacearum* hosts.

a, The *Brg11-EBE* is conserved across multiple *R. solanacearum* host species. Nucleotides that differ with respect to the *Brg11-EBE* in *SlADC1/2* (uppermost sequence) are highlighted by black font on white background. **b**, Nucleotide polymorphisms in *Brg11-EBEs* of distinct host species do not affect Brg11-mediated gene activation. *Uida* reporter gene constructs, driven by *Bs3p* promoter-derivatives containing the depicted *Brg11-EBEs*, were co-delivered with either a *35S* promoter-driven *Brg11* (Brg11) or empty vector control (EV) into *N. benthamiana* leaves via *A. tumefaciens*. GUS staining of leaf discs was carried out at two days post infiltration. **c-e**, Brg11 induces increase of *ADC* transcripts in three representative host species. Plant leaves were infiltrated with either *R. solanacearum* strains (**c**) or *A. tumefaciens* strains (**d, e**) containing either a *35S* promoter-driven *Brg11* or EV. Infiltrated leaves were harvested at one day (**c**) or two days (**d, e**) after inoculation for qPCR analysis. Data are mean \pm SD ($n = 4$ for eggplant and *N. benthamiana*, $n = 3$ for *N. tabacum*); $*P < 0.05$; $**P < 0.01$; $***P < 0.001$ (Student's t-test); solid circles, individual biological replicates.

Figure 3

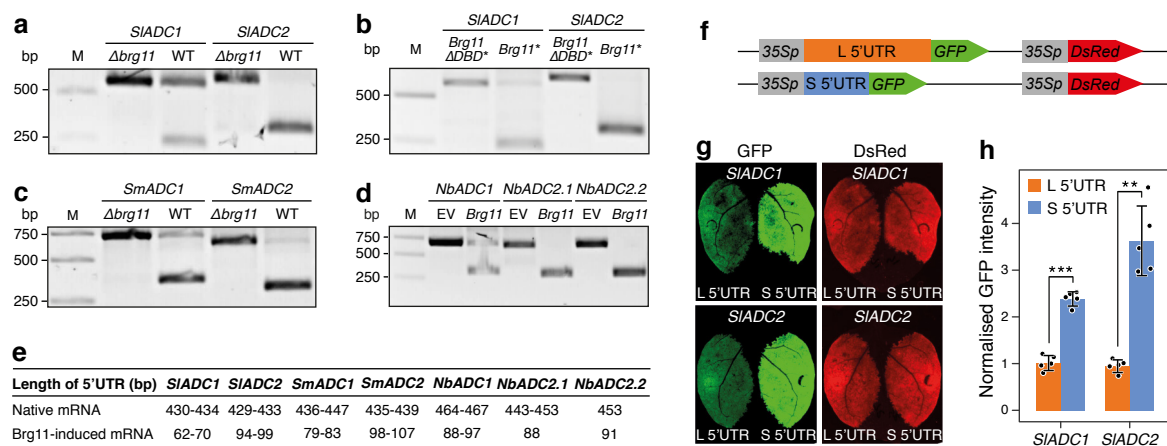


Figure 3 | Brg11 induced *ADC* transcripts with short 5'UTRs have higher translational activity than native *ADC* transcripts with long 5'UTRs.

a-d, 5'RACE in three representative *R. solanacearum* hosts shows that Brg11 induces *ADC* transcripts with short 5'UTRs. 5'RACE was conducted on (a) tomato (*Solanum lycopersicum* [*Sl*]) inoculated with *R. solanacearum*, (b) tomato inoculated with *X. euvesicatoria*, (c) eggplant (*Solanum melongena* [*Sm*]) inoculated with *R. solanacearum* or (d) *N. benthamiana* (*Nb*) inoculated with *A. tumefaciens*. M, DNA marker. **e**, Length of 5'UTRs of native and Brg11-induced *ADC* transcripts in three representative *R. solanacearum* host species. **f**, Schematic display of the dual reporter constructs used to determine *in vivo* translational activity of *SIADC1/2* 5'UTRs. 35S-promoter driven *DsRed* was used for normalization. L 5'UTR, long 5'UTR from native *ADC* transcripts; S 5'UTR, short 5'UTR of Brg11-induced *ADC* transcripts. **g, h**, The short 5'UTR of Brg11-induced *ADC* mRNAs and the long 5'UTR of native *ADC* mRNAs have high and low translational activity, respectively. 36 hours after *A. tumefaciens* mediated delivery of reporter constructs with depicted 5'UTRs into *N. benthamiana* leaves GFP fluorescence was monitored visually (**g**) and evaluated quantitatively (**h**). n = 5. Data are mean \pm SD; ** P < 0.01; *** P < 0.001 (Student's t test); solid circles, individual biological replicates.

Figure 4

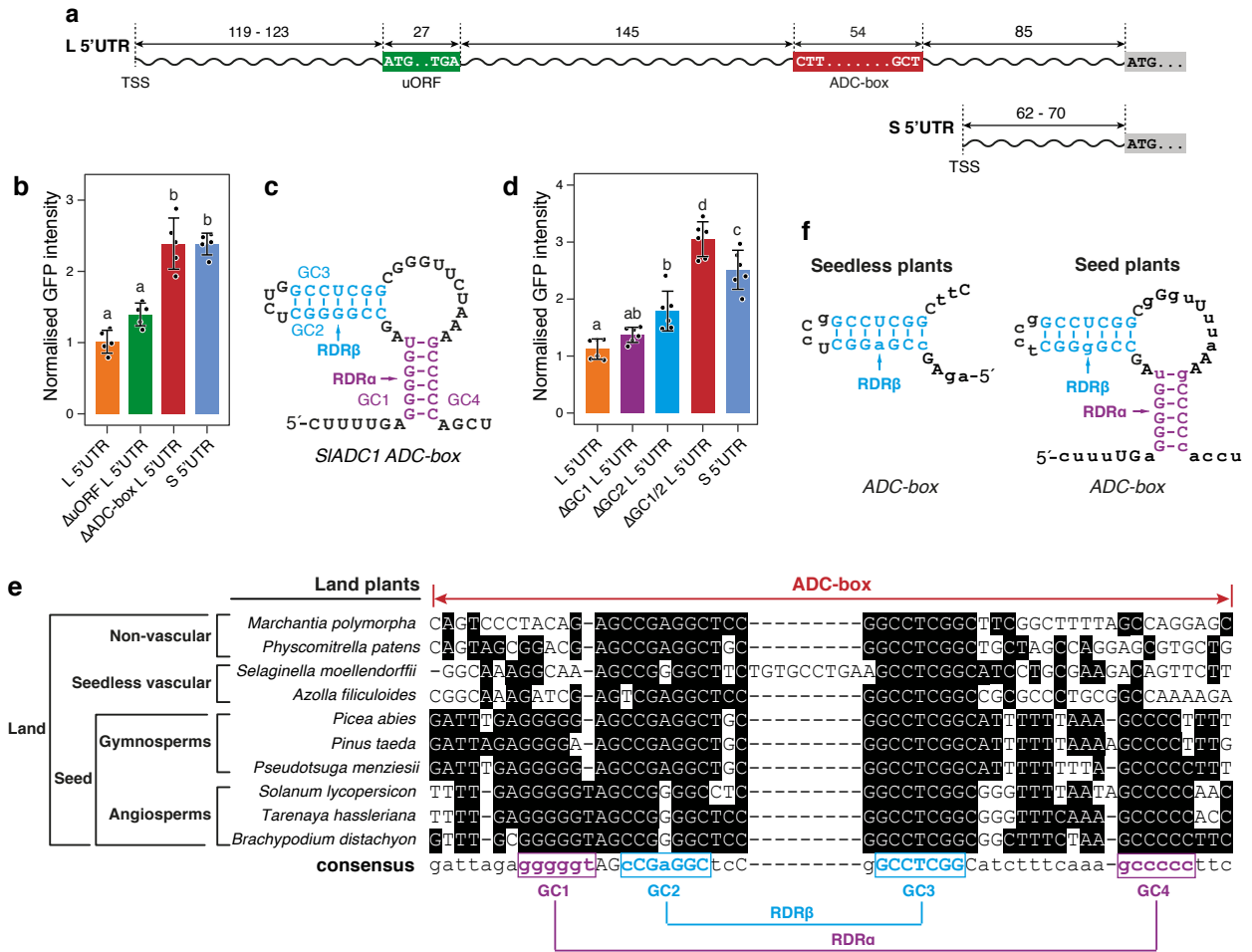


Figure 4 | The *ADC-box* is conserved across land plant species and acts as a translational repressor.

a, Schematic display of the 5'UTRs of long native *SIADC1* transcripts (L 5' UTR) and short Brg11-induced *SIADC1* transcripts (S 5' UTR). Numbers indicate bp-distances between depicted 5'UTR elements. TSS, transcription start site. **b**, Deletion of the *ADC-box* increases translation of corresponding 5'UTRs. Reporter constructs containing the L 5'UTR, the S 5'UTR or derivatives lacking either the uORF (Δ uORF) or the *ADC-box* (Δ ADC) were delivered into *N. benthamiana* leaves via *A. tumefaciens*. GFP fluorescence was quantified at 36 hpi. n = 5. **c**, Predicted RNA secondary structure of the *ADC-box*. GC-rich regions (GC1-4) and RNA duplex regions (RDR α [purple font], RDR β [blue font]) are depicted. **d**, The two predicted duplex regions in the 5'UTR of *SIADC1* have additive translational inhibitory effects. Reporter constructs containing the L 5'UTR, the S 5'UTR or corresponding derivatives with mutations in GC1 (Δ GC1), GC2 (Δ GC2) or both (Δ GC1/2) were delivered into *N. benthamiana* leaves using *A. tumefaciens*. GFP fluorescence was quantified at 36 hpi. n = 6. Data are mean \pm SD; ** P < 0.01; *** P < 0.001 (Student's t-test); lowercase letters indicate significance in one-way analysis of variance (ANOVA, TukeyHSD); solid circles, individual biological replicates. **e**, Seedless plants are conserved in GC2/3 but not in GC1/4. **f**, Tentative RNA secondary structure formed by *ADC-boxes* of seedless plants and seed plants. Capital letter indicates conserved nucleotides.

Figure 5

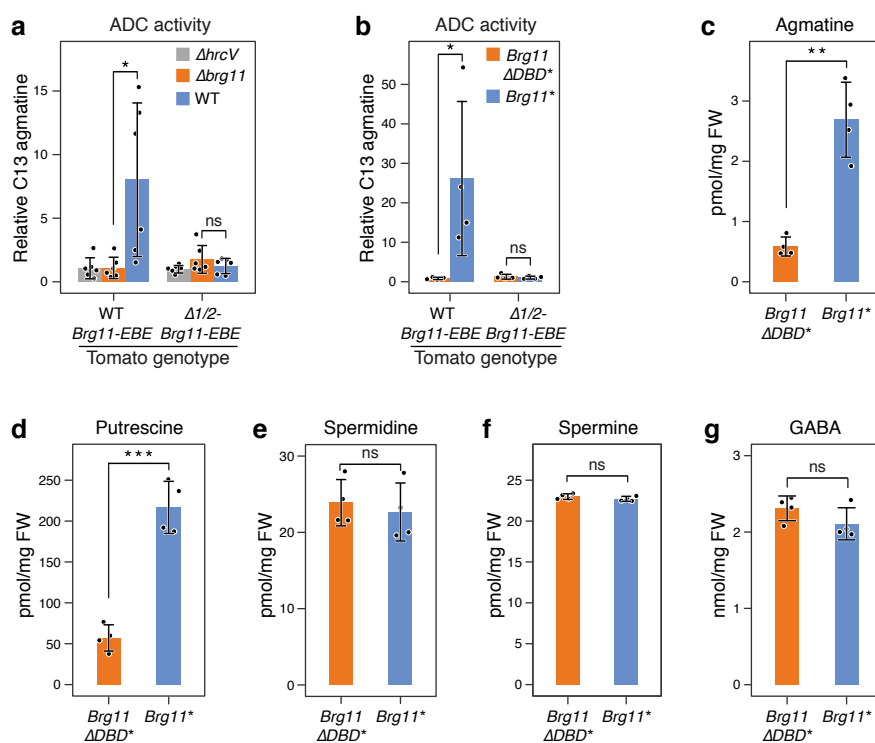


Figure 5 | *Brg11* increases ADC activity and putrescine levels.

a, b, *Brg11* increases ADC activity in a *Brg11*-*EBE*-dependent manner in tomato. Tomato leaves were inoculated with depicted *R. solanacearum* (**a**) or *X. euvesicatoria* (**b**) strains and inoculated tissue was collected 18 h (**a**) or 24 h (**b**) after infiltration. ¹³C arginine was added to homogenized tissue of inoculated tomato leaves and one hour later ¹³C agmatine was quantified by mass spectrometry (MS) thus providing a proxy for ADC activity. **c-g**, The depicted metabolites were quantified by MS, 24 hours after inoculation with depicted *X. euvesicatoria* strains in wild-type tomato. n = 4. Data are mean \pm SD; ***P* < 0.01; ****P* < 0.001; ns, not significant (Student's t test); solid circles, individual biological replicates.

Figure 6

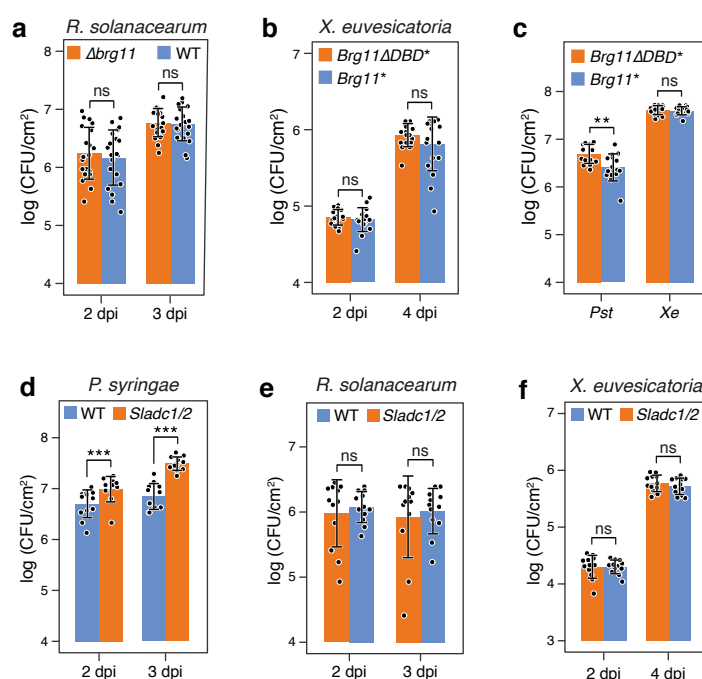


Figure 6 | Brg11 inhibits *in planta* growth of *P. syringae* but has no impact on *in planta* growth of *X. euvesicatoria* and *R. solanacearum*.

a, b, Brg11 has no impact on *in planta* growth of *R. solanacearum* and *X. euvesicatoria* in tomato. Bacterial counts of *R. solanacearum* (**a**) and *X. euvesicatoria* (**b**) were determined at indicated days post inoculation (dpi) upon infiltration with bacteria at 10⁵ CFU/ml (n = 20). **c**, *X. euvesicatoria* strain containing Brg11 reduces *in planta* growth of co-inoculated *P. syringae*. Bacterial populations in tomato wild-type plants were quantified upon mixed inoculation of *P. syringae* pv. *tomato* DC3000 (*Pst*) and *X. euvesicatoria* (*Xe*) delivering Brg11* or Brg11 Δ DBD* at 10⁵ CFU/ml and 10⁸ CFU/ml, respectively, at 2 dpi (n = 15). **d**, *Sladc1/2* double mutants are more susceptible to *Pst* than tomato wild-type plants. **e-f**, *In planta* growth of *R. solanacearum* and *X. euvesicatoria* in tomato *Sladc1/2* double mutants and tomato wild-type plants does not differ. Bacterial growth of inoculated tomato leaves (d-f) was quantified at depicted timepoints. Inoculation was carried with depicted bacteria at 10⁵ CFU/ml (n = 12). Data are mean \pm SD; **P* < 0.05; ***P* < 0.01; ****P* < 0.001; ns, not significant (Student's t-test); solid circles, individual biological replicates.

METHODS

EBE prediction

365 *EBE* prediction was carried out using Talvez v.3.1³² against putative promoter regions (1kb upstream of the translation start codon, both strands) of annotated tomato genes (SL3.0/ITAG3.10). The RVD-nucleotide matrix (Supplementary Table 2) used for prediction was modified to allow pairings for Brg11 (e.g. "G" at the zero position)¹⁰. The score indicates the likelihood of the predicted *Brg11-EBEs* to be activated by Brg11.

370 **Promoter-*uidA* reporter assays**

brg11 and *avrBs3* were assembled into pGWB641 via Gateway Cloning. The pepper *Bs3* promoter (343 bp upstream of ATG) and *SlADC1/2* promoters (350 bp upstream of ATG) were first cloned into pUC57 and then transferred to pGWB3* via Golden Gate assembly³³. Candidate *Brg11-EBEs* and targeted mutations were integrated into the *Bs3* promoter or
375 *SlADC1/2* promoters by PCR based mutagenesis. Primers used in this study were listed in Supplementary Table 3.

All constructs were transformed into *A. tumefaciens* strain GV3101 by electroporation. *A. tumefaciens* were grown in YEB medium supplemented with spectinomycin and rifampicin (for pGWB641-containing strains), or kanamycin and rifampicin (for pGWB3*-
380 containing strains) at 28°C for 24 h. Bacterial cells were collected by centrifugation, resuspended in inoculation medium (pH 5.6, 10 mM MgCl₂, 5 mM MES and 150 μM acetosyringone) and adjusted to an optical density at 600 nm (OD₆₀₀) of 0.8. Equal amount of *A. tumefaciens* strains delivering either the effector or the promoter-*uidA* fusions were mixed and infiltrated into 4-week-old *N. benthamiana* leaves with blunt-end syringe.

385 At 2 days post inoculation (dpi), leaf discs from infiltrated area were harvested and stained in GUS staining solution (pH= 7.0, 0.1 M sodium phosphate, 5 mM EDTA, 1 mM K₃[Fe(CN)₆], 1 mM K₄[Fe(CN)₆], 0.1% Triton X-100 and 0.05% X-Gluc) for 24 h, followed by washing in 70% ethanol for 2 days. Three representative stained leaf discs were scanned.

Bacterial strains and growth conditions

390 The *R. solanacearum* wild-type strain GMI1000 (WT), *brg11* mutant strain (Δ *brg11*) and *hrcV* mutant strain (Δ *hrcV*) were kind gifts from Stephane Genin and Nemo Peeters (LIPM, INRA, Toulouse, France). *R. solanacearum* were grown overnight in B medium (1% peptone, 0.1% tryptone, 0.1% yeast extract, 2.5% glucose) (for WT strain) or B medium supplemented

with gentamycin (for $\Delta brg11$ strain) or spectinomycin (for $\Delta hrcV$ strain) at 28°C. Bacterial
395 cells were collected by centrifugation, resuspended in sterile MiliQ water and adjusted to
required OD₆₀₀.

The *X. euvesicatoria* strains translocating Brg11* or Brg11 Δ DBD* (also named as
Hpx17)³⁴ were generated as follows: the type III secretion signal (T3S signal) of AvrBs3 (N-
terminal 152 amino acids) and the full-length coding sequence of Brg11 or Brg11 Δ DBD
400 were PCR amplified and cloned together into pENTR CACC-AAGG. pENTR carrying the
above fragments were then digested with BamHI. The products at right size were gel purified
and further ligated into BamHI digested pDSK602 vector in which contains the *lac*
constitutive promoter in front of BamHI restriction site to drive the expression of the inserted
genes. Cloned constructs were transformed into *X. euvesicatoria* 85-10 by electroporation. *X.*
405 *euvesicatoria* strains delivering Brg11* or Brg11 Δ DBD* were grown in NYG medium (0.5%
peptone, 0.3% yeast extract, 2% glycerol) supplemented with spectinomycin and rifampicin
at 28°C. Bacterial cells were collected by centrifugation, resuspended in sterile MiliQ water
and adjusted to required OD₆₀₀.

P. syringae pv. *tomato* DC3000 was kindly provided by Andrea Gust (ZMBP,
410 University of Tübingen) and grown in NYG medium supplemented with rifampicin at 28°C.
Bacterial cells were collected by centrifugation, resuspended in sterile MiliQ water and
adjusted to required OD₆₀₀.

Plant inoculation, RNA extraction and quantitative real-time PCR

Four- to five-week-old tomato plants (Moneymaker or its corresponding mutants) were
415 inoculated with either the *R. solanacearum* WT strain, $\Delta brg11$ or $\Delta hrcV$ at OD₆₀₀ 0.1, and
harvested at 18 hpi, or *X. euvesicatoria* strains expressing Brg11* or Brg11 Δ DBD* at OD₆₀₀
0.4 and harvested at 24 hpi. Five-week-old eggplant plants (Zebrina) were inoculated with the
R. solanacearum WT strain, $\Delta brg11$ and $\Delta hrcV$ at OD₆₀₀ 0.1, and harvested at 24 hpi. For *A.*
tumefaciens mediated transient expression of Brg11 in *N. benthamiana* and *N. tabacum*,
420 bacterial suspensions were adjusted to OD₆₀₀ 0.4 and infiltrated into four- to five-week-old
plants. Infiltrated leaves were sampled at 2 dpi.

Total RNA were isolated from infiltrated tissue with the GeneMATRIX Universal
RNA Purification Kit (EURx) according to the manufacturer's instruction. The quality of
total RNA was checked by nanodrop. cDNA was synthesised from 500 ng of total RNA with
425 the RevertAid First Strand cDNA Synthesis Kit (Thermo Scientific) according to the
procedure provided by the company. Quantitative real-time PCR (qPCR) was performed in 8

μl reactions (BioRad, CFX384), each containing 1 pmol of forward and reverse primer, 2 μl of 1 to 20 diluted cDNA and 4 μl of MESA BLUE qPCR MasterMix Plus for SYBR® Assay (Eurogentec). The specificity of qPCR primers were checked by running a melting curve.
430 *TIP41* from tomato, *18S rRNA* from eggplant, *PP2A* from *N. benthamiana* and *EF 1α* from *N. tabacum* were used as reference genes for internal normalization, respectively³⁵⁻³⁸. Relative expression was calculated with $2^{-\Delta\Delta CT}$.

RNA sequencing and analysis

RNA quality was assessed with the Agilent 2100 Bioanalyzer system. Samples with RNA integrity number higher than 7.0 were selected for library generation. Poly(A) selected sequencing libraries were generated from 100 ng of total RNA using the NEBNext Ultra II Directional RNA Library Prep Kit for Illumina. All libraries were sequenced on the Illumina NextSeq 500 platform in single-end mode with read length 75 bp and at a depth of approx. 20 million clusters each. Library preparation and sequencing were performed by the same
440 individual and a sequencing design aimed to minimize technical batch effects was chosen.

Quality of raw RNA-seq data in FASTQ files was assessed using ReadQC (ngs-bits version 2018_06) to identify potential sequencing cycles with low average quality and base distribution bias. Reads were preprocessed with skewer (version 0.2.2) and aligned using STAR (version 2.5.4a) allowing spliced read alignment to the tomato reference genome
445 (version SL3.0, International Tomato Genome Sequencing Project). Alignment quality was analyzed using MappingQC (ngs-bits version 2018_06) and visually inspected with Broad Integrative Genome Viewer (version 2.4.11). Based on the genome annotation ITAG (version 3.20), read counts for all genes were obtained using subread (version 1.6.0).

For differential gene expression analysis, raw gene counts were filtered to only retain
450 genes with at least 1 cpm (count per million) in at least half of the samples, leaving >17,000 genes for determining differential expression in each of the pair-wise comparisons between experimental groups. The analysis was performed with edgeR (version 3.22.3).

CRISPR-Cas9 mediated mutation of the *Brg11-EBEs* and *SLADC1/2* in tomato

The one-vector CRISPR-Cas9 cloning system (p201N Cas9)³⁹ was used to mutate the
455 *Brg11-EBEs* in wild-type tomato money maker. Since the *Brg11-EBEs* and their surrounding regions were conserved between *SLADC1* and *SLADC2* promoters, one guide RNA (gRNA) was designed to target the *Brg11-EBEs* in both promoters. The cloning of the gRNA into the T-DNA vector was done as previously described³⁹. The construct was introduced into *A.*

tumefaciens strain GV3101 by electroporation. *A. tumefaciens* containing both the gRNA and the *Cas9* gene was transformed into tomato as previously described (Wittmann et al., 2016). For screening of mutant lines, total genomic DNA was extracted from individual lines and the regions containing the target sites were PCR amplified and sequenced. The mutant line (#20) that had homozygous mutations in *Brg11-EBEs* of both *SLADC1/2* promoters was kept for producing seeds. In the next generation, *Cas9* transgene free plants were screened by PCR amplification of the *Cas9* coding sequence. The inoculation assay was performed on T3 progeny. The generation of *SLADC1* and *SLADC2* CDS single mutants (*Sladc1* and *Sladc2*) were the same as for the *Brg11-EBEs* mutant except that two gRNAs were designed for each target gene. The *SLADC1/2* double mutants (*Sladc1/2*) were obtained by crossing *Sladc1* with *Sladc2*. F3 generation were used for inoculation analysis.

470 **5' Rapid amplification of cDNA ends**

5'RACE was carried out with the SMARTer™ RACE cDNA Amplification Kit (Clontech). Briefly, high quality RNA samples were synthesized into first-strand cDNA with SMARTScribe™ Reverse Transcriptase. PCR were then performed with PrimeSTAR GXL DNA Polymerase (Clontech) using diluted cDNA as template. To improve the specificity of the PCR products, nested PCR were performed in all cases. PCR products from 5'RACE PCR were gel purified and cloned into the commercial cloning vector CloneJET (Thermo Fisher Scientific). Several colonies from each cloning were sequenced and analyzed.

RNA secondary structure prediction for the *ADC-box*

Based on the highly conserved *Brg11-EBE* sequence a multiple-sequence alignment was created using the plant subset of the RefSeq nucleotide database⁴⁰. A *Picea abies* sequence was also extracted from GenBank. To find additional homologs of this region, we performed repeated searches using the Infernal software, version 1.1⁴¹. By using the CMfinder software⁴², potential conserved secondary structures were analyzed. To evaluate genes associated with the conserved element, we used genome annotations available in RefSeq and domain predictions from the conserved domain database⁴³ version 2.25. Predicted elements adjacent to annotated pseudogenes were not investigated further. Notably, no base pairs in the proposed structure are convincingly supported by covariation⁴⁴, i.e. mutations that modify both nucleotides in a base pair, yet preserve Watson-Crick pairing. Additionally, some *ADC-box* sequences contain base pairs that are not usually energetically favorable in Watson-Crick pairs. For these reasons, the proposed structure must be regarded as tentative.

***In vitro* translation**

Different 5'UTRs were fused to the *GFP* reporter gene and driven by the *T7* promoter. Capped mRNA was transcribed *in vitro* in the presence of the cap analog m²⁷,3'-OG[5']ppp[5']G (Jena Bioscience, *Jena, Germany*) using the HiScribe™ T7 High Yield
495 RNA Synthesis Kit (New England Biolabs, *Ipswich, MA, USA*). Either PCR products amplified by Phusion polymerase (New England Biolabs) or plasmid DNA linearized with EcoRI were used as template for RNA synthesis. The RNA was purified using the DyeEx 2.0 Spin Kit (Qiagen, *Hilden, Germany*).

In vitro translation was carried out in a 50 µl scale containing 50% (v/v) tobacco BY-
500 2 cell-free lysates, 16% (v/v) TR buffer (30 mM HEPES-KOH, pH 7.6, 40 mM potassium glutamate, 0.5 mM magnesium glutamate, 2 mM DTT), 0.75 mM ATP, 0.1 mM GTP, 25 mM creatine phosphate, 50 µM of each amino acid, 0.1 mg/ml creatine phosphokinase (Roche Diagnostics) and 8.5 pmol purified mRNA. The magnesium concentration was adjusted to 1.5 mM with magnesium glutamate and the potassium concentration was adjusted
505 to 38 mM with potassium glutamate. Any existing magnesium and potassium in tobacco BY-2 cell-free lysates were ignored. The batch translation reactions were carried out in a LT-X (Lab-Therm) shaker (Kuhner, *Birsfelden, Switzerland*) at 25°C and 500 rpm. The GFP fluorescence signal from each reaction were quantified using a Synergy HT Multi-Mode Microplate Reader (Biotek, *Bad Friedrichshall, Germany*) with 485/20 nm excitation and
510 528/20 nm emission.

Fluorescence reporter based *in vivo* translational assay

A GFP/DsRed dual fluorescence reporter system was used for different 5'UTRs-driven reporter gene translational studies. The constructs were assembled by Golden Gate Cloning³³. Firstly, *35S* promoter, 5'UTRs, *GFP*, *DsRed*, *35S* terminator were cloned into LI vector.
515 Taking advantage of Golden Gate Cloning, GATG, in which G is the last base of the 5'UTRs and ATG is the first three bases of *GFP*, was defined as overhang between the 5'UTRs and *GFP* so that those two fragments were seamlessly connected without introducing extra bases. Secondly, individual functional units expressing *GFP* or *DsRed* were assembled as LII vector. *GFP* was designed as the translational reporter and *DsRed* was used as the internal control.
520 Lastly, the assembled LII vectors were combined into a LIII binary vector for expression of both reporters within one T-DNA.

The plasmids were transformed into *A. tumefaciens* GV3101 by electroporation. *A. tumefaciens* mediated reporter gene transient expression in *N. benthamiana* was performed as described above. Leaf tissue were harvested at 36 hpi for fluorescence scanning and
525 quantification. For GFP and DsRed protein quantification, 6 leaf discs (0.25 cm²) were ground in liquid nitrogen and total protein was extracted in 300 µl of isolation buffer (50 mM Tris-HCl, pH=7.5, 150 mM NaCl, 0.1% Tween 20, 0.1% β-mercaptoethanol) as previously described⁴⁵. GFP and DsRed intensity from protein extracts were measured using a fluorometer (Berthold Plate Reader).

530 **Bacterial growth assay**

For growth curve of *R. solanacearum*, *X. euvesicatoria* and *P. syringae*, bacteria suspensions were adjusted to 10⁵ CFU/ml with sterile water and infiltrated into 4- to 5-week-old tomato leaves. Inoculated plants were incubated at 27°C with a 12-h light cycle (*R. solanacearum*) or
535 25°C with a 14h/10h day/night cycle (*X. euvesicatoria* and *P. syringae*). Leaf discs were harvested at 2, 3 or 4 dpi and ground in MiliQ water in a Retsch MM200 (25 f) for 1 min. Series of dilutions were plated out on agar plate and incubated at 28°C for 36 to 48 h.

For competitive growth of *P. syringae* and *X. euvesicatoria*, *P. syringae* were adjusted to 10⁵ CFU/ml and *X. euvesicatoria* were adjusted to 10⁸ CFU/ml. Equal volume of
540 *P. syringae* and *X. euvesicatoria* were mixed and infiltrated into 4- to 5-week-old tomato leaves. Inoculated plants were incubated at 25°C with a 14h/10h day/night cycle. Bacteria growth were measured as described above.

ADC activity assay and polyamine analysis

Bacteria infected tissue were homogenized in ADC activity isolation buffer (5 mM Tris, pH 7.5, 1 mM ascorbate, 50 µM pyridoxal 5 phosphate (Sigma Aldrich), 5%
545 polyvinylpyrrolidone) (3 µl buffer/mg tissue). After centrifugation at 17,000 g for 20 min at 4°C, supernatants were carefully transferred to a new tube and kept on ice. ADC activity assays were set up as follows: 90 µl of protein extract was combined with either 5 µl of Milli-Q water or 5 µl of 1 mM DL-α-(Difluoromethyl) arginine (DFMA; Santa Cruz Biotechnology, Germany). The reaction was started by adding 5 µl of 1 mM U-13C6 L-
550 arginine (Euroisotop, Germany). After incubation at 37°C for 1 h – gently mixing - the enzymatic reaction was stopped with 5 µl of heptafluorobutyric acid (HFBA, pKs=0.4; Sigma Aldrich) and centrifuged at 17,000 g for 20 min at 10°C. The supernatant was diluted either 1 to 5 or 1 to 10 and subjected to metabolite analysis.

The LC-MRM-MS profiling was performed as reported previously⁴⁶ using an Ekspert
555 Micro-LC 200 and a QTRAP4000 (ABSciex, USA). Chromatographic separation was
achieved on a HaloFused C18 column (150 x 0.5 mm; 2.7 μ m; AB Sciex) applying the
following binary gradient at a flow rate of 11 μ l/min and 35°C: 0 – 0.5 min isocratic 90% A;
0.5 – 4 min, linear from 90% A to 1% A; 4 – 4.8 min, isocratic 1% A (water, 0.1% aq. formic
acid, 0.05% heptafluorobutyric acid); 4.8-5 min, linear from 1% A to 90% A; 5-5.5 min,
560 linear to 99% A; 5.5-5.8 min, linear to 90% A; 5.8– 6 min, isocratic 10% B (acetonitrile,
0.1% aq. formic acid, 0.05% heptafluorobutyric acid). The injection volume was 2 μ l.
Analytes were ionized using a TurboV ion source equipped with an Assy 65 μ m ESI
electrode in positive ion mode. The following instrument settings were applied: nebulizer and
heater gas, nitrogen, 25 and 10 psi; curtain gas, nitrogen, 20 psi; collision gas, nitrogen,
565 medium; source temperature, 200°C; ionspray voltage, 5000 V; entrance potential, 10 V;
collision cell exit potential, 5V; scan time 25msec. The transitions monitored for each analyte
were listed in Supplementary Table 4. The MRM data acquired were analyzed using the
vendors MultiQuant software.

Data analysis

570 All statistical analysis (Student's t-test, ANOVA and wilcox.test) were performed in R.

Data availability

RNA-seq data generated in this study have been deposited to GEO under accession number
GSE125558.

575 REFERENCES

- 1 García-Bayona, L. & Comstock, L. E. Bacterial antagonism in host-associated microbial communities. *Science* **361**, eaat2456 (2018).
- 2 Galán, J. E. & Waksman, G. Protein-injection machines in bacteria. *Cell* **172**, 1306-1318 (2018).
- 580 3 Rüter, C., Lubos, M. L., Norkowski, S. & Schmidt, M. A. All in-multiple parallel strategies for intracellular delivery by bacterial pathogens. *Int. J. Med. Microbiol.* **308**, 872-881 (2018).
- 4 Ma, L. S., Hachani, A., Lin, J. S., Filloux, A. & Lai, E. M. *Agrobacterium tumefaciens* deploys a superfamily of type VI secretion DNase effectors as weapons for interbacterial competition *in planta*. *Cell Host Microbe* **16**, 94-104 (2014).
- 585 5 Souza, D. P. *et al.* Bacterial killing via a type IV secretion system. *Nat. Commun.* **6**, 6453 (2015).
- 6 Büttner, D. Behind the lines-actions of bacterial type III effector proteins in plant cells. *FEMS Microbiol. Rev.* **40**, 894-937 (2016).
- 590 7 Macho, A. P., Guidot, A., Barberis, P., Beuzon, C. R. & Genin, S. A competitive index assay identifies several *Ralstonia solanacearum* type III effector mutant strains with reduced fitness in host plants. *Mol Plant Microbe Interact* **23**, 1197-1205, (2010).
- 8 Salanoubat, M. *et al.* Genome sequence of the plant pathogen *Ralstonia solanacearum*. *Nature* **415**, 497-502, (2002).
- 595 9 Boch, J., Bonas, U. & Lahaye, T. TAL effectors - pathogen strategies and plant resistance engineering. *New Phytol.* **204**, 823-832 (2014).
- 10 de Lange, O. *et al.* Breaking the DNA binding code of *Ralstonia solanacearum* TAL effectors provides new possibilities to generate plant resistance genes against bacterial wilt disease. *New Phytol.* **199**, 773-786 (2013).
- 600 11 Deslandes, L. & Genin, S. Opening the *Ralstonia solanacearum* type III effector tool box: insights into host cell subversion mechanisms. *Curr. Opin. Plant Biol.* **20**, 110-117 (2014).
- 12 Genin, S. & Denny, T. P. Pathogenomics of the *Ralstonia solanacearum* species complex. *Annu Rev Phytopathol* **50**, 67-89 (2012).
- 605 13 Alcazar, R. & Tiburcio, A. F. Plant polyamines in stress and development: an emerging area of research in plant sciences. *Front. Plant Sci.* **5**, (2014).
- 14 von Arnim, A. G., Jia, Q. D. & Vaughn, J. N. Regulation of plant translation by upstream open reading frames. *Plant Science* **214**, 1-12 (2014).
- 15 Kay, S., Hahn, S., Marois, E., Hause, G. & Bonas, U. A bacterial effector acts as a plant transcription factor and induces a cell size regulator. *Science* **318**, 648-651 (2007).
- 610 16 Römer, P. *et al.* Recognition of AvrBs3-like proteins is mediated by specific binding to promoters of matching pepper *Bs3* alleles. *Plant Physiol.* **150**, 1697-1712 (2009).
- 17 Buntru, M., Vogel, S., Stoff, K., Spiegel, H. & Schillberg, S. A versatile coupled cell-free transcription-translation system based on tobacco BY-2 cell lysates. *Biotechnol. Bioeng.* **112**, 867-878 (2015).
- 615

- 18 Buntru, M., Vogel, S., Spiegel, H. & Schillberg, S. Tobacco BY-2 cell-free lysate: an alternative and highly-productive plant-based *in vitro* translation system. *BMC Biotechnol.* **14**, (2014).
- 620 19 Barrett, L. W., Fletcher, S. & Wilton, S. D. Regulation of eukaryotic gene expression by the untranslated gene regions and other non-coding elements. *Cell Mol Life Sci* **69**, 3613-3634 (2012).
- 20 Wachter, A. Gene regulation by structured mRNA elements. *Trends Genet* **30**, 172-181 (2014).
- 625 21 Bitonti, A. J., Casara, P. J., Mccann, P. P. & Bey, P. Catalytic irreversible inhibition of bacterial and plant arginine decarboxylase activities by novel substrate and product analogs. *Biochem. J.* **242**, 69-74 (1987).
- 22 Tiburcio, A. F., Altabella, T., Bitrian, M. & Alcazar, R. The roles of polyamines during the lifespan of plants: from development to stress. *Planta* **240**, 1-18 (2014).
- 630 23 Liu, J. H., Wang, W., Wu, H., Gong, X. Q. & Moriguchi, T. Polyamines function in stress tolerance: from synthesis to regulation. *Front. Plant Sci.* **6** (2015).
- 24 Jimenez-Bremont, J. F. *et al.* Physiological and molecular implications of plant polyamine metabolism during biotic interactions. *Front. Plant Sci.* **5** (2014).
- 635 25 Kwak, M.-J. *et al.* Rhizosphere microbiome structure alters to enable wilt resistance in tomato. *Nat. Biotechnol.* **36**, 1100-1109 (2018).
- 26 Khan, M., Seto, D., Subramaniam, R. & Desveaux, D. Oh, the places they'll go! A survey of phytopathogen effectors and their host targets. *Plant J.* **93**, 651-663 (2018).
- 27 Miller-Fleming, L., Olin-Sandoval, V., Campbell, K. & Ralser, M. Remaining mysteries of molecular biology: the role of polyamines in the cell. *J Mol Biol* **427**, 3389-3406 (2015).
- 640 28 Thalor, S. K., Berberich, T. & Kusano, T. in *Polyamines: a universal molecular nexus for growth, survival, and specialized metabolism* (eds Tomonobu Kusano & Hideyuki Suzuki), 111-118 (Springer Japan), (2015).
- 29 Denancé, N. *et al.* Two ancestral genes shaped the *Xanthomonas campestris* TAL effector gene repertoire. *New Phytol.* **219**, 391-407 (2018).
- 645 30 O'Neill, E. M. *et al.* Phevamine A, a small molecule that suppresses plant immune responses. *Proc Natl Acad Sci USA* **115**, E9514-E9522 (2018).
- 31 Lou, Y. R., Bor, M., Yan, J., Preuss, A. S. & Jander, G. Arabidopsis NATA1 acetylates putrescine and decreases defense-related hydrogen peroxide accumulation. *Plant Physiol.* **171**, 1443-1455 (2016).
- 650 32 Pérez-Quintero, A. L. *et al.* An improved method for TAL effectors DNA-binding sites prediction reveals functional convergence in TAL repertoires of *Xanthomonas oryzae* strains. *PLoS One* **8**, e68464 (2013).
- 33 Binder, A. *et al.* A modular plasmid assembly kit for multigene expression, gene silencing and silencing rescue in plants. *PLoS One* **9**, e88218 (2014).
- 655 34 Mukaiharu, T., Tamura, N. & Iwabuchi, M. Genome-wide identification of a large repertoire of *Ralstonia solanacearum* type III effector proteins by a new functional screen. *Mol Plant Microbe Interact* **23**, 251-262 (2010).

- 660 35 Lacerda, A. L. M. *et al.* Reference gene selection for qPCR analysis in tomato-bipartite begomovirus interaction and validation in additional tomato-virus pathosystems. *PLoS One* **10**, (2015).
- 36 Gantasala, N. P. *et al.* Selection and validation of reference genes for quantitative gene expression studies by real-time PCR in eggplant (*Solanum melongena* L). *BMC research notes* **6**, 312 (2013).
- 665 37 Liu, D. S. *et al.* Validation of reference genes for gene expression studies in virus-infected *Nicotiana benthamiana* using quantitative real-time PCR. *PLoS One* **7** (2012).
- 38 Schmidt, G. W. & Delaney, S. K. Stable internal reference genes for normalization of real-time RT-PCR in tobacco (*Nicotiana tabacum*) during development and abiotic stress. *Mol Genet Genomics* **283**, 233-241 (2010).
- 670 39 Jacobs, T. B., LaFayette, P. R., Schmitz, R. J. & Parrott, W. A. Targeted genome modifications in soybean with CRISPR/Cas9. *BMC Biotechnol.* **15** (2015).
- 40 O'Leary, N. A. *et al.* Reference sequence (RefSeq) database at NCBI: current status, taxonomic expansion, and functional annotation. *Nucleic Acids Res* **44**, D733-745 (2016).
- 675 41 Nawrocki, E. P. & Eddy, S. R. Infernal 1.1: 100-fold faster RNA homology searches. *Bioinformatics* **29**, 2933-2935 (2013).
- 42 Yao, Z. Z., Weinberg, Z. & Ruzzo, W. L. CMfinder - a covariance model based RNA motif finding algorithm. *Bioinformatics* **22**, 445-452 (2006).
- 680 43 Marchler-Bauer, A. *et al.* CDD/SPARCLE: functional classification of proteins via subfamily domain architectures. *Nucleic Acids Res* **45**, D200-D203 (2017).
- 44 Michel, F. & Westhof, E. Modelling of the three-dimensional architecture of group I catalytic introns based on comparative sequence analysis. *J Mol Biol* **216**, 585-610 (1990).
- 685 45 Stauffer, E., Westermann, A., Wagner, G. & Wachter, A. Polypyrimidine tract-binding protein homologues from Arabidopsis underlie regulatory circuits based on alternative splicing and downstream control. *Plant J.* **64**, 243-255 (2010).
- 46 Sanchez-Lopez, J. *et al.* Underivatized polyamine analysis in plant samples by ion pair LC coupled with electrospray tandem mass spectrometry. *Plant Physiology and Biochemistry* **47**, 592-598 (2009).

690

END NOTES

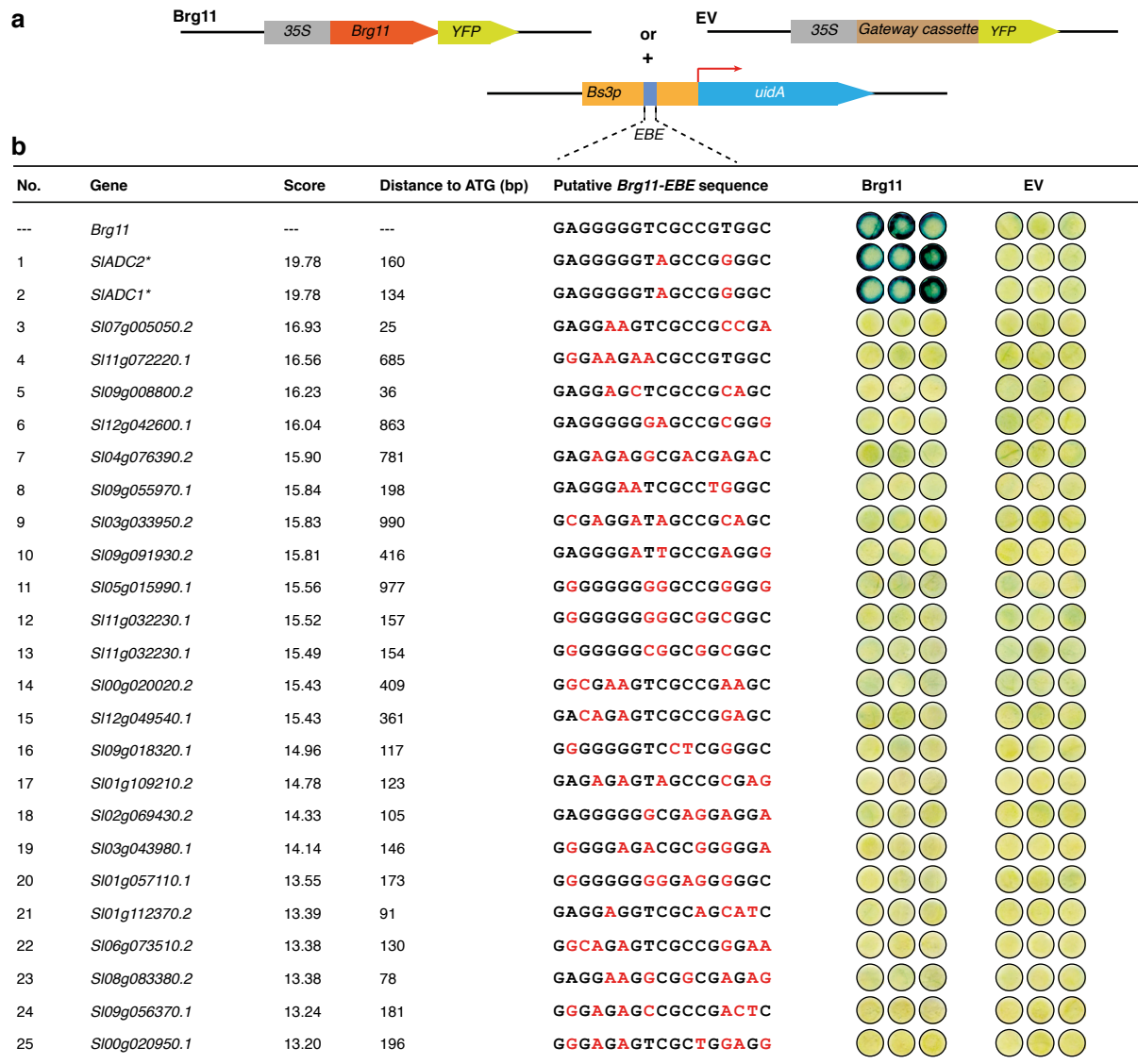
Supplementary Information is linked to the online version of the paper.

Acknowledgments

We thank the Lahaye Group, and especially Robert Morbitzer and Annett Strauß, for their
695 technical support and constructive suggestions. We also would like to thank Stephane Genin
and Nemo Peeters for providing us with *R. solanacearum* strains and useful advice on how to
work with them; Andreas Wachter for discussion on the RNA secondary structure prediction
and helpful comments on the manuscript; Axel Strauss and Chang Liu for help on statistical
analysis and figure preparation; Caterina Brancato for help on tomato transformation and the
700 ZMBP gardeners Johanna Schröter and Sofia Riegger for handling tomato plants. We thank
Eric Kemen, Diana Horvath, Erin Ritchie, and Danalyn Holmes for helpful comments on an
earlier version of this manuscript. This work was supported by grants from Deutsche
Forschungsgemeinschaft (DFG) to T.L. (LA1338/6-1 and LA1338/11-1).

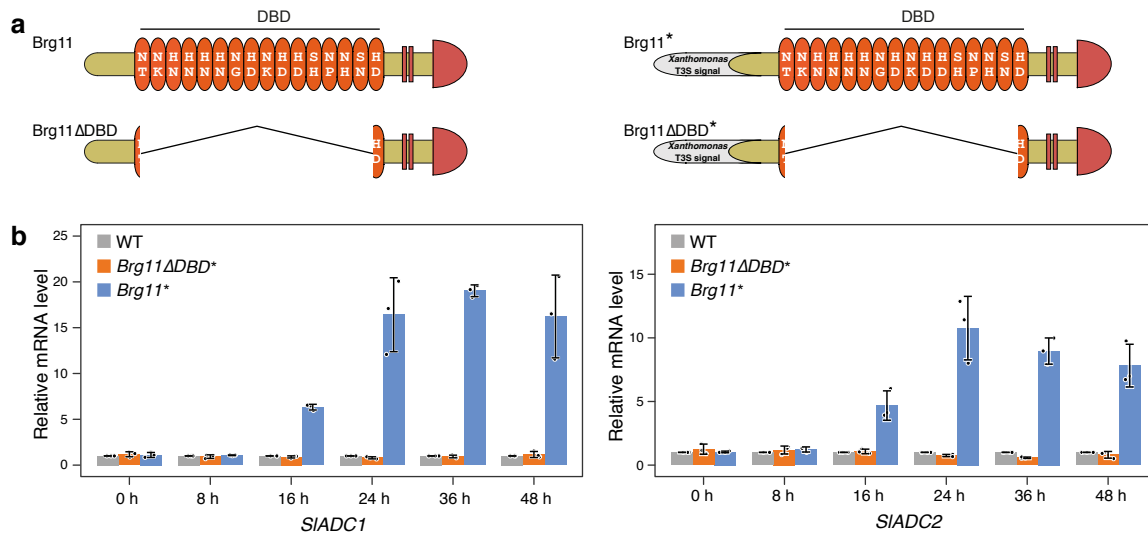
Author contributions

705 D.W. and T.L. conceived, designed and coordinated the study. E.v.R.-L. performed the ADC
activity and metabolic assays. O.L. and N.S. initiated the project and provided preliminary
material and data. M.B. performed the *in vitro* transcription-translation experiment under the
supervision of S.S.. A.P. carried out the *EBE* prediction under the supervision of B.S.. Z.W.
performed the RNA secondary structure prediction. T.M.L. provided the *SIADC* CDS
710 CRISPR vectors. D.W. performed all other experiments. C.A. provided helpful comments on
the impact of putrescine on *R. solanacearum*. A.J.M. provided helpful comments on
polyamine and translational regulation of *ADC* transcripts. D.W. and T.L. wrote the
manuscript with input from all co-authors.



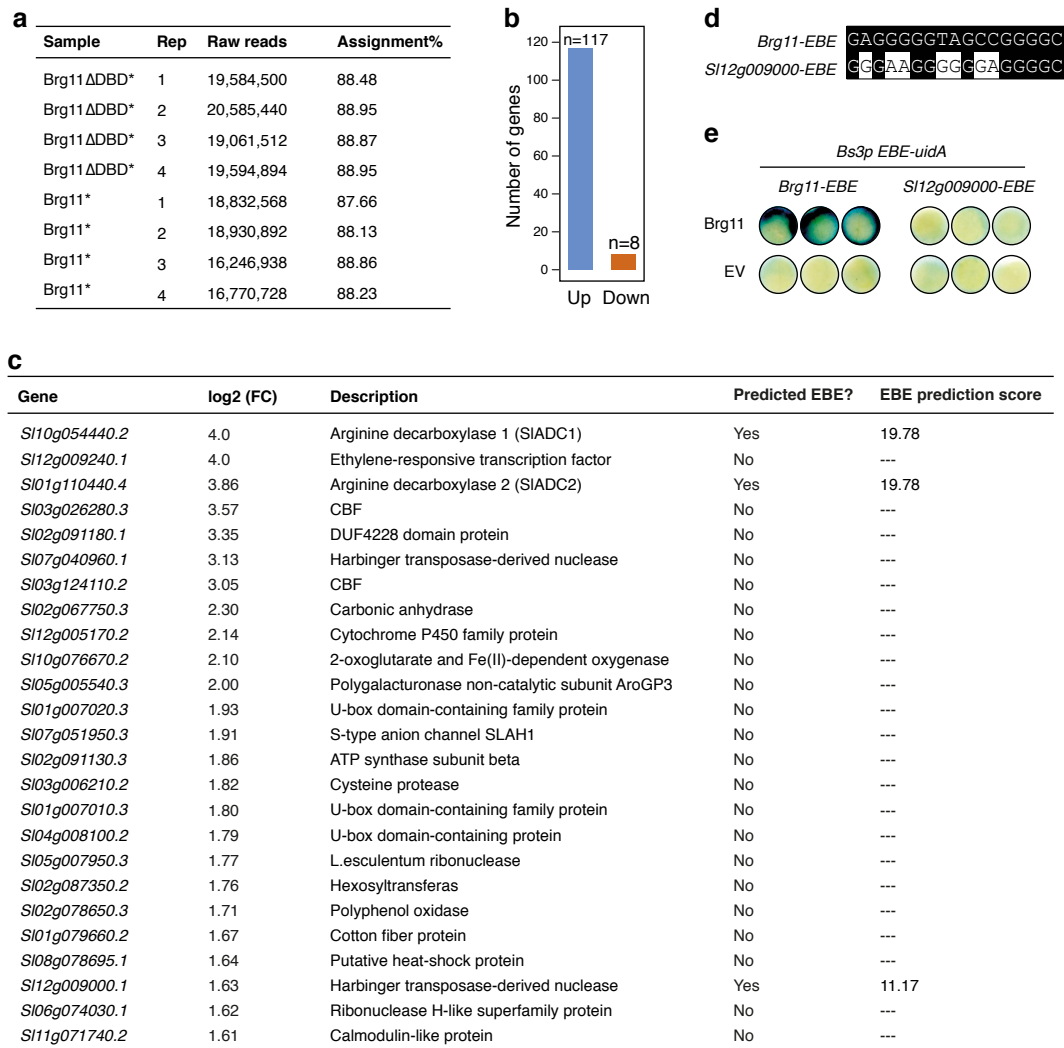
Extended Data Figure 1 | Brg11 activates a *Bs3* promoter derivative containing the putative *Brg11*-EBEs located upstream of *SIADC1/2* genes.

a, Schematic display of T-DNA constructs used for functional analysis of predicted *Brg11*-EBEs in promoter-reporter assays. **b**, Summary of the top 25 predicted *Brg11*-EBEs in tomato and their recognition by Brg11. The *Brg11*-EBE prediction was carried out with Talvez v.3.1 against the tomato promoterome (1 kb upstream of the ATG start codon). Scores indicate the likelihood of the predicted *Brg11*-EBEs to be activated by Brg11. The 17 bp *Brg11*-EBE, previously determined in transient assays, is shown on top. Predicted *Brg11*-EBEs are shown below, ordered by prediction score. Nucleotide polymorphisms between the previously determined *Brg11*-EBE and predicted *Brg11*-EBEs are highlighted by red font. To study functionality, the putative *Brg11*-EBEs were integrated into the pepper *Bs3* promoter (*Bs3p*). Promoter-*uidA* fusion constructs were co-delivered with 35S promoter-driven Brg11 or empty vector (EV) into *N. benthamiana* leaves via *A. tumefaciens*. GUS staining of leaf discs was carried out at 2 dpi. **Brg11*-EBEs in *SIADC1* and *SIADC2* are identical and accordingly the same three leaf discs are shown twice. Three representative leaf discs are shown for each promoter-effector combination.



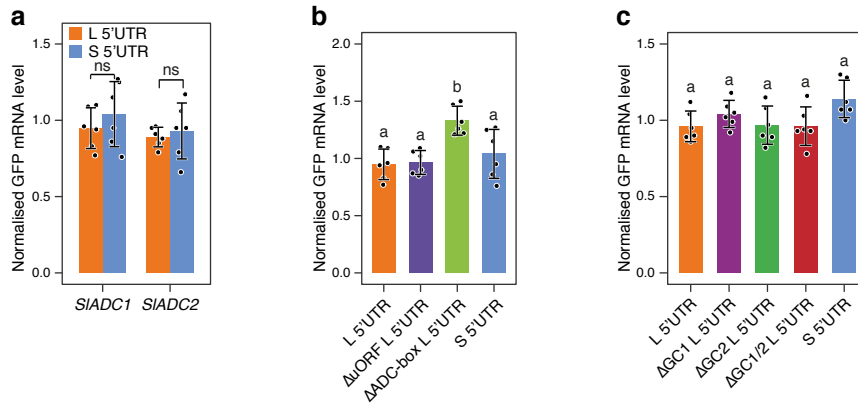
Extended Data Figure 2 | *X. euvesicatoria* mediated Brg11 delivery transcriptionally activates *SIADC1/2*.

a, Schematics of Brg11 structure and its derivative Brg11ΔDBD. Brg11ΔDBD is identical to Brg11 in its N- and C-terminal regions but lacks the DNA binding domain (DBD) and thus cannot activate promoters containing *Brg11*-EBE. For T3SS-mediated delivery of Brg11 via *X. euvesicatoria*, the type III secretion signal (T3S signal, indicated by gray colour) from the *X. euvesicatoria* effector AvrBs3 (N-terminal 152 amino acids) was fused to N-terminus of Brg11 or its derivative Brg11ΔDBD yielding Brg11* or Brg11ΔDBD*. **b**, Brg11* transcriptionally activates *SIADC1/2*. Tomato leaves were infiltrated with *X. euvesicatoria* wild-type strain 85-10 (WT), or *X. euvesicatoria* strains delivering either Brg11ΔDBD* or Brg11*. Inoculated tomato leaves were harvested at indicated time points for qPCR analysis. Data are mean ± SD (n = 3); solid circles, individual biological replicates.



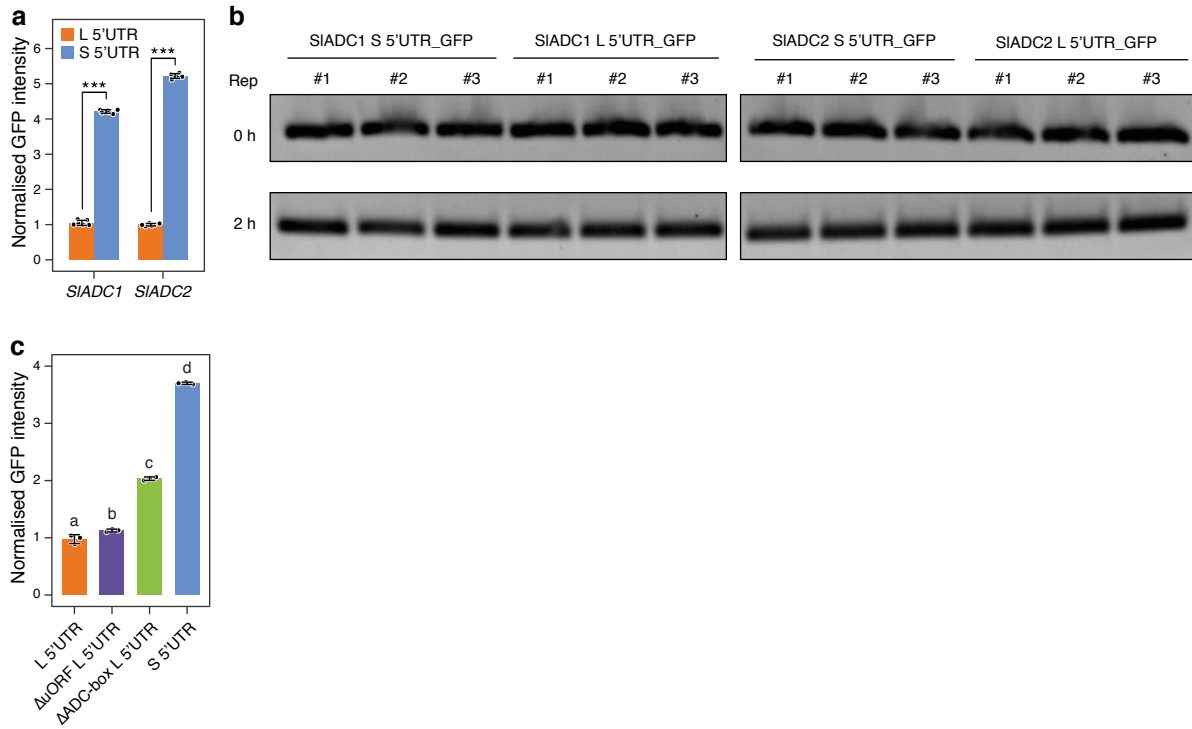
Extended Data Figure 3 | *SIADC1/2* are the only Brg11-induced genes containing a functional *Brg11-EBE*.

a, Summary of the RNA-seq-based differential transcriptome profiling. Tomato leaves were infiltrated with *X. euvesicatoria* delivering either Brg11* or Brg11ΔDBD* and harvested at 24 hpi for RNA extraction and sequencing. Rep, replicate. **b**, Number of tomato genes that were either up-regulated (Up) or down-regulated (Down) by Brg11. **c**, *EBE* prediction on the top 25 Brg11-induced genes. The prediction was carried out with Talvez v.3.1 with cut-off score of 10. **d**, Sequence alignment of the *Brg11-EBE* from *SIADC1/2* promoters and the predicted *EBE* from *SI12g009000* promoter (*SI12g009000-EBE*). Black letters on white background indicate polymorphic nucleotides. **e**, Brg11 cannot activate promoter-reporter constructs containing the predicted *Brg11-EBE* upstream of *SI12g009000*. The promoter-reporter fusion constructs were co-delivered with 35S promoter-driven *Brg11* or empty vector (EV) into *N. benthamiana* leaves via *A. tumefaciens*. GUS staining of leaf discs was carried out at 2 dpi. Three representative leaf discs are shown for each promoter-effector combination.



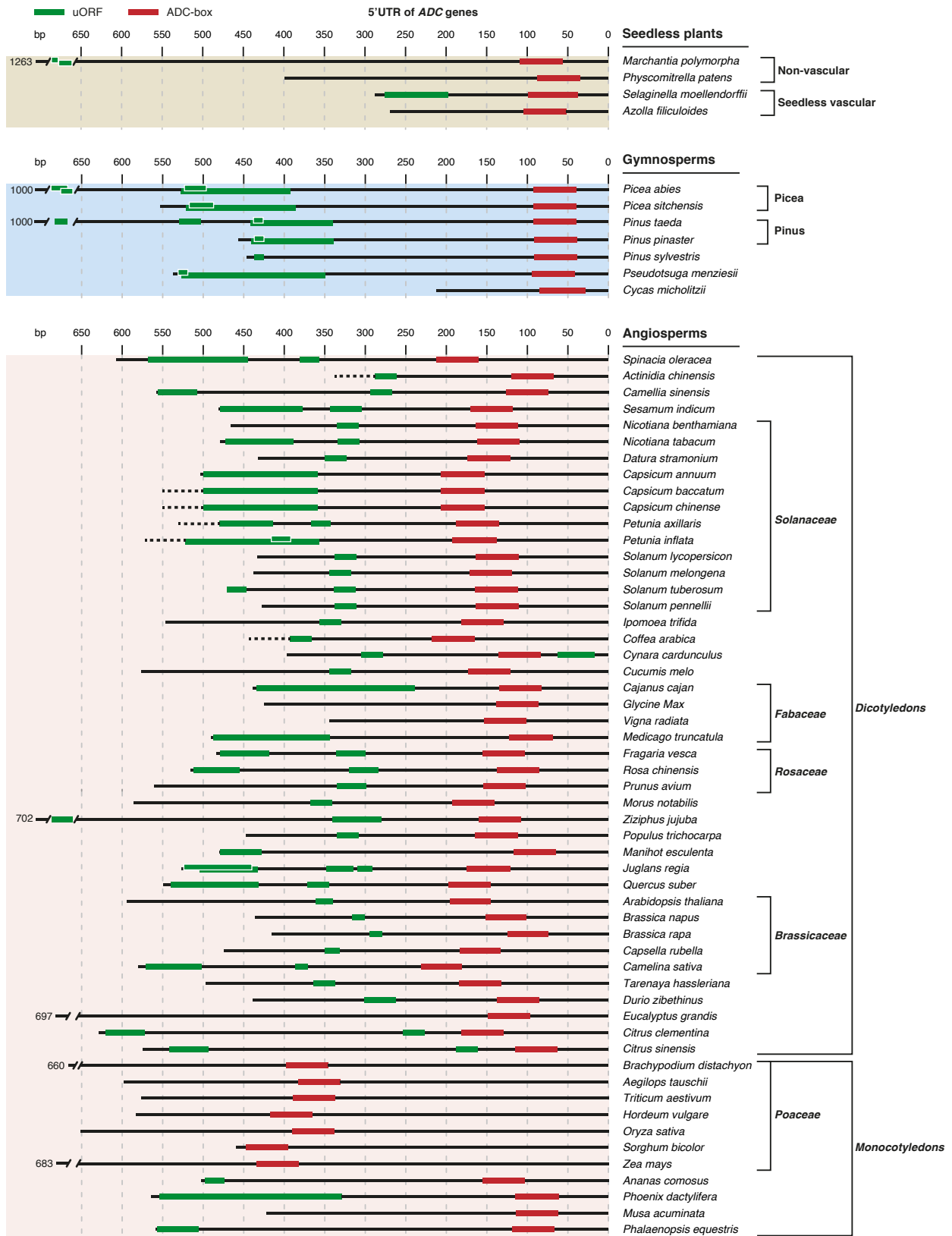
Extended Data Figure 4 | *SIADC* 5'UTRs and their derivatives have no impact on mRNA stability *in vivo*.

a-c, Transcript level of 35S promoter-driven *GFP* reporter genes fused to depicted 5'UTRs after transient expression in *N. benthamiana*. **a**, Long 5'UTRs of native *SIADC1/2* transcripts (L 5'UTR) and short 5'UTRs of Brg11-induced transcripts (S 5'UTR) fused to the *GFP* reporter gene. **b**, Derivatives of *SIADC1*: L 5'UTR-*GFP* lacking either the uORF (Δ uORF) or the *ADC-box* (Δ ADC-box). **c**, Derivatives of *SIADC1*: L 5'UTR-*GFP* mutated in either GC1, GC2 or both stretches (Δ GC1, Δ GC2 and Δ GC1/2, respectively). *A. tumefaciens*-containing reporter constructs were infiltrated into *N. benthamiana* leaves and harvested at 36 hpi. n = 6. Data are mean \pm SD; ns, not significant; lowercase letters indicate significance in one-way analysis of variance (ANOVA, TukeyHSD); solid circles, individual biological replicates.



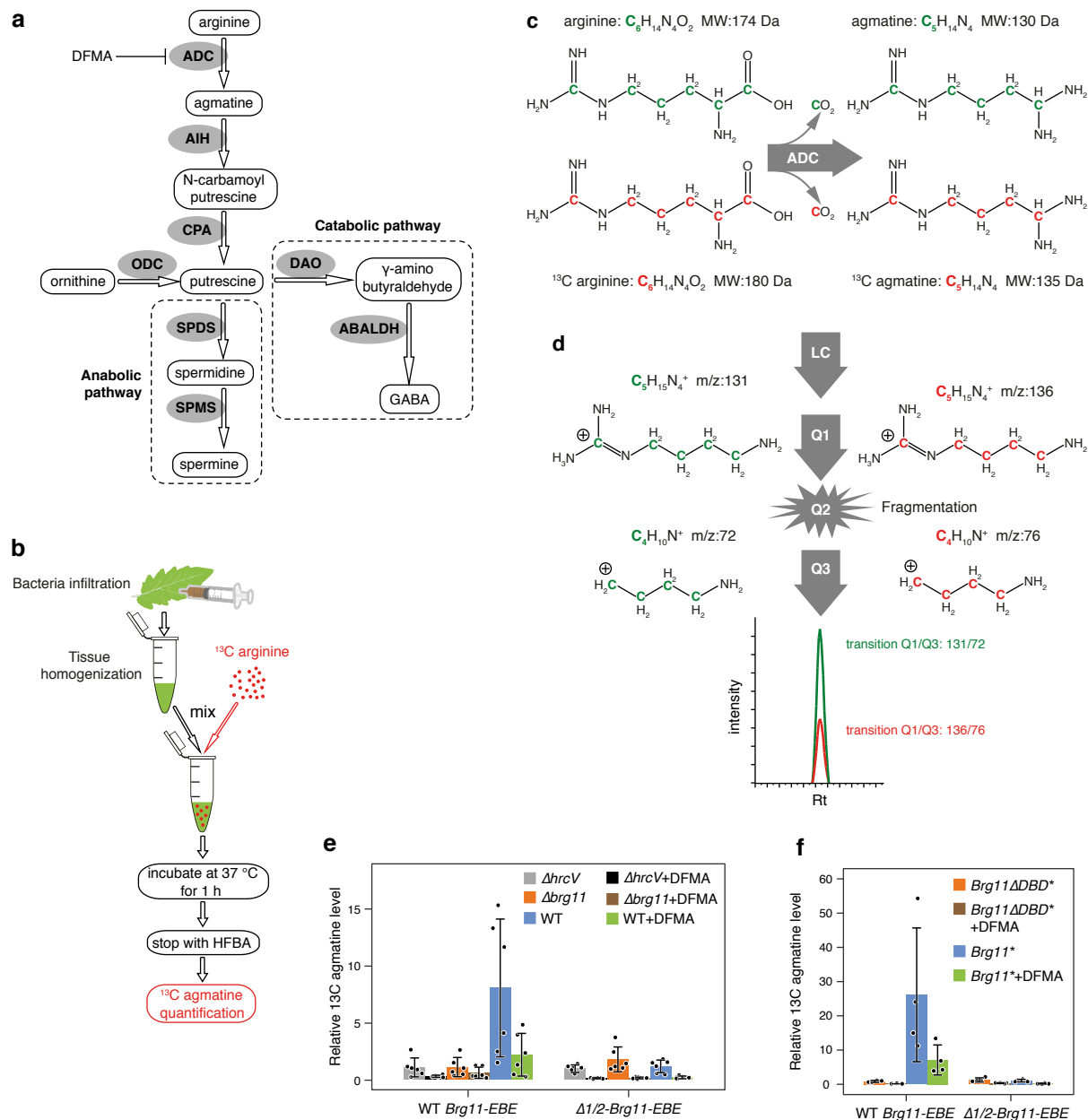
Extended Data Figure 5 | Translation activity of Brg11-induced and native *SIADC1/2* 5'UTR and their corresponding mutant variants *in vitro*.

a, Brg11-induced short *SIADC1/2* 5'UTRs mediate high level of translation *in vitro*. Translation efficiency of either *SIADC1/2* L 5'UTR- or the S 5'UTR-*GFP* fusions were determined *in vitro* using tobacco BY2 cell-free lysates. GFP intensity was quantified 2 h after addition of mRNA (n = 6). Data are mean ± SD; ****P* < 0.001 (Student's t-test); solid circles, individual biological replicates. **b**, *GFP* transcript level of *SIADC1/2* L 5'UTR- and S 5'UTR-*GFP* fusions before (0 h) and two hours (2 h) after addition of reporter mRNA. mRNA was quantified by RT-PCR. Three replicates (Rep) for each 5'UTR-*GFP* fusion at each time point. **c**, Deletion of the *ADC-box* but not the uORF from the long 5'UTR of native *SIADC1* transcripts causes increased reporter expression *in vitro*. *In vitro* translation activity of the *SIADC1* S 5'UTR, the *SIADC1* L 5'UTR, and corresponding uORF or *ADC-box* deletion derivatives (ΔuORF and Δ*ADC-box*, respectively) were determined 2 h after addition of *in vitro*-transcribed reporter mRNAs (n = 3). Data are mean ± SD; lowercase letters indicate significance in one-way analysis of variance (ANOVA, TukeyHSD); solid circles, individual biological replicates.



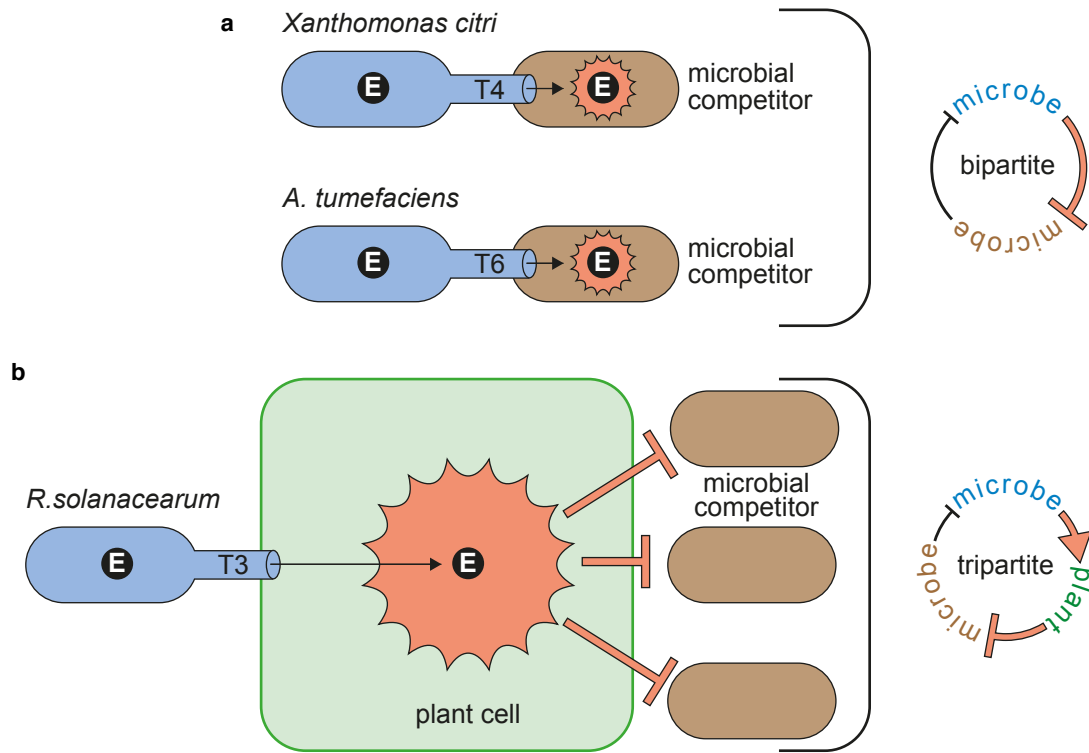
Extended Data Figure 7 | uORFs and *ADC-boxes* in 5'UTRs of seedless plant, gymnosperm and angiosperm *ADC* genes.

Black horizontal lines indicate the 5'UTRs of *ADC* transcripts that are displayed to scale. Green boxes and red boxes indicate uORFs and *ADC-boxes*, respectively. Green boxes with white border indicate independent overlapping uORFs with a distinct reading frame. Species designations of displayed *ADC* 5'UTRs are given on the right side of the horizontal bars. Plant species forming taxonomic groups are indicated by square brackets with the designation of the taxonomic group on the far right. Gray vertical dashed lines are placed at a distance of 50 bp as indicated on the top. Terminal short cross lines indicate 5'UTRs that are not displayed to scale. The length of these 5'UTRs is indicated by numbers at the far left. 5'UTR nucleotide sequences are given in supplementary sequence list 2.



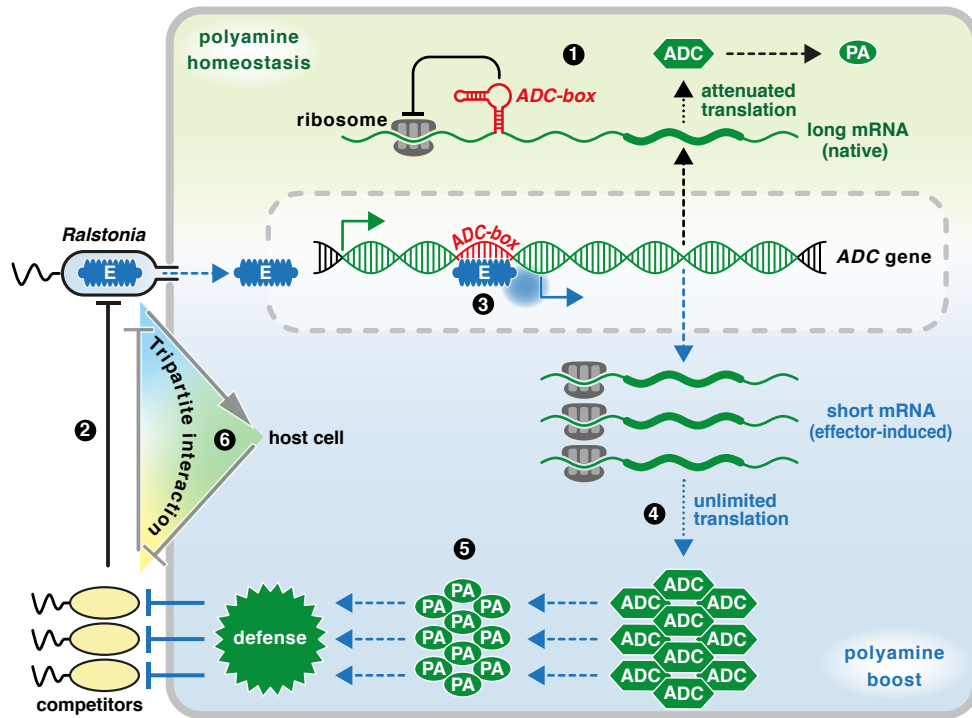
Extended Data Figure 8 | Brg11 causes an increase in ADC activity.

a, Simplified display of anabolic and catabolic polyamine pathways in tomato. Metabolites and relevant enzymes are shown in white boxes and gray ovals, respectively. AIH, agmatine iminohydrolase; CPA, N-carbamoyl-putrescine amidohydrolase; ODC, ornithine decarboxylase; SPDS, spermidine synthase; SPMS, spermine synthase; DAO, diamine oxidase; ABALDH, aminobutyraldehyde dehydrogenase; DFMA, difluoromethylarginine, an specific ADC inhibitor. **b**, Schematics describing the experimental procedure to study the impact of bacterial strains on activity of host ADC proteins. HFBA, heptafluorobutyric acid. **c**, **d**, A rapid and sensitive method for quantification of ADC activity by targeted LC-MS. **c**, Structures and molecular weights (MW) of the ADC substrates arginine (^{12}C atoms, highlighted in green) and its stable isotope-labeled analog (^{13}C atoms, highlighted in red) and their corresponding products. **d**, Agmatine and its labeled analog were separated by RP18 liquid chromatography (LC) using HFBA as an ion-pair reagent. Quantification was achieved by electrospray multiple reaction monitoring mass spectrometry (ESI-MRM-MS). The positively charged precursor ions were isolated in Q1 (quadrupole), fragmented in Q2 and scanned in Q3 resulting in the transitions Q1/Q3: 131/72 and Q1/Q3: 136/76 for agmatine (green) and its heavy analog (red). **e**, **f**, Supplementation of the ADC inhibitor DFMA significantly reduced synthesis of ^{13}C agmatine (ADC activity). ^{13}C agmatine levels in wild-type tomato and the $\Delta 1/2\text{-Brg11-EBE}$ mutant tomato (**e**) 18 h after infiltration with *R. solanacearum* ($n = 6$) or (**f**) 24 h after infiltration with *X. euvesicatoria* ($n = 4$). Strain+DFMA, DFMA was supplemented to the enzymatic reaction of given strain infected tissue. Data are mean \pm SD; solid circles, individual biological replicates.



Extended Data Figure 9 | A *Ralstonia* type III effector mediates tripartite microbe-host-microbe interactions.

a, Pathogen effectors involved in dipartite microbe-microbe interactions. The depicted bacterial plant pathogens (blue shapes) deliver effector proteins (E) into target cells of bacterial niche competitors (brown shapes) via type IV (T4) and type VI (T6) secretion systems. These toxic effectors kill bacterial niche competitors thus promoting growth of effector-delivering bacterial pathogens. **b**, Pathogen effectors mediating tripartite microbe-host-microbe interaction. The depicted bacterial pathogen (blue shape) delivers type III (T3) effector proteins (E) into plant target cells (green shape). Effector-mediated manipulation of host cells triggers a plant immune reaction that inhibits growth of niche competitors of the effector-delivering bacteria.



Extended Data Figure 10 | A *R. solanacearum* effector overcomes translational regulation of ADC expression to inhibit growth of bacterial niche competitors.

(1) Translation of native *ADC* transcripts (long mRNA) is attenuated by the *ADC-box*, an ancient *cis*-element in the 5'UTR that regulates polyamine (PA) homeostasis. (2) Growth of the bacterial plant pathogen *Ralstonia solanacearum* is suppressed by bacterial niche competitors. (3) *R. solanacearum* injects a type III effector (E) that binds to the *ADC-box* and initiates a 5' truncated (effector-induced) mRNA lacking the transcribed *ADC-box*. (4) Effector-induced *ADC* transcripts bypass translational regulation, resulting in high ADC expression. (5) High ADC expression results in high PA levels and triggers a plant defense that inhibits growth of *R. solanacearum* niche competitors. (6) In summary, a type III effector manipulates the tripartite interaction of *R. solanacearum* with host cells and bacterial competitors.

865 **Supplementary table 1 Total list of Brg11 up-regulated genes from RNA-seq**

Gene ID	Description	Log2(FC)*	p value
<i>Sl01g110430.3</i>	Nudix hydrolase homolog 11	4.09	0.0000
<i>Sl10g054440.2</i>	Arginine decarboxylase 1	4.00	0.0000
<i>Sl12g009240.1</i>	Ethylene-responsive transcription factor ERF017	4.00	0.0000
<i>Sl01g110440.4</i>	Arginine decarboxylase 2	3.86	0.0000
<i>Sl03g026280.3</i>	CBF	3.57	0.0000
<i>Sl02g091180.1</i>	DUF4228 domain protein	3.35	0.0000
<i>Sl07g040960.1</i>	Harbinger transposase-derived nuclease	3.13	0.0000
<i>Sl03g124110.2</i>	CBF	3.05	0.0073
<i>Sl02g067750.3</i>	Carbonic anhydrase	2.30	0.0169
<i>Sl12g005170.2</i>	Cytochrome P450 family protein	2.14	0.0008
<i>Sl10g076670.2</i>	2-oxoglutarate (2OG) and Fe(II)-dependent oxygenase	2.10	0.0039
<i>Sl05g005540.3</i>	Polygalacturonase non-catalytic subunit	2.00	0.0167
<i>Sl01g007020.3</i>	U-box domain-containing family protein	1.93	0.0002
<i>Sl07g051950.3</i>	S-type anion channel SLAH1	1.91	0.0016
<i>Sl02g091130.3</i>	ATP synthase subunit beta	1.86	0.0100
<i>Sl03g006210.2</i>	Cysteine protease	1.82	0.0399
<i>Sl01g007010.3</i>	U-box domain-containing family protein	1.80	0.0006
<i>Sl04g008100.2</i>	U-box domain-containing protein	1.79	0.0003
<i>Sl05g007950.3</i>	LERNALE <i>L. esculentum</i> ribonuclease le	1.77	0.0002
<i>Sl02g087350.2</i>	Hexosyltransferase	1.76	0.0001
<i>Sl02g078650.3</i>	Polyphenol oxidase	1.71	0.0357
<i>Sl01g079660.2</i>	Cotton fiber protein	1.67	0.0035
<i>Sl08g078695.1</i>	Heat-shock protein, putative	1.64	0.0358
<i>Sl12g009000.1</i>	Harbinger transposase-derived nuclease	1.63	0.0003
<i>Sl06g074030.1</i>	Polynucleotidyl transferase, ribonuclease H-like protein	1.62	0.0001
<i>Sl11g071740.2</i>	Calmodulin-like protein	1.61	0.0206
<i>Sl06g076160.3</i>	Cytochrome P450	1.61	0.0062
<i>Sl02g067610.1</i>	DNA helicase INO80-like protein	1.57	0.0097
<i>Sl01g107090.2</i>	Beta-1,4-xylosidase	1.56	0.0006
<i>Sl11g069560.2</i>	Glycosyl transferase, family 2	1.56	0.0011
<i>Sl06g073830.1</i>	Calcium-binding protein	1.54	0.0034
<i>Sl04g074450.2</i>	Phosphate-responsive 1 family protein	1.49	0.0001

<i>SI04g072280.3</i>	Laccase	1.43	0.0367
<i>SI05g055080.1</i>	P-loop containing nucleoside triphosphate hydrolases	1.42	0.0021
<i>SI04g079360.1</i>	R2R3MYB transcription factor 77	1.41	0.0092
<i>SI09g097960.3</i>	NAD(P)-linked oxidoreductase superfamily protein	1.39	0.0065
<i>SI04g071480.1</i>	Plant/F1M20-13 protein	1.39	0.0002
<i>SI02g072210.1</i>	DUF1685 family protein	1.39	0.0023
<i>SI01g009340.3</i>	SUN-domain protein2	1.37	0.0030
<i>SI03g093130.3</i>	Xyloglucan endotransglucosylase-hydrolase 3	1.37	0.0056
<i>SI11g011330.2</i>	Alcohol dehydrogenase, putative	1.37	0.0254
<i>SI09g065850.3</i>	Auxin-regulated IAA3	1.37	0.0005
<i>SI08g067300.1</i>	F-box family protein	1.36	0.0011
<i>SI01g009160.2</i>	Harpin-induced1-like	1.35	0.0011
<i>SI03g020030.3</i>	Pin-II type proteinase inhibitor 69	1.35	0.0080
<i>SI12g010540.1</i>	UDP-glucuronate 4-epimerase 4	1.35	0.0001
<i>SI03g119530.3</i>	LOB domain protein 40	1.33	0.0070
<i>SI02g062300.3</i>	BURP domain protein RD22	1.32	0.0011
<i>SI03g020010.1</i>	Miraculin	1.31	0.0032
<i>SI05g054250.1</i>	Heavy metal transport/detoxification superfamily protein	1.31	0.0400
<i>SI12g010420.1</i>	NHL domain protein	1.31	0.0001
<i>SI03g098740.1</i>	Kunitz trypsin inhibitor	1.30	0.0193
<i>SI06g065060.2</i>	FAD-binding Berberine family protein	1.29	0.0039
<i>SI08g079190.1</i>	Bifunctional inhibitor/lipid-transfer protein	1.29	0.0040
<i>SI12g005450.1</i>	Kinase family protein	1.27	0.0138
<i>SI04g077980.1</i>	C2H2-type zinc finger protein	1.25	0.0001
<i>SI09g098160.3</i>	Pirin	1.25	0.0015
<i>SI07g052990.1</i>	Ypt/Rab-GAP domain of gyp1p superfamily protein	1.22	0.0039
<i>SI02g082450.3</i>	Auxin efflux carrier family protein	1.21	0.0253
<i>SI02g087210.3</i>	Zinc finger AN1 domain- and stress-associated protein 12	1.20	0.0085
<i>SI03g097410.1</i>	Inositol-tetrakisphosphate 1-kinase	1.20	0.0070
<i>SI10g006130.1</i>	EAR motif SIERF36	1.20	0.0000
<i>SI12g017240.2</i>	Xyloglucan endo-transglycosylase B1	1.19	0.0002
<i>SI06g061080.3</i>	NAC domain protein	1.18	0.0027
<i>SI04g011750.3</i>	Protein TIC 214	1.18	0.0002
<i>SI08g080630.3</i>	Ethylene-responsive proteinase inhibitor 1	1.16	0.0269
<i>SI01g066680.3</i>	Pollen Ole 1 allergen and extensin family protein	1.16	0.0472

<i>SI10g084880.3</i>	Avr9/Cf-9 rapidly elicited protein 137	1.15	0.0028
<i>SI08g016150.1</i>	Avr9/Cf-9 rapidly elicited protein 180	1.15	0.0002
<i>SI06g070960.2</i>	ABC transporter family protein	1.14	0.0019
<i>SI05g015880.3</i>	Regulator of nonsense transcript protein	1.14	0.0117
<i>SI03g020040.3</i>	Pin-II type proteinase inhibitor 69	1.14	0.0100
<i>SI01g087980.3</i>	BPS1, putative	1.14	0.0007
<i>SI03g120020.3</i>	Boron transporter, putative	1.13	0.0100
<i>SI05g052040.1</i>	Ethylene-responsive transcription factor	1.13	0.0008
<i>SI07g063700.2</i>	Serine/threonine-protein kinase	1.13	0.0330
<i>SI08g068790.2</i>	Tyramine n-hydroxycinnamoyl transferase	1.13	0.0001
<i>SI03g116510.1</i>	Cotton fiber protein	1.13	0.0017
<i>SI07g052370.3</i>	Cytochrome P450	1.13	0.0076
<i>SI01g091590.3</i>	BON1-associated protein 2	1.13	0.0023
<i>SI11g010250.1</i>	Avr9/Cf-9 rapidly elicited protein 75	1.13	0.0002
<i>SI03g093560.1</i>	Ethylene response factor C.6	1.12	0.0005
<i>SI12g099120.2</i>	Abscisic acid induced MYB1	1.12	0.0038
<i>SI08g081610.3</i>	WRKY family transcription factor, putative	1.11	0.0030
<i>SI12g036650.2</i>	Translocase subunit seca	1.10	0.0025
<i>SI11g072310.2</i>	Gibberellin 20-oxidase-3	1.10	0.0089
<i>SI04g080660.3</i>	Carboxyl methyltransferase	1.10	0.0014
<i>SI03g093550.1</i>	Ethylene-responsive transcription factor	1.09	0.0001
<i>SI10g006700.1</i>	Calcium-binding family protein	1.09	0.0002
<i>SI04g005480.1</i>	Nodulin-related protein 1, putative	1.09	0.0003
<i>SI04g007580.1</i>	DUF4228 domain protein	1.09	0.0087
<i>SI12g011030.2</i>	Xyloglucan endotransglucosylase-hydrolase 9	1.09	0.0068
<i>SI10g055820.2</i>	Chitinase	1.09	0.0126
<i>SI02g065570.1</i>	Rotundifolia-like protein	1.08	0.0146
<i>SI08g076850.3</i>	Tetraspanin family protein	1.08	0.0241
<i>SI04g055050.1</i>	VQ motif-containing protein	1.08	0.0046
<i>SI08g005640.3</i>	Terpene synthase	1.07	0.0148
<i>SI03g093120.4</i>	Xyloglucan endotransglucosylase-hydrolase	1.07	0.0396
<i>SI09g082690.3</i>	Superoxide dismutase	1.07	0.0173
<i>SI03g112540.3</i>	NAD(P)-binding Rossmann-fold superfamily protein	1.06	0.0067
<i>SI06g070990.3</i>	WRKY transcription factor 74	1.06	0.0277
<i>SI09g005830.1</i>	ACI49	1.06	0.0016

<i>SI11g073060.2</i>	Zinc finger family protein	1.06	0.0020
<i>SI05g018820.1</i>	Cotton fiber protein	1.05	0.0476
<i>SI02g091700.3</i>	Hydroxyproline-rich glycoprotein family protein	1.05	0.0003
<i>SI04g011767.1</i>	Pentatricopeptide repeat-containing protein	1.05	0.0079
<i>SI02g067800.3</i>	High affinity nitrate transporter	1.05	0.0004
<i>SI01g065510.2</i>	CheY-like responsive regulator family protein	1.04	0.0009
<i>SI06g075780.2</i>	Zinc finger, C2H2	1.04	0.0006
<i>SI01g109250.2</i>	DUF4228 domain protein	1.04	0.0003
<i>SI08g077900.3</i>	Expansin-like protein	1.03	0.0175
<i>SI09g014350.3</i>	Glycerol-3-phosphate acyltransferase	1.03	0.0000
<i>SI06g008620.1</i>	TolB protein-like protein	1.03	0.0000
<i>SI12g057160.1</i>	Arabinogalactan protein	1.03	0.0005
<i>SI11g005820.1</i>	Pectinesterase inhibitor	1.03	0.0030
<i>SI03g026230.1</i>	Protein DETOXIFICATION	1.00	0.0308
<i>SI06g083470.3</i>	NAD(P)-binding Rossmann-fold superfamily protein	1.00	0.0157

* FC, fold-change

Supplementary table 2 The Brg11 RVD-nucleotide matrix used for *Brg11-EBE* prediction

RVD	Binding possibility of each RVD to each nucleotide			
	A	C	G	T
NT	30	5	10	1
NK	1	1	30	1
HN	30	1	30	0
NG	5	5	5	50
HD	15	50	5	5
SH	1	1	30	1
NP	30	10	10	20
NH	20	10	30	1
SN	25	1	30	1

870

Supplementary table 2 Primers used in this study

Name	Sequence (5' - 3')	Description
qSIADC1 F	TAGCGAAAGTGGCAGAGCAA	qPCR for <i>SIADC1</i> in tomato
qSIADC1 R	AGGTATCGTACTCTCCGCGA	qPCR for <i>SIADC1</i> in tomato
qSIADC2 F	TTGGTCGCAAGAAAGCTCCT	qPCR for <i>SIADC2</i> in tomato
qSIADC2 R	TGGCCAGAATGCTTTGTCCT	qPCR for <i>SIADC2</i> in tomato
qTIP41 F	GCTTAGGGTTGATGGAGTGC	qPCR in tomato (Reference gene)
qTIP41 R	CTCTCCAGCAGCTTTCACG	qPCR in tomato (Reference gene)
qSmADC1 F	CAGCTCGGGGAATTTTATCA	qPCR for <i>SmADC1</i> in eggplant
qSmADC1 R	GCAAAGCTGTGAGGGCTATC	qPCR for <i>SmADC1</i> in eggplant
qSmADC2 F	GTAAGGGCGTAAAGCATCCA	qPCR for <i>SmADC2</i> in eggplant
qSmADC2 R	GGTAGTCAACACGGGCATCT	qPCR for <i>SmADC2</i> in eggplant
qSm18S rRNA-F	CGCGCGCTACACTGATGTATTCAA	qPCR in eggplant (Reference gene)
qSm18S rRNA-R	TACAAAGGGCAGGGACGTAGTCAA	qPCR in eggplant (Reference gene)
qNbADC1 F	GGTAGTGGTGTGGTGGGAA	qPCR for <i>NbADC1</i> in <i>N. benthamiana</i>
qNbADC1 R	CCGGAGAACATCAGCACAA	qPCR for <i>NbADC1</i> in <i>N. benthamiana</i>
qNbADC2.1 F	CGATTATTCCAATTCACCGC	qPCR for <i>NbADC2.1</i> in <i>N. benthamiana</i>
qNbADC2.1 R	CAAACAGGTTGTGGAGTCCG	qPCR for <i>NbADC2.1</i> in <i>N. benthamiana</i>
qNbADC2.2 F	CCAATTGTTCCAATACACCGT	qPCR for <i>NbADC2.2</i> in <i>N. benthamiana</i>
qNbADC2.2 R	CAAACAAGTTGTGGAGTCTT	qPCR for <i>NbADC2.2</i> in <i>N. benthamiana</i>
qNbPP2A F	GCATATCATTCCTCAGGTCTTGG	qPCR in <i>N. benthamiana</i> (Reference gene)
qNbPP2A R	GGTGCAAGCAATGAAATCGC	qPCR in <i>N. benthamiana</i> (Reference gene)
qNtADC1.1 F	ACATTGAACAGCTTGCTGCC	qPCR for <i>NtADC1.1</i> in <i>N. tabacum</i>
qNtADC1.1 R	CGATAATATTCCTCGGACTC	qPCR for <i>NtADC1.1</i> in <i>N. tabacum</i>
qNtADC1.2 F	GACATTGAACAACCTTGCTGCA	qPCR for <i>NtADC1.2</i> in <i>N. tabacum</i>
qNtADC1.2 R	CCGATAAAAATTCCTCGAACTA	qPCR for <i>NtADC1.2</i> in <i>N. tabacum</i>
qNtADC2.1 F	TGTTTGGTGGACCAAGTGTC	qPCR for <i>NtADC2.1</i> in <i>N. tabacum</i>
qNtADC2.1 R	CTGCTGGCCAAAGATTCAACA	qPCR for <i>NtADC2.1</i> in <i>N. tabacum</i>
qNtADC2.2 F	TGTTTGGTGGACCAAGCGTG	qPCR for <i>NtADC2.2</i> in <i>N. tabacum</i>
qNtADC2.2 R	TGCTGGCCAAAGATGCAATG	qPCR for <i>NtADC2.2</i> in <i>N. tabacum</i>
qNtEF 1a F	TGAGATGCACCACGAAGCTC	qPCR in <i>N. tabacum</i> (Reference gene)
qNtEF 1a R	CCAACATTGTCACCAGGAAGTG	qPCR in <i>N. tabacum</i> (Reference gene)
qGFP F	CACATGAAGCAGCAGACTT	qPCR for <i>GFP</i>
qGFP R	TCCTTGAAGTCGATGCCCTT	qPCR for <i>GFP</i>
qDsRed F	CATCCCCGACTACAAGAAGC	qPCR <i>DsRed</i>
qDsRed R	TGGTCTTCTTCTGCATCAG	qPCR <i>DsRed</i>
Brg11-EBE F	5'PHO- GGGGCAATCACAACCTTCAAGTTATCAT	Integration of the <i>Brg11-EBE</i> from <i>SIADC1/2</i> into <i>Bs3</i> promoter

	C	
Brg11-EBE R	GGCTACCCCCTCATAAAAATTGGTCAG	Integration of the <i>Brg11-EBE</i> from <i>SIADC1/2</i> into <i>Bs3</i> promoter
EBE CaADC1 F	5'PHO- GAGGCAATCACAACCTTCAAGTTATCAT C	Integration of the <i>Brg11-EBE</i> from pepper <i>ADC1</i> into <i>Bs3</i> promoter
EBE CaADC1 R	GGCTACCTCCTCATAAAAATTGGTCAG	Integration of the <i>Brg11-EBE</i> from pepper <i>ADC1</i> into <i>Bs3</i> promoter
EBE SI07g005050 F	GAGGAAGTCGCCGCCGAAATCACAAC TCAA	Ingegration of the candidate EBE from <i>SI07g005050</i> into <i>Bs3</i> promoter
EBE SI11g072220 F	GGGAAGAACGCCGTGGCAATCACAAC TTCAA	Ingegration of the candidate EBE from <i>SI11g072220</i> into <i>Bs3</i> promoter
EBE SI09g008800 F	GAGGAGCTCGCCGCAGCAATCACAAC TCAA	Ingegration of the candidate EBE from <i>SI09g008800</i> into <i>Bs3</i> promoter
EBE SI12g042600 F	GAGGGGGGAGCCGCGGGAATCACAAC TTCAA	Ingegration of the candidate EBE from <i>SI12g042600</i> into <i>Bs3</i> promoter
EBE SI04g076390 F	GAGAGAGGCGACGAGACAATCACAAC TTCAA	Ingegration of the candidate EBE from <i>SI04g076390</i> into <i>Bs3</i> promoter
EBE SI09g055970 F	GAGGGAATCGCCTGGGCAATCACAAC TCAA	Ingegration of the candidate EBE from <i>SI09g055970</i> into <i>Bs3</i> promoter
EBE SI03g033950 F	GCGAGGATAGCCGCAGCAATCACAAC TCAA	Ingegration of the candidate EBE from <i>SI03g033950</i> into <i>Bs3</i> promoter
EBE SI09g091930 F	GAGGGGATTGCCGAGGGAATCACAAC TTCAA	Ingegration of the candidate EBE from <i>SI09g091930</i> into <i>Bs3</i> promoter
EBE SI05g015990 F	GGGGGGGGGGCCGGGGAATCACAAC TTCAA	Ingegration of the candidate EBE from <i>SI05g015990</i> into <i>Bs3</i> promoter
EBE SI11g032230 1F	GGGGGGGGGGCGGCGGCAATCACAAC TTCAA	Ingegration of the candidate EBE1 from <i>SI11g032230</i> into <i>Bs3</i> promoter
EBE SI11g032230 2F	GGGGGGGGCGGCGGCGGCAATCACAAC TTCAA	Ingegration of the candidate EBE2 from <i>SI11g032230</i> into <i>Bs3</i> promoter
EBE SI00g020020 F	GGCGAAGTCGCCGAAGCAATCACAAC TCAA	Ingegration of the candidate EBE from <i>SI00g020020</i> into <i>Bs3</i> promoter
EBE SI12g049540 F	GACAGAGTCGCCGAGCAATCACAAC TCAA	Ingegration of the candidate EBE from <i>SI12g049540</i> into <i>Bs3</i> promoter
EBE SI09g018320 F	GGGGGGGTCTCGGGGCAATCACAAC TCAA	Ingegration of the candidate EBE from <i>SI09g018320</i> into <i>Bs3</i> promoter
EBE SI01g109210 F	GAGAGAGTAGCCGCGAGAATCACAAC TTCAA	Ingegration of the candidate EBE from <i>SI01g109210</i> into <i>Bs3</i> promoter
EBE SI02g069430 F	GAGGGGGGCGAGGAGGAAATCACAAC	Ingegration of the candidate EBE from

	TTCAA	<i>SI02g069430</i> into <i>Bs3</i> promoter
EBE <i>SI03g043980</i> F	GGGGGAGACGCGGGGGAAATCACAAC TTCAA	Ingegration of the candidate EBE from <i>SI03g043980</i> into <i>Bs3</i> promoter
EBE <i>SI01g057110</i> F	GGGGGGGGGAGGGGGCAATCACAAC TTCAA	Ingegration of the candidate EBE from <i>SI01g057110</i> into <i>Bs3</i> promoter
EBE <i>SI01g112370</i> F	GAGGAGGTCGCAGCATCAATCACAAC TCAA	Ingegration of the candidate EBE from <i>SI01g112370</i> into <i>Bs3</i> promoter
EBE <i>SI06g073510</i> F	GGCAGAGTCGCCGGGAAAATCACAAC TTCAA	Ingegration of the candidate EBE from <i>SI06g073510</i> into <i>Bs3</i> promoter
EBE <i>SI08g083380</i> F	GAGGAAGGCGGCGAGAGAATCACAAC TTCAA	Ingegration of the candidate EBE from <i>SI08g083380</i> into <i>Bs3</i> promoter
EBE <i>SI09g056370</i> F	GGGAGAGCCGCGACTCAATCACAAC TCAA	Ingegration of the candidate EBE from <i>SI09g056370</i> into <i>Bs3</i> promoter
EBE <i>SI00g020950</i> F	GGGAGAGTCGCTGGAGGAATCACAAC TTCAA	Ingegration of the candidate EBE from <i>SI00g020950</i> into <i>Bs3</i> promoter
EBE <i>AtADC2</i> F	GAGGGGGTAGCCGAGGCAATCACAAC TTCAAG	Ingegration of the candidate EBE from <i>AtADC2</i> into <i>Bs3</i> promoter
EBE <i>MtADC1</i> F	GGGGGGGTAGCCGGGGCAATCACAA	Ingegration of the candidate EBE from <i>MtADC1</i> into <i>Bs3</i> promoter
EBE <i>GmADC1</i> F	GAGGGGGAAGCCGGGGCAATCACAAC TTC	Ingegration of the candidate EBE from <i>GmADC1</i> into <i>Bs3</i> promoter
EBE R	5'PHO-ATAAAATTGGTCAGGCAAACGT GTTCATTG	Integraton of the candidate EBE into <i>Bs3</i> promoter, shared reverse primer
<i>SIADC1p 350</i> F	TTTGGTCTCTCACCTTTCTTCTTCTCCG GTGAACTATTCCG	Clone of <i>SIADC1p 350</i> bp
<i>SIADC1p 350</i> R	AAAGGTCTCACCTTCTCGTAAAATCTT CACAAAAAAGAAATC	Clone of <i>SIADC1p 350</i> bp
<i>SIADC2p 350</i> F	TTTGGTCTCTCACCATTAATATCTGTAT GGTGTCTTCTT	Clone of <i>SIADC2p 350</i> bp
<i>SIADC2p 350</i> F	AAAGGTCTCACCTTCTTCCCCGATCT GTTTTGATTTGTTAAG	Clone of <i>SIADC2p 350</i> bp
Δ <i>SIADC1p 350</i> F	GTGGGGCTCTGGCCTCGGCGGGTT	Mutagenesis of the <i>Brg11</i> -EBE in <i>SIADC1</i> promoter
Δ <i>SIADC2p 350</i> F	AGGGGGCCTCGGCCTCGGCGGGTT	Mutagenesis of the <i>Brg11</i> -EBE in <i>SIADC2</i> promoter
Δ <i>SIADC1/2p 350</i> R	5'PHO-CCCCTCAAAAGAAGCAAAAAA	Mutagenesis of the <i>Brg11</i> -EBE in <i>SIADC1/2</i> promoter, shared reverse P
Δ 1- <i>Brg11</i> -EBE F	TAGCCGGGGAATCACAACCTCAAG	Mutagenesis of the <i>Brg11</i> -EBE in <i>Bs3</i> promoter based on CRISPR mutation

Δ1-Brg11-EBE R	5'PHO- ACCCCCTCATAAAATTGGTCAGGC	Mutagenesis of the <i>Brg11-EBE</i> in <i>Bs3</i> promoter based on CRISPR mutation
Δ2-Brg11-EBE F	AGCCGGGGCAATCACAACCTCA	Mutagenesis of the <i>Brg11-EBE</i> in <i>Bs3</i> promoter based on CRISPR mutation
Δ2-Brg11-EBE R	5'PHO-CCTCATAAAATTGGTCAGGCAA	Mutagenesis of the <i>Brg11-EBE</i> in <i>Bs3</i> promoter based on CRISPR mutation
EBE <i>Sl12g009000</i> F	GGGAAGGGGGAGGGGCAATCACAAC TTCAA	Inegration of the candidate EBE from <i>Sl12g009000</i> into <i>Bs3</i> promoter
SIADC1 N R1	CGGAAGAATTAACGGTGAAATAC	5'RACE PCR on <i>SlADC1</i> in tomato
SIADC1 N R2	CCAATGGGTGGTAAGAGGGA	5'RACE PCR on <i>SlADC1</i> in tomato
SIADC2 N R1	CCAAGTCCACCCAAATTTTTC	5'RACE PCR on <i>SlADC2</i> in tomato
SIADC2 N R2	CCCGGTACAAATCAGATGACA	5'RACE PCR on <i>SlADC2</i> in tomato
SmADC1 N R1	CCAAGTCCACCAGAATTTATCGGATCG	5'RACE PCR on <i>SmADC1</i> in eggplant
SmADC1 N R2	TGGTGAGGAAGGGTATCTGTAC	5'RACE PCR on <i>SmADC1</i> in eggplant
SmADC2 N R1	CAAGTCCACCCAAATTTTCTGGGTCAG	5'RACE PCR on <i>SmADC2</i> in eggplant
SmADC2 N R2	ATGACATATCCGTTGACCAATG	5'RACE PCR on <i>SmADC2</i> in eggplant
NbADC1 N R1	GACTCCAACCGATTTTTTCAGAATATC	5'RACE PCR on <i>NbADC1</i> in <i>N. benthamiana</i>
NbADC1 N R2	TAGAATAAAGAGCGGATGAGTGCG	5'RACE PCR on <i>NbADC1</i> in <i>N. benthamiana</i>
NbADC2.1 N R1	ACAATATCTTCTACCACGAACCTGT	5'RACE PCR on <i>NbADC2.1</i> in <i>N. benthamiana</i>
NbADC2.1 N R2	CCGTACAAAGAAGAGGACAAATCC	5'RACE PCR on <i>NbADC2.1</i> in <i>N. benthamiana</i>
NbADC2.2 N R1	CTGATTGCATTTACGGGATAAACAC	5'RACE PCR on <i>NbADC2.2</i> in <i>N. benthamiana</i>
NbADC2.2 N R2	CCCGTACAAAGCAGATGATAAATCC	5'RACE PCR on <i>NbADC2.2</i> in <i>N. benthamiana</i>
Brg11 F	AGGTCTCACACCATGAGAATAGGCAAA TCAAGCGGTTGG	Clone of full-length <i>Brg11</i> and its derivate
Brg11 R	TCAGGTCTCTCCTTCGTTTCCAATATTT GCAGAAGCCAGTC	Clone of full-length <i>Brg11</i> and its derivate
SwaI_MtU6 F	GATATTAATCTCTTCGATGAAATTTATG CCTATCTTATATGATCAATGAGG	Clone of <i>MtU6</i> promoter into CRISPR vector
MtU6 R	AAGCCTACTGGTTCGCTTGAAG	Clone of <i>MtU6</i> promoter into CRISPR vector
Scaffold F	GTTTTAGAGCTAGAAATAGCAAGTT	Clone of gRNA scaffold into CRISPR vector
SpeI Scaffold R	GTCATGAATTGTAATACGACTCAAAA	Clone of gRNA scaffold into CRISPR

	AAAGCACCGACTCGGTG	vector
StUbi218R	ACATGCACCTAATTTCACTAGATGT	Colony PCR of assembled CRISPR constructs
ISceIR	GTGATCGATTACCCTGTTATCCCTAG	Colony PCR of assembled CRISPR constructs
UNS1_MtU6 F	CATTACTCGCATCCATTCTCATGCCTAT CTTATATGATCAATGAGG	Clone of <i>MtU6</i> promoter for CRISPR with multiply gRNAs
UNS1_Scaffold R	GAGAATGGATGCGAGTAATGAAAAAA AGCACCGACTCGGTG	Clone of gRNA scaffold for CRISPR with multiply gRNAs
Brg11-EBE g225	GCTATTTCTAGCTCTAAAACGCTACCC CCTCAAAGAAGCAAGCCTACTGGTTC GCTTGA	Clone of gRNA into CRISPR vector
SIADC1 g426	TCAAGCGAACCAGTAGGCTTGGATATG AGGCTCATTACCAGTTTATAGACTAGA AATAGC	Clone of gRNA into CRISPR vector
SIADC1 g560	TCAAGCGAACCAGTAGGCTTGGCCATG AGCTCTCTATGCAGTTTATAGACTAGA AATAGC	Clone of gRNA into CRISPR vector
SIADC2 g512	GCTATTTCTAGCTCTAAAACGCCGAA TCGGTATGGCGACAAGCCTACTGGTTC GCTTGA	Clone of gRNA into CRISPR vector
SIADC2 g564	GCTATTTCTAGCTCTAAAACCTTGGACA GACAGTTCATCGCAAGCCTACTGGTTC GCTTGA	Clone of gRNA into CRISPR vector
ScrnADC1 F	TACAGATACCCTTCCTCACCA	Screen for <i>Sladc1</i> CRISPR mutants
ScrnADC1 R	TGTCAATCACCAATCAAGC	Screen for <i>Sladc1</i> CRISPR mutants
ScrnADC2 F	AATCGGCTTTTGACATGGCG	Screen for <i>Sladc2</i> CRISPR mutants
ScrnADC2 R	AAGGAGCTTCTTGCGACCA	Screen for <i>Sladc2</i> CRISPR mutants
SIADC1p 434 F	TTGAAGACTGTACGGGTCTcTCTGGCT CATTTTCGAGTTGTTTAC	Clone of <i>SIADC1</i> long 5'UTR
SIADC1p 434 R	AAGAAGACGTCAGAGGTCTCaCATCTC GTAAAATCTTCACAAAAAA	Clone of <i>SIADC1</i> long/short 5'UTR
SIADC1p 70 F	TTGAAGACTGTACGGGTCTcTCTGAAC AAATCATTTCTGTATAATTAG	Clone of <i>SIADC1</i> short 5'UTR
SIADC2p 433 F	TTGAAGACTGTACGGGTCTcTCTGGCT CACTTCATAAGCTGTTA	Clone of <i>SIADC2</i> long 5'UTR
SIADC2p 433 R	AAGAAGACGTCAGAGGTCTCaCATCTC TTCCCCGATCTGTTTTG	Clone of <i>SIADC2</i> long/short 5'UTR
SIADC2p 99 F	TTGAAGACTGTACGGGTCTcTCTGGGG	Clone of <i>SIADC2</i> short 5'UTR

	AAGAAGAACATCAATCT	
ΔuORF F	GTCTGGTGGGGTGTGTTGTTT	Mutagenesis of the uORF in <i>SIADC1</i> long 5'UTR
ΔuORF R	5'PHO-AACTTTTAACCGGAATAGTT	Mutagenesis of the uORF in <i>SIADC1</i> long 5'UTR
ΔADC-box F	AGCTATTACAACATTGGTCAA	Mutagenesis of the ADC-box in <i>SIADC1</i> long 5'UTR
ΔADC-box R	5'PHO-AAAAGAAGCAAAAAAAGAAGCT	Mutagenesis of the ADC-box in <i>SIADC1</i> long 5'UTR
L 5'UTR ΔGC1 F	5'PHO-TAGCCGGGGCTCTGGCCTCG	Mutagenesis of the GC stretch 1 in <i>SIADC1</i> long 5'UTR
L 5'UTR ΔGC1 R	GGGGGTCAAAGAAGCAAAAAAAGAACTT	Mutagenesis of the GC stretch 1 in <i>SIADC1</i> long 5'UTR
L 5'UTR ΔGC2 F	5'PHO-TCTGGCCTCGGCGGGTTCTA	Mutagenesis of the GC stretch 2 in <i>SIADC1</i> long 5'UTR
L 5'UTR ΔGC2 R	CGGGGCCCTACCCCCTCAAAGAAGCA	Mutagenesis of the GC stretch 2 in <i>SIADC1</i> long 5'UTR
L 5'UTR ΔGC1/2 F	GACCCCTAGGGCCCGTCTGGCCTCGGCGGGTTCTAAAG	Mutagenesis of the GC stretch 1/2 in <i>SIADC1</i> long 5'UTR
L 5'UTR ΔGC1/2 R	5'PHO-AAAAGAAGCAAAAAAAGAAGCTT	Mutagenesis of the GC stretch 1/2 in <i>SIADC1</i> long 5'UTR
EGFP F	TTGGTCTCTACCGAAGACTCGATGGTGAGCAAGGGCGAGGA	Clone of <i>EGFP</i>
EGFP R	AAGGTCTCAGATTTTACTTGTACAGCTCGTCC	Clone of <i>EGFP</i>
DsRed F	TTGGTCTCTACCATGGCCTCCTCCGAGAACGT	Clone of <i>DsRed</i>
DsRed R	AAGGTCTCACCTTCTACAGGAACAGGTGGTGG	Clone of <i>DsRed</i>
In vitro 1	TCGCCACCTCTGACTTGAGC	<i>In vitro</i> translation PCR
In vitro 2	GCTGCGCAACTGTTGGGAAG	<i>In vitro</i> translation PCR

Supplementary table 4 The transitions monitored for each analyte in polyamine analysis

Q1 mass (Da)	Q3 mass (Da)	declustering potential (volts)	collision energy (volts)	compound	quantifier ion
89.1	72	22	14	putrescine1	+
175	158	50	20	arginine 1	+
175	116.1	50	20	arginine2	-
133	116	50	10	ornithine 1	-
133.01	70	50	20	ornithine 2	+
146.1	129	20	20	spermidine 1	+
146.1	72	20	21	spermidine 2	-
203.2	112	48	15	spermine 1	-
203.2	129.1	48	24	spermine 2	+
131.1	114.1	22	15	agmatine 1	-
131.1	72.1	22	15	agmatine 2	+
176.2	159.3	20	10	citrulline 1	+
176.2	113.1	20	10	citrulline 2	-
181.1	164.1	50	20	13C arginine 1	+
181.1	121.1	50	20	13C arginine 2	-
136.1	119.1	22	15	13C agmatine 1	-
136.11	76.1	22	15	13C agmatine 2	+
93.1	76.1	22	14	13C putrescine	+
104.01	69	90	23	GABA 1	+
104	87	90	17	GABA 2	-

875

6 Discussion

In this thesis I have established a toolkit for cloning of *R. solanacearum* gene knockout and complementation constructs. I have also identified *arginine decarboxylase* (*ADC*) genes as the sole host targets of the *R. solanacearum* TAL effector Brg11 in tomato. Brg11 binds to the *EBE* (*Brg11-EBE*) in *SIADC1/2* promoters and transcriptionally activates *SIADC1/2* expression. All investigated *ADC* genes from different host species contain a functional Brg11-*EBE* in their promoters, suggesting that Brg11 targets *ADC* genes across multiple hosts. *ADC*s are rate-limiting enzymes involved in polyamine biosynthesis. I found that 5'UTR of native *ADC* mRNAs contain an *ADC-box* that attenuates translation and that is conserved across land plant species. Interestingly, Brg11 targets the *ADC-box* region in *ADC* promoters and induces new *ADC* mRNA variants lacking the *ADC-box*, bypassing translational control and boosting host polyamine levels. *ADC* genes have no impact on *in planta* growth of *R. solanacearum*, however, I demonstrate that *ADC* genes are involved in a plant defense reaction against *P. syringae*. I hypothesize that Brg11-mediated *ADC* activation and polyamine boost helps *R. solanacearum* to better colonize host tissue by inhibiting bacterial niche competitors.

6.1 Golden-Gate based cloning simplifies gene functional studies in *R. solanacearum*

Assembly of *R. solanacearum* gene knockout and complementation constructs mostly relies on classical DNA cloning and Gateway cloning (Jacobs et al., 2013; Monteiro et al., 2012). Classical cloning is relatively time consuming, inflexible and the cloning efficiency can be very low when large fragments are assembled. Though Gateway cloning enables very effective construction of recombinant DNA and is independent on particular restriction sites, it's still limited in its flexibility. However, Golden-Gate (GG) cloning allows economic, efficient and flexible assembly of multiple fragments in one reaction (Engler et al., 2008). I established a GG toolbox for the constructions of plasmids for gene knockout and complementation in *R. solanacearum*. This toolkit simplifies the cloning strategy for genetic manipulation in this pathogen. Gene knockout is normally achieved by replacing the gene of interest with a resistance selection marker. Thus mutating multiple genes requires different selection markers. In the toolkit I have created several LI selection marker modules

(e.g. gentamycin and kanamycin) which extends the flexibility of the use of selection markers. The conceptual design of the toolkit is based on a previously published GG toolkit for construct assembly for *in planta* expression (Binder et al., 2014). The 4-bp overhangs of functionally equivalent modules are identical between both toolkits. This enables shared use of epitope tags for expression in *R. solanacearum* and *in planta*. Furthermore, it allows the gene of interest from *R. solanacearum* to be studied in a bacteria and plant context. For example, cloned type III effector genes can be used for complementation studies in *R. solanacearum* as well as for transient expression or overexpression studies in plants. Therefore, the establishment of this toolkit will simplify and facilitate gene functional studies in *R. solanacearum*.

To stably express genes in *R. solanacearum*, the constructs normally are integrated into the bacterial genome. A target site at nucleotide position 203, 337, located in one of the intergenic regions in the chromosome, has been shown to be a safe site for integration (Monteiro et al., 2012). However, *R. solanacearum* is a species complex and consists of four different phlotypes. Because of genetic diversity the target site for gene integration in different phlotype strains is polymorphic. The previously established pRC series allows integration of complementation constructs into phlotype I and phlotype II strains (Monteiro et al., 2012), it is relatively time consuming if one wants to change the integration site that matches to multiple strains. With GG cloning, it simplifies the cloning procedure for exchanging the integration site and thus allows genetic manipulation in any *R. solanacearum* strains whose genome information is available.

Another purpose for gene functional studies is to track the expression of the gene of interest. This can be achieved by fusing the native promoter to a reporter gene. Accordingly one can monitor the reporter expression. The previously established pRC system also enables such application (Monteiro et al., 2012). In our GG toolkit there are multiple fluorophore reporters and other reporter modules which significantly improves the flexibility for promoter probing. In addition, one could easily combine different reporters in one construct with the GG toolkit. For example, one can combine a fluorophore reporter with a *uidA* reporter; the fluorophore reporter enables cellular resolution of expression visualization and the *uidA* reporter is very sensitive and enables visualization without microscopy.

6.2 Identification of *ADCs* as *Brg11* host targets ---- What makes *Brg11* different with TALEs from *Xanthomonas*?

A TALE target gene typically has three major characters: 1) contains a functional *EBE* in its promoter; 2) is transcriptionally activated by the corresponding TALE; 3) is responsible for a certain disease phenotype. Based on the current knowledge on TALE targeted *EBEs*, all have the identical preference for the nucleotide thymine at the 5' of the *EBE* (T_0). This preference is mediated by the N-terminal non-canonical repeats (Mak et al., 2012). It has been previously shown that the RipTAL *Brg11* from *R. solanacearum* uniquely has preference for the nucleotide guanine at the 5' of the inferred *EBE* (G_0) (de Lange et al., 2013). In this thesis I demonstrate that *Brg11* targets host *ADC* genes. The *Brg11-EBE* upstream of *ADC* coding sequences contains the G_0 , which is totally different with *EBEs* of *Xanthomonas* TALEs (Figure 4A). This suggests that though *Brg11* is a TALE homology, it has its own features. It's likely that the G_0 preference for *Brg11* is also mediated by its N-terminal non-canonical repeats.

Xanthomonas TALEs normally target several genes in a given host (Boch et al., 2014). This means that TALEs can bind to several similar *EBEs* and activate their downstream gene expression (Figure 4B). Yet, among all targeted genes typically only one of them contributes to a disease phenotype and this gene is defined as the TALE target gene. The other TALE-induced genes with a compatible *EBE* are considered as off-target genes since they have no detectable virulence phenotype. My RNA-seq experiment on tomato leaves infiltrated with strains containing or lacking *Brg11* identified 117 *Brg11* up-regulated genes. Interestingly, only *SIADC1* and *SIADC2* genes contain a *Brg11* compatible *EBE* in their promoter regions and the *Brg11-EBE* is identical between *SIADC1* and *SIADC2*. This suggests that, unlike any known TALEs, *Brg11* only binds to one *EBE* sequence in the host genome. Since *SIADC1* and *SIADC2* are just two copies of *ADC* genes having the same function, I conclude that *Brg11* exclusively targets the same gene without activating additional off-target genes (Figure 4B). It's noteworthy that the *Brg11* containing *R. solanacearum* strain has a broad host range. I found that *Brg11* activates *ADC* genes in all investigated host plants, which is also different with TALEs from *Xanthomonas* spp. that have a limited host range.

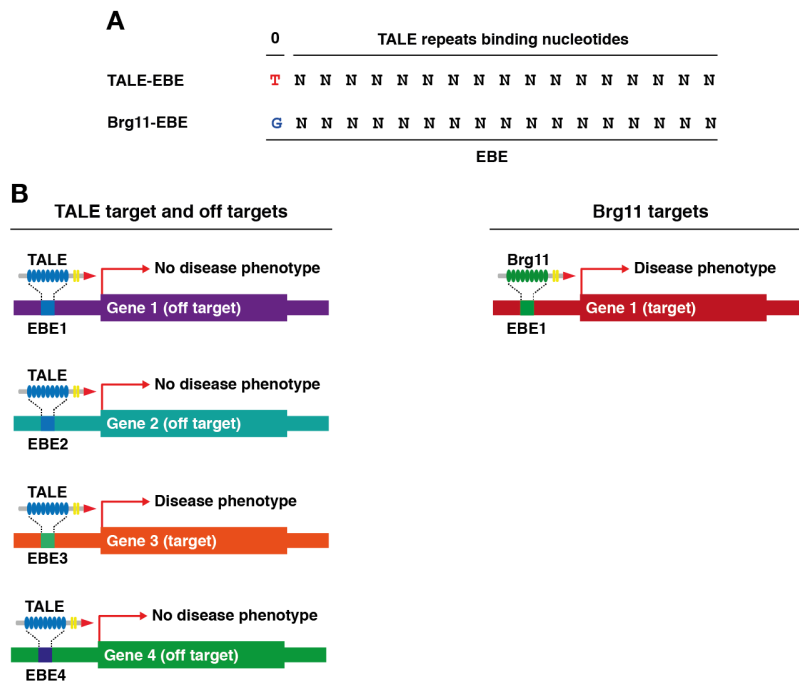


Figure 4 Differences between *Xanthomonas* TALE target genes and Brg11 target genes.

A, The Brg11-EBE is different with the TALE-EBE at the 0 position. An intact EBE includes a nucleotide at the 0 position (colored) and nucleotides that the TALE repeat units bind to (indicated by N). For TALEs, the nucleotide at the 0 position is always a T. However, the nucleotide at the 0 position is a G for Brg11. **B**, Brg11 does not have off target genes while TALEs typically have several off target genes. Brg11 only recognizes and binds to one specific EBE located at the upstream of the target gene (Gene 1). TALEs can bind to similar EBE sequences (EBE1-EBE4) and transcriptionally activate their downstream genes (Gene 1-4). However, only one of the targeted genes is responsible for a disease phenotype (Gene 3).

6.3 ADCs are new members of *R. solanacearum* type III effector target genes

R. solanacearum possess a large number of type III effectors. Due to the fact that knocking out a single effector gene in most cases has no effect on bacterial virulence (Cunnac et al., 2004), the mechanistical study of how effectors promote bacterial wilt disease is challenging. Till so far, only a few effectors's host targets have been identified and characterized. The effector RipP2 from strain GMI1000 interacts with RRS1-R (Resistance to *Ralstonia solanacearum* 1) in *Arabidopsis ecotpye* Nd-1 (Deslandes et al., 2003). RRS1-R triggers immune activation through intercepting RipP2-mediated immune suppression (Le Roux et al., 2015).

The RipTAL Brg11 has been previously studied *in planta* and shown to work as a transcription activator by binding to DNA in target promoters (de Lange et al., 2013). This work leads to the identification of ADC genes as sole host target genes of

Brg11. Although Brg11 is not recognized as a core type III effector in *R. solanacearum*, since some sequenced strains lack this effector (Peeters et al., 2013b). However, Brg11 homologies are prevalent in most of the phylotype I and IV strains (Schandry et al., 2016). Interestingly, Brg11 and Brg11 homologies from broad host strains conservatively targets *ADC* genes in all investigated host species. This suggests that *ADC* genes and their downstream metabolite putrescine possibly play important role in bacterial wilt disease development. I speculate that Brg11-mediated host *ADCs* induction and putrescine accumulation attenuate growth of competitive microbes which in return provides a competitive advantage to *R. solanacearum*. It has been shown that the Brg11 knockout strain is less competitive in eggplant leaves when co-infiltrated with the wild-type *R. solanacearum* strain (Macho et al., 2010). This competitive assay is a mixed inoculation between two different strains, but they are the same species *R. solanacearum*. Nevertheless Brg11 seems to promote the competitive advantage of *R. solanacearum*.

Though most of the type III effectors in *R. solanacearum* are not mechanistically studied, a large proportion of them have been assigned with a putative function. Several recent publications even confirmed the putative functions of a few distinct effectors *in planta* (Fujiwara et al., 2016; Mukaihara et al., 2016; Sang et al., 2018; Wei et al., 2017; Zheng et al., 2018). The identification of Brg11 host targets is based on its validated putative function as a transcription activator. Thus the *in planta* studies of other *R. solanacearum* effectors will facilitate the identification of their host targets and the characterization of how the interaction between effectors and host targets promote disease.

6.4 Induction of new transcription start sites by Brg11 and its biological impact

5' Rapid amplification of cDNA ends (5'RACE) PCR on *ADC* genes from tomato, aubergine and *N. benthamiana* showed that, Brg11-induced and native *ADC* transcripts differ in their transcription start sites (TSS). TALEs from *Xanthomonas* are also known to induce new TSSs of their target genes (Kay et al., 2007; Romer et al., 2009). The TALE AvrBs3 induces the expression of *upa20*, a master transcription factor controlling cell size. It was shown that in the presence of AvrBs3, *upa20* has an additional transcript variant which is 37 bp shorter in the 5'UTR compare to the native transcript (Kay et al., 2007). This suggests that AvrBs3 induces new TSS that

is downstream of the native TSS (Figure 5). However, different with TALEs, Brg11-induced TSSs are consistently >300 bp downstream of native TSSs. For example, Brg11-induced TSS in *SIADC1* gene is 363 bp downstream of its native TSS (Figure 5). This mainly because the native 5'UTR of *ADC* genes are much longer than the native 5'UTR of *upa20*.

The biological meaning of AvrBs3-induced short 5'UTR of *upa20* remains unclear. It most likely will not have a big impact on the behaviour of *upa20* transcript since the size difference between AvrBs3-induced and native 5'UTR of *upa20* is not that huge. Interestingly, Brg11-induced short 5'UTR of *ADC* genes have much higher translation efficiency compare to the native 5'UTR of *ADC* genes. Therefore, Brg11-induced TSS affect the translation activity of target transcripts. In the past, less attention has been paid to TALE-mediated TSS induction. Based on the result from Brg11, it seems important to perform 5'RACE PCR on TALE targets of interest. On one hand, it provides strong evidence that the targets are indeed direct target genes of a given TALE. On the other hand, it can provide information on the 5'UTR of the transcripts. Some other TALEs might use similar mechanisms to bypass translational control of target genes.

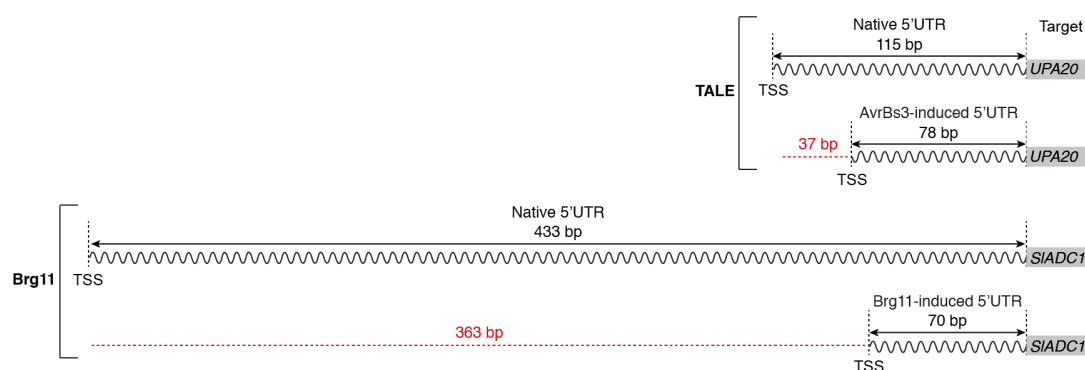


Figure 5 AvrBs3 and Brg11 induce new transcription start sites and thus distinct 5'UTRs.

The TALE AvrBs3 and the RipTAL Brg11 induce distinct transcription start site (TSS) in their target genes *UPA20* and *SIADC1*, respectively. The wavy lines indicate the 5'UTRs. The red dash line indicates the difference between the native TSS and the TALE- or Brg11-induced TSS.

6.5 Translational regulation of *ADC* and other polyamine pathway genes

ADC genes are involved in plant polyamine biosynthesis. Polyamines are important metabolites found in almost all living organisms. Maintaining intracellular polyamine

homeostasis is essential for normal cell functions and is achieved by a multi-level regulation from biosynthesis, transport to catabolism (Flynn and Hogarty, 2018). The regulation of polyamine biosynthesis is mainly maintained by translational control of polyamine pathway gene transcripts.

5'RACE PCR on *ADC* genes showed that native *ADC* transcripts contain a relatively long 5'UTR (about 430 bp, Figure 5). In eukaryotes, the 5'UTR of transcripts is important for ribosome recruitment and plays a critical role in the control of translation efficiency of downstream genes (Hinnebusch et al., 2016). Interestingly, there are two putative translational regulatory elements in the 5'UTR of native *ADC* transcripts (Figure 6). One of the putative element is a 27 bp uORF which is about 280 bp upstream of its main ORF. uORFs are widely involved in translation regulation of mRNAs. A large proportion (49%) of human transcripts contain one or more uORFs in their 5'UTRs (Calvo et al., 2009). In plants, about 30% to more than 40% of transcripts contain at least one uORF depending on the plant species (Von Arnim et al., 2014). It has been shown that mRNA of *AdoMetDC*, which encodes a rate limiting enzyme in the synthesis of polyamines spermidine and spermine (Tabor et al., 1984), contains one uORF in mammals and two uORFs in plants (Ivanov et al., 2009) (Figure 6). uORFs have also been predicted in other polyamine pathway genes including spermine synthase (Ivanov et al., 2009). The two uORFs of plant *AdoMetDC* mRNA overlaps by one nucleotide but only the second uORF whose sequence is conserved across land plant species is involved in translational regulation (Hanfrey et al., 2002, 2005). However, I found that the uORF in 5'UTR of native *SIADC* transcripts has no significant inhibitory effect on translation of *ADC* mRNA based on the transient reporter assay. It's possible that the transient assay might be not a good assay to identify subtle changes at the translational level. Analysis of stable uORF mutant tomato will be needed to study the functional relevance of this element in translational regulation. Nevertheless, the number and the size of uORFs in *ADC* transcript from different plant species differ quite a lot and the uORF is even absent in some plant *ADC* mRNAs. These together suggest that uORF is likely not a key translational regulatory element in plant *ADC* genes.

5'UTR of native *ADC* transcripts also contains a \approx 50 bp GC rich motif sequence (Figure 6). For simplicity, this GC rich motif is designated as *ADC-box*. Typically, 5'UTRs that allow efficient translation have short 5'UTR and a low GC content

(Kochetov et al., 1998). In contrast, 5'UTRs of mRNAs with low protein expression are more GC rich and have a higher degree of predicted RNA secondary structure (Barrett et al., 2012; Pickering and Willis, 2005). This suggests that GC-rich sequences are possibly involved in translational regulation of corresponding transcripts. In agreement with these observations, deletion of the *ADC-box* significantly increased translation efficiency of native *SIADC1* 5'UTR under both *in vivo* and *in vitro* conditions, suggesting that the *ADC-box* controls translation of native *ADC* transcripts. Similar to the second uORF in 5'UTR of plant *AdoMetDC* mRNA that is conserved in all land plants (Hanfrey et al., 2002), the *ADC-box* is extremely conserved across the plant kingdom, from the very ancient seedless plants like *Marchantia polymorpha* to the recently evolved higher plants like *Brachypodium distachyon*. These indicate that, on one hand, individual polyamine pathway gene use very conserved regulatory element for translational regulation; on the other hand, different polyamine pathway genes possess distinct translational regulatory elements. This allows very precise translational control of different genes. Different elements are likely controlled by unique metabolites.

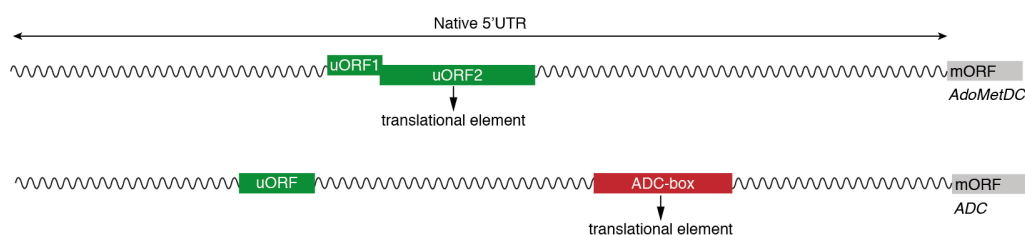


Figure 6 *ADC* genes use the *ADC-box* for translational regulation while *AdoMetDC* uses the uORF for translational regulation.

The 5'UTR of *AdoMetDC* has two upstream ORFs (uORF1 and uORF2, as indicated by green boxes). The uORF1 consists of 4 codons. The uORF2 consists of 53 codons. The uORF1 and uORF2 overlaps by one nucleotide but only the uORF2 is involved in translational regulation. The 5'UTR of *ADC* contains an uORF and a GC rich motif called *ADC-box*. The uORF consists of 9 codons but has no significant impact on translation. The *ADC-box* consists of about 50 bp and is involved in translational regulation. mORF, main ORF.

The *ADC-box* is predicted to form a tentative RNA secondary structure that consists of four GC stretches, termed GC1-4. GC1 is predicted to pair with GC4 forming RNA duplex region α (RDR α), and GC2 is predicted to pair with GC3 forming RNA duplex region β (RDR β). Although the *ADC-box* is very conserved across all land plant species, there are still some polymorphisms between ancient seedless plants and seed plants, especially in GC1 and GC4. Thus the tentative RNA secondary structure

of the *ADC-box* in seedless plants possibly only consists of GC2 and GC3. Interestingly, mutational analysis showed that GC2/GC3 pair (RDR β) has a much stronger impact on the translational inhibition compare to GC1/GC4 pair (RDR α). This indicates that GC2/GC3 pair is the original and core sequence controlling translation efficiency and the *ADC-box* is evolved from a relatively simple RNA secondary structure to a more complex structure during speciation via two alternative ways (Figure 7).

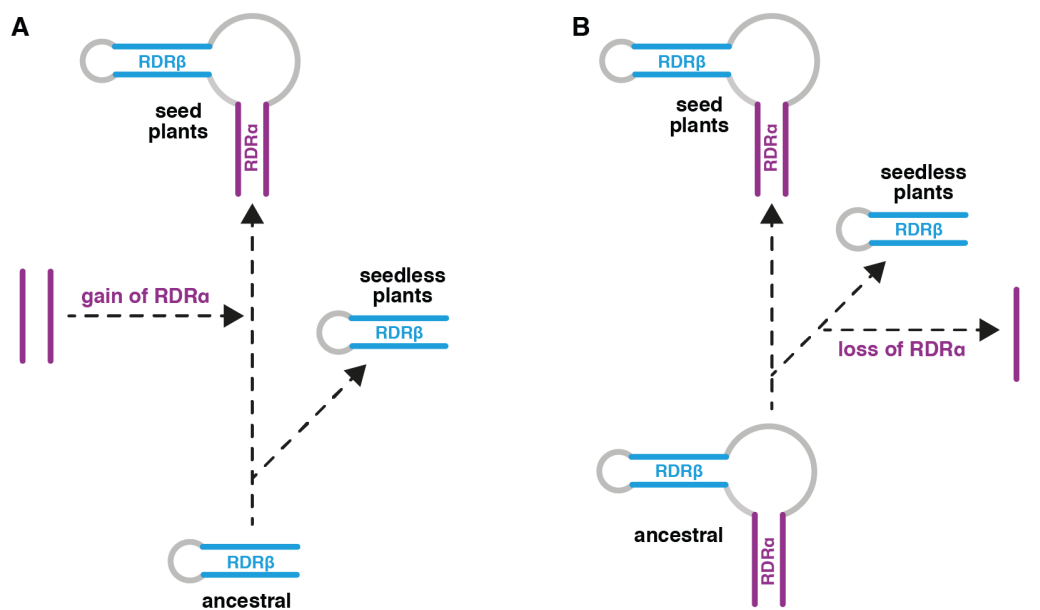


Figure 7 Two alternative evolutionary models that explain the polymorphisms in the *ADC-box* of seedless plants and seed plants.

A, The RNA duplex region α (RDR α) of the *ADC-box* is absent from ancestral plants and evolved in seed plant species. **B,** The RDR α of the *ADC-box* is present in ancestral plants, but it was lost during evolution to seedless plants and gained again during evolution to seed plants. The RDR α and RDR β are indicated by purple and blue color, respectively. The RDR α refers to GC1/4 pair. The RDR β refers to GC2/3 pair.

6.6 Polyamines represent a centre hub in host-microbe interactions

Brg11 not only exclusively increases host *ADC* transcript levels but also induces distinct *ADC* transcript variants that lack the cis-element *ADC-box* and mediate high level of translation. This strongly indicates that *ADC* genes play an important role in *R. solanacearum*-host interaction. *ADC* genes encode a rate limiting enzyme in polyamine biosynthesis where the amino acid arginine is converted to agmatine. Agmatine can be further processed to the diamine putrescine by agmatine iminohydrolase. Putrescine is the substrate for synthesis of higher polyamines

including the triamine spermidine and the tetraamines spermine and thermospermine (Jimenez-Bremont et al., 2014). Metabolic analysis showed that elevated transcription and translation of *ADC* genes by Brg11 lead to significant increase in agmatine and putrescine levels, but have no impact on spermidine and spermine levels. Notably, the concentration of putrescine is about 100 times higher than that of agmatine suggesting that putrescine is the functionally relevant metabolite induced by Brg11.

It has been shown that *ADC* genes in Arabidopsis (*AtADC1* and *AtADC2*) are involved in defense response against *Pseudomonas viridiflava* and *Pseudomonas syringae* pv. *tomato* DC3000 (Kim et al., 2013b; Rossi et al., 2015). *P. viridiflava* infection specifically induced *AtADC1* expression and putrescine accumulation in wild-type Arabidopsis. Interestingly, *P. viridiflava* inoculation induced *AtADC2* expression as well as ADC activity in the *adc1* mutant plants, suggesting that there is a certain degree of functional redundancy between *AtADC1* and *AtADC2* (Rossi et al., 2015). Different with *P. viridiflava*, *P. syringae* inoculation highly induced *AtADC2* expression in Arabidopsis. The *adc2* mutant plants are more susceptible upon *P. syringae* infection (Kim et al., 2013b). These studies consistently indicate that *ADC* genes play an important role in defense reaction against bacterial pathogens. Similar to these observations, *R. solanacearum* infection also activates tomato *ADC* genes. However, instead of a general defense response to pathogen infection, activation of host *ADC* expression upon *R. solanacearum* infection is mediated by the type III effector Brg11 that the bacteria injects into the host cells. Intriguingly, unlike *P. syringae-AtADC2* interaction, Brg11-mediated host *ADC* genes activation and putrescine accumulation are neither beneficial nor detrimental to *in planta* growth of *R. solanacearum*. Knockout of *ADC1* and *ADC2* in tomato (*Sladc1/2*) also have no impact on *in planta* growth of *R. solanacearum*. However, in agreement with the previous study in Arabidopsis (Kim et al., 2013b), the *Sladc1/2* double mutant tomato is more susceptible to *P. syringae* infection. These observations suggest that, depending on the target microbe or pathogen, *ADC* genes can be either neutral or harmful. *R. solanacearum* resides in soil, a microbe-rich environment, it's likely that *R. solanacearum* has to compete with other microbes for nutrition and resources. Therefore, it's hypothesized that Brg11-mediated *ADC* activation and polyamine

boost indirectly contributes to *R. solanacearum* virulence by inhibiting competitive microbes.

If the hypothesis is true, one would expect that *ADC* genes or other polyamine pathway genes or polyamines are widely involved in host-microbe interactions. Indeed, a TAL effector from *Xanthomonas campestris* is predicted to target the *ADC* gene in *Brassicaceae* (Denanc et al., 2018). It is noteworthy that, similar to *R. solanacearum*, *X. campestris* infecting *Brassicaceae* is also a vascular pathogen. This suggests that vascular pathogens might conservatively target host *ADC* genes. It has also been shown that AvrBsT, an effector protein from *X. campestris* pv *vesicatoria*, interacts with pepper ADC1 (Kim et al., 2013a). The interaction of pepper ADC1 with AvrBsT in *N. benthamiana* leads to accumulation of polyamines and enhanced cell death reaction. Polyamines are also involved in fungal infection. Polyamine biosynthetic genes and polyamine content are induced after *Fusarium* infection (Wojtasik et al., 2015).

Except for polyamine biosynthetic genes, polyamine oxidase genes are also found to be involved in host-microbe interaction. The soil-borne fungal pathogen *Verticillium dahliae* significantly induced cotton polyamine oxidase (*GhPAO*) gene expression during infection (Mo et al., 2015). GhPAO is responsible for converting spermine to spermidine. Silencing of *GhPAO* in cotton strongly reduced spermidine levels and increased spermine levels, resulting in enhanced susceptibility to *V. dahliae* infection. This suggests that *GhPAO* is involved in a host defense reaction against *V. dahliae* through the control of host spermine level.

Polyamines are involved in defense response against pathogens (Jimenez-Bremont et al., 2014). To overcome this defense reaction, some pathogens have evolved unique mechanisms to reduce polyamine levels. For example, *P. syringae* produces an effector molecule called coronatine during infection. Coronatine can significantly induce host *N-Acetyltransferase activity1* (*NATA1*) expression (Lou et al., 2016). *NATA1* acetylates putrescine to *N*-acetylputrescine reducing free putrescine content. Therefore, production of coronatine by *P. syringae* can lead to reduction of host free putrescine levels and accordingly inhibition of defense response. A recent study found that *P. syringae* also produces another small molecule phevamine A.

Phevamine A can suppress spermidine-mediated reactive oxygen species burst triggered by recognition of bacterial flagellin (O'Neill et al., 2018).

Altogether, these studies strongly indicate that polyamine pathway genes and their downstream metabolites are widely involved in plant-microbe interactions. Intriguingly, some microbes specifically up-regulate host polyamine levels while other microbes decrease host polyamine levels for their own benefit. This supports the hypothesis that Brg11-mediated putrescine boost enhances *R. solanacearum* pathogenicity through inhibition of competitive microbes.

It is noteworthy that *R. solanacearum* itself secretes huge amount of putrescine into its residing environment xylem and exogenous application of putrescine accelerate bacterial wilt disease development (Lowe-Power et al., 2018). One might wonder why *R. solanacearum* uses the effector Brg11 to increase host putrescine levels, since itself can secrete a lot. I speculate that *R. solanacearum* produced putrescine only accumulate in the extracellular space, while the effector Brg11 induced host putrescine increase most likely stay in the intracellular space. Different distribution of cellular putrescine can result in different biological functions. How *R. solanacearum* benefits from its own secreted putrescine is unclear. Interestingly, a recent study found that polyamines can elevate the flg22-induced ROS burst in *N. benthamiana* (O'Neill et al., 2018). Thus it's possible that Brg11-mediated intracellular putrescine accumulation acts as defense associated signaling molecules to defend against certain microbes.

6.7 Bacteria type III effectors mediate inhibition of competitive microbes

Brg11-mediated putrescine accumulation has no impact on *in planta* growth of *R. solanacearum* but attenuates *in planta* growth of *P. syringae*, suggesting the distinct or opposite role of putrescine on different microbes. This supports the above proposed hypothesis that regulation of host putrescine by the effector Brg11 benefits *R. solanacearum* via suppression of niche competitors.

R. solanacearum is a soil-borne pathogenic bacteria that infects plants through roots, which represent a microbe-rich environment for beneficial microbes as well as for pathogens (Castrillo et al., 2017; Finkel et al., 2017; Garrido-Oter et al., 2018). A recent study found that *R. solanacearum* infection strongly reduced the diversity and

abundance of rhizosphere microbiota (Wei et al., 2018). This suggests that *R. solanacearum* suppresses a substantial amount of competitive microbes in order to successfully invade the host plants. Comparison of root microbiota between a *R. solanacearum* resistant tomato cultivar Hawaii 7996 and a susceptible cultivar Moneymaker revealed distinct microbiome structures, and the resistant tomatoes possibly recruit microbiome composition to protect themselves from *R. solanacearum* infection (Kwak et al., 2018). In addition, the authors also identified a flavobacterium that was more abundant in the resistant tomato rhizosphere and that could suppress *R. solanacearum* infection in a susceptible tomato plants. This further confirms that the root microbiota play an important role in *R. solanacearum* disease development.

Interestingly, bacteria have evolved different protection mechanisms, for example, production of toxic compounds and type IV effectors, in order to thrive in a competitive environment. For example, a previous study reported that the soil bacterium *Agrobacterium tumefaciens* secretes a group of type VI DNase effectors that can attack both sibling cells and *Pseudomonas aeruginosa* and improve the competitive advantage of the bacteria (Ma et al., 2014). The size of bacteria and their competitors are similar. To gain a significant competitive advantage, it's very likely that the bacteria need a lot of energy to kill competitors. However, in the case of the hypothesis proposed here, where the *R. solanacearum* type III effector Brg11 manipulates a central host metabolism to inhibit growth of microbial niche competitors, it makes more sense, since plant cells are much bigger than microbe cells which most likely will have a much stronger impact on determining the structure of the surrounding microbiome. This is especially important during early stages of infection where the population of the pathogenic bacteria is still low. It also explains why we failed to see a virulence phenotype of Brg11 when inoculation assays were done in a microbe-poor soil.

6.8 Outlook

This thesis leads to the identification of *ADC* genes as sole host targets of the *R. solanacearum* type III effector Brg11. Brg11 targets *ADC* promoters and transcriptionally activates downstream *ADC* gene expression. However, it remains unknown by which time and at which cell type Brg11 is delivered during a natural infection. Based on the reporter assays, the transcriptional fusion of the *ADC* 5'UTR

(350 bp upstream of ATG) upstream of a GFP reporter did not result in fluorescence, suggesting that expression under this 5' sequence is not leaky. Thus one can fuse this UTR upstream of a fluorophore reporter and transform the fusion construct into tomato. The resulting transgenic plants should facilitate Brg11-dependent fluorescence visualization, which will provide cellular resolution for further functional characterization of Brg11 during bacterial wilt disease development.

5'UTR of *ADC* transcripts contains the *ADC-box* that works as a *cis*-element and controls translation. Though it has been demonstrated that the *ADC-box* attenuates translation and the sequence of the *ADC-box* is very conserved across all land plant species, it will be interesting to confirm that the *ADC-box* is functional in ancient plants such as *M. polymorpha*. On the other hand, how the *ADC-box* works as a translational regulatory element remains unknown. Since *ADC* genes are involved in polyamine biosynthesis, I speculate that one metabolite in this pathway can bind to the *ADC-box* and thus control translation of the corresponding transcript in a feedback manner. Future studies aimed to understand the mechanism would help us better understand the polyamine regulation in plants.

This thesis also leads to the proposal of the hypothesis that Brg11-mediated manipulation of host putrescine are involved in suppression of niche competitors. The data that support the hypothesis are based on the *in planta* growth of the leaf pathogen *P. syringae*. This is an artificial test system since *R. solanacearum* and *P. syringae* do not colonize the same niche under natural conditions. Therefore in the future it would be important to demonstrate the hypothesis in a more natural system. For example, it would be interesting to see if *R. solanacearum* delivery of Brg11 can inhibit growth of microbes that are known to affect growth of *R. solanacearum* in root. It would also be interesting to test if knockout of *ADC* genes in a given host can change the microbiome structure compare to wild-type plants.

References

- Antony, G., Zhou, J., Huang, S., Li, T., Liu, B., White, F., and Yang, B. (2010). Rice *xa13* recessive resistance to bacterial blight is defeated by induction of the disease susceptibility gene *Os-11N3*. *Plant Cell* 22, 3864–3876.
- Arnim, A.G., Jia, Q., and Vaughn, J.N. (2014). Regulation of plant translation by upstream open reading frames. *Plant Sci.* 214, 1–12.
- Barrett, L.W., Fletcher, S., and Wilton, S.D. (2012). Regulation of eukaryotic gene expression by the untranslated gene regions and other non-coding elements. *Cell. Mol. Life Sci.* 69, 3613–3634.
- Beaudoin, J.D., and Perreault, J.P. (2010). 5'-UTR G-quadruplex structures acting as translational repressors. *Nucleic Acids Res.* 38, 7022–7036.
- Binder, A., Lambert, J., Morbitzer, R., Popp, C., Ott, T., Lahaye, T., and Parniske, M. (2014). A modular plasmid assembly kit for multigene expression, gene silencing and silencing rescue in plants. *PLoS One* 9, e88218.
- Boch, J., and Bonas, U. (2010). Xanthomonas AvrBs3 family-type III effectors: discovery and function. *Annu. Rev. Phytopathol.* 48, 419–436.
- Boch, J., Scholze, H., Schornack, S., Landgraf, A., Hahn, S., Kay, S., Lahaye, T., Nickstadt, A., and Bonas, U. (2009). Breaking the code of DNA binding specificity of TAL-type III effectors. *Science.* 1509, 1509–1512.
- Boch, J., Bonas, U., and Lahaye, T. (2014). TAL effectors - pathogen strategies and plant resistance engineering. *New Phytol.* 204, 823–832.
- Bogdanove, A.J., Schornack, S., and Lahaye, T. (2010). TAL effectors: Finding plant genes for disease and defense. *Curr. Opin. Plant Biol.* 13, 394–401.
- Brito, B., Aldon, D., Barberis, P., Boucher, C., and Genin, S. (2002). A signal transfer system through three compartments transduces the plant cell contact-dependent signal controlling *Ralstonia solanacearum* hrp genes. *Mol. Plant-Microbe Interact.* 15, 109–119.
- Büttner, D., and He, S.Y. (2009). Type III protein secretion in plant pathogenic bacteria. *Plant Physiol.* 150, 1656–1664.
- Büttner, D. (2016). Behind the lines-actions of bacterial type III effector proteins in plant cells. *FEMS Microbiol. Rev.* 40, 894–937.
- Calvo, S.E., Pagliarini, D.J., and Mootha, V.K. (2009). Upstream open reading frames cause widespread reduction of protein expression and are polymorphic among humans. *Proc. Natl. Acad. Sci. U. S. A.* 106, 7507-7512
- Castrillo, G., Teixeira, P.J.P.L., Paredes, S.H., Law, T.F., de Lorenzo, L., Feltcher, M.E., Finkel, O.M., Breakfield, N.W., Mieczkowski, P., Jones, C.D., et al. (2017).

Root microbiota drive direct integration of phosphate stress and immunity. *Nature* **543**, 513–518.

Cernadas, R.A., Doyle, E.L., Niño-Liu, D.O., Wilkins, K.E., Bancroft, T., Wang, L., Schmidt, C.L., Caldo, R., Yang, B., White, F.F., et al. (2014). Code-assisted discovery of TAL effector targets in bacterial leaf streak of rice reveals contrast with bacterial blight and a novel susceptibility gene. *PLoS Pathog.* **10**, e1003972

Chen, L.Q. (2014). SWEET sugar transporters for phloem transport and pathogen nutrition. *New Phytol.* **201**, 1150–1155.

Chisholm, S.T., Coaker, G., Day, B., and Staskawicz, B.J. (2006). Host-microbe interactions: Shaping the evolution of the plant immune response. *Cell* **124**, 803–814.

Cohn, M., Bart, R.S., Shybut, M., Dahlbeck, D., Gomez, M., Morbitzer, R., Hou, B.H., Frommer, W.B., Lahaye, T., and Staskawicz, B.J. (2014). *Xanthomonas axonopodis* virulence is promoted by a transcription activator-like effector-mediated induction of a SWEET sugar transporter in cassava. *Mol. Plant-Microbe Interact.* **27**, 1186–1198.

Coll, N.S., and Valls, M. (2013). Current knowledge on the *Ralstonia solanacearum* type III secretion system. *Microb. Biotechnol.* **6**, 614–620.

Cox, K.L., Meng, F., Wilkins, K.E., Li, F., Wang, P., Booher, N.J., Carpenter, S.C.D., Chen, L., Zheng, H., Gao, X., et al. (2017). TAL effector driven induction of a SWEET gene confers susceptibility to bacterial blight of cotton. *Nat. Commun.* **8**, 1–14.

Cui, H., Tsuda, K., and Parker, J.E. (2014). Effector-triggered immunity: from pathogen perception to robust defense. *Annu. Rev. Plant Biol.* **66**, 487–511.

Cunnac, S., Occhialini, A., Barberis, P., Boucher, C., and Genin, S. (2004). Inventory and functional analysis of the large Hrp regulon in *Ralstonia solanacearum*: Identification of novel effector proteins translocated to plant host cells through the type III secretion system. *Mol. Microbiol.* **53**, 115–128.

Denanc, N., Szurek, B., Doyle, E.L., Lauber, E., Fontaine-bodin, L., Guy, E., Hajri, A., Cerutti, A., Boureau, T., Arlat, M., et al. (2018). Two ancestral genes shaped the *Xanthomonas campestris* TAL effector gene repertoire. *New Phytol.* **219**, 391–407.

Deslandes, L., and Genin, S. (2014). Opening the *Ralstonia solanacearum* type III effector tool box: Insights into host cell subversion mechanisms. *Curr. Opin. Plant Biol.* **20**, 110–117.

Deslandes, L., Olivier, J., Peeters, N., Feng, D.X., Khounlotham, M., Boucher, C., Somssich, I., Genin, S., and Marco, Y. (2003). Physical interaction between RRS1-R, a protein conferring resistance to bacterial wilt, and PopP2, a type III effector targeted to the plant nucleus. *Proc. Natl. Acad. Sci. U. S. A.* **100**, 8024–8029.

Doyle, E.L., Booher, N.J., Standage, D.S., Voytas, D.F., Brendel, V.P., Vandyk, J.K., and Bogdanove, A.J. (2012). TAL effector-nucleotide targeter (TALE-NT) 2.0: tools

- for TAL effector design and target prediction. *Nucleic Acids Res.* *40*, 117–122.
- Engler, C., Kandzia, R., and Marillonnet, S. (2008). A one pot, one step, precision cloning method with high throughput capability. *PLoS One* *3*, e3647.
- Finkel, O.M., Castrillo, G., Herrera Paredes, S., Salas González, I., and Dangl, J.L. (2017). Understanding and exploiting plant beneficial microbes. *Curr. Opin. Plant Biol.* *38*, 155–163.
- Flynn, A., and Hogarty, M. (2018). Myc, oncogenic protein translation, and the role of polyamines. *Med. Sci.* *6*, 41.
- Fujiwara, S., Kawazoe, T., Ohnishi, K., Kitagawa, T., Popa, C., Valls, M., Genin, S., Nakamura, K., Kuramitsu, Y., Tanaka, N., et al. (2016). RipAY, a plant pathogen effector protein, exhibits robust γ -glutamyl cyclotransferase activity when stimulated by eukaryotic thioredoxins. *J. Biol. Chem.* *291*, 6813–6830.
- Garrido-Oter, R., Nakano, R.T., Dombrowski, N., Ma, K.W., McHardy, A.C., and Schulze-Lefert, P. (2018). Modular traits of the rhizobiales root microbiota and their evolutionary relationship with symbiotic rhizobia. *Cell Host Microbe* *24*, 155–167.
- Genin, S., and Denny, T.P. (2012). Pathogenomics of the *Ralstonia solanacearum* species complex. *Annu. Rev. Phytopathol.* *50*, 67–89.
- Gill, S.S., and Tuteja, N. (2010). Polyamines and abiotic stress tolerance in plants. *Plant Signal. Behav.* *5*, 26–33.
- Greenland, J.A., and Lewis, D.H. (1984). Amines in barley leaves infected by brown rust and their possible relevance to formation of green islands. *New Phytol.* *96*, 283–291.
- Gu, K., Yang, B., Tian, D., Wu, L., Wang, D., Sreekala, C., Yang, F., Chu, Z., Wang, G.L., White, F.F., et al. (2005). R gene expression induced by a type-III effector triggers disease resistance in rice. *Nature* *435*, 1122–1125.
- Guerrero-González, M.L., Rodríguez-Kessler, M., and Jiménez-Bremont, J.F. (2014). uORF, a regulatory mechanism of the *Arabidopsis* polyamine oxidase 2. *Mol. Biol. Rep.* *41*, 2427–2443.
- Hanfrey, C., Franceschetti, M., Mayer, M.J., Illingworth, C., and Michael, A.J. (2002). Abrogation of upstream open reading frame-mediated translational control of a plant S-adenosylmethionine decarboxylase results in polyamine disruption and growth perturbations. *J. Biol. Chem.* *277*, 44131–44139.
- Hanfrey, C., Elliott, K.A., Franceschetti, M., Mayer, M.J., Illingworth, C., and Michael, A.J. (2005). A dual upstream open reading frame-based autoregulatory circuit controlling polyamine-responsive translation. *J. Biol. Chem.* *280*, 39229–39237.
- Hellens, R.P., Brown, C.M., Chisnall, M.A.W., Waterhouse, P.M., and Macknight,

- R.C. (2016). The emerging world of small ORFs. *Trends Plant Sci.* 21, 317–328.
- Heuer, H., Yin, Y.N., Xue, Q.Y., Smalla, K., and Guo, J.H. (2007). Repeat domain diversity of *avrBs3*-like genes in *Ralstonia solanacearum* strains and association with host preferences in the field. *Appl. Environ. Microbiol.* 73, 4379–4384.
- Hinnebusch, A.G., Ivanov, I.P., and Sonenberg, N. (2016). Translational control by 5'-untranslated regions of eukaryotic mRNAs. *Science.* 352, 1413–1416.
- Hu, Y., Zhang, J., Jia, H., Sosso, D., Li, T., Frommer, W.B., Yang, B., White, F.F., Wang, N., and Jones, J.B. (2014). Lateral organ boundaries 1 is a disease susceptibility gene for citrus bacterial canker disease. *Proc. Natl. Acad. Sci. U. S. A.* 111, E521–E529.
- Ivanov, I.P., Atkins, J.F., and Michael, A.J. (2009). A profusion of upstream open reading frame mechanisms in polyamine-responsive translational regulation. *Nucleic Acids Res.* 38, 353–359.
- Jacobs, J.M., Milling, A., Mitra, R.M., Hogan, C.S., Ailloud, F., Prior, P., and Allen, C. (2013). *Ralstonia solanacearum* requires *pops*, an ancient *avrE*-family effector, for virulence and to overcome salicylic acid-mediated defenses during tomato pathogenesis. *MBio* 4, 1-12
- Jimenez-Bremont, J.F., Marina, M., Guerrero-Gonzalez, M. de la L., Rossi, F.R., Sanchez-Rangel, D., Rodriguez-Kessler, M., Ruiz, O.A., and Garriz, A. (2014). Physiological and molecular implications of plant polyamine metabolism during biotic interactions. *Front. Plant Sci.* 5, 1–14.
- Jones, J.D.G., and Dangl, L. (2006). The plant immune system. *Nature* 444, 323–329.
- Kang, Y., Liu, H., Genin, S., Schell, M., and Denny, T.P. (2002). *Ralstonia solanacearum* requires type 4 pili to adhere to multiple surfaces and for natural transformation and virulence. *Mol. Microbiol.* 46, 427–437.
- Kay, S., Hahn, S., Marois, E., Hause, G., and Bonas, U. (2007). A bacterial effector acts as a plant transcription factor and induces a cell size regulator. *Science.* 318, 648–651.
- Kim, N.H., Kim, B.S., and Hwang, B.K. (2013a). Pepper arginine decarboxylase is required for polyamine and γ -aminobutyric acid signaling in cell death and defense response. *Plant Physiol.* 162, 2067–2083.
- Kim, S.H., Kim, S.H., Yoo, S.J., Min, K.H., Nam, S.H., Cho, B.H., and Yang, K.Y. (2013b). Putrescine regulating by stress-responsive MAPK cascade contributes to bacterial pathogen defense in *Arabidopsis*. *Biochem. Biophys. Res. Commun.* 437, 502–508.
- Kochetov, A. V., Ischenko, I. V., Vorobiev, D.G., Kel, A.E., Babenko, V.N., Kisselev,

- L.L., and Kolchanov, N.A. (1998). Eukaryotic mRNAs encoding abundant and scarce proteins are statistically dissimilar in many structural features. *FEBS Lett.* **440**, 351–355.
- Kwak, M.J., Kong, H.G., Choi, K., Kwon, S.K., Song, J.Y., Lee, J., Lee, P.A., Choi, S.Y., Seo, M., Lee, H.J., et al. (2018). Rhizosphere microbiome structure alters to enable wilt resistance in tomato. *Nat. Biotechnol.* **36**, 1110-1117
- Laing, W.A., Martínez-Sánchez, M., Wright, M.A., Bulley, S.M., Brewster, D., Dare, A.P., Rassam, M., Wang, D., Storey, R., Macknight, R.C., et al. (2015). An upstream open reading frame is essential for feedback regulation of ascorbate biosynthesis in *Arabidopsis*. *Plant Cell* **27**, 772–786.
- de Lange, O., Schreiber, T., Schandry, N., Radeck, J., Braun, K.H., Koszinowski, J., Heuer, H., Strauß, A., and Lahaye, T. (2013). Breaking the DNA-binding code of *Ralstonia solanacearum* TAL effectors provides new possibilities to generate plant resistance genes against bacterial wilt disease. *New Phytol.* **199**, 773–786.
- Li, L., Atef, A., Piatek, A., Ali, Z., Piatek, M., Aouida, M., Sharakuu, A., Mahjoub, A., Wang, G., Khan, S., et al. (2013). Characterization and DNA-binding specificities of *Ralstonia* TAL-like effectors. *Mol. Plant* **6**, 1318–1330.
- Lou, Y.R., Bor, M., Yan, J., Preuss, A.S., and Jander, G. (2016). *Arabidopsis* NATA1 acetylates putrescine and decreases defense-related hydrogen peroxide accumulation. *Plant Physiol.* **171**, 1443-1455.
- Lowe-Power, T.M., Hendrich, C.G., von Roepenack-Lahaye, E., Li, B., Wu, D., Mitra, R., Dalsing, B.L., Ricca, P., Naidoo, J., Cook, D., et al. (2018). Metabolomics of tomato xylem sap during bacterial wilt reveals *Ralstonia solanacearum* produces abundant putrescine, a metabolite that accelerates wilt disease. *Environ. Microbiol.* **20**, 1330–1349.
- Ma, L.S., Hachani, A., Lin, J.S., Filloux, A., and Lai, E.M. (2014). *Agrobacterium tumefaciens* deploys a superfamily of type VI secretion DNase effectors as weapons for interbacterial competition in planta. *Cell Host Microbe* **16**, 94–104.
- Macho, A.P. (2016). Subversion of plant cellular functions by bacterial type-III effectors: Beyond suppression of immunity. *New Phytol.* **210**, 51–57.
- Macho, A.P., Guidot, A., Barberis, P., Beuzon, C.R., and Genin, S. (2010) A competitive index assay identifies several *Ralstonia solanacearum* type III effector mutant strains with reduced fitness in host plants. *Mol. Plant-Microbe Interact.* **23**, 1197-1205.
- Macho, A.P., and Zipfel, C. (2015). Targeting of plant pattern recognition receptor-triggered immunity by bacterial type-III secretion system effectors. *Curr. Opin. Microbiol.* **23**, 14–22.

- Mak, A.N., Bradley, P., Cernadas, R., Bogdanove, A.J., and Stoddard, B. (2012). The crystal structure of TAL effector PthXo1 bound to its DNA target. *Nature* 5, 13–15.
- Mansfield, J., Genin, S., Magori, S., Citovsky, V., Sriariyanum, M., Ronald, P., Dow, M., Verdier, V., Beer, S. V., Machado, M.A., et al. (2012). Top 10 plant pathogenic bacteria in molecular plant pathology. *Mol. Plant Pathol.* 13, 614–629.
- McGillivray, P., Ault, R., Pawashe, M., Kitchen, R., Balasubramanian, S., and Gerstein, M. (2018). A comprehensive catalog of predicted functional upstream open reading frames in humans. *Nucleic Acids Res.* 46, 3326–3338.
- Michael, A.J. (2016). Polyamines in eukaryotes, bacteria, and archaea. *J. Biol. Chem.* 291, 14896–14903.
- Mo, H., Wang, X., Zhang, Y., Zhang, G., Zhang, J., and Ma, Z. (2015). Cotton polyamine oxidase is required for spermine and camalexin signalling in the defence response to *Verticillium dahliae*. *Plant J.* 83, 962–975.
- Monteiro, F., Solé, M., van Dijk, I., and Valls, M. (2012). A chromosomal insertion toolbox for promoter probing, mutant complementation, and pathogenicity studies in *Ralstonia solanacearum*. *Mol. Plant-Microbe Interact.* 25, 557–568.
- Moscou, M., and Bogdanove, A. (2009). A simple cipher governs DNA recognition by TAL effectors. *Science* 326, 1501.
- Mukaihara, T., Hatanaka, T., Nakano, M., and Oda, K. (2016). *Ralstonia solanacearum* type III effector RipAY is a glutathione-degrading enzyme that is activated by plant cytosolic thioredoxins and suppresses plant immunity. *MBio* 7, 1–14.
- Nürnbergger, T., Brunner, F., Kemmerling, B., and Piater, L. (2004). Innate immunity in plants and animals: striking similarities and obvious differences. *Immunol. Rev.* 198, 249–266.
- O'Neill, E.M., Mucyn, T.S., Patteson, J.B., Finkel, O.M., Chung, E.-H., Baccile, J.A., Massolo, E., Schroeder, F.C., Dangl, J.L., and Li, B. (2018). Phevamine A, a small molecule that suppresses plant immune responses. *Proc. Natl. Acad. Sci. U. S. A.* 115, E9514–E9522.
- Occhialini, A., Cunnac, S., Reymond, N., Genin, S., and Boucher, C. (2005). Genome-wide analysis of gene expression in *Ralstonia solanacearum* reveals that the *hrpB* gene acts as a regulatory switch controlling multiple virulence pathways. *Mol. Plant-Microbe Interact.* 18, 938–949.
- Peeters, N., Guidot, A., Vaillieu, F., and Valls, M. (2013a). *Ralstonia solanacearum*, a widespread bacterial plant pathogen in the post-genomic era. *Mol. Plant Pathol.* 14, 651–662.
- Peeters, N., Carrère, S., Anisimova, M., Plener, L., Cazalé, A.-C., and Genin, S.

- (2013b). Repertoire, unified nomenclature and evolution of the Type III effector gene set in the *Ralstonia solanacearum* species complex. *BMC Genomics* *14*, 859.
- Perez-Leal, O., and Merali, S. (2012). Regulation of polyamine metabolism by translational control. *Amino Acids* *42*, 611–617.
- Pérez-Quintero, A.L., Rodriguez-R, L.M., Dereeper, A., López, C., Koebnik, R., Szurek, B., and Cunnac, S. (2013). An improved method for TAL effectors DNA-binding sites prediction reveals functional convergence in TAL repertoires of *Xanthomonas oryzae* strains. *PLoS One* *8*. e68464
- Pickering, B.M., and Willis, A.E. (2005). The implications of structured 5' untranslated regions on translation and disease. *Semin. Cell Dev. Biol.* *16*, 39–47.
- Rahmani, F., Hummel, M., Schuurmans, J., Wiese-Klinkenberg, A., Smeekens, S., and Hanson, J. (2009). Sucrose control of translation mediated by an upstream open reading frame-encoded peptide. *Plant Physiol.* *150*, 1356–1367.
- Romer, P., Strauss, T., Hahn, S., Scholze, H., Morbitzer, R., Grau, J., Bonas, U., and Lahaye, T. (2009). Recognition of AvrBs3-Like proteins is mediated by specific binding to promoters of matching pepper Bs3 alleles. *Plant Physiol* *150*, 1697–1712.
- Römer, P., Hahn, S., Jordan, T., Strauß, T., Bonas, U., and Lahaye, T. (2007). Plant pathogen recognition mediated by promoter activation of the pepper Bs3 resistance gene. *Science.* *318*, 645–648.
- Rossi, F.R., Marina, M., and Pieckenstain, F.L. (2015). Role of arginine decarboxylase (ADC) in *Arabidopsis thaliana* defence against the pathogenic bacterium *Pseudomonas viridiflava*. *Plant Biol.* *17*, 831–839.
- Le Roux, C., Huet, G., Jauneau, A., Camborde, L., Tremousaygue, D., Kraut, A., Zhou, B., Levailant, M., Adachi, H., Yoshioka, H., et al. (2015). A receptor pair with an integrated decoy converts pathogen disabling of transcription factors to immunity. *Cell* *161*, 1074–1088.
- Salanoubat, M., Genin, S., Artiguenave, F., Gouzy, J., Mangenot, S., Arlat, M., Billault, A., Brottier, P., Camus, J.C., Cattolico, L., et al. (2002). Genome sequence of the plant pathogen *Ralstonia solanacearum*. *Nature* *415*, 497–502.
- Sang, Y., Wang, Y., Ni, H., Cazalé, A.-C., She, Y.-M., Peeters, N., and Macho, A.P. (2018). The *Ralstonia solanacearum* type III effector RipAY targets plant redox regulators to suppress immune responses. *Mol. Plant Pathol.* *19*, 129–142.
- Schandry, N., de Lange, O., Prior, P., and Lahaye, T. (2016). TALE-like effectors are an ancestral feature of the *Ralstonia solanacearum* species complex and converge in DNA targeting specificity. *Front. Plant Sci.* *7*, 1225.
- Srivastava, A.K., Lu, Y., Zinta, G., Lang, Z., and Zhu, J.K. (2018). UTR-dependent control of gene expression in plants. *Trends Plant Sci.* *23*, 248–259.

- Strauss, T., van Poecke, R.M.P., Strauß, A., Römer, P., Minsavage, G. V, Singh, S., Wolf, C., Strauß, A., Kim, S., Lee, H.A., et al. (2012). RNA-seq pinpoints a *Xanthomonas* TAL-effector activated resistance gene in a large-crop genome. *Proc. Natl. Acad. Sci. U. S. A.* *109*, 19480–19485.
- Streubel, J., Pesce, C., Hutin, M., Koebnik, R., Boch, J., and Szurek, B. (2013). Five phylogenetically close rice SWEET genes confer TAL effector-mediated susceptibility to *Xanthomonas oryzae* pv. *oryzae*. *New Phytol.* *200*, 808–819.
- Tabor, C.W., Tabor, C.W., Tabor, H., and Tabor, H. (1984). Polyamines. *Metab. Clin. Exp.* 749–790.
- Tans-Kersten, J., Brown, D., and Allen, C. (2007). Swimming motility, a virulence trait of *Ralstonia solanacearum*, is regulated by FlhDC and the plant host environment. *Mol. Plant-Microbe Interact.* *17*, 686–695.
- Tian, D., Wang, J., Zeng, X., Gu, K., Qiu, C., Yang, X., Zhou, Z., Goh, M., Luo, Y., Murata-Hori, M., et al. (2014). The rice TAL effector-dependent resistance protein XA10 triggers cell death and calcium depletion in the endoplasmic reticulum. *Plant Cell* *26*, 497–515.
- Walters, D. (2003). Resistance to plant pathogens: Possible roles for free polyamines and polyamine catabolism. *New Phytol.* *159*, 109–115.
- Walters, D.R., Wilson, P.W.F., and Shuttleton, M.A. (1985). Relative changes in levels of polyamines and activities of their biosynthetic enzymes in barley infected with the powdery mildew fungus, *Erysiphe graminis* D.C. ex *merat* f.sp. *hordei* *marchal*. *New Phytol.* *101*, 695–705.
- Wang, C., Fan, Y., Zheng, C., Qin, T., Zhang, X., and Zhao, K. (2014). High-resolution genetic mapping of rice bacterial blight resistance gene *Xa23*. *Mol. Genet. Genomics* *289*, 745–753.
- Wei, Y., Sang, Y., and Macho, A.P. (2017). The *Ralstonia solanacearum* type III effector RipAY is phosphorylated in plant cells to modulate its enzymatic activity. *Front. Plant Sci.* *8*, 1–7.
- Wei, Z., Hu, J., Gu, Y., Yin, S., Xu, Y., Jousset, A., Shen, Q., and Friman, V.P. (2018). *Ralstonia solanacearum* pathogen disrupts bacterial rhizosphere microbiome during an invasion. *Soil Biol. Biochem.* *118*, 8–17.
- Wojtasik, W., Kulma, A., Namysł, K., Preisner, M., and Szopa, J. (2015). Polyamine metabolism in flax in response to treatment with pathogenic and non-pathogenic *Fusarium* strains. *Front. Plant Sci.* *6*, 1–12.
- Xiang, T., Zong, N., Zou, Y., Wu, Y., Zhang, J., Xing, W., Li, Y., Tang, X., Zhu, L., Chai, J., et al. (2008). *Pseudomonas syringae* effector AvrPto blocks innate immunity by targeting receptor kinases. *Curr. Biol.* *18*, 74–80.

- Xiang, T., Zong, N., Zhang, J., Chen, J., Chen, M., and Zhou, J.M. (2010). BAK1 is not a target of the *Pseudomonas syringae* effector AvrPto . *Mol. Plant-Microbe Interact.* *24*, 100–107.
- Yang, B., Sugio, A., and White, F.F. (2006). Os8N3 is a host disease-susceptibility gene for bacterial blight of rice. *Proc. Natl. Acad. Sci. U. S. A.* *103*, 10503–10508.
- Yu, Y., Streubel, J., Balzergue, S., Champion, A., Boch, J., Koebnik, R., Feng, J., Verdier, V., and Szurek, B. (2011). Colonization of rice leaf blades by an african strain of *Xanthomonas oryzae* pv. *oryzae* depends on a new TAL effector that induces the rice nodulin-3 Os11N3 gene . *Mol. Plant-Microbe Interact.* *24*, 1102–1113.
- Zheng, X., Li, X., Wang, B., Cheng, D., Li, Y., Li, W., Huang, M., Tan, X., Zhao, G., Song, B., et al. (2018). A systematic screen of conserved *Ralstonia solanacearum* effectors reveals the role of RipAB, a nuclear-localized effector that suppresses immune responses in potato. *Mol. Plant Pathol.* *20*, 547–561.
- Zipfel, C. (2014). Plant pattern-recognition receptors. *Trends Immunol.* *35*, 345–351.

Acknowledgments

The PhD life is colorful and unforgettable. I experienced exciting moments when experiments went smoothly; I experienced stress when things were not working so well. I learned a lot from success; I also learned a lot from failure. But no matter what happened, there are always people supporting me and helping me.

First of all I would like to give my special gratitude to my supervisor Prof. Thomas Lahaye. Thank you for giving me the opportunity to work in the group. I am very appreciate for all the things you have supported me. All these have made a big difference. Thank you, Thomas.

I would like to thank Orlando de Lange and Niklas Schandry who have helped me, scientifically and personally, so much from the very beginning. Without your previous work and support, I would not be able to take over the project so quickly.

It is really great to work in Lahaye group. Everybody is so nice and inclusive. Many thanks to all my colleagues. Robert Morbitzer and Annett Strauß, thank you for constant help and suggestions in the lab. Markus Wunderlich and Angela Dressel, thank you for technical support. Christina Wolf, Christina Krönauer, Patrizia Ricca, Thi Thu Trang Phan, Kyrylo Schenstnyi, Danalyn Holmes and Erin-samantha Ritchie, thank you for all the help, discussions, chats and lunch times.

I thank Niels Gallas for choosing one part of my project as his master thesis and Maximilian Werner Epple for doing the bachelor thesis with me. Thank the student assistants Katharina-elizabeth Gabor and Alexander Müller for helping me with some lab work.

Outside the Lahaye group, I would like to thank our nice secretary Charlotte Rehm for all the paper work.

I would like to thank Ulrike Zentgraf and Andrea A. Gust for being my thesis advisory committee and for all the valuable suggestions during the TAC meetings.

I would like to thank the whole General Genetics, especially Andreas Wachter and Chang Liu for all the help and impressive discussions during my progress reports and literature seminars.

Within the ZMBP, I would like to thank Edda von Roepenack- Lahaye for help on the metabolomic analysis; Kenneth Berendzen and Caterina Brancato for help on the protoplast and tomato transformation; Johanna Schröter and Sofia Riegger for help on the preparation of tomato plants. Special thanks to Christopher Grefen and Farid El Kasmi for organising the ZMBP graduate program.

I would also like to thank all of the collaborators. Especially those who are not listed as co-authors on the publications. Richard Berthome, thank you for showing me the nice Arabidopsis hydroponic system. Fabien Lonjon, thank you for working on the Brg11 secretion assay.

I thank Yong Zhang and Gaofei Jiang in China for helping me before and during my PhD.

I am very grateful to all the people who have helped me. Thank you.

Finally and most importantly, I would like to thank my parents, my wife and my sisters. No matter where I am and what I am doing, you always encourage me and support me to pursue my goals.

Curriculum vitae

Dousheng Wu (伍斗生)

Date of birth: 04.07.1989

Place of birth: Hunan, China

Education:

2015.01 – 2019.09 PhD student, Centre for Plant Molecular Biology,
University of Tuebingen, Germany

2008.09 – 2012.06 Bachelor student, College of Plant Protection, Southwest
University, China

2005.09 – 2008.06 High school student, The Third Middle School of Xinhua,
Hunan, China